NASA CR-60035

Final Report

A STUDY OF TECHNIQUES FOR REDUCING THE NOISE TEMPERATURE OF PASSIVE PARABOLOIDAL REFLECTOR ANTENNAS

By: K. D. McDonald

A.G.A. Project 1196

Prepared for

NATIONAL AERONAUTICS AND SPACE ADMINISTRATION
GODDARD SPACE FLIGHT CENTER
GREENBELT, MARYLAND

Contract NAS 5-1951

October 1962

AERO GEO ASTRO CORPORATION
EDSALL AND LINCOLNIA ROADS
ALEXANDRIA, VIRGINIA

A STUDY OF TECHNIQUES FOR REDUCING THE NOISE TEMPERATURE OF PASSIVE PARABOLOIDAL REFLECTORS

ABSTRACT

12814

Results of this study include presentation and analysis of the basic physical factors influencing the effective noise temperature of passive paraboloidal reflector antennas; description of a novel shaped beam "fluted feed" surface wave structure capable of improving conventional paraboloidal antenna low noise performance by a factor of between two and five; and presentation of design information and experimental results for a completely new Cassegrainian sectoral horn-reflector antenna which is physically compact, attains an equivalent antenna noise temperature of less than five degrees Kelvin, and appears in nearly all respects to be superior to all other low noise antennas currently available.

A discussion of external noise sources is presented including contributions due to galactic radiation, atmospheric absorption, ground radiation and various other influences. The dependence upon internal noise sources such as transmission line losses, mismatch losses, reflector surface error, and aperture blocking are discussed. An analysis of various feed shaping techniques for optimizing the ratio of gain to effective antenna temperature is presented and experimental results of various feeds employing these techniques are presented. Primary and secondary pattern evaluation techniques are also developed providing a means by which the low noise characteristics of existing and developmental feeds or antenna systems may be evaluated. Characteristics for a novel surface wave feed structure designated the fluted feed are presented. The fluted feed is shown to have several significant advantages over conventional feeds resulting in a substantial noise temperature performance improvement for conventional paraboloidal reflector antennas. The fluted

author

feed design is shown to have nearly uniform reflector illumination maximizing gain and efficiency, low spillover at the aperture edges minimizing minor-lobe energy, equal beamwidths in the E and H-planes, complete polarization flexibility, negligible aperture blocking in high gain applications and to be adaptable to monopulse tracking.

The Cassegrainian sectoral horn-reflector antenna, designated the KSK Antenna, is a Cassegrainian adaptation of the sectoral horn-reflector "sugar scoop" antenna. The latter antenna has obtained excellent low noise performance, but is mechanically complex and of large physical size. The KSK Antenna overcomes these mechanical disadvantages by the use of a hyperboloidal reflector at the mouth of the horn transforming the antenna into a Cassegrainian system. Advantages gained by the KSK Antenna are exceptional low noise characteristics with high efficiency, physical compactness, mechanical simplicity, negligible aperture blocking, operation without radome, adaptability to monopulse operation and economic feasibility.

TABLE OF CONTENTS

LIST OF TABLES

LIST OF ILLUSTRATIONS

I INTRODUCTION

1.0 INTRODUCTION

1.1 Low Noise Antenna Requirement

The development of low noise solid state amplifier systems, such as maser and parametric amplifiers has caused a re-evaluation of the role which the antenna plays in limiting the performance of a communications system. The extreme sensitivities attainable by the solid state "cooled" amplifiers, corresponding to equivalent amplifier noise temperatures of but a few degrees Kelvin, indicates that the noise contributions entering the receiving system from environmental sources external to the antenna and from the losses occurring within the antenna may place an important limitation on system sensitivity. The noise received by a radio or radar system from external radiating sources has become of increasing importance as the effective apertures of antennas have become larger, and as receiver systems have become more sensitive.

The overall system sensitivity is generally limited by the noise contributions generated either internal or external to the system which have a tendency to mask the received signal energy. The problem is hence one basically of obtaining the optimum, or highest, output signal-to-noise ratio (SNR) for a given set of input conditions. This infers directly that the solution may involve a minimization of the total system noise source level, including both internal and external sources.

Antenna system design in the past has been primarily concerned with achieving a specified directive gain from a given antenna configuration. Factors such as aperture efficiency, spillover energy, minor-lobe level, mismatch losses, feed losses, transmission line losses, and aperture blocking effects have often been considered important only in the manner in which they effect gain or side-lobe characteristics. However, the influence which these and other antenna parameters have in

determining the noise characteristics fo the antenna system must be analyzed and evaluated in order to obtain the optimal relations for these factors in the low noise antenna application.

The total system sensitivity, expressed as a signal power density level at a given signal-to-noise ratio (SNR) is directly influenced by the background noise level with which the desired signal must be interpreted. The ability of microwave receiver systems to detect small signal power levels at a given SNR relates directly to the internal noise generated within the receiver system. For this reason, the sensitivity of a receiver system may be expressed in terms of its equivalent noise temperature. The improvement in receiver system sensitivities, which has occurred during the past three decades, is in certain respects quite amazing. During this interval, an overall sensitivity improvement of about three orders of magnitude has been realized. Maser systems in particular have attained operating temperatures in the order of a few degrees Kelvin and it appears questionable whether any improvement in their operating noise temperature characteristics causes an appreciable improvement in the total system signal-to-noise ratio. The more advanced maser systems presently operate at noise temperatures in the order of the minimum externally generated noise. It is not surprising that conventional passive paraboloidal reflector antenna systems which generally have not been designed specifically for the low noise application should become significant contributors to the degradation of the total system sensitivity.

To illustrate the present state-of-the-art in receiver systems, refer to Figure 1-1 , which is a survey of operational receivers for use in the microwave region and somewhat below. It is clear from these plots that effective receiver noise temperatures in the order of 30° Kelvin or less are possible throughout the

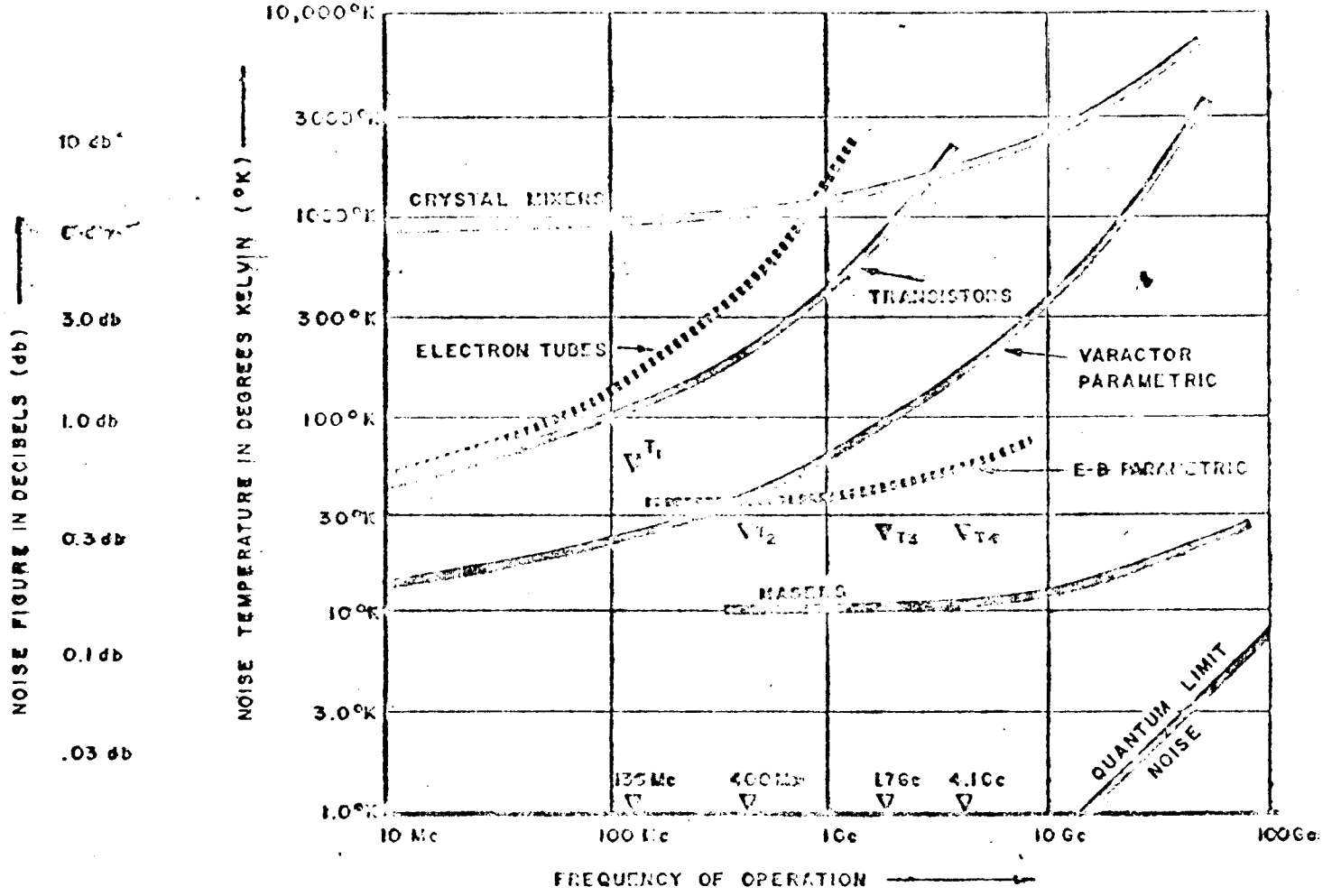

NOISE CHARACTERISTICS FOR VARIOUS OPERATIONAL RECEIVER SYSTEMS

Figure 1-1.

entire NASA frequency range of interest. The low receiver noise temperatures available with masers, paramps, and certain other devices may be compared with older techniques such as receivers utilizing crystal mixers operating in the microwave region, or conventional detection techniques employing electron tubes. It is apparent that noise temperatures for the older systems operating in the microwave region of approximately 500 - 2000° Kelvin were not uncommon. The abscissa on the receiver low noise capability plot represents operating frequency, and the ordinate on the plot indicates the noise temperature in degrees Kelvin and is also represented by the noise figure ($\overline{NF}$) in decibels. There is a simple relation converting noise figure in decibels to noise temperature in degrees Kelvin which is given by the expression

$$T_A = (\overline{NF} - 1)\ T_o$$

where T_o is the reference temperature generally taken as 290° Kelvin. This may also be written in terms of the noise figure as

$$\overline{NF} = 1 + T_A / T_o$$

or in logarithmic form, the noise figure may be written as

$$\overline{NF}\ (db) = 10 \log (1 + T_A / T_o).$$

It is also interesting to note the relative advantages of low noise antenna systems in terms of overall system sensitivity. To illustrate this, a hypothetical lunar space probe example has been devised involving transmission of information from a telemetry transmitter in the region of the lunar surface to a ground station on the earth. Figure 1-2 shows a plot of the power required at the space probe transmitter in the vicinity of the moon for various low noise receiving antenna systems. The separation between the antenna systems is taken as the mean lunar distance of approximately 250,000 miles. It is clear from this plot that if payload

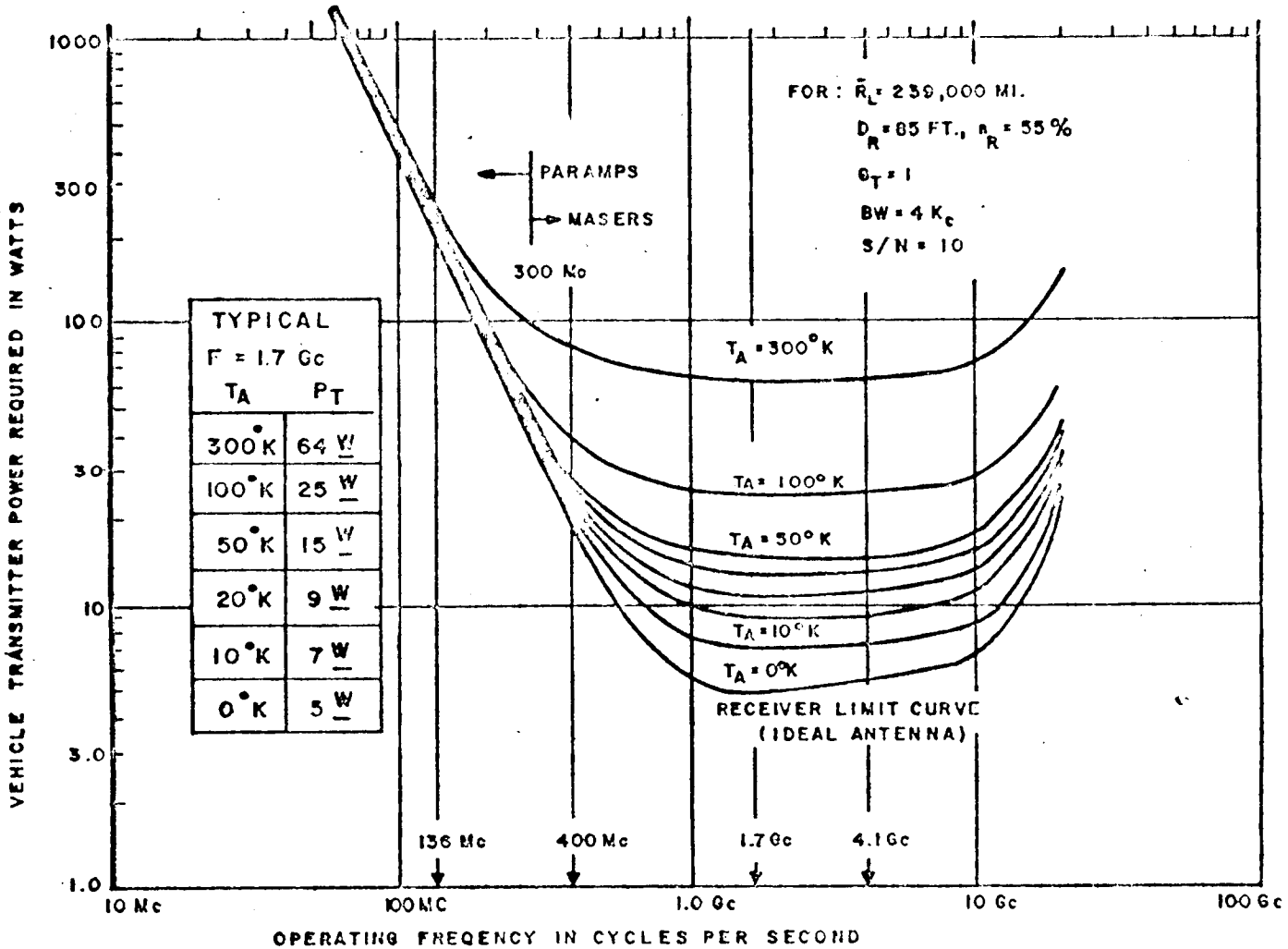

LUNAR RANGE SPACE VEHICLE TRANSMITTER POWER VS FREQUENCY OF OPERATION FOR VARIOUS LOW NOISE ANTENNA SYSTEMS

Figure 1-2.

transmitter power is to be kept at a reasonable level, i. e., in the order of ten watts or less, and if the information rate and signal-to-noise factors are to be maintained within the specified limits, a sensitive and therefore low noise antenna and receiver system must be employed. The conditions for this example are described in the figure and are believed reasonable design relations for a space mission of this type.

1.2 Objectives of the Study

The general objective of the study program is the investigation of techniques by which a reduction in the effective antenna noise temperature of passive paraboloidal reflector antennas may be achieved. Attainment of this objective is desired within the framework of the system performance requirements involving an optimization of the various relations including antenna gain, SNR, and other factors.

Three specific study objectives were considered quite important, and may be listed as follows:

1. Consolidation of information describing and establishing relations concerning the various physical factors involved which influence the noise temperature characteristics of passive paraboloidal reflector antennas.

2. An investigation of means and the determination of general design criteria by which the effective noise temperature of passive paraboloidal reflector systems of three general classes might be minimized or optimized with other antenna considerations; and derivation of evaluation methods by which the developmental designs may be analyzed.

3. Development and fabrication of antenna feed designs and antenna system configurations which demonstrate the developed design criteria and result in significant improvements in the low noise performance characteristics of existing or

future passive paraboloidal reflector antenna systems.

1.3 Antenna Noise Temperature Concept

The antenna noise temperature concept for describing antenna noise temperature or other components of circuit noise is based upon the equivalence in the radio frequency region of the received noise power density spectrum averaged over a specified bandwidth and the corresponding black body radiation temperature for a totally emissive source radiating an equivalent noise power density spectrum. The antenna noise temperature is actually an "effective" noise temperature related to an equivalent power density spectrum for a black body radiator which may replace the antenna system and will provide an equivalent power in the specified bandwidth. Since this characterization of noise power is fundamental to the low noise antenna field, it appears worthwhile to develop the "effective noise temperature" concept in sufficient detail to insure appreciation of its validity and limitations.

The effective noise temperature representation is based on the variation in radiation intensity per unit bandwidth for black body radiation in the Raleigh-Jeans approximation region of the Planck radiation law. The Planck radiation law expresses the intensity of radiation within an enclosure in thermodynamic equilibrium at a temperature T as a function of frequency, f, as:

$$I_f(T) = \frac{2hf^3}{c^2} \left[\exp\left(-\frac{hf}{KT} \right) - 1 \right]^{-1}$$

where c is the velocity of propagation, h is Planck's constant, and k is Boltzmann's constant. Since the peak region of the Planck radiation law occurs at wavelengths somewhat shorter than those generally encountered in the microwave region, it is possible to use the approximation for the long wavelength region in describing the

character of the radiation in the radio frequency range. This region may be approximated by setting

$$\frac{hf}{kT} << 1 \quad \text{for} \quad f << f_{peak}.$$

Using the expansion for the exponential term we have

$$I_f(T) = \frac{2hf^3}{c^2}\left(1 + \frac{hf}{kT} + \cdots - 1\right)^{-1}.$$

which simplifies to

$$I_f(T) = \frac{2kTf^2}{c^2} = \frac{2kT}{\lambda^2}$$

This is known as the Raleigh-Jeans approximation to the Planck radiation law. This expression indicates that the intensity of the radiation, and hence the power received per unit bandwidth is directly proportional to the temperature T. The direct relation existing in the Raleigh-Jeans region between intensity, or spectral power density, and temperature enables expression of received noise or signal energy in terms of an effective temperature instead of power density. The effective noise temperature may therefore be defined as a fictitious absolute temperature (usually in degrees Kelvin) such that the noise power per unit bandwidth, or spectral power density, for a given polarization is expressed as

$$S_n = k\,T_n$$

where k is Boltzmann's constant (1.38×10^{-23} joules/deg K),

The noise power density in a bandwidth B is

$$\mathcal{P}_n = k\,T_n\,B$$

which is the "available" power density of the noise power in watts per square meter, or similar units, and B is the bandwidth over which the noise power is measured. In the case of a generalized bandpass response, such as that of a following receiver,

the bandwidth may be defined as

$$B = \frac{1}{\left| H(f_o) \right|^2} \int_{-\infty}^{+\infty} \left| H(f) \right|^2 df$$

where H(f) is the frequency response function of the particular device and f_o is the frequency of maximum response. The noise bandwidth, B, may be considered equivalent to the bandwidth of a filter network of rectangular bandpass characteristics of height $H(f_o)$ and width B.

The total noise of a receiving system may be expressed as a system noise temperature, T_{SN}, which is simply the sum of the various effective noise temperature components as illustrated in Figure 1-3, i. e., of the system,

$$T_{SN} = \sum_{i=1}^{n} T_i$$

where T_1, T_2, $T_3 \ldots T_n$ might be the effective noise temperature contributions from the various external and internal noise sources. These noise sources may be regarded as the sum of the contributions from the following general areas:

a) Receiver internal noise contributions

b) Transmission line, feed or sub-reflector support, and mis-match losses

c) Antenna noise contributions.

The receiver noise and transmission line loss effects may be considered as internal noise sources; the antenna noise contributions are generally taken as externally generated contributions. Figure 1-4 illustrates the general manner in which the internal and external contributions influence an antenna system.

The effective antenna noise temperature is determined principally by the antenna power gain function and the corresponding environmental noise temperature distribution

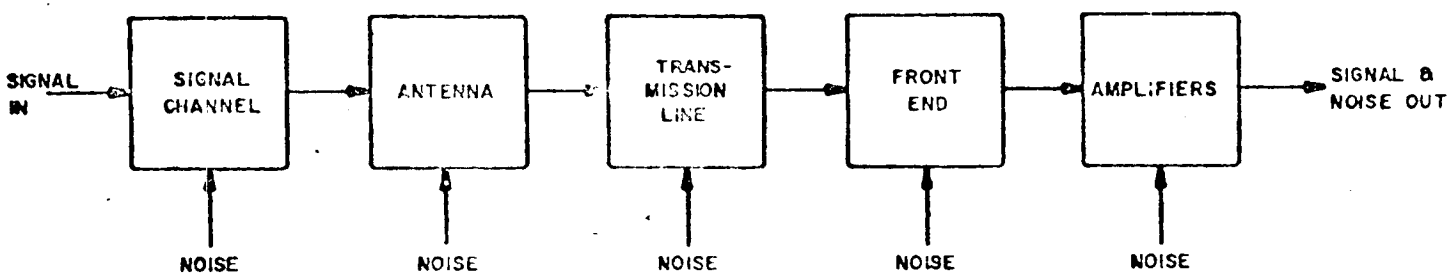

Block Diagram of Conventional Receiving System

Figure 1-3.

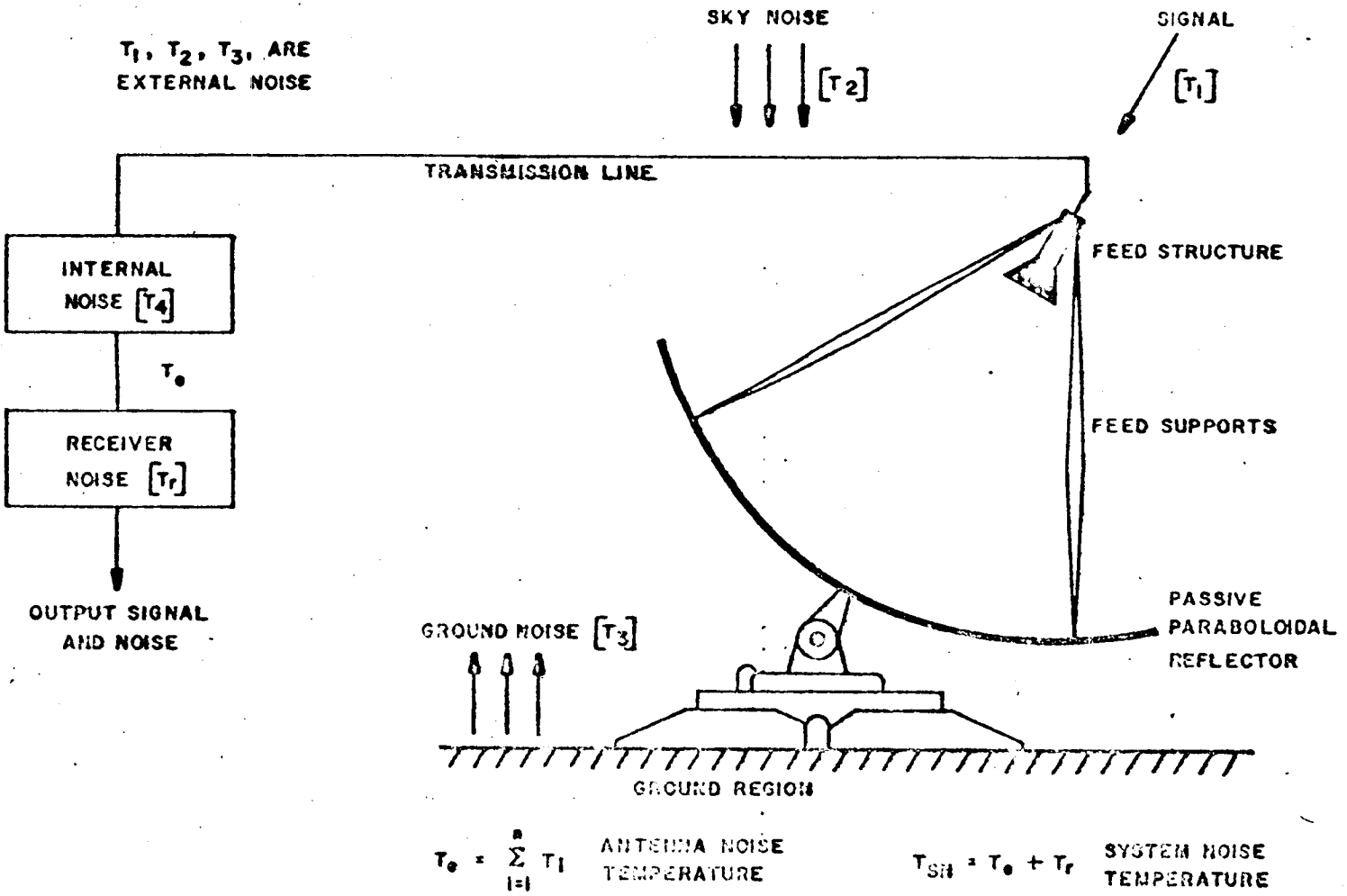

Figure 1-4. System Noise Sources and Contributing Mechanisms.

throughout all of space.

The nature of the antenna environmental noise characteristics must be analyzed, as well as the manner in which the antenna operates on the environmental effective temperature distribution.

The total antenna noise temperature may be determined by integrating the noise power spectral density expressed as a noise temperature over all space weighted by the corresponding antenna gain function over all space. This may be written

$$T_a = \frac{\int_0^{4\pi} T_s(\Omega)\, G(\Omega)\, d\Omega}{\int_0^{4\pi} G(\Omega)\, d\Omega}$$

which may be placed in conventional spherical coordinate form where $d\Omega$ is the solid angle given by $\sin\theta\, d\theta\, d\phi$, and $\int_0^{4\pi} G(\Omega)\, d\Omega = 4\pi$ steradians, assuming a radiation efficiency approaching unity. We therefore have for the effective antenna noise temperature determined essentially from appropriate gain "weightings" of the environmental noise temperature distribution at all angles in space:

$$T_a = \frac{1}{4\pi} \int_0^{\pi} \int_0^{2\pi} T_s(\theta, \phi)\, G(\theta, \phi) \sin\theta\, d\theta\, d\phi.$$

It is important to note that the function $T_s(\theta, \phi)$ represents the effective space temperature as a function of direction referenced to the antenna, and is often a quite complicated function involving many factors. Certain of these factors are not functions of spatial location only, but are dependent upon time, geographical location, weather conditions, position in galactic frame, and many other considerations.

1.4 Environmental Noise Distribution

The relations have been presented which specify the effective antenna noise temperature primarily as a function of the antenna far field power gain response

function and the corresponding environmental noise temperature distribution integrated over all space. This relation may be written as

$$\overline{T}_a = \frac{1}{4\pi} \int_0^{4\pi} G(\Omega)\, T(\Omega)\, d\Omega$$

which neglects heating and reflection losses in the system, generally a valid assumption.

The antenna gain function can generally be determined, hence it becomes necessary to determine the environmental noise temperature distribution in order to interpret the manner in which the various noise sources and contributing spatial regions influence the effective antenna noise temperature.

A reasonably complete analysis of the environmental noise factors was believed desirable and is presented in the Analysis section of this report in detail. A brief discussion of the general considerations relating to this phase of the investigation appears to be in order and is presented to assist in furnishing an overall view of the relations involved in this aspect of the study.

Three principal noise factors contribute to the antenna noise temperature which are characteristic of the antenna's operating environment. These three noise generating mechanisms are space related in that two constitute "sky noise" sources and the third refers to radiation from the ground, or "ground noise". These principal noise sources are:

1. Thermal radiation noise associated with the ground region.

2. Galactic radiation noise associated with the distribution of stellar sources and certain galactic "continuum" effects.

3. Atmospheric absorption losses and re-radiation noise due to the components of the atmosphere.

The thermal noise associated with the thermal radiation characteristics of the ground in the vicinity of the antenna system appears as a noise source extending over the half-space bounded by the sky region, and of an effective noise temperature essentially that of the ambient ground temperature. An effective value of about 300° Kelvin is often taken as a reasonable estimate for the noise temperature of the ground region. The actual noise temperature is actually somewhat less, since the ground region is not a perfect black body radiator but has an emissivity factor which in general differs appreciably from unity. Corrected values of about 240-250° Kelvin are probably more realistic on an average basis.

At microwave frequencies, reasonably high values of noise temperature are associated with the ground region relative to the noise temperature values of the sky region. This factor emphasizes the importance of improving the radiation characteristics of the antenna system in the ground region if the influence of the ground temperature distribution upon the effective antenna noise temperature is to be minimized.

Noise energy of galactic nature is primarily due to the various radiative mechanisms of stellar sources and is therefore unevenly distributed in space and is frequency dependent. The maximum intensity galactic radiation is, as expected, from the direction of the galactic center or nucleus. The minimum intensity of galactic noise is generally associated with the direction of the galactic pole. There are also a number of reasonably strong discreet source radiators, however, due to their relatively small angular extent in terms of most antenna systems, these strong sources will be neglected.

Atmospheric absorption and re-radiation is principally due to water vapor, oxygen and nitrogen pressure broadened molecular resonances occurring in the millimeter wavelength range. This effect is therefore directly proportional to atmospheric conditions, and the extent of the atmosphere through which the antenna beam must pass. Therefore, in general, the atmospheric absorption and re-radiation effects are maximum along the horizon corresponding to the longest path through the atmosphere. The frequencies of maximum loss or noise temperature degradation correspond to the wavelengths at which the pressure broadened molecular line resonances occur. Noise temperature degradation due to atmospheric absorption at frequencies less than one Gc are extremely small, and rise steadily to noise temperatures of 50-300° Kelvin at Zenith for the first line resonance, occurring for water vapor at about 25 Gc.

1.5 Low Noise Antenna Optimization Criteria

The development of optimum criteria for the design of low noise antennas may be considered as essentially a problem in obtaining the maximum signal-to-noise ratio (SNR) for the antenna system.

It has been indicated that various techniques which result in considerable improvement in antenna noise temperature are often quite undesirable and actually degrade the SNR capabilities of the antenna system. A typical example of one of these techniques is the under-illumination of an aperture. It is possible in this manner to obtain considerable improvements in the antenna noise temperature since a considerably larger fraction of the primary energy may be considered as contained within the secondary aperture extent. The disadvantage of this approach is a reduced aperture efficiency with resulting loss in gain. The decreased gain reduces the available signal power but generally does not influence the antenna noise power.

Hence, an immediate degradation of the antenna system SNR may occur if the improvement in antenna noise temperature does not at least match the loss in gain. The gain loss which occurs in a particular system is directly described by the ratio of the aperture efficiencies, before and after improvement of the antenna temperature. The noise temperature improvement, however, is a function of principally the feed characteristics, and to some extent the reflector characteristics. For example, an under-illuminated antenna may achieve a factor of two reduction in effective antenna noise temperature by means of a factor of four decrease in aperture efficiency. This antenna would be more desirable by a factor of two in its noise temperature characteristics than previously, but would be simultaneously less desirable in its overall performance characteristics expressed as a signal-to-noise ratio, again by a factor of two. This apparent inconsistency should stress the fact that antenna temperature in itself may have small significance in describing certain antenna systems; the resulting antenna system SNR is the important factor. For antenna systems of constant, and in particular reasonably high, aperture efficiencies, the defining factor becomes simply the antenna noise temperature.

An optimization procedure is therefore required involving gain improvement with corresponding high values of aperture efficiency and antenna system noise temperature improvement which is principally a function of the primary feed illumination and the environmental noise distribution.

An analysis of these considerations was believed to be important and necessary for effective design and evaluation of low noise antenna systems. The discussion of these considerations is presented and includes the relation between the principal factors involved in determining the optimization criteria. In particular, the significance of primary beam-shaping techniques is discussed as a means for obtaining both

high efficiency and minimal antenna noise contributions from the environmental noise distribution providing a means for maximizing the antenna system SNR.

1.6 Aperture Distribution Factors

It is possible to analyze various aperture distributions and to evaluate their characteristics in terms of aperture efficiency and equivalent antenna noise temperature for a typical temperature distribution. Analysis of a number of aperture distributions was accomplished using this principle, and the results are presented.

Since the antenna gain determines the intensity of the signal power received, high aperture efficiency appears desirable in order to maximize gain. However, if an attempt is made to attain high values of aperture efficiency by uniform illumination over an aperture, it is found that high levels of spillover generally occur because of the difficulty in realizing the sharp illumination taper required at the aperture edge. Rapid tapering of the energy distribution in the region of the aperture edge to a low value is necessary and requires a primary feed aperture sufficient to obtain the desired taper. Primary feeds must be limited in physical extent and therefore it infers that a compromise, or optimum, condition exists. The amount of feed blockage which may be accepted in the aperture region is an important factor in establishing the optimum feed system extent and hence the resulting aperture distribution.

A discussion of the various factors influencing the low noise characteristics and limitations of conventional aperture illuminations and the applicability and feasibility of certain optimal aperture illumination techniques is included in the report.

2.0 INVESTIGATIONS

A considerable amount of worthwhile information was obtained during the course of the study of theoretical, analytical and experimental nature. Information is presented which relates to the extent and distribution of environmental noise sources and the means by which they influence a general antenna system. Investigation of these relations and their dependence upon the various design parameters, such as frequency, antenna pointing direction, and other factors, forms an important basis for the ensuing discussion of low noise optimization techniques. The design criteria necessary for the improvement of low noise antenna feeds and antenna systems is a necessary prerequisite to the intelligent development and evaluation of low noise antenna systems. Of considerable practical importance and possibly the most beneficial investigations performed during the study relate to the development of several practical techniques by which a reduction in the noise temperature of passive paraboloidal reflectors may be attained. Experimental effort enlarging upon and verifying the analytical investigations resulted in a number of fabricated antenna feeds and antenna systems. These antennas and antenna feed systems demonstrated significant improvement in low noise antenna performance over that available by conventional means.

In order to place the investigations in the proper perspective, it appears worthwhile to discuss individually each of the principal investigative areas. As indicated previously, it is quite important that a reasonably thorough treatment be given the basic considerations determining the low noise performance of general antenna systems. Consolidation and analysis of this information is essential to providing the effective design criteria required for a sound approach to the low noise antenna design problem. For these reasons, a reasonably complete investigation of the

fundamental parameters influencing the effective antenna noise temperature and the basic relations governing related antenna performance were believed necessary.

Low noise antenna evaluation methods were also believed to deserve attention since the merit of a particular design or design approach is determined by its low noise performance characteristics, which generally are quite difficult or at times impossible to measure. Hence, a reasonable effort was believed desirable in developing analytical or graphical means by which existing antennas or antenna designs could be evaluated.

It is important to note the extent and limitations of the program. The antenna systems of interest are generically passive paraboloidal reflectors. This includes, fortunately, nearly all present antenna systems of proven low noise capability in the frequency range of interest to NASA, i. e., about 136 Mc to 4.1 Gc. The types of passive paraboloidal reflectors treated may be separated into the following general categories. First, the conventional focal point feed-reflector systems which is the antenna class to which most of the NASA large tracking antennas belong. Second, the Cassegrainian antenna systems which have met with considerable success in many low noise applications. Third is the sectoral horn-reflector, or "sugar scoop" antenna, which is essentially also a passive paraboloidal reflector surface coupled to a moderately flared sectoral horn feed system. A fourth antenna type is also included as a new system developed under the study program. This antenna class consists of a Cassegrainian adaptation of the sectoral horn-reflector system. This configuration, designated the KSK antenna, also utilizes a passive paraboloidal surface and appears to have significant advantages over the sectoral horn-reflector system.

The areas of investigative effort concerning passive paraboloidal reflector

antennas therefore reduce to the following:

1. Focal point feed-reflector antennas
2. Cassegrainian antennas
3. Sectoral horn-reflector antennas
4. Cassegrainian sectoral horn-reflector antennas.

The general plan of the investigation was to treat the first and second categories separately. A comparative evaluation was then planned including the known characteristics of the sectoral horn-reflector antenna with the results obtained from a fabricated developmental model of the Cassegrainian sectoral horn-reflector antenna. In this manner, all significant configurations of passive paraboloidal reflector systems would be included in the investigation.

The important factor determining the merit of a focal point feed-reflector antenna system is found to concern the energy distribution from the primary feed. This criteria is found of general importance if low noise antenna characteristics are to be combined with reasonable gain values for the antenna. For this reason, a rather detailed section of the investigation is devoted to shaped beam feed approaches.

The general features of the Cassegrainian configuration were found to be of value in themselves and were therefore treated in some detail. The shaped beam feed requirement for Cassegrainian systems was also believed important. To this end a somewhat unusual Cassegrainian antenna utilizing an ellipsoidal sub-reflector was investigated.

The Cassegrainian sectoral horn-reflector system was next investigated and compared with the sectoral horn-reflector system. An evaluation of the various low noise designs was considered worthwhile and is included.

The important areas of the investigation may be outlined in brief detail in order to present a general outline of the program effort.

2.1 Low-Noise Antenna Design Criteria

The various parameters involved in the effective design of an antenna system for low noise applications were analytically related and evaluated. Factors found to play an important part in the antenna temperature determination include two categories of noise sources. The first of these may be designated as external noise sources, and the second as internal noise sources. External sources include such factors as the galactic noise power density distribution, the atmospheric absorption losses and re-radiation noise and the ground thermal radiation noise. Internal losses occurring within the antenna which degrade the low noise performance of the antenna include factors such as transmission line losses, mismatch losses, reflector surface losses, surface error, and miscellaneous other items. Other important parameters essential to the design of low noise antenna systems include the average level of the minor-lobe radiation, the primary feed beam shape, the aperture efficiency, and other factors.

2.2 Evaluation and Performance Prediction Techniques

In order to analyze certain low noise feed systems which were developed during the program, a graphical technique was developed for evaluation of the antenna feed illumination. This technique also served as an aid in the prediction of antenna system noise temperature. The method involves essentially an integration of the measured pattern characteristics weighted by an estimated spatial temperature distribution which may be accomplished by means of a planimeter on a linear graphed pattern plot, or by the use of a digital computer programmed to accomplish in general the same integration. This technique has been of considerable assistance and has

proven quite successful in evlauating feed designs developed during the program. The evaluation results have been demonstrated to predict values in close agreement with those measured and calculated by others. Methods by which both primary and secondary patterns may be evaluated are presented.

2.3 Shaped Beam Feed Approaches

A dielectric lens feed employing a half-pillbox horn fed by a broad beam waveguide was designed and tested during the program. Measured patterns for this feed are presented along with a discussion of its features and difficulties.

A feed design which appeared early in the study to warrant investigation and subsequently developed into a very satisfactory low noise feed system involves the surface wave field energy "trapping" principle. It was basically desired to broaden the beamwidth of a primary illumination by the use of either dielectric or metallic plates in the shape of possibly a cone fed by a conventional dipole or waveguide horn. It was felt that if effective trapping of the electromagnetic energy along the surfaces of the surface wave structure could be maintained, a triple lobed primary pattern instead of a single lobed pattern could be achieved. This pattern offers a good approximation to the uniform illumination primary pattern desired across the secondary aperture. It would have the additional advantage of a reasonably rapid taper of the energy distribution in the region of the aperture edge. Minor difficulties were encountered concerning the response of the surface wave structures to small variations in certain parameters such as illumination horn protrusion depth, surface wave structure included angle, and length of the surface wave structure. The principal difficulty inherent in the surface wave feed structure appears to concern the difference in energy trapping efficiency of a given surface wave device to the polarization of the incident wave. Investigation of this effect and experimental

results are presented including a low noise feed design, designated the fluted feed, which overcomes this problem in a novel but very successful manner.

2.4 Cassegrainian System Considerations

Cassegrainian antenna systems have found increased application as low noise antennas due primarily to their favorable spillover placement characteristics. A large variety of Cassegrainian configurations are possible; however, the surface pair conventionally employed is the hyperboloidal sub-reflector imaging the focal point of the paraboloidal surface to a point near the center region of the paraboloidal surface. In addition to placing the spillover portion of the antenna radiation pattern in the relatively "cool" sky region in place of the relatively "hot" ground region, there are certain other inherent advantages to the Cassegrainian configuration. Modern low noise receivers such as maser systems are often quite complex requiring considerable cooling, stable "pump" source power, and various other services. There is a definite advantage in placing this equipment in the vicinity of the secondary surface of the Cassegrainian antenna, instead of at the focal point of the paraboloidal surface. A discussion of typical improvements brought about by means of the Cassegrainian antenna and other areas of difficulty principally relating to illumination problems are discussed.

2.5 Cassegrainian Ellipsoidal Sub-Reflector

An unusual configuration of the Cassegrainian system employing an ellipsoidal sub-reflector in place of the conventional hyperboloidal sub-reflector appears to offer certain advantages in the low noise application. A brief analysis of the advantages and difficulties associated with this configuration are presented. Experimental work which was done in this area illustrates the principal features and describes certain desirable aspects of this technique.

2.6 Cassegrainian Sectoral Horn-Reflector Antenna

A quite interesting and practical adaptation of the sectoral horn-reflector system employing a Cassegrainian approach has been investigated. This antenna system appears from experimental measurements to have extremely desirable low noise characteristics coupled with a very compact and practical mechanical configuration. This completely new paraboloidal reflector system appears capable of replacing the large sectoral horn-reflector antenna systems of the type used by BTL in the Telstar communication satellite program. A model of this unit has been fabricated and experimentally measured. The design has been experimentally verified from the model. The antenna appears to have essentially the desirable characteristics of the low noise BTL antenna system which is generally considered the present state-of-the-art. The Cassegrainian adaptation of the sectoral horn-reflector unit, designated the KSK horn, avoids the mechanical difficulties and drawbacks of the extreme size involved in the BTL antenna. The KSK horn actually appears to have more desirable characteristics than the existing BTL system due to the reduction in the existing diffraction lobe of approximately 30 db associated with the ring gear on the large BTL sectoral horns. The apparent practicality of operation of the KSK horn without a large radome avoids significant losses associated with operation in this manner. The use of the Cassegrainian approach in the sectoral horn design drastically reduces the horn in size. It is possible to achieve a configuration in which the maximum dimensions of this antenna closely approximate the radiating aperture dimensions. It appears that the compact KSK horn structure provides a significant improvement in practical low noise antenna design and may produce an antenna system establishing a new operational state-of-the-art whose cost may closely approximate that of the present 85 foot reflectors for equivalent gain and low noise performance.

2.7 Evaluation of Low Noise Antenna Designs

During the study, a number of methods and criteria by which low noise antennas and antenna feeds may be evaluated were developed. These criteria and evaluation techniques form an important basis for low noise antenna selection and operation. An evaluation is performed of the relative merits and measured performance figures for various low noise antennas.

III ANALYSIS

3.0 Analysis

3.1 Low Noise Design Criteria

A significant amount of general background information concerning the behavior of the various parameters influencing the design of low noise antenna systems and corresponding analytical results relating to the necessary criteria required for the effective design of low noise feeds and antennas was considered essential to the study.

A reasonably valid estimate of the environmental noise considerations was particularly desired due to the great importance of the spatial noise distribution in determining the effective antenna noise temperature. Several other factors were found to be of considerable importance in the establishment of a well-defined set of design criteria. Certain of these factors are closely related to the particular requirements of the NASA large paraboloidal reflector tracking systems; however, the general features of the analysis are believed to have wide application. Examples of the areas in which a reasonably thorough analysis was believed essential include aperture illumination considerations, gain optimization, monopulse operation, multiband operation, primary feed design, and polarization considerations.

It is often convenient to represent the total antenna noise temperature as a summation of several average components, each relating to a particular spatial region or class of noise source. In this form we may express the effective antenna noise temperature as

$$\bar{T}_a = \alpha_1 \bar{T}_{sky} + \alpha_2 \bar{T}_{gnd} + \sum_{n=3}^{n} \alpha_n \bar{T}_n$$

where

$$\sum_{n=1}^{n} \alpha_n = 1.$$

The α's represent fractions of the antenna power or radiation pattern extent integrated over the spatial, or other, region of interest. These fractional relations are determined from the fundamental relation governing the magnitude of an effective antenna noise temperature contribution from any region of space which may be written as

$$\bar{T}_n = \frac{1}{\Omega_n} \int_{\Omega_1}^{\Omega_2} G(\Omega)\, T(\Omega)\, d\Omega.$$

The $\bar{T}_n$'s shown in the series expression represent noise sources of other than the conventional ground and sky noise contributions. These $\bar{T}_n$'s may be used to indicate ohmic losses in a transmission line, feed and reflector surface losses, feed support losses, antenna side lobes pointing at the sun or other discrete galactic noise sources.

In general, the environmental noise considerations warrant the principal effort. The non-environmental noise sources are often important but a reasonably simple evaluation of these contributions can generally be made which can frequently be verified experimentally. However, the environmental noise distribution and behavior is quite complex but important to proper evaluation of the antenna and to development of optimum design criteria.

3.1.1 Environmental Noise Temperature Distribution

The environmental distribution of noise power is a predominant factor influencing the effective antenna noise temperature. The relation which defines the effective antenna temperature may be written as

$$\bar{T}_a = \frac{1}{4\pi} \int_{o(v)}^{4\pi} G(\Omega)\, T(\Omega)\, d\Omega$$

where $G(\Omega)$ is the antenna power gain function which is integrated over the angular extent of all of space with the corresponding environmental noise temperature distribution, $T(\Omega)$.

Environmental noise may be broadly separated into three components: ground radiation noise, galactic emission noise, and atmospheric absorption and re-radiation noise. Ground noise is of thermal character and is due to the emissive nature of the ground region at the ambient level. A value of 300° Kelvin is often used for the effective nose temperature of the ground region; however, this value assumes perfect black body radiation which is certainly not the case. An assumed emissivity for the ground region of about 0.8 to 0.9 appears reasonable and results in a corrected average effective noise temperature for the ground region of about 240° to 270° Kelvin. A value of 250° Kelvin appears to be a reasonable estimate and may generally be considered as an isothermal component for the spatial region defined by the ground half-space bound by the sky region.

The sky noise sources of galactic and atmospheric origin are additional noise contributions of importance. Galactic noise is principally due to the power density spectrum received from extensive and rather diffused stellar sources. The radiation mechanism for these stellar bodies has a characteristic in opposition to the conventional black body radiation, resulting in very large effective noise temperature values at low frequencies and vanishing values of noise temperature in the microwave region. Figure 3-1 illustrates a plot by Kraus and Ko[1] of the maximum and minimum galactic sky temperature as a function of frequency, prepared from various observed

---

1. J. D. Kraus and H. C. Ko, "Celestial Radio Radiations", Technical Note TN-57-537: AFCRC Contr. No. AF 19 (604(-1591, Ohio State Univ. Research Foundation, Columbus, Ohio (Dec. 1958)).

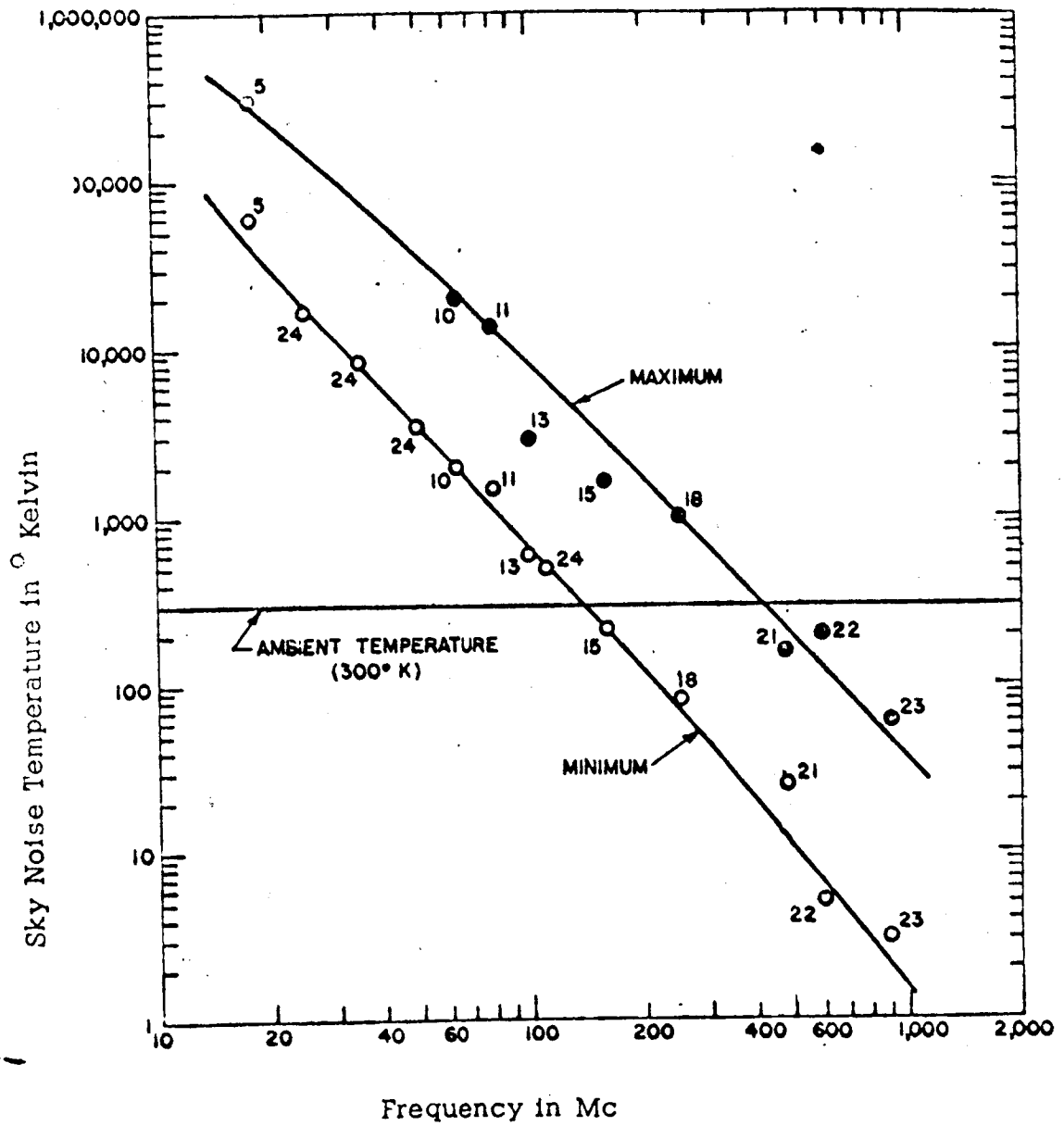

Sky Noise Temperature of Galactic Origin
As A Function of Frequency.

Figure 3-1.

data. The numbered points refer to various investigators and their reported observations.

The atmospheric noise is principally due to the absorption and re-radiation characteristics caused by the broadened molecular resonances of water vapor, oxygen, and nitrogen in the atmosphere. Accurate information has been obtained for this noise source, experimentally by Crawford, Hogg, Mumford[2,3] and other which are in-close agreement with theoretical values obtained by Van Vleck[4] which indicate that a reasonably well defined physical model for this noise contribution mechanism exists.

We have essentially determined the characteristics of the ground region by stipulating it to be of thermal nature and approximately an extended black-body radiator at about 250°K. The sky noise principal mechanisms have also been briefly discussed. It now remains to obtain reasonably accurate estimate for the behavior of the sky noise contributors to the environmental noise. To obtain realistic values for the effective noise temperature of the sky as seen by a passive directional antenna, several assumptions must be initially made. The principal assumptions may be briefly stated as follows:

1. The measurements will be corrected to obtain an "ideal" receiving antenna of infinitesimally narrow beamwidth and zero minor-lobe level.

---

2. A. B. Crawford and D. C. Hogg, Bur. Standards Tech. Journal, Vol. 35, July 1956 pp. 907.

3. D. C. Hogg and W. W. Mumford, "The Effective Noise Temperature of the Sky", Microwave Journal, Vol. 3, March 1960, pp. 80-84.

4. J. H. Van Vleck, Phys. Rev., Vol. 71, 1947, pp. 413 - 427.

2. Certain choices of antenna direction measured from the zenith will be selected; the values tentatively selected are for a minimum value of 0^{o}, at zenith; a maximum value of 90^{o} at the horizon and an intermediate value of 80^{o}, at 10^{o} above the horizon. A restricted number of antenna pointing directions is desirable to avoid unnecessary complexity in the plots of the several variables involved. The particular values chosen were selected primarily from the atmospheric noise considerations.

3. Certain choices of galactic enter or galactic "nucleus" orientation will be selected; the values tentatively selected are for a value of 0^{o}, at Zenith, and for 90^{o}, at the horizon. This restriction enables demonstration of the dependence of the galactic center on the effective antenna noise at selected antenna pointing orientations.

4. The noise temperature plots obtained will be taken as average plots for the conditions described and some variation about the plotted values is to be expected. Causes for the variation are many; a partial listing of some of the more significant influences includes the following factors. First, for those primarily influencing the galactic contributions, we have the following:

a) Van Allen radiation belt influences

b) Solar bursts and storms

c) Lunar intercept effects

d) Effects of ionized regions, Aurorae

e) Planetary source contributions

f) High intensity stellar sources

g) Noctilucent "cloud" obstruction.

And for those primarily influencing the atmospheric contributions, we have the following:

h) Variation in atmospheric water vapor content with latitude, nature of surface region, season

i) Atmospheric changes due to diurnal solar heating.

j) Atmospheric refractive effects.

k) Atmospheric turbulence.

l) Ionization discharges occurring in the atmosphere.

m) Particle precipitation in the lower atmosphere.

The various factors which influence the noise background presented by a directional receiving antenna may be categorized as follows:

1. The sky noise associated with the galactic noise sources, atmospheric effects, lightning activity and similar contributions in the main beams of the antenna system.

2. The ground radiation due to the "black body" radiation emitted from the earth's surface which intercepts part of the antenna radiation pattern.

3. Various other noise contributions due to the inclusion in the antenna pattern of sky noise sources out of the main beam, absorption material in the sky or on the ground, and various other contributors. If we set $\alpha_1, \alpha_2, \ldots\ldots \alpha_n$ as the multipliers associated with the main beam and side and back lobes of the antenna system, we obtain after Hogg and Mumford[1] a simple expression for the total effective

---

1. D. C. Hogg and W.W. Mumford, "The Effective Noise Temperature of the Sky", Microwave Journal, Vol. 3, March 1960, pp. 80-84.

antenna noise temperature for the antenna of:

$$\bar{T}_{ant} = \alpha_1 \bar{T}_{sky} + \alpha_2 \bar{T}_{gnd} + \sum_{n=3}^{N} \alpha_n \bar{T}_n ,$$

However, each of the α's and each of the $\bar{T}$'s represents either an antenna radiation response distribution or a noise distribution; therefore, for a solution to be obtained the entire expression must be integrated over the spatial and temperature distributions of interest. The effective noise temperature of an arbitrary noise temperature distribution included in the solid angle of an antenna which has a gain function of $G(\Omega)$ is given by

$$\bar{T} = \frac{\int_0^{4\pi} \bar{T}(\Omega)\, G(\Omega)\, d\Omega}{\int_0^{4\pi} G(\Omega)\, d\Omega}$$

where we assume that the gain over all of space

$$\int_0^{4\pi} G(\Omega)\, d\Omega = 4\pi.$$

Hence, we obtain

$$\bar{T} = \sum_{n=1}^{N} \frac{1}{4\pi} \int_0^{4\pi} \alpha_n \bar{T}_n(\Omega)\, G_n(\Omega)\, d\Omega$$

for the series of terms.

If we consider an idealized antenna pattern in which the minor-lobe energy is zero, the first appear to drop out of the expression. Therefore the effective noise temperature for an idealized antenna may be written as

$$\bar{T}_{ant} = \frac{1}{4\pi} \int_0^{4\pi} \alpha_1 \bar{T}_{sky}(\Omega)\, G_1(\Omega)\, d\Omega$$

which is seen to be simply the noise contribution from the sky region such as galactic noise and atmospheric absorption. For this reason, it is apparent that the minimal noise temperature attainable from an ideal antenna system will be the sky noise. Therefore, an accurate measure of the sky noise for various antenna orientations, locations of the galactic plane, and as a function of frequency, is worthwhile. In addition to establishing the value of the minimum attainable noise temperature, it also establishes the range of variation for the noise temperature under given restrictions.

Brown and Hazard [1] have analyzed observed data for the noise contribution from galactic sources and have proposed a model of the galaxy which represents in reasonably close agreement the essential aspects of the observed data. The model separates the "galactic" noise into the following three components:

1) Localized sources within the galaxy.

2) Ionized interstellar gas.

3) An isotropic component which may be of extra-galactic origin.

Corrections of the observed data have been made by Brown and Hazard to idealize the temperature distribution by constraining the receiving antenna beamwidth to an infintesimal angle. The noise temperature distribution with frequency is then obtained for the case in which the antenna beam is pointed into the galactic plane, or the galactic "nucleus". The isotropic noise component is tabulated neglecting the absorption characteristics of certain atmospheric gases and vapors. These two cases give the maximum and minimum noise distributions and are found to be in good agreement with Jansky's observations [2] and with other more recent

---

1. R. H. Brown and C. Hazard, "A Model of The Radio-Frequency Radiation From the Galaxy", Phil. Mag., Ser 7, Vol. 44, Sept. 1953; pp. 939-963.

2. K. G. Jansky, Proc. IRE., Vol. 25, December, 1957; p. 1517.

observations. Referring to Figures 3-2 and 3-3 , we utilize these two values as the average maximum and minimum values for the noise temperature as a function of frequency. Two additional values are employed, a noise distribution with frequency for the antenna pointed 10° off from the galactic plane and another orientation 80° off from the galactic plane.

The calculations from the Brown and Hazard model are quite good for the low frequency region, i. e. from about 10 Mc to 1 Gc. In the region of 1 Gc the galactic contributions become quite small and the noise contributions due to oxygen and water vapor absorption in the atmosphere become more significant.

Many factors influence the absorption of radio waves by the atmosphere including the temperature, pressure and oxygen and water vapor content of the atmosphere. Expressions for the absorption of radio frequency energy by the oxygen and water vapor constituents have been worked out by Van Vleck [1] which are in close agreement with the experimentally measured data of Crawford and Hogg [2], and others. The pronounced peaking shown in Figures 3-2 and 3-3 in the 25 Gc region is caused by a broadened strong absorption line of atmospheric water vapor. In addition to this K-band absorption region centered at 1.35 cm, there is some background absorption due to the tails of strong water vapor absorption lines occurring in the far infra-red.

The absorption effects due to oxygen are principally form a strong set of absorption lines occurring in the 50-75 Gc (4-6mm) range. The broadened skirts or tails of these lines influence to a degree the absorption values at lower

---

1. J. H. Van Vleck, Phys. Rev., Vol. 71, 1947, pp. 413 - 427.

2. A. B. Crawford and D. C. Hogg, Bur. Standards Tech. Journal, Vol. 35, July 1956, pp. 907.

Figure 3-2. Effective Idealized Antenna Noise Temperature As A Function of Frequency ($\phi_G = 0^0$).

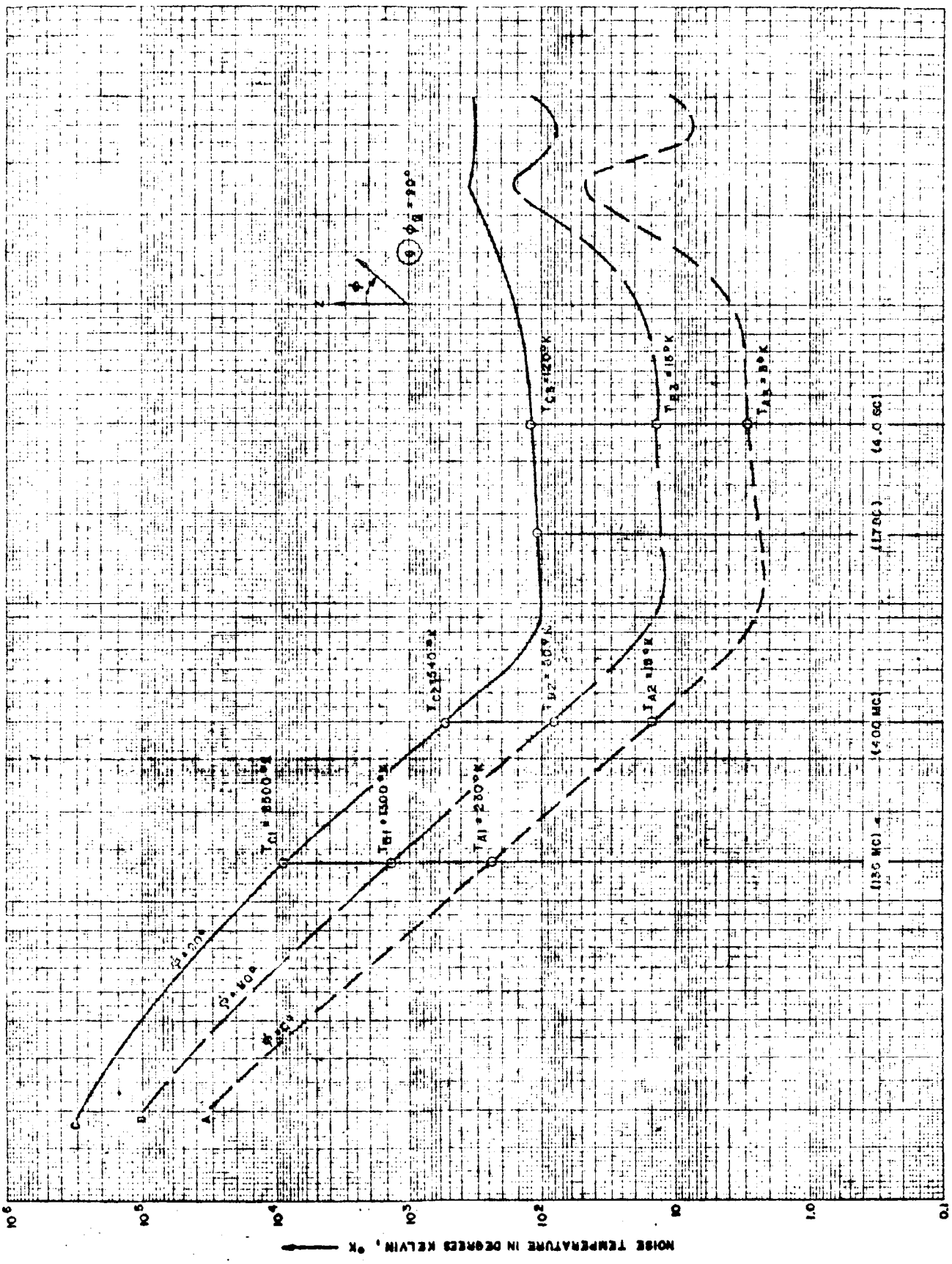

Figure 3-3. Effective Idealized Antenna Noise Temperature As A Function of Frequency ($\phi_G = 90^\circ$).

frequencies. Figures 3-2 and 3-3 include the minor influences due to oxygen absorption but principally show the galactic noise and water vapor absorption effects since the plots are terminated at about 50 Gc, well above our region of operation.

Referring to Figure 3-2, we have a plot of the average noise temperature with frequency for three antenna orientations. In this set of plots the galactic center is assumed to be at zenith ($\phi_A = 0^o$). Taking first the antenna orientation for the antenna pointing at zenith ($\phi_A = 0^o$) shown in Plot A, we find that at low frequencies the effective noise temperature of the antenna indicating the galactic noise contributions, is quite high. This is as expected since the antenna is pointed into the galactic center. However, for this zenith antenna orientation, the effective antenna temperature at high frequencies, especially at about 3-10 Gc, is quite low (about 3-4°K). This is because the galactic contributions in this range become very small and the zenith orientation of the antenna "looks" through a minimum of atmosphere allowing the noise contributions from atmospheric absorption also to remain small. Next considering the antenna orientation along the horizon shown in plot C, we find that the galactic contributions at low frequencies are at a minimum, as would be expected. At the higher frequencies, the increased length of the antenna beam path through the atmosphere causes an appreciable increase in the antenna noise due to atmospheric absorption effects. The 3-10 Gc region for this plot is at an effective noise temperature of about 110-160°K and the minimum noise region has been lowered in frequency to the 300-500 Mc range, and now has a value of about 35-40° K.

For the third antenna orientation shown in plot B, which is ten degrees above the horizon ($\phi_A = 80^o$), we find that at low frequencies the galactic contributions

are very nearly those of the antenna pointed at the horizon, i.e., the minimum galactic noise condition. At higher frequencies, the ten degree elevation angle assists in reducing considerably the atmospheric noise contributions. The plot for this antenna orientation reaches a minimum noise temperature of about 10°K in the 600-800 Mc region. The plot remains reasonably flat throughout the high frequency range to about 10 Gc (T = 20°K), at which point it begins to rise due to water vapor and oxygen absorption in the atmosphere.

Figure 3-3 is a plot similar to the previous plot except that the galactic center is now oriented at the horizon. For the antenna orientation set to zenith, $\beta_A = 0°$, represented by plot A, we find that the galactic noise contributions at low frequency are at a minimum, and since the atmospheric noise contributions are also at a minimum for this pointing direction, the high frequency region is at minimum noise. For this somewhat optimal condition, the plot reaches a minimum effective noise temperature at 1 Gc of about 2°K and remains quite flat over a wide range attaining a value of 4°K at 10 Gc and then rising to a maximum of about 46°K at 25 Gc. It is interesting to note that an effective noise temperature of less than 1 db (75.5°K) is maintained from about 200 Mc to over 50 Gc. An effective noise temperature of less than 0.5 db (34.8°K) is maintained from about 300 Mc to 20 Gc; less than 0.25 db (17.4°K) is maintained from about 400 Mc to 14 Gc; and a noise factor of less than 0.1 db (5.8°K) is maintained over a range from 600 Mc to 12 Gc. These values for noise temperature in terms of decibels are obtained from the relation

$$T_e = (\overline{NF} - 1)\, T_o$$

or

$$\overline{NF} = 1 + \frac{T_e}{T_o}$$

$\phi_G = 0^\circ$ Antenna Orientation	Effective Noise Temperature, °K					Frequency or Bandwidth, Gc				
	136 Mc	400 Mc	1.7 Gc	4.0 Gc	T_{min}	$f(T_{min})$	$f_L(BW)$	$f_H(BW)$	BW	f_{mean}
(A) $\phi_A = 0^\circ$	8500°K	540°K	18°K	3°K	2.6°K	6.0 Gc	2.4 Gc	12 Gc	9.6 Gc	5.4 Gc
(B) $\phi_A = 80^\circ$	280°K	19°K	13°K	15°K	9.5°K	0.68 Gc	0.40 Gc	10 Gc	9.6 Gc	2.0 Gc
(C) $\phi_A = 90^\circ$	230°K	34°K	100°K	120°K	33°K	0.38 Gc	0.25 Gc	0.70 Gc	0.45 Gc	0.31 Gc

TABLE III - 1

Antenna noise characteristics at various antenna orientations for galactic center oriented at Zenith.

$\phi_G = 90^\circ$ Antenna Orientation	Effective Noise Temperature, °K					Frequency or Bandwidth, Gc				
	136 Mc	400 Mc	1.7 Gc	4.0 Gc	T_{min}	$f(T_{min})$	$f_L(BW)$	$f_H(BW)$	BW	f_{mean}
(A) $\phi_A = 0^\circ$	230°K	15°K	2.3°K	3°K	2.2°K	1.2 Gc	0.65 Gc	11 Gc	10.4 Gc	2.7 Gc
(B) $\phi_A = 80^\circ$	1300°K	300°K	13°K	15°K	12°K	1.3 Gc	0.65 Gc	11 Gc	10.4 Gc	2.7 Gc
(C) $\phi_A = 90^\circ$	8500°K	540°K	110°K	120°K	95°K	1.0 Gc	0.60 Gc	13 Gc	12.4 Gc	2.8 Gc

TABLE III - 2

Antenna noise characteristics at various antenna orientations for galactic center oriented on horizon.

and in decibels

$$\overline{NF}\ (db) = 10 \log_{10} \left(1 + \frac{T_e}{T_o}\right),$$

where T_o is taken as equal to 290°K.

Referring again to Figure 3-3 and considering now the antenna orientation pointed at the horizon $\phi_A = 90°$, shown as plot C, which is directed into the galactic center, we find as expected a maximum galactic noise distribution at the lower frequencies. At the higher frequencies, the atmospheric noise contributions are also at a maximum due to the low angle of the antenna to the horizon. The intermediate antenna orientation of ten degrees above the horizon, shown as plot B, is seen to avoid a considerable amount of the galactic noise contribution at low frequencies and attains a moderately low noise temperature of about 10-20°K in the high frequency region of from 700 Mc to 10 Gc.

Tables III-1 and III-2 summarize the results of the effective antenna noise temperature characteristics from the plots of Figures 3-2 and 3-3 . The frequencies selected are those desired for use with the 85 foot diameter paraboloidal antenna operating for NASA at Fairbanks, Alaska. Since the frequencies of 4.080 Gc and 4.170 Gc are quite close to 4 Gc, the latter frequency is used in place of the former two. The noise frequency bandwidth appearing in the tables is defined here as the frequency range over which no greater than a doubling of the minimum effective antenna noise temperature occurs. The designation T_{min} is the minimum noise temperature for a particular set of conditions, and $f(t_{min})$ is the frequency at which that lowest effective noise temperature occurs. In the bandwidth calculation f_L and f_H are the low frequency and high frequency values corresponding to the end points of the noise frequency bandwidth (the 2 T_{min} points). The bandwidth is therefore simply,

$$BW = f_H - f_L$$

of the best data for this phenomena but unfortunately include both summer and winter measurements. The plots have been corrected in the higher frequency regions to give better agreement with winter conditions. However, since it appears that the available experimental data is possibly not all that might be desired, the plots may need some further tailoring to the conditions found in the region of a particular antenna facility, but in any case appear to be realistic estimates.

Relating the plots of Figures 3-2 and 3-3 , and Tables III-1 and III-2 to the probable operating characteristics of the NASA 85 foot paraboloidal antennas now appears in order. It should be realized that the information presented in the plots if for an idealized antenna configuration considering only an infinite simally narrow main beam and assuming zero minor-lobe contributions.

A plot summarizing the determined environmental noise temperature characteristics is presented in Figure 3-4 and illustrates the typical and extreme characteristics of the environmental noise temperature as a function of frequency.

The effective noise temperature variation due to finite but limited antenna beamwidths is quite small, especially for the reasonably narrow antenna beamwidths available with the NASA 85 foot paraboloids. Since the idealized effective noise temperature generally has a slow variation with antenna "look" angle, the effective noise temperature from the main beam due to integration of the sky temperature distribution over a solid angle of coverage determined by the finite beamwidth will be in most cases practically the same value as the idealized values shown in the plot. The two conditions for which somewhat greater variation may occur are first, for the antenna pointed into the region of the galactic center and second, for the antenna pointed toward the horizon. For the first condition, the broadened antenna beam integrates a temperature distribution which includes sources of somewhat lower values

and the mean frequency is conventionally

$$f_{mean} = (f_H f_L)^{\frac{1}{2}}$$

The values for effective antenna noise temperature presented in the plots of Figures 3-2 and 3-3 , and in Tables III-1 and III-2 are believed reasonably accurate for the conditions specified. Actual measured values in both the galactic and atmospheric regions may show some variations due to certain factors mentioned previously. In general, this effective noise temperature variation may be somewhat greater and of a more irregular function of the antenna orientation for lower frequencies corresponding to the galactic region than to the analogous frequencies in the atmospheric region. The idealized antenna noise variation at the microwave frequencies will be largely determined by the "look" angle of the antenna into the atmosphere and will be influenced only to a slight degree by the location of the galactic center.

It is apparent from the plots of Figure 3-3 that by orienting the antenna ten degrees above the horizon, an appreciable decrease in the effective noise temperature due to atmospheric absorption is obtained. It appears from simple trigonometric relations, that for antenna pointing angles measured from the zenith of about 60° or less, the noise contribution from atmospheric absorption will be no more than about twice the value of the minimum antenna noise temperature attained for the antenna pointed directly at zenith. The variation of the effective noise temperature in the region of primarily atmospheric absorption effects as a function of antenna "look" angle can be seen to be an easily tabulated and reasonably stable parameter.

The water vapor and oxygen absorption of the atmosphere, as shown in Figures 3-2 and 3-3 may be somewhat high for certain areas. These plots are a combination

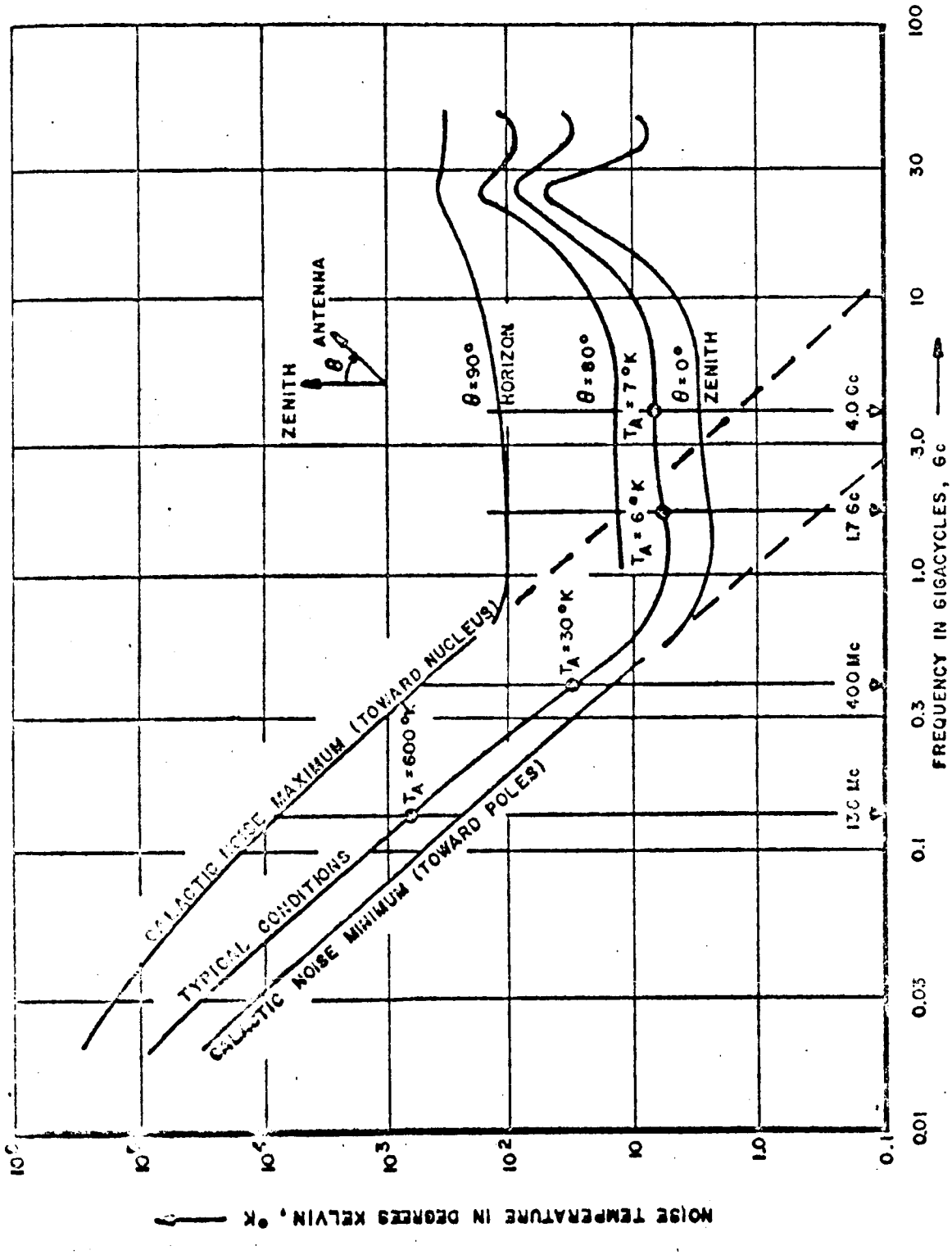

Figure 3-4. Summary Plot of Environmental Noise Temperature Characteristics.

than the maximum temperature obtained from the galactic center. The second condition for which the NASA 85 foot antenna characteristics may vary somewhat from those shown on the plots is for the case of directing the antenna toward the horizon. For this condition a finite beam width places a portion of the antenna pattern in the ground, thereby allowing terrestial noise contributions to increase the effective antenna noise temperature. The degree of this effect will be dependent upon the temperature and r-f reflectance characteristics of the terrain in the region and the portion of the antenna radiation pattern which intersects the earth. Directing the antenna a few degrees above the horizon would possibly avoid all but relatively small minor-lobe contributions from terrestial noise. The ground contribution in this case would displace the entire plot by the increased effective noise temperature due to the ground contribution. For the conditions specified, this increased noise contribution, for an estimated three percent of the antenna pattern intersecting the earth, would be about eight or nine degrees Kelvin.

The other important factor which should be considered is the influence of the minor-lobe and feed spillover energy on the effective noise temperature. These effects are naturally excluded from the plots. Evaluation of the degree of their influence is difficult [illegible] of both antenna orientation, frequency of operation, and antenna feed-reflector design. However, certain assumptions can be made which enable reasonable estimates to be made for their effects. We can determine from the form of the feed pattern and the aperture distribution the fraction of the radiation pattern which appears as spillover and other minor-lobe energy. From these considerations and a knowledge of the temperature distribution, the "excess" noise temperature of these minor-lobe contributions can be determined. For instance, a typical antenna system having a cosine squared aperture

distribution such as the NASA large paraboloidal antennas may have a combined spillover and minor-lobe content of approximately 10^{-15} percent. The corresponding value of effective antenna noise temperature due to spillover and minor-lobes would then be this fraction times the ground noise temperature, or about 25 - 38°K. This value may easily be as high as 30 - 50°K and it may range at certain antenna positions to less than 15°K. However, values of approximately 30°K appear reasonable for the contribution to the effective antenna noise temperature for the NASA 85 foot paraboloidal reflectors.

Figure 3-5 illustrates noise temperature profile plots indicating the behavior of the environmental noise at the particular NASA frequency ranges of interest. These plots essentially represent elevation plane cuts through the antenna location and are arranged to include the regions of maximal noise temperature variation. A space weighted mean of the noise temperature is presented for the ground region and separately for the sky region at each of the frequency ranges. Also shown on the profile plots is the typical variation in effective environmental noise temperature as a function of antenna pointing angle. The galactic center contributions shown in the 136 Mc and 400 Mc noise profiles are shown displaced from the Zenith to indicate the fact that these maxima are not related to the antenna coordinate system.

A significant noise factor which influences considerably at particular times the effective antenna noise temperature is the solar radiation energy which may be intercepted or reflected into a minor-lobe. This effect is not considered of great overall importance, however, large antenna noise degradation may occur for reasonably extended periods due to this factor. Figures 3-6 and 3-7 illustrate the variation in power flux density per unit bandwidth for various temperatures

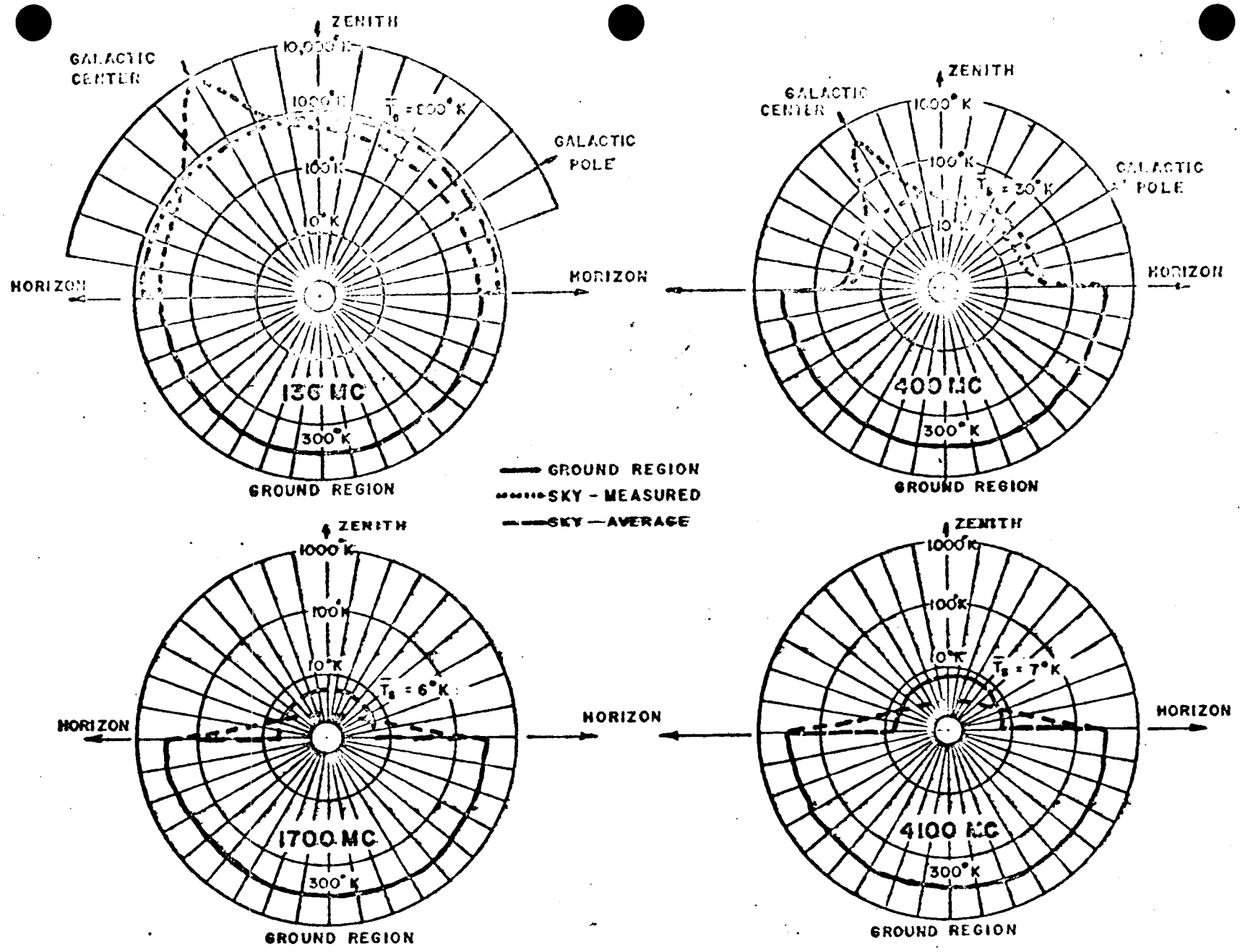

NOISE TEMPERATURE PROFILES FOR SELECTED FREQUENCIES

Figure 3-5.

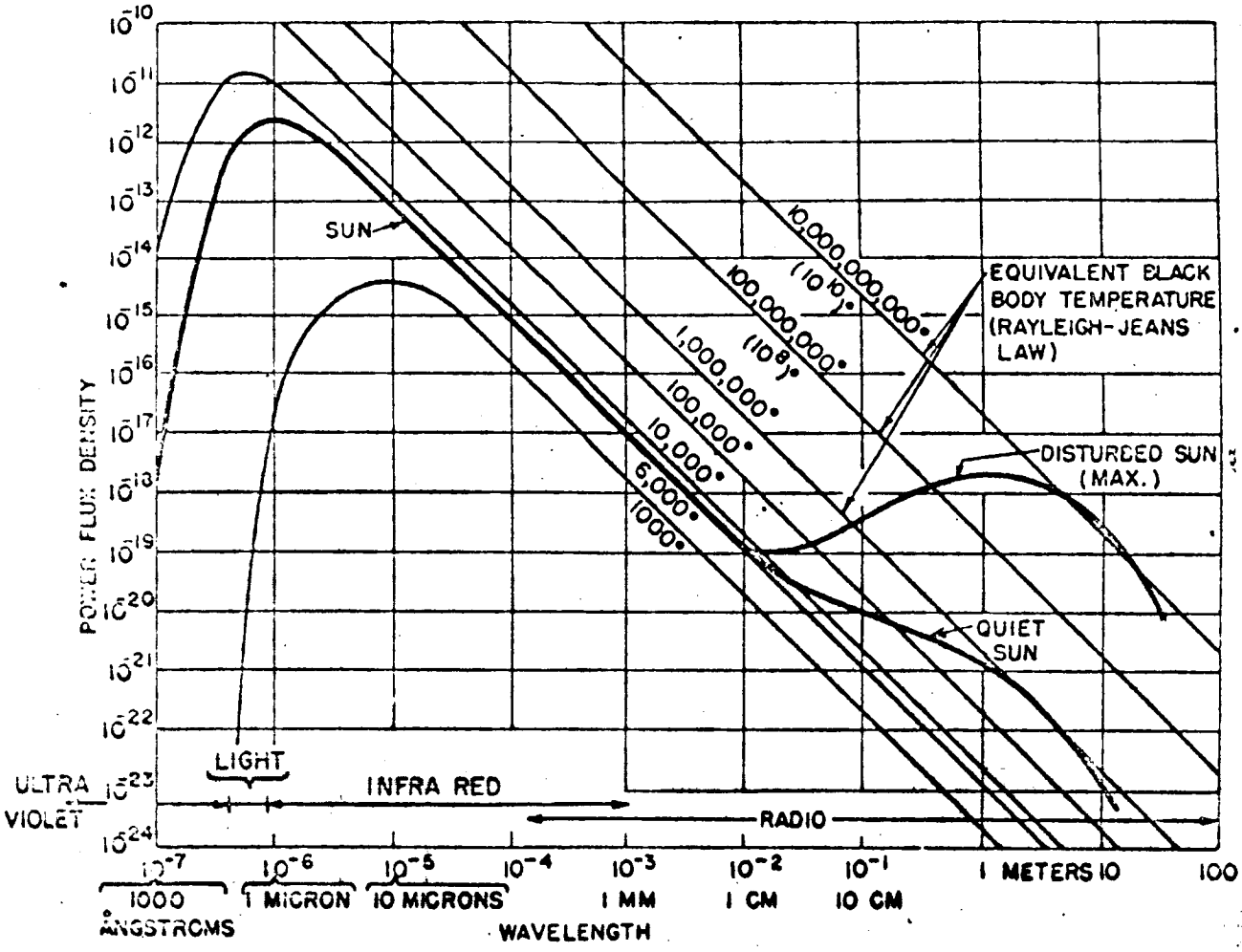

Figure 3-6. Solar and Black Body Radiation Power Flux Density As A Function of Frequency.

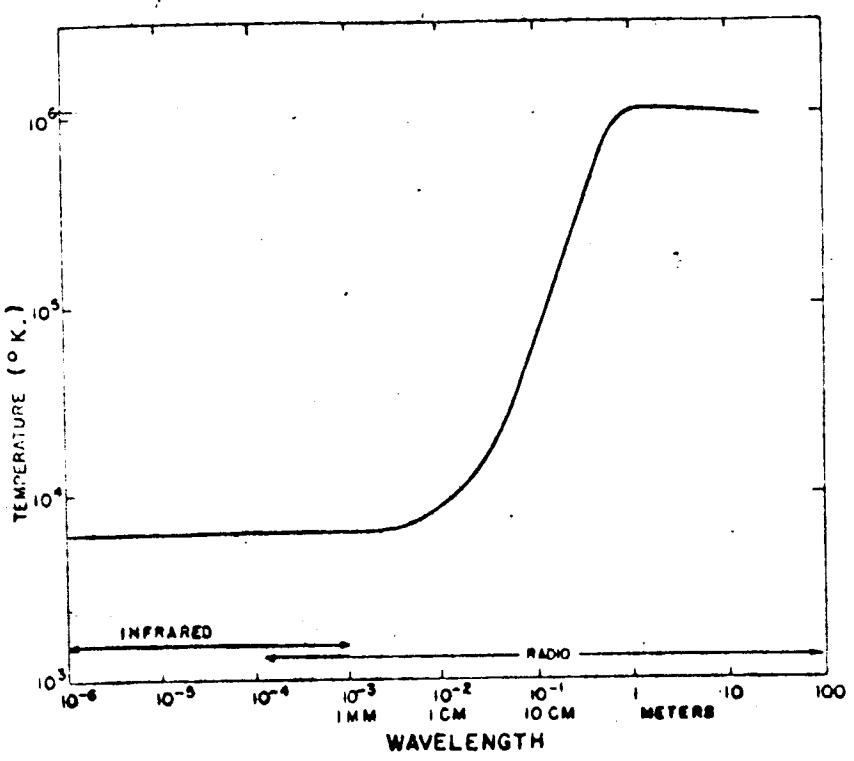

Figure 3-7. Effective Noise Temperature For The Quiet Sun As A Function Of Wavelength.

of black-body radiation and the character of the solar radiation as a function of frequency. The somewhat surprising increase in the effective noise temperature characteristics of solar radiation to the order of several million degrees in the lower radio frequency ranges may be noted in the figures.

The angular extent of the described noise component is reasonably uniform over the 0.5° visible angular extent of the solar disc. The indicated temperature would therefore be observed with antennas of comparable beamwidth, corresponding to gains of about 50 db or greater. The effective solar noise contribution is reduced in proportion to the antenna gain characteristic, i. e. a 20 db gain antenna pointed at the solar disc would receive an effective solar noise temperature component of about 30 db less than indicated.

3.1.2 Transmission Line Loss and Mismatch Effects

The power loss effects of the transmission line are of considerable importance in low noise systems. This loss degrades the amount of signal power transferred through the system and contributes an effective noise temperature component of its own to the system noise determined by its loss factor and operating temperature. The power loss factor, or loss ratio, is defined as the ratio of power input to power output for the device or network, and may be written as

$$L_r = P_{in} / P_{out}$$

Hence, the expression for determining the loss factor for a transmission line from its attenuation characteristic, α, in decibels may be written as simply

$$L_r = \text{antilog}_{10} (\alpha/10)$$

It is apparent that the transmission line loss factor modifies the antenna temperature contribution to the system noise temperature by $1/L_r$. The system noise temperature, T_n, for the system under consideration may therefore be written as

$$T_n = T_a/L_r + T_l + T_r$$

where T_l is the effective noise temperature of the transmission line and T_r is the receiver noise temperature. The transmission line effective noise temperature is dependent upon the termal equilibrium characteristics of its dissipative components, designated as a temperature T_{ot}. This relation may be written as

$$T_l = T_{ot} \left(\frac{L_r - 1}{L_r} \right) = T_{ot} \left(1 - \frac{1}{L_r} \right)$$

This relation may be also conveniently expressed by the use of a fractional change in the exchangeable power available, or

$$\gamma = \frac{P_{in} - P_{out}}{P_{out}}$$

The available, or exchangeable power loss or gain is specified by the relation

$$\frac{P_{avail.}}{P_{deliv.}} = \frac{(Z_1 + Z_2)^2}{4R_1 R_2}$$

The effective noise temperature of the transmission line becomes simply

$$T_1 = \gamma T_{ot}$$

And the excess noise figure of the transmission line for an exchangeable gain ratio of $(1 - \gamma)$ becomes,

$$\overline{NF}_1 - 1 = \frac{\gamma T_{ot}}{(1 - \gamma) T_o} ,$$

where T_o is a reference temperature usually taken as 290°Kelvin.. The equivalent expression in terms of the loss ratio is

$$\overline{NF}_1 - 1 = \frac{T_{ot}}{T_o} \left(1 - \frac{1}{L_r}\right) .$$

The derivation of the preceding results expressing the noise temperature of a linear passive four terminal network, such as a transmission line or waveguide, was originally given by Dicke' for the case of a matched load impedance. Dicke's argument; however, may be employed without the matched load restriction and some interesting results are obtained.

For a two port transducer terminated by a source and load, all of which are assumed to be linear passive elements at specified thermodynamic equilibrium temperatures, a noise power is generated by each component. The noise power

generated has a value determined by Nyquist's theorem which states that a resistance R at equilibrium temperature T produces a noise power density which may be expressed as an RMS noise voltage proportional to the bandwidth B, and of magnitude

$$e_n \text{ (RMS)} = \sqrt{4kTRB}$$

where k is Boltzmann's constant.

The source noise temperature must therefore be equivalent to its thermal equilibrium temperature since the noise power density available from any linear passive source is simply kT_s watts per cycle per second. The networks following the source may be assumed to be at zero temperature and hence generate zero noise power. For this condition, the available or exchangeable noise power at the input of the twoport is $k\ T_s\ B/L_r$, where L_r is the loss of the twoport.

Let us now assume that the thermal equilibrium temperature of the twoport is made equal to the source noise temperature, T_s. Both the source termination and the twoport may now be considered as a linear passive network at noise temperature T_s. Hence, the available noise power at the load must be $k\ T_s\ B$, by Nyquist's theorem.

The contribution of the source to the available power at the load input must be the same as before, the contribution of the two port network, designated P_2, must be the difference. Therefore, we may write for the available power loss of the twoport,

$$P_2 = kT_2B = kT_sB - kT_sB/L_r \ .$$

Hence,

$$T_2 = T_s \left(1 - \frac{1}{L_r}\right)$$

which is the result which was to be verified.

It may seem strange that a mismatch at the source affects the noise temperature of the network measured at the load. Since Nyquist's theorem expresses noise voltage and power in relation to dissipative circuit elements, it might seem that the noise temperature of a circuit should depend only upon the dissipative losses of the circuit. For a four-terminal network, it should be realized that the internally generated noise power is delivered to the equivalent of two external loads which are effectively in series. Hence, the source impedance characteristic should be expected to influence the power available at the load. The definition of L_r as the available or exchangeable loss indicates the dependence discussed.

In discussing the character of the effective noise temperature degradation which occurs in a general antenna aystem due to the impedance mismatch which may exist following the antenna, we may consider the antenna as a general two-port network. The effective input noise temperature for a two-port transducer such as an antenna is defined [1] as the noise temperature of an input termination which would result in the same output noise power as that of the actual transducer (antenna) connected to a noise free input termination. The conditions are specified such that the equivalent input termination is to be connected to a noise-free equivalent of the transducer. The precautions regarding the input impedance relations are necessary because the effective input noise temperature depends directly upon the impedance of the input termination. The variation in noise factor of a

---

1. "IRE Standards on Methods of Measuring Noise in Linear Two-ports, 1959". '59 IRE 20.S1, Proc. IRE, Vol. 48, No. 1, pp 60-68; January, 1960.

linear two-port transducer such as an antenna system characterized by its output admittance, Y_a, as a function of source admittance, Y_s, is given by

$$\overline{NF} = \overline{NF}_a + (R_n/G_s) \left| Y_s - Y_a \right|^2$$

and since we may relate noise factor, or excess noise factor, to effective noise temperature by

$$T_e = T_o \, (\overline{NF} - 1), \text{ where } T_o \sim 250^\circ K$$

we find that the admittance relation in terms of noise temperature is

$$T_e = T_a + T_o \, (R_n/G_s) \left| Y_s - Y_a \right|^2 \quad .$$

The terms $\overline{NF}_a$ and T_a are the optimum noise values for a given antenna obtained by adjustment of the source admittance, Y_s. The optimum source admittance, $Y_S = G_S + jB_S$, is the particular value of Y_s for which the optimum value of noise factor or noise temperature is realized. The parameter R_n is a positive resistance and represents the rapidity with which T_e increases above T_a and Y_s departs from Y_a. The relations here are important to note since the necessity for using more than one parameter to specify the noise properties of linear transducers has not been generally recognized.

It is usually necessary to calculate T_a, Y_a and R_n from the theory of the transducer, in this case an antenna, or to determine the values empirically from experimental data. For the general antenna case in which it is assumed that a good match exists between the radiation resistance of the antenna and the following input network, the latter mismatch dependent term is negligible. Hence, the problem is one of determining the inherent optimal characteristics of the antenna,

specifically T_a. The values for Y_a and R_n must also be determined if accurate information is desired concerning the performance degradation of the antenna as a function of mismatch.

3.1.3 . General Low Noise Antenna Relations

A brief but reasonably comprehensive discussion is included of the more significant antenna relations with particular emphasis given to the development of the describing performance parameters for low noise antennas, following in part the work of Barrett [1] and others.

In all radio observations, an antenna is needed to serve as a coupling between the receiver and the field of incident radiation. In this regard, an antenna is characterized by its effective area, frequency response, and polarization. When used as a transmitting antenna, either the power gain or directivity is often referred to instead of its effective area. However, as will be shown, the power gain, directivity, and effective area are related and may be used interchangeably with the appropriate modifications.

Consider an antenna used for purposes of transmitting power and let θ and ϕ be polar angles with the antenna at the origin. If P_{TR} is the total power radiated by the antenna, and $P(\theta,\phi,)$ is the power radiated per unit solid angle in the direction θ,ϕ, then the antenna directive gain function or directivity function, $D(\theta,\phi)$, is defined as

$$D(\theta,\phi) = \frac{P(\theta,\phi)}{P_{TR}/4\pi} = \frac{4\pi P(\theta,\phi)}{P_{TR}}$$

For an isotropic antenna, one which radiates equally in all directions, $P(\theta,\phi)$ equals $P_{TR}/4\pi$ and the directivity function is unity for all directions. Thus the directivity function, as defined by represents the increase in power radiated per unit solid angle in a given direction over that of an isotropic antenna.

---

1. A. H. Barrett, "Concepts on the Specification and Detection of Thermal Radiation", unpublished notes from Radio Astronomy Special Program; MIT, 1962.

Since we must have

$$\int_{4\pi} P(\theta,\phi)\, d\Omega = P_{TR}$$

it follows immediately from the definition of the directivity function that

$$\int_{4\pi} D(\theta,\phi)\, d\Omega = 4\pi.$$

Frequently antenna performance is specified in terms of the power gain function, $G(\theta,\phi)$, defined in a manner similar to the directivity function. If P_T is the total power supplied to the antenna terminals, then the power gain function is defined as

$$G(\theta,\phi) = \frac{P(\theta,\phi)}{P_T/4\pi}$$

If the antenna radiation efficiency, N_R, is defined as the fraction of the total power supplied to an antenna that is radiated by the antenna, then we have

$$P_{TR} = \eta_R P_T$$

and it follows that

$$G(\theta,\phi) = \eta_R D(\theta,\phi)$$

The antenna radiation efficiency accounts for the ohmic losses in the antenna, has a value between zero and one, and is very difficult to determine in practice. The losses in the transmission lines between the antenna terminals and the receiver input terminals can generally be easily determined and are not included in the radiation efficiency.

For most antennas there will be a particular value of θ and ϕ for which the antenna functions $D(\theta,\phi)$ and $G(\theta,\phi)$ will have maximum values. These are usually spoken of as the "directivity" and "gain", respectively, and will be denoted by D_o and G_o. Another term frequently used is that of the "antenna pattern" defined simply as the directivity function, or the power gain function, normalized to unity.

If $f(\theta,\phi)$ is the antenna pattern, then

$$f(\theta,\phi) = \frac{D(\theta,\phi)}{D_o} = \frac{G(\theta,\phi)}{G_o}$$

The equation $r = f(\theta,\phi)$ is an equation for a surface of unit maximum radius and any cross section of this surface which includes the axis of the coordinate system is known as a "polar diagram." Note that it follows from Eq. 14 that the directivity D_o may be written as

$$D_o = \frac{4\pi}{\int_{4\pi} f(\theta,\phi)\, d\Omega}$$

When considering an antenna for purposes of receiving signal or noise energy, the concept of <u>effective area</u> is perhaps more useful than that of gain or directivity. Consider an antenna exposed to an incident power flux density $d\,S(f)$ arriving from an incremental solid angle $d\Omega$ specified by the polar angles θ and ϕ with respect to the antenna. Then the incremental power $dP(f)$ absorbed by the antenna in the frequency range between f and $f + \Delta f$ and delivered to the input of the receiver is given by

$$d\,P(f) = \frac{1}{2}\,\Delta f\, A(\theta,\phi)\, dS(f)$$

The factor 1/2 is inserted in the expression because in general the antenna will be capable of absorbing only radiation of one polarization, and hence, for randomly polarized radiation, will absorb only one-half of the incident radiation. The total power absorbed by the antenna $P(f)$ is given by

$$P(f) = \frac{\Delta f}{2} \int_{4\pi} I(f) A(\theta,\phi)\, d\Omega.$$

In general when observing radiation from a source in space, the power detected will be a maximum for a particular orientation of the antenna. For this orientation the effective area will have a maximum value A_o. As with the directivity function or the gain function, it is possible to define an antenna

pattern $f(\theta,\phi)$ from the concept of effective area. Thus,

$$f(\theta,\phi) = \frac{A(\theta,\phi)}{A_o}$$

It may be shown that the directional characteristics of an antenna are the same whether it is used for transmitting or for reception of radiation.

The received power P(f) can be related to the effective noise temperature, T_B, of a source by the following relation

$$P(f) = \frac{P_R f^2 \Delta f}{C^2} \int_{4\pi} T_B A(\theta,\phi) d\Omega$$

Now it can be shown that for an antenna surrounded by an enclosure at a uniform temperature T the power absorbed by the antenna in bandwidth Δf will be $kT\Delta f$. Thus for an antenna exposed to any type of radiation field it is customary to define the antenna temperature T_A by the relation

$$P(f) = kT_A \Delta f = kT_A B$$

Combining the preceding two expressions, we have

$$T_A = \frac{1}{\lambda^2} \int_{4\pi} T_B A(\theta,\phi)\, d\Omega$$

This equation is one of the most fundamental equations of radio astronomy for it relates the experimentally determined antenna temperature T_A to the noise temperature T_B of a source in space in terms of the physical characteristics of the antenna.

With the equations derived above, it is now possible to obtain a relation between the gain function $G(\theta,\phi)$ and the effective area $A(\theta,\phi)$ of an antenna. This is a general relationship derived from thermodynamical considerations. Consider an antenna and a black body subtending a solid angle Ω when viewed from the antenna in an enclosure in thermodynamic equilibrium. Assume that the black body is at a uniform temperature T and that Ω is small so that $A(\theta,\phi)$ may be considered constant

over Ω_A. Then the power per unit bandwidth from the black body absorbed by the antenna will be $kTA\,\Omega\lambda^{-2}$. On the other hand, the power radiated by the antenna and absorbed by the black body is $kTG\Omega/4\pi$ as follows from the gain function. Since the system is in thermodynamic equilibrium, the power radiated from the black body to the antenna must equal the power radiated inthe opposite direction. Thus these two expressions may be equated. Furthermore, since the argument did not depend on specifying the angles θ and ϕ, it musthold for all angles. Hence,

$$G(\theta,\phi) = \frac{4\pi}{\lambda^2} \quad A(\theta,\phi)$$

in general, and in particular

$$G_o = \frac{4\pi}{\lambda^2} A_o$$

Combining these expressions with the normalized gain or directivity "pattern" functions, expressions is obvious.

It follows, that

$$\int_{4\pi} A(\theta,\phi)\, d\Omega = \lambda^2 \eta_R$$

which allows the expression for the antenna noise temperature to be written as

$$T_A = \frac{\eta_R \int_{4\pi} T_B A(\theta,\phi) d\Omega}{\int_{4\pi} A(\theta,\phi)\, d\Omega}$$

Alternative forms of several of these expressions often appear in the literature and are included here for completeness. The <u>mean</u> <u>effective</u> area, $\bar{A}$, is defined as

$$\bar{A} = \frac{1}{4\pi} \int_{4\pi} A(\theta,\phi) \quad d\Omega$$

from which the following expressions may be derived.

$$\bar{A} = \frac{\eta_R \lambda^2}{4}$$

$$D(\theta,\phi) = \frac{A(\theta,\phi)}{\bar{A}}$$

$$T_A = \frac{A_o}{\lambda^2} \int_{4\pi} T_B \; f(\theta,\phi) \; d\Omega$$

$$T_A = \frac{1}{4\pi} \int_{4\pi} T_B \, G(\theta,\phi) \; d\Omega$$

A useful quantity is the effective solid angle Ω_B defined as

$$\Omega_B = \int_{4\pi} f(\theta,\phi) \; d\Omega$$

which can be related directly to the directivity by

$$\Omega_B = \frac{4\pi}{D_o} .$$

Suppose that T_B has a value greater than zero over the solid angle subtended at the antenna by the source, Ω_S, and is zero outside this solid angle. In addition assume that the source may be considered as essentially a point source. Thus we may equate $G(\theta,\phi)$ to G_o over the solid angle Ω_S. Thus Eq. 32 may be written as

$$T_A = \frac{G_o}{4\pi} \int_{\Omega_S} T_B \, (\theta,\phi) \; d\Omega$$

This may be written as

$$T_A = \frac{A_o S(f)}{2k}$$

which illustrates that the flux density is the more appropriate way to refer to a point source.

If it is assumed that $T_B \, (\theta,\phi)$ is constant over the solid angle Ω_S, then there are alternate expressions for the antenna temperature T_A obtained from a point source.

$$T_A = \frac{A_o T_B \Omega_S}{\lambda_2}$$

or

$$T_A = \eta_R T_B \frac{\Omega_S}{\Omega_B}$$

Both equations serve to illustrate important results. From the first equation we see that as long as T_B is independent of frequency, as it is for purely thermal radiation from an opaque body, then the received power, and hence T_A, will be proportional to λ^{-2}, thus favoring observation at the shorter wavelengths. We see that aside from the power loss represented by the radiation efficiency η_R we may regard T_A as equal to T_B weighted by the ratio of the solid angle of the source Ω_S to that of the antenna Ω_B. This same result might have been obtained by intuitive reasoning and is a specific case of the more general weighting process which has been described. Note also, as expected, that the more directive an antenna is, the the greater will be the received power from a point source. This is only valid for point sources and does not hold true in general.

The interpretation of the observations of the extended intensity distribution, such as the environmental noise distribution are considerably more complicated than for a point source. The basic reason for this is that the antenna is generally responsive to radiation incident upon it from all directions. It is true that the antenna power gain (or directivity) is very much smaller over most directions than it is in the main beam; however, the integrated effect of the side and back-lobes can be an appreciable fraction of the integral over only the main beam. Thus, to deal with the interpretation of the observations occurring within extended intensity distributions, further definitions are needed and special caution is often necessary in their application.

It is desired to be able to evaluate the antenna temperature due to the intensity distribution in the main beam only, to relate this to the noise temperature distribution of the extended region, and to exclude the effects of side and back-lobes of the antenna. In this effort we shall follow the terminology and procedures introduced by the Dutch workers as closely as it is feasible with our previous terminology. The term "main beam" will be taken to include all portions of the antenna pattern within the solid angle defined by some multiple of the main lobe half-power width, i.e., some multiple of antenna beam width. The multiple to be chosen depends entirely on the characteristics of the problem, such as the variations in the intensity distribution, the sensitivity of the receiver, the antenna pattern, etc., but it is normally taken sufficiently large as to enclose all the main lobe and perhaps the near side lobes. Having chosen the main beam, one can define a stray factor, β, which is related to the radiation which is received from solid angles not included in the main beam. The stray factor is fedined as

$$\beta = \frac{\int_{4\pi-MB} f(\theta,\phi)\,d\Omega}{\int_{4\pi} f(\theta,\phi)\,d\Omega}$$

Analogous to the directivity, we define the beam directivity, D_o', as

$$D_o' = \frac{4\pi}{\int_{MB} f(\theta,\phi)\,d\Omega}$$

It follows that

$$D_o = (1-\beta)\, D_o'.$$

One can also define a beam solid angle, Ω_β

$$\Omega_B' = \int_{MB} f(\theta,\phi)\, d\Omega = \frac{4\pi}{D_o'}$$

In these equations the notation MB under the integral sign implies integration over the solid angle including only the main beam.

To evaluate the antenna temperature T_A due to an extended intensity distribution, we obtain

$$T_A = \frac{G_o}{4\pi}\left\{\int_{MB} T_B\, f(\theta,\phi)\, d\Omega + \int_{4\pi-MB} T_B f(\theta,\phi)\, d\Omega\right\}$$

which can be written as

$$T_A = \eta_R \left[(1-\beta)\,\bar{T}_B + \beta T'\right]$$

where the temperatures T' and $\bar{T}_B$ are defined by

$$T' = \frac{\int_{4\pi-MB} T_B f(\theta,\phi)\, d\Omega}{\int_{4\pi-MB} f(\theta,\phi)\, d\Omega}$$

$$\bar{T}_B = \frac{\int_{MB} T_B f(\theta,\phi)\, d\Omega}{\int_{MB} f(\theta,\phi)\, d\Omega}$$

$\bar{T}_B$ may be referred to as the main beam brightness temperature, familiar in radio astronomy work, and is clearly the average of T_B over the main beam, as T' is the average of T_B over the balance of the antenna pattern.

It should be obvious from the discussion of both the point source and extended source cases that a detailed knowledge of the antenna pattern and the antenna losses is important to the proper interpretation of the resulting antenna temperature. These factors should prove even more important with the trend toward larger and more precise antennas and the resulting improvement in resolving power attainable.

A discussion may be in order of certain of the basic considerations of antenna design and antenna measurements, pointing out the principal areas of difficulty in the design and measurement of low noise antennas.

As we have discussed, the antenna pattern and power gain are characterized by the beamwidth, beam solid angle, effective solid angle, stray radiation factor, antenna radiation efficiency, and other quantities. Many of these quantities are interrelated, and we will consider the factors that determine these quantities for a paraboloidal reflector with either a microwave horn or a dipole at the focus.

The antenna pattern of a receiving antenna will be identical with the pattern of the same antenna when used as a transmitter. Thus, when it is convenient, we will discuss the transmitting pattern of the antenna, but the results will be applicable to use of the antenna for reception.

In general, the power distribution in the field of a transmitting antenna will depend on the distribution of currents in the conductors of the system. Thus, it is possible by a suitable choice of currents (amplitude and phase) and of geometrical arrangement of conductors to produce many different antenna patterns. Furthermore, many applications of this principle, particularly in interferometry, involve the superposition of the field patterns (not power patterns) of two or more simple antennas.

Many of the large antennas utilized in space applications have paraboloidal reflectors of one kind or another. Often these reflectors are limited to sectors of a paraboloid for reasons of mechanical design or economics. The reason for the popularity of these reflectors is that the antenna pattern is nearly symmetrical about the axis of the paraboloid, and gives rise to the so-called "pencil beam".

The reflector, when used as a receiving antenna, collects energy from the incident radiation field and concentrates it at the focus of the paraboloid where it is fed to the receiver input. When used as a transmitting antenna, the reflector intercepts energy from the active element at its focus and concentrates it into a preferred direction. Thus, in either case, a principal part of the antenna is a device at the focus whose electrical properties are matched to those of the reflector. This can be a dipole, a microwave horn, or possibly other configurations, depending on the wavelength to be used and, to a leaser extent, on the ratio of the focal length to the diameter of the reflector, the f/D ratio. For purposes of illustration, we shall consider a microwave horn, but it is to be understood that it could just as well be a dipole feed, although the latter would not be the simple dipole discussed above.

The unit at the focus is often spoken of as the "feed", a term carried over from radar where the horn is used to feed energy to the reflector. It should be recognized that the horn itself is actually an antenna, but without the directivity possible when used in conjunction with a reflector, and the pattern of the feed horn is referred to as the primary pattern. The pattern of the reflector is called the secondary pattern. The secondary pattern is a property of both the reflector and the primary pattern. A change in the primary pattern will affect the secondary pattern. In the previous discussions of directivity, beamwidth, and other antenna factors, we have been referring to the secondary pattern.

A single paraboloidal reflector defines a beamwidth unambiguously, and this can be related to the properties of the reflector, the wavelength, and the primary pattern. It can be shown that if the primary pattern is uniform in amplitude and phase over the aperture of the reflector, and if the reflector surface is of

sufficient mechanical precision so as not to introduce any distortion into the secondary pattern, the beamwidth Θ_B, i.e., the half-power width of the main lobe, is given by

$$\Theta_B = 2 \sin^{-1} (0.51\frac{\lambda}{D}) \simeq 1.02\frac{\lambda}{D}$$

where λ is the wavelength and D is the diameter of the reflector, assumed to have a circular aperture. The beamwidth given by this expression, may be regarded as of little more than academic interest since it requires an aperture illumination, i.e., primary pattern, which is uniform in amplitude and phase. Such an illumination is generally considered impossible with present techniques. With a uniform illumination, the peak of the first side lobe is only 17.6 db less than the peak of the main lobe, and this is considered to be quite high by current standards. A more realistic value for the beamwidth, Θ_B, is

$$\Theta_B \simeq 1.2\frac{\lambda}{D} ,$$

but this expression should not be considered rigorous as it depends on the primary feed pattern.

In general, it is not possible to have the primary pattern uniform in amplitude and phase over the entire aperture of the antenna, but great care is usually taken to keep the phase variation small, i.e., the phase at the periphery of the aperture should not differ from that at the center by more than about 1/16th of a wavelength. Phase variations over the aperture can arise from deviations of the reflector from a paraboloid, displacement of the feed horn from the focus of the reflector, and departures of the wavefronts from the feed horn from spherical waves. It is these considerations which make the construction of large paraboloids for use at short wavelengths such a difficult engineering

problem. The inability to have uniform amplitude illumination across the surface of the aperture results in reduced directivity and an increased beamwidth; however, there is an advantage in that the side-lobe level will be lower than in the case of uniform illumination. This effect is often important and the primary pattern is tapered so the illumination at the edge is a small fraction of that at the center. Generally, tapers of at least 10 db are employed; i.e., the illumination at the edge is at least 1/10 as small as at the center, and frequently smaller. Needless to say, considerations such as these dictage the design of the feed system.

It can be seen that not all the energy radiated by the feed horn will be intercepted by the reflector and concentrated into the main beam. The power that is not intercepted by the reflector is referred to as "spill-over". In the case of a receiving antenna, it implies that the feed horn will receive radiation from beyond the edge of the reflector, such as ground radiation. This source of power loss is one of the major contributions to the stray radiation factor β, as previously defined. Other sources are radiation scattered by the supports for the feed horn, side-lobes outside the main beam, and, if the reflector is made of a wire or metal mesh, radiation lost through the holes in the reflector. A reduction in spill-over is another major advantage in tapering the illumination of the aperture. Considerable effort has been expended in designing feed systems that will illuminate the aperture in a desired fashion, but sharply taper the illumination at the edge.

We have discussed three sources of power loss which affect the power gain of the antenna. These are: (1) the ohmic losses in the feed horn and reflector, represented by the antenna radiation efficiency η_R, (2) the side lobe, spill-over, and scattered power, represented by the stray factor β, and (3) the power gain

deterioration due to phase effects, which we shall represent by η_D, called the diffractive efficiency. These terms can be combined into the antenna efficiency η, which may be defined as

$$\eta = \frac{A_o}{A_g} = \frac{\lambda^2 G_o}{4\pi A_g}$$

where A_g is the geometrical area of the aperture and A_o is the maximum effective area defined previously as related to the power gain. The diffractive efficiency is defined by the relation

$$\eta_D = \frac{\lambda^2}{4\pi A_g} D_o'$$

and its value would be unity if all the power reflected from the paraboloid were concentrated in the main beam. Thus, in a sense, it represents the "concentration efficiency" of the reflector. We have therefore

$$\eta = (1-\beta)\, \eta_D\, \eta_R$$

which relates the over-all antenna efficiency η to the three sources of power loss from the main beam. Typical values of η range between 0.40 and 0.65, of which the main contribution comes from the stray radiation factor β, in most cases.

It seems possibly worthwhile to mention certain of the difficulties associated with the experimental measurement of the directivity and power gain of large paraboloids. The procedure is difficult, at best, and the accuracy obtained is generally of the order of five or ten per cent. The uncertainties in large antenna measurements usually result almost entirely from the inability to determine the antenna pattern with precision.

Antenna measurements generally involve a distant transmitter which illuminates the antenna under test with a nearby plane wave and the relative power received by the test antenna is recorded as it is moved in various positions. One of the major difficulties in performing these measurements for large reflectors is that the distance between the transmitter and the receiving antenna must be sufficiently large so that the received wave is a reasonable approximation to a plane wave; i.e., the transmitter must be in the Fraunhofer region of the test antenna. The minimum acceptable distance can be easily worked out from geometrical considerations from the requirement that the phase difference of the incident wave between the center and the edge of the refelctor should not exceed $\lambda/16$. The distance is given by

$$R = \frac{2D^2}{\lambda}$$

where D is the diameter of the reflector. For example, the distance is between 11 and 12 miles for a 100' paraboloid used at 10 cm wavelength. The magnitude of this distance can present a problem to proper antenna measurements because it is desired that the path be free from nearby obstructions which will cause unwanted reflections of the transmitted power.

It is clear that the antenna pattern $f(\theta,\phi)$ can be obtained by relative power measurements without the necessity of an absolute calibration; however, it is usually impossible to make these measurements over all solid angles. Generally, measurements are taken in the E-plane and H-plane, and perhaps at an intermediate position, and values at other positions are inferred from these. The directivity D_o follows from the pattern measurements.

If the ohmic losses in the antenna can be determined, then the power gain follows from the directivity. However, as has been mentioned, this is usually difficult to determine so that the power gain must be measured directly. The principal difference between the directivity and power gain measurements is that the latter require an absolute power calibration. The characteristics of microwave horns can be calculated fairly accurately, and this fact is often employed in making absolute gain measurements. If the microwave horn is considered as a standard, whose gain G_s is known, then the gain of the test antenna can be determined by measuring the relative power received by the test antenna P_t and by the standard horn P_s. The gain of the test antenna then follows from the equation

$$G = \frac{P_t}{P_s} G_s.$$

Many precautions must be taken in performing these measurements. The field at the test antenna should be uniform, the same detection equipment should be used for both power measurements, the power output of the distant transmitter should be monitored at the test antenna, and the received powers should be corrected for the law of the detector if it does not follow the square law.

If both directivity and power gain data are available, then one can determine the over-all antenna efficiency, η, and the stray factor, β. However, measurements are rarely carried out which make this feasible. Usually the antenna ohmic losses, represented by η_R, are estimated or considered to be negligible, and the diffractive efficiency η_D and the stray factor β are determined from observations.

3.1.4 Low Noise Antenna Performance Optimization

The principal justification for the attainment of low noise antenna systems is to enable an improvement in the system sensitivity for a specified output signal-to-noise ratio (SNR). The importance of system SNR has been briefly described previously. The possibility of confusion which may result if the low noise characteristics of a system are interpreted as being generally equivalent to the maximum output SNR characteristics of the system. An example was presented of a low noise antenna of poor aperture efficiency which was found to be a factor of two improvement in low noise characteristics relative to a reference antenna, but was a factor of two less desirable in its SNR characteristics. In this case, the improvement in low noise characteristics achieved by under-illuminating a reflector did not compensate for the loss in gain due to the considerably decreased aperture efficiency. An optimization process appeared necessary to achieve the desired maximum output SNR available from the antenna far-field response resulting from a given primary illumination and the antenna noise temperature environment.

In the output SNR optimization process, it is important to determine the significance of the optimization criteria in terms of the antenna parameters. To this end, we may assume an optimally matched receiver connected to the antenna by means of a linear passive twoport which will be assumed of loss ratio, L_1. We may also assume a receiver noise temperature of T_n. The antenna may also be viewed as a four terminal device in which the source impedance is essentially the antenna radiation resistance. The available or exchangeable noise power spectral density developed at the input which is assumed to be principally a function of the environmental noise distribution, T_n, and appears as an extended source, i. e. independent of antenna beamwidth, may be written as simply $S_n = k\,T_n$ watts per cycle

per second. The factor k is Boltzmann's constant which has a value of 1.38×10^{-23} watt-sec/°K. The signal power density entering the antenna may be expressed as an equivalent noise temperature of T_s °Kelvin which indicates an available spectral power density, $S_s = k\,T_s$ watts per cps. Again the available, or exchangeable power is the power which could be delivered to a matched load, or specified more precisely for an arbitrary network as

$$\frac{P_{avail.}}{P_{deliv.}} = \frac{|Z_a + Z_s|^2}{4R_a\,R_s} .$$

The signal power captured by the receiving antenna effective aperture, A_c, is

$$P_{RA} = S_R\,A_C$$

and the effective aperture "capture" area may be written

$$A_c = \frac{G_R \lambda^2}{4\pi} ,$$

therefore we have for the signal power available at the antenna terminals,

$$P_{RA} = \frac{S_R\,G_R \lambda^2}{4\pi} .$$

Similarly the system input noise temperature, T_n, for the configuration we have taken of a receiving system consisting of an antenna, a passive linear twoport representing a transmission line of available loss ratio L_t, and a receiver of noise temperature T_e, as

$$T_N = T_a/L_t + T_t + T_e .$$

The receiver noise temperature, T_e, is defined by IRE standards to be related to the receiver noise factor, or noise figure, $\overline{NF}$, by

$$T_e = (\overline{NF} - 1)\,T_o$$

where T_o is a standard reference temperature, usually taken (by IRE standards, again) to be 290° Kelvin. The effective output noise temperature of the transmission line, T_t, is found by the relation

$$T_t = (1 - 1/L_t)\, T_o' ,$$

where T_o' is the thermal equilibrium temperature of the transmission line or twoport device, often set equal to T_o of 290°K. This assumes antenna performance in which there are negligible ohmic losses, usually the case for the large passive paraboloidal antennas under consideration.

For a given noise bandwidth characteristic for the receiver as defined by North [1], we have

$$B_n = \frac{1}{G_o} \int G(f)df$$

where G(f) is the gain-frequency characteristic and G_o is the value at the nominal frequency of the passband. Using the bandwidth B_n, we may express the system input noise power as a function of the system input noise power as

$$P_n = S_n B = kT_n B.$$

Referring the system noise temperature to a reference point at the receiver output, we obtain for the available received signal power

$$P_R = \frac{S_S G_R \lambda^2}{4\pi L_t}$$

where L_t is the overall available loss between the antenna and the reference point.

---

1. D. O. North, "The Absolute Sensivity of Radio Receivers", RCA Review 6:332-343 (Jan. 1942).

We may now obtain the output signal-to-noise ratio (SNR) as the available signal power gain divided by the system input noise power, or

$$SNR = \frac{P_R}{P_N} = \frac{S_s G_R \lambda^2}{4\pi L_t \, kT_n B} \quad .$$

This expression holds for actual powers as well as the available powers since both signal and noise are subject to the same mismatch losses.

Separating the factors which are not influenced by the antenna characteristics from those which are, we may write

$$SNR = C \frac{G_R}{T_N} \quad .$$

This indicates the relative importance, before only intuitively believed reasonable, of the receiving antenna gain and the system input noise temperature. The receiving antenna gain is a function of the primary feed illumination and may be arbitrarily expressed as

$$G_R = \xi G_M$$

where ξ is the fraction of the total power radiated by the feed incident on the reflector aperture. The efficiency of the aperture in collimating the incident energy may be represented by G_M.

A series of numerical integrations of various primary pattern illuminations coupled with the influence of the corresponding spillover and minor-lobe energy on the input noise temperature may be performed to determine the optimum value for ξ and G_M. Evaluations of this type were performed during the program and as expected, the form of the primary illumination was found of great importance in

establishing high gain values for corresponding low input noise, or antenna noise temperatures.

Analytical and numerical integration calculations have been performed by Livingston [1] and others to obtain optimum operating relations for feed configurations having conventional or specified illumination characteristics.

In general, the defined relations were employed to obtain the maximum gain characteristics from the aperture by approximating a uniform illumination over as great an aperture extent possible consistent with obtaining the desired aperture edge illumination taper available from the primary feed aperture extent. This approach appears to represent near optimum characteristics from the secondary aperture since simultaneous gain improvement and greatly reduced antenna noise temperatures were found practicable through this technique. Both of these factors improve the system SNR.

The low noise antenna figure-of-merit designation, $M = G_A/T_A$, represented by the antenna dependent term of the SNR general expression is of value in analyzing the relative values of various low noise antennas.

---

1. M. L. Livingston, "The Effect of Antenna Characteristics on Antenna Noise Temperature and System SNR", IRE Trans. on Space Electronics and Telemetry, Sept. 1961; pp. 71 - 79.

3.1.5 Monopulse Operation Considerations

The principal difficulties generally associated with monopulse operation of an antenna system relate to the employment of several primary feed systems in a limited spatial extent, generally limited by the maximum permissable blocking of the secondary aperture. This limitation of the available primary aperture coupled with the requirement for axial symmetry of the primary response in the case of conventional paraboloidal configurations place significant constraints on the primary feed design.

3.1.6 Multiple Band Feeds

The requirement for single antenna operation over a considerable range of frequencies, extending for certain present NASA requirements from the VHF region well into the microwave region, compounds to an extent the design constraints mentioned in connection with monopulse operation. Techniques are available, relying generally upon either broadband or frequency selective techniques for satisfying the design requirements placed upon the configuration of primary feeds necessary for effective antenna operation.

3.1.7 Polarization Requirements

It is generally desirable that the antenna perform satisfactorily under all polarization conditions. This in general specifies a circular polarization requirement which is generally compatible with the antenna symmetry considerations. There are a number of inherent difficulties in the attainment of desirable circular polarization characteristics from multi-band feed systems of moderate mechanical and electrical complexity. One of these difficulties concerns achievement of constant antenna beamwidth with polarization for an aperture containing significant reactive and diffraction influences.

3.2 Antenna Performance Evaluation Techniques

3.2.1 Far-Field, Near-Field Relations

A reasonably detailed discussion has been presented concerning the behavior of the far-field radiation characteristics of an aperture as a function of the near-field energy distribution in the region of the aperture. The important factor concerning this relation is to realize that the form of the near-field, or Fresnel region, energy distribution as determined by a particular feed configuration specifies with certain phase constraints the characteristics of the far field, or Fraunhofer region, characteristics. Mathematically the far-field response may be expressed as the Fourier transform of the field distribution at the region of the aperture surface. This fact allows analysis, and under certain conditions synthesis, of the desired antenna characteristics either in general form or by numerical integration techniques applied to the appropriate radiation field distributions.

3.2.2 Absolute Gain, Efficiency Considerations

The relation presented in the section on Low Noise Performance Optimization govern the general antenna performance optimization criteria. The determined overall relation indicating the optimal SNR performance of an antenna was designated the low noise antenna figure of merit, which is

$$M = G_A/T_A ,$$

where G_A is the antenna gain and T_A is the effective noise temperature of the antenna. A further relation may be described relating the gain of an antenna system for a specified aperture area to the maximum gain attainable for the aperture area as

$$G_A = \eta G_o$$

where G_o is the maximum gain obtainable, which corresponds to a uniform illumination over the aperture, and is the aperture efficiency. Hence, we may rewrite the figure of merit as

$$M = \frac{\eta G_o}{T_A}$$

which for a specified aperture area and frequency of operation reduces to simply

$$M_A = \eta / T_A .$$

It is therefore apparent from these relations that maximal aperture efficiency consistent with low values of degradation in T_A due to spillover and minor-lobe level interaction with the environmental temperature distribution appears to be the principal feed design objective.

3.2.3 Gain-Temperature Integration Technique

Formulation of a general method for determining the effective antenna noise temperature appears worthwhile in that quite often it is not possible or feasible to obtain an accurate far-field pattern for a large or isolated antenna. However, accurate primary feed information is generally available. Also, it appears that an analysis of this type would serve to establish on a practical basis the desired characteristics of primary feed systems. A comparison of the calculated results with the measured experimental data should allow development of a consistent and accurate means for the determination of the effective antenna noise temperature.

Determination of the effective noise temperature of an antenna from the form of its primary pattern and the spatial temperature distribution is based upon the fact that the far-field pattern may be synthesized from the primary pattern and reflector considerations. The far-field power gain function integrated over the spatial temperature distribution represents the total effective noise temperature for the antenna. This may be expressed as

$$T_a = (1/4\pi) \int_{\Omega} G(\Omega)\, T(\Omega)\, d\Omega$$

or in spherical coordinates

$$T_a = (1/4\pi) \iint G(\phi,\theta)\, T(\phi,\theta) \sin\theta\, d\theta\, d\phi \ .$$

Synthesis of the far-field radiation pattern to a close approximation may be obtained by Fourier transform techniques applied to the form of the primary illumination function combined with the amount and extent of the spillover energy. By then making reasonable simplifying assumptions concerning the spatial temperature distribution, the preceding integration may be accomplished. Initially the temperature distribution simplifying assumption is to consider the distribution to have symmetry in the azimuth plane and to have a simple "step" form of temperature

variation in the elevation plane. A further simplification may be accomplished by referring the temperature distribution assumptions back to the primary feed illumination patterns which were obtained experimentally.

An analysis of the experimentally obtained primary patterns may be obtained by means of a pattern integration technique of the recorded primary patterns. This feed evaluation technique enables a comparison of the measured feed performance with that obtained by certain optimum and conventional illuminations.

The directivity of an antenna is given by:

$$D = 4\pi \frac{P(max)}{\int P(\Omega)\ d\Omega}$$

$$D = 4\pi \frac{P(max)}{\iint P(\theta,\phi)\ \sin\theta d\theta d\phi}$$

Assuming the radiation pattern is symmetrical about the X-axis, we may write,

$$P(\theta,\phi) = P(\theta) = P(max)\ \ r\ \ (\theta)$$

and

$$D = 4\pi \frac{P(max)}{\int_0^{2\pi}\int_0^{\pi} P(max)\ r \sin\theta d\theta d\phi}$$

$$= \frac{4\pi}{2\pi \int_0^{\pi} r \sin\theta d\theta}$$

or

$$D = \frac{2}{\int_0^{\pi} r \sin\theta\ d\theta}$$

where r is the relative power as a function of θ and is expressed as a pure ratio of the normalized power.

Considering the ϕ = constant plane in a conventional r, θ, ϕ spherical coordinate system such as that shown in Figure 3-8, we find that the area measured or "integrated" by the planimeter is given by

$$A = 1/2 \int R^2\ d\theta, \quad R = R(\theta)$$

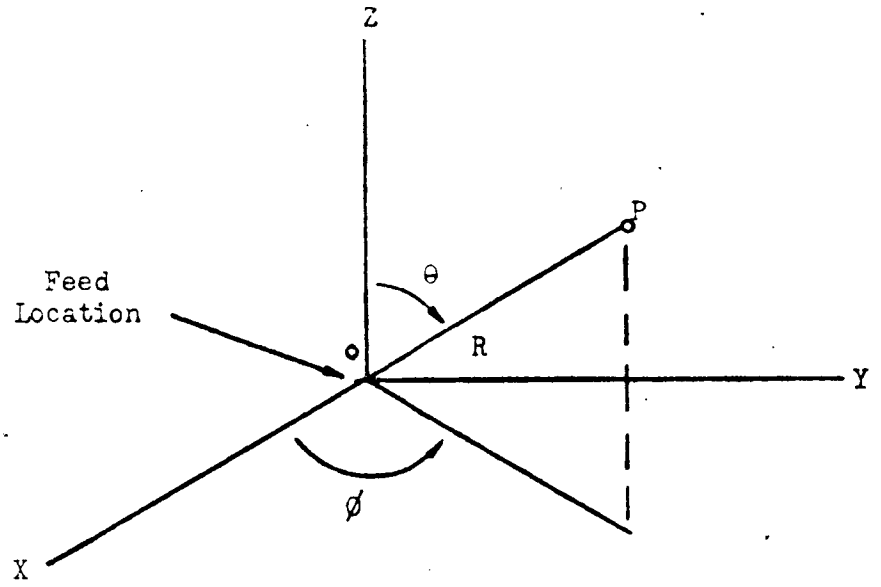

Feed Evaluation Coordinate System Geometry.

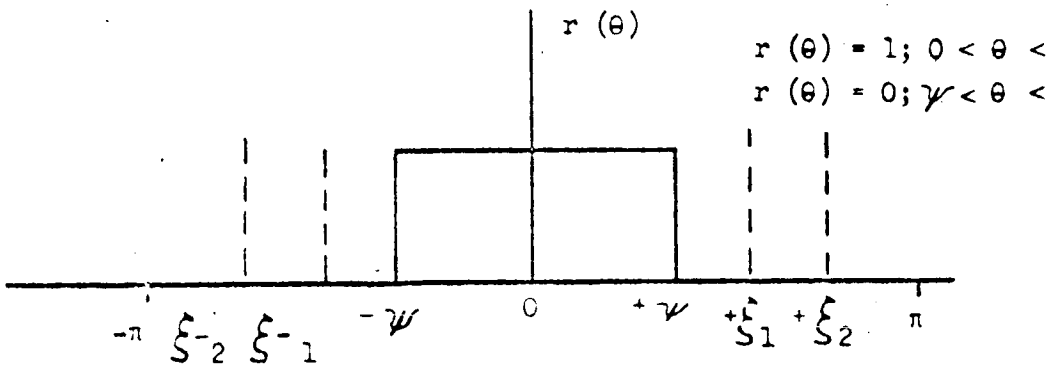

Feed System Integration Regions.

Figure 3-8. Coordinate System Geometry and Integration Regions For Feed Evaluation Technique.

The area indicated by the planimeter may be written as

$$2A = \int_0^{\pi} R^2 \, d\theta$$

$$= \int_0^{\pi} r \sin \theta \, d\theta$$

Hence if a plot is made for

$$R = (r \sin \theta)^{1/2}$$

and integrated with a planimeter, the value of the power density integral is given by 2A. For our particular case, referring to Figure 3-8, we have the indicated idealized primary pattern for a constant primary illumination over the aperture. Comparison of the primary power pattern obtained experimentally with the idealized power distribution enables a determination to be made of the relative merit of the various feeds.

In graphical integration we herefore want

$$\int R^2(\theta) d\theta = \int r(\theta) \sin \theta d\theta = \text{max. for } 0 < \theta < \psi$$

and

$$\int r(\theta) \sin \theta d\theta = \text{min. for } \psi < \theta < \pi .$$

The procedure may be modified slightly if the integration is to be done in cartesian form by replacing the polar planimeter integration expression by,

$$A = \int_0^{\pi} y \, d\theta , \quad y = y(\theta)$$

where y is the relative power ratio. For this case it is necessary only to plot $y = r \sin \theta$ in place of the square root as required in polar form. The graphical integration therefore consists of

$$A = \int_0^{\pi} y(\theta) d\theta = \int_0^{\pi} r \sin \theta \, d\theta .$$

Hence, we may plot r sin θ and integrate with the planimeter.

Actually it appears desirable to separate the primary feed patterns into several regions in order to properly evaluate the noise temperature contributions in the various spatial regions. These regions are shown as $\pm\xi_1$, $\pm\xi_2$, etc. in Figure 3-8.

To evaluate a feed pattern we may list the following steps:

(1) Convert normalized power measured in decibels to a linear relative power ratio as a function of angle.

(2) Multiply the value obtained in step 1 by the sine of the angular coordinate.

(3) In cartesian form plot r sin θ as a function of θ; in polar form plot $(r \sin \theta)^{1/2}$ as a function of θ.

(4) Integrate with a planimeter from 0 to ψ and record value.

(5) Integrate with planimeter from ψ to π and record value.

(6) The ratio of the result of step 4 to step 5 determines the figure of merit.

(7) The influence of the various temperature distributions in the appropriate regions of space may be multiplied by the fraction of the total energy contained in that region to provide an estimate of the noise contribution of the primary feed. The result will have the dimensions of an equivalent temperature.

The secondary patterns may be treated in a similar manner.

Temperature Distribution Data

The following table indicates nominal values for the spatial effective noise temperature distributions as a function of frequency. The selected NASA frequency regions are used as a basis. Zenith pointing of the secondary pattern is assumed in the following table. Mean values of the galactic contributions are also assumed.

	$0 < \theta < +62^\circ$	$62^\circ < \theta < 90^\circ$	$90^\circ < \theta < 100^\circ$	$100^\circ < \theta < 180^\circ$
136 Mc	1300°K	290°K	600°K	500°K
400 Mc	30°K	290°K	50°K	30°K
1700 Mc	7°K	290°K	40°K	7°K
4000 Mc	3°K	290°K	40°K	7°K

TABLE III-3

Effective noise temperature spatial distributions for galactic and absorption noise at various selected frequencies.

3.2.4 Typical Evaluation Results

A comparative evaluation of the primary response patterns of the surface-wave feed structure developed during the program and the best available information on other low noise antenna feed systems appeared worthwhile. The technique consists of determining the ratio of the power contained in the spillover region and in the minor-lobes to the total power and relating these values to their appropriate noise temperature distributions. This may be done by re-plotting the pattern in a linear coordinate system and integrating the regions of interest by means of a planimeter as described previously. In re-plotting, it is necessary to make appropriate corrections for the geometry of the illuminated surface. This generally takes the form of a sin θ factor appearing as a multiplier of the original pattern intensity. A computer technique has also been programmed for this integration which enables more rapid evaluation of the patterns and is believed to be of somewhat greater accuracy.

The patterns which have been evaluated by this technique are:

1. The H and E plane patterns for the surface-wave cone structure with sleeve-dipole feed.
2. The H and E-plane patterns for the surface wave cone structure with the circular polarization horn feed.
3. A conventional horn feed.
4. A low noise feed recently reported on by JPL[1], which is a shaped beam feed used with a large paraboloidal dish.

The JPL feed information is presented as an average of the H and E-plane responses. The surface-wave feed information will be given separately for H and E-plane responses and also as an average figure for comparison purposes. The JPL measurements were conducted at 960 and 2388 mc, using an 85 foot paraboloidal reflector with several antenna feed configurations. The published data for the JPL low noise and comparison feed horns have been analyzed and processed in a similar manner to the surface-wave feed patterns.

The integration process for the primary patterns has been divided into several regions to enable a more effective determination to be made of the resulting equivalent noise temperature. Since the sky noise temperature distribution is found to be generally a function of the pointing angle, especially at the higher microwave frequencies, it is desirable to separate the principal

---

1. D. Shuster, C. T. Stelzried and G. S. Levy, "The determination of Noise Temperatures of Large Paraboloidal Antennas", IRE Trans. on Antennas and Propagation, Vol. AP-10, No. 3, May 1962; pp. 286 - 291.

regions of variation. The half-space which the ground represents may be set to a fixed equivalent noise temperature, generally about 250-300°K. The remaining half-space which the antenna "sees" represents the sky noise distribution. The sky distribution has been arbitrarily divided into two regions of interest; the region within about ten degrees of the horizon and the remaining space. This separation results from the sky noise temperature attributed to atmospheric absorption influences and is significantly greater at low pointing angles to the horizon than in the regions near the zenith. The regions under consideration may be summarized as follows as illustrated in Figure 3-9:

1. The region subtended at the primary feed by the secondary aperture. For the designated f/D = 0.42, this region corresponds to $-62^\circ<\theta<+62^\circ$. The angle θ is taken with respect to the primary feed and corresponds to the deviation from the forward axial pointing direction of the primary feed.
2. The region between the secondary surface aperture edge and the horizon corresponding to $62^\circ < \theta < 90^\circ$ and $-62^\circ > \theta > -90^\circ$.
3. The remaining sky region including the zenith at $\theta = 180^\circ$. This region corresponds to $100^\circ < \theta < 180^\circ$ and $-100^\circ > \theta > -180^\circ$.

Temperature distributions which are dependent upon the frequency of operation and certain other factors may be established quite readily for the assigned regions. In this manner a reasonably accurate determination of the theoretical primary feed performance may be made for a given feed pattern. The behavior of the sky temperature as a function of frequency and the other factors involved has been reported on previously in some detail. The section on Environmental Noise Temperature Distribution frequency plots which graphically present the factors influencing noise temperature and its variation with frequency.

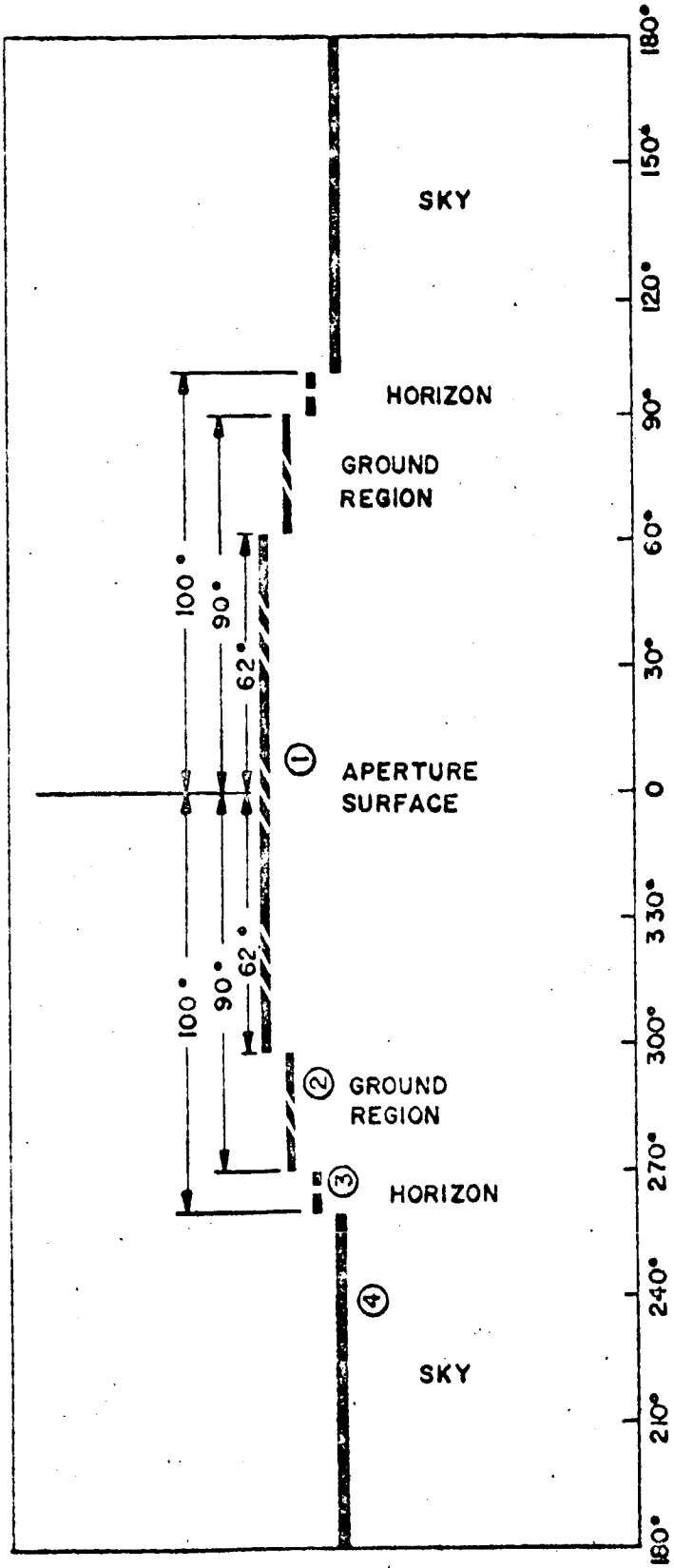

Figure 3-9. Multiple Regions of Integration For Noise Temperature Determination.

It appears desirable to evaluate the general performance of the developed feed structures and to compare this information to available information on other state-of-the-art low noise feed systems. It then appears desirable to set in the appropriate temperature distributions for a given operating frequency and compare the actual low-noise performance of the antenna systems.

A tabulation for the results of the various pattern integrations over the regions of interest is presented in Table III-4. It is interesting to note that both surface-wave cone feed structures indicate average values for the spillover and minor-lobe energy compared to the total energy of about 2.6 percent or better. Comparing this figure to the shaped-beam low-noise feed of JPL which has a combined spillover and minor-lobe average value of about 4.6 percent, we find an improvment factor for the AGA surface-wave primary feed structures of about two to one. This performance corresponds to an improvement over a conventional 10 db horn feed of about five to one. These values are believed to represent true, practically attainable improvement factors for the large paraboloidal antenna configuration. It is important to note that these improvements are obtained by more optimum primary feed design only, and no changes are required of the secondary surface.

Calculation of the antenna equivalent noise temperatures may be accomplished by establishing a frequency of operation for which the sky noise temperature is desired and summing the contributions throughout all space for the integrated pattern responses. Since the JPL data is established for a frequency of 2388 mc which does not differ significantly from one of the NASA operating frequencies, this frequency will be utilized. This should also allow an accurate comparative evaluation of the various feed systems on an equivalent noise temperature basis.

FEED NO.	DESCRIPTION	$0 < \theta < 62°$ PARABOLOID	$62° < \theta < 90°$ GROUND	$90° < \theta < 100°$ HORIZON	$100° < \theta < 180°$ SKY	TOTAL GROUND-SKY
1	CONVENTIONAL HORN	87.6 %	9.8 %	1.1 %	1.5 %	12.4 %
2	SHAPED BEAM HORN	95.4	4.3	0.1	0.2	4.6
3	AGA CONE WITH HORN	97.4	2.1	0.1	0.4	2.6
4	AGA CONE WITH DIPOLE	98.0	1.8	0.1	0.1	2.0

Note: Values shown are for average of both polarizations.

SPATIAL DISTRIBUTION OF FEED ENERGY

Table III-4.

CONTRIBUTING REGION	$0 < \theta < 62°$ PARABOLOID	$62° < \theta < 90°$ GROUND	$90° < \theta < 100°$ HORIZON	$100° < \theta < 180°$ SKY
GALACTIC RADIATION	2°K	—	3°K	4°K
ATMOSPHERIC ABSORBTION	1°K	—	35°K	3°K
GROUND RADIATION	—	240°K	—	—
TOTAL	3°K	240°K	38°K	7°K

Note: Frequency of operation taken as 1Gc. Above results hold for about 1–10Gc.

SPATIAL NOISE TEMPERATURE DISTRIBUTION

Table III-5.

Actually, the equivalent sky noise temperature distribution is reasonably constant in the region from about 2.0 - 2.5 Gc, so the following evaluation should hold for this frequency range.

For the various spatial regions of interest, the following nominal values for the effective noise temperature are taken. This data is believed to represent the best galactic and atmospheric noise evaluation sources available. Table III-5 contains this information in tabular form for the specified spatial regions of interest.

From the information in the previous two Tables, the antenna noise temperature values of Table III-6 are calculated. The average values are used in these calculations, since it is assumed that a signal sensing system such as circular polarization is employed.

Considering a combined contribution due to the scattering of ground energy by the feed supports and transmission line losses equivalent to about 3°K, the values obtained in the latter Table reconcile quite well with the JPL measured equivalent noise temperature value of about 15°K.

Summarizing the preceding determinations including consistent feed support scattering and transmission line losses for all antennas, the results shown in Table III-7 are obtained.

A determination may also be obtained of the noise temperature characteristics of an antenna from the nature of its secondary pattern. This may be accomplished for most of the microwave region with reasonable accuracy by considering the predominant degrading factor, the minor-lobe energy intercepting the ground region, and the corresponding temperature distribution. The temperature distribution for the ground may be generally assumed constant and of a value equal to either 300°K

FEED NO.	DESCRIPTION	$0<\theta<62°$ PARABOLOID	$62°<\theta<90°$ GROUND	$90<\theta<100°$ HORIZON	$100°<\theta<180°$ SKY	TOTAL GROUND-SKY
1	CONVENTIONAL HORN	2.6°K	24°K	0.4°K	0.1°K	~27°K
2	SHAPED BEAM FEED	2.9°K	10°K	.04°K	.01°K	~13°K
3	AGA CONE WITH HORN	2.9°K	5.0°K	.04°K	.03°K	~8°K
4	AGA CONE WITH DIPOLE	2.9°K	4.3°K	.04°K	.01°K	~7°K

SPATIAL CONTRIBUTIONS TO ANTENNA TEMPERATURE

Table III-6.

FEED NO.	DESCRIPTION	CALCULATED NOISE TEMP.	FEED SUPPORT, TRANS. LINE, ETC	TOTAL EQUIV. NOISE TEMP.
1	CONVENTIONAL HORN	27°K	3°K	~30°K
2	SHAPED BEAM FEED	13°K	3°K	~16°K
3	AGA CONE WITH HORN	8°K	3°K	~11°K
4	AGA CONE WITH DIPOLE	7°K	3°K	~10°K

SUMMARY OF ANTENNA EQUIVALENT NOISE TEMPERATURE RESULTS

Table III-7.

as is often assumed in the literature, or about 250°K which includes a ground emissivity factor and is probably more realistic. For an isotropic antenna, the antenna noise temperature contribution would be the fraction of the antenna energy intercepting the ground multiplied by the assumed ground temperature. In this case, a resulting value of about 125 - 150°K. For decreased average back-lobe levels, the corresponding antenna noise temperature will also be decreased.

Figure 3-10 is a plot showing the antenna noise temperature contributions due to an average back-lobe level, $\bar{G}_{BL}$, intercepting the ground region. The two linear plots represent the two conditions of ground temperature which were noted to be functions of the ground emissivity.

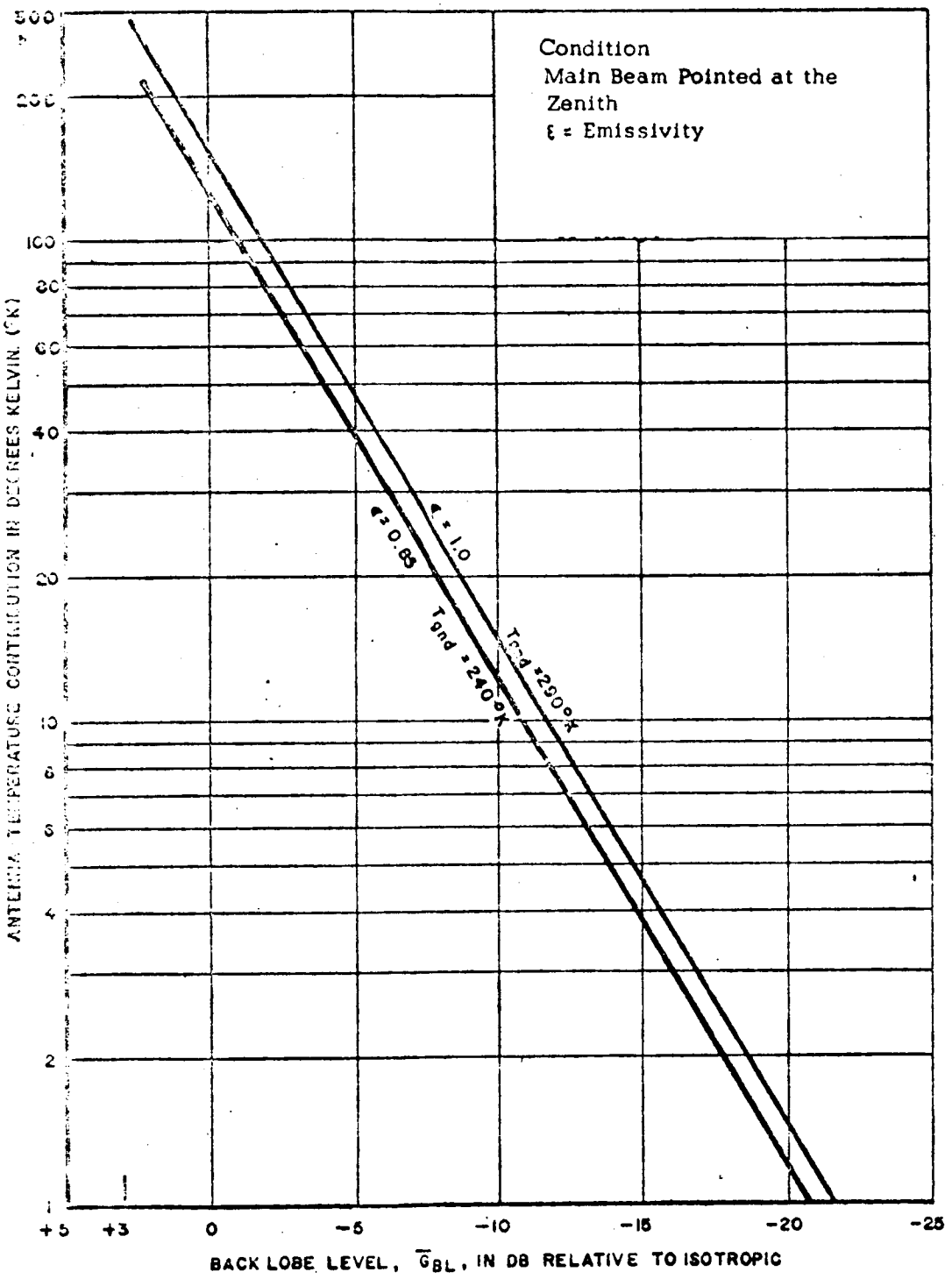

Figure 3-10. Antenna Noise Temperature Contributions Calculated From Average Back-Lobe Level ($\bar{G}_{BL}$).

3.2.5 Low Noise Evaluation of NASA 85 Foot Paraboloidal Reflectors

The secondary patterns for a typical antenna system of the large paraboloidal reflector type employed by NASA were not available, therefore an evaluation was made based on the reasonably well-defined characteristics of the feed system primary patterns. Assuming an approximately cosine form of illumination distribution across the aperture and a ten db taper level at the aperture edge, we find by pattern integration techniques that the fraction of feed energy lost as spillover is about 0.22. Combining this with an average ground temperature, including the ground emissivity factor, of about 250°K, we find a resulting noise contribution due to spillover in the ground region of about 55°K. We should add to this figure the noise degradation due to energy losses in the feed supports, of nominally ten degrees, for a total reasonably frequency independent noise contribution of about 65°K.

The environmental contributions from the main beam must also be considered which for the four principal NASA frequency ranges of interest may be described as follows:

At 136 Mc, the galactic noise contribution of about 600°K combines with the previous contribution for an average equivalent antenna noise temperature of about 660°K.

At 400 Mc, the galactic contributions are considerably reduced to a value of about 30-50° Kelvin. Hence, a nominal antenna noise temperature value of about 100°K may be expected.

At both the 1.7 Gc and the 4.1 Gc frequency ranges, the environmental noise contribution is due primarily to atmospheric absorption and, at Zenith, is quite small, about 3-4° Kelvin. Therefore, the resulting effective antenna noise temperature for these conditions is about 70° Kelvin.

These estimates are approximations to the true conditions and neglect certain factors of varying importance. As reasonable approximation to the actual antenna noise temperatures, the presented estimates are believed to be realistic and generally valid for the conditions specified.

IV SHAPED BEAM FEED APPROACHES

4.1 General Considerations

Physical considerations which have been elaborated upon previously, dictate that for maximum aperture efficiency corresponding to maximum gain and minimal spillover energy, the secondary reflector illumination should appear ideally as a pie-shaped response on a polar plot. Neglecting the space attenuation effects between feed and reflector, this requires essentially a primary feed system providing uniform illumination over most of the solid angle intercepted by the secondary surface and a rapid response taper with angle in the region of the reflector edge. This type of illumination is in distinct contrast with the gradual energy taper from the aperture center associated with primary illuminations which provide low values of side-lobe energy in the region of the main beam.

The minor-lobe energy which is separated considerably from the main beam provides the principal means for ground radiation to enter the antenna and generally results in significant noise temperature degradation of the antenna system. Hence, the "far out" minor-lobe levels must be suppressed at the expense of increasing the "near in" side-lobe levels if a minimization of the antenna noise temperature contributions due to ground radiation is to be realized. The evaluation of a low noise antenna should then be based to a considerable degree, upon a careful examination of the far out side-lobe response characteristics of the antenna.

Figure 4-1 illustrates the primary pattern beam shaping approach taken. The conventional horn feed in this illustration may be seen to have a rather gradual decrease in energy with angle of departure from the center of the feed pattern resembling a cosine or cosine squared primary response. The shaded area of the primary pattern indicates the energy contained in the feed illumination which does not intercept the secondary aperture. The energy which is not effectively utilized in illuminating the secondary aperture results in rather large spillover lobes and in a degradation of the antenna system aperture efficiency and maximum gain. The ideal feed illumination shown in the center plot consists of a uniform illumination over the angular extent of the secondary sperture decreasing to a value of zero at the aperture edge. The ideal feed illumination results in a reasonably constant illumination over the secondary aperture surface and hence the familiar uniformly illuminated circular aperture secondary pattern would be obtained which corresponds to the maximum gain condition for the antenna.

It may be worthwhile to briefly discuss certain of the important characteristics of the far field patterns for a constant illumination ideal primary pattern such as that illustrated in the center figure. In particular, the relative levels of the near inside lobes and the rate of decrease of the minor lobe energy are desired. The secondary pattern in the far field for constant illumination of a paraboloidal aperture of circular symmetry may be written as simply the product of the aperture area and the first order Lambda function, or expressed in terms of the field as

$$g(u) = \pi a^2 \Lambda_1(u)$$

which in terms of the power response may be written as simply

$$p(u) = F(a) \left[\Lambda_1(u)\right]^2$$

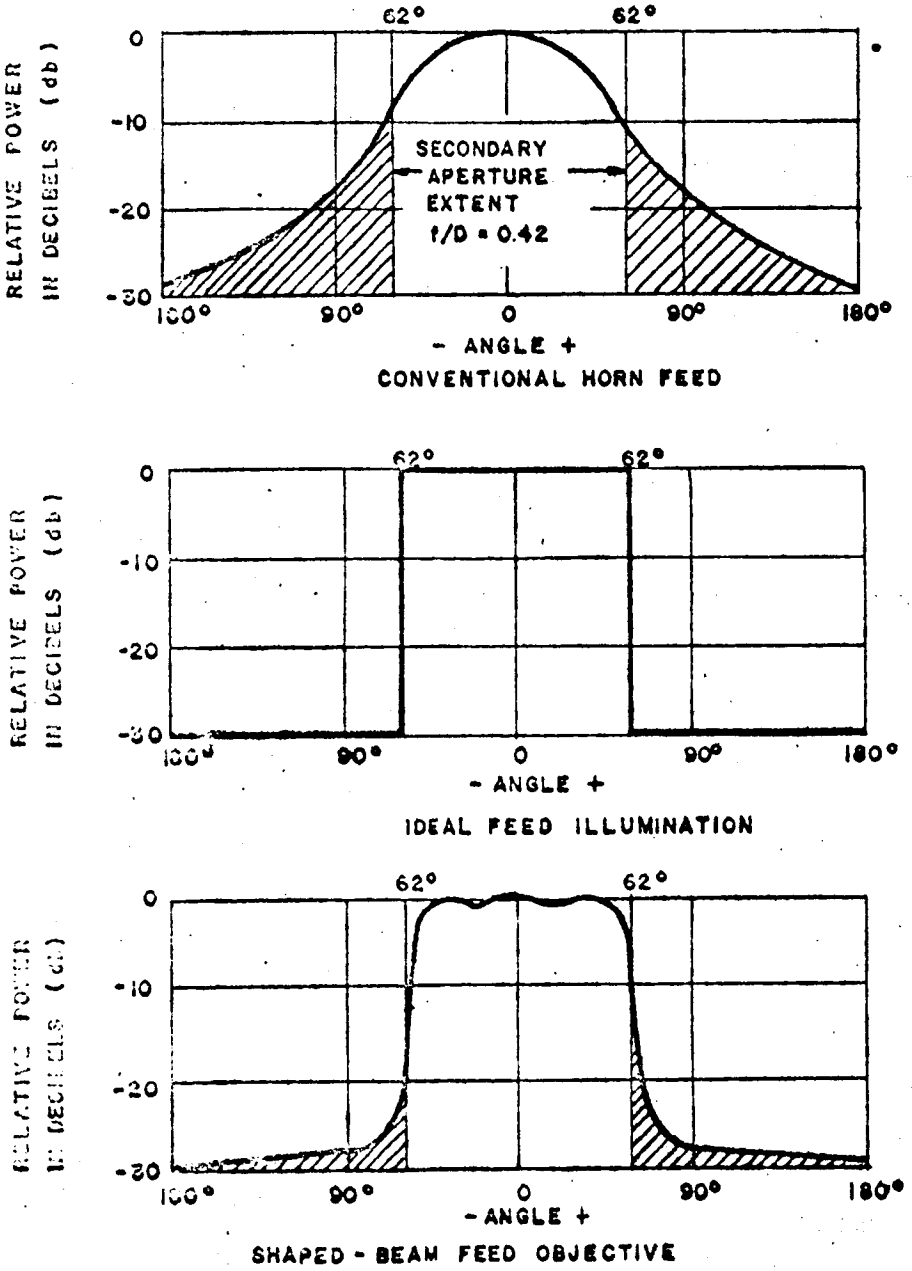

Figure 4-1. Shaped Beam Primary Pattern Approaches.

The argument, u, represents the departure from the axis of symmetry of the paraboloidal surface in terms of the aperture dimension in wavelengths and the sine of the angle of departure, θ. This relation is written as

$$u = \frac{D}{\lambda} \pi \sin \theta .$$

More conventionally this relation is given as the square of twice the product of the aperture area and the first order Bessel function divided by the argument, or as

$$p(u) = \left[\frac{\pi D}{\lambda} \frac{J_1(u)}{u}\right]^2$$

which may be recognized as a rapidly converging expression in the argument. Pattern characteristics for the uniformly illuminated circular aperture have been worked out by Silver[2] and others. It is found that the first side-lobe is down about 17 db from the main lobe, the second side-lobe about 24 db below the main lobe, and all others over 30 db below the main beam. For space tracking and communications applications, these relatively high minor lobe levels appear to be quite acceptable.

The ideal primary illumination characteristic described in the figure results in 100 percent aperture efficiency and maximum gain at the expense of an acceptable increase in the side-lobe levels near the main beam. However, it is apparent that the actual primary pattern obtained by any practical feed shaping approach must have a finite illumination taper at the aperture edge, since we are naturally concerned only with feeds of reasonable physical extent, and are not concerned with the actual

---

2. S. Silver, "Microwave Antenna Theory and Design", McGraw-Hill Book Co., Inc., New York, 1949, pp. 192-195.

or approximate limiting condition of aperture to wavelength ratios approaching infinity or of even very large values. With a primary feed of reasonable size a gradual illumination taper at the aperture edge will be required. The pattern also will not be uniform but will contain minor deviations from uniformity within the angular extent of the secondary aperture. The important considerations are to greatly reduce spillover in the region not containing the secondary aperture and to provide reasonably uniform illumination over the aperture surface by means of a moderately sized primary feed. The shaped beam feed objective plot illustrates these desirable features more realistically presented.

4.2 Dielectric Lens Feed

4.2.1 Aperture - Illumination - Slope Relations

Initially the dielectric lens feed design was directed toward obtaining wedge shaped patterns having a slope of approximately one db per degree at the aperture edge with beamwidths on the order of approximately 100 - 120 degrees at the 10 db points. Several different techniques were investigated, all of which depended upon an increase in the size of the feed structure in order to obtain the increased beam slope at the aperture edge. Several general techniques which appeared appropriate might be reviewed. These techniques included the following:

1. Endfire radiators.
2. Aperture type radiators.
3. Hybrid systems (for example: corner reflectors)

For the aperture type antenna, the simplest configuration might possibly be a Luneberg Lens with an extended feed system. A single feed on the lens produces a good beam slope and a combination of several feeds arranged to provide the desired

beam slope at the edges and maintain a pattern without nulls over the region of interest appeared to be a feasible approach. Another aperture technique involves a single feed with a shaped dielectric lens. The purpose of the lens is to divert energy from the center of the beam into the regions at either side of the beam. In this manner a reasonably uniform illumination pattern appeared attainable. A reasonably rapid illumination taper at the aperture edge should be possible if the horn illuminating the lens has desirable characteristics. Hybrid feed systems were of interest at the longer wavelengths in particular. It appeared that a simple endfire feed system, possibly a dipole element, might be combined with either a reflecting surface or a surface wave structure to obtain the desired primary radiation pattern.

4.2.2 Experimental Results

Several primary feed systems consisting of sectoral horns and dielectric lens configurations were fabricated and experimentally tested. Figure 4-2 illustrates a shaped lens feed pattern in which the reflector is nearly uniformly illuminated while the reasonably sharp illumination taper at the edges tend to reduce spillover. This horn lens system was designed for a 10 db beamwidth of about 130 degrees. In order to obtain far-field patterns for this and other feeds under investigation, a paraboloidal cylinder reflector was constructed. Figure 4-3 illustrates the paraboloidal cylinder with the H-plane sectoral horn feed with dielectric lens in place. Secondary patterns taken by means of this arrangement indicate a considerable improvement in the level of the minor lobes formed by the spillover energy for the lens system compared to the conventional horn feed.

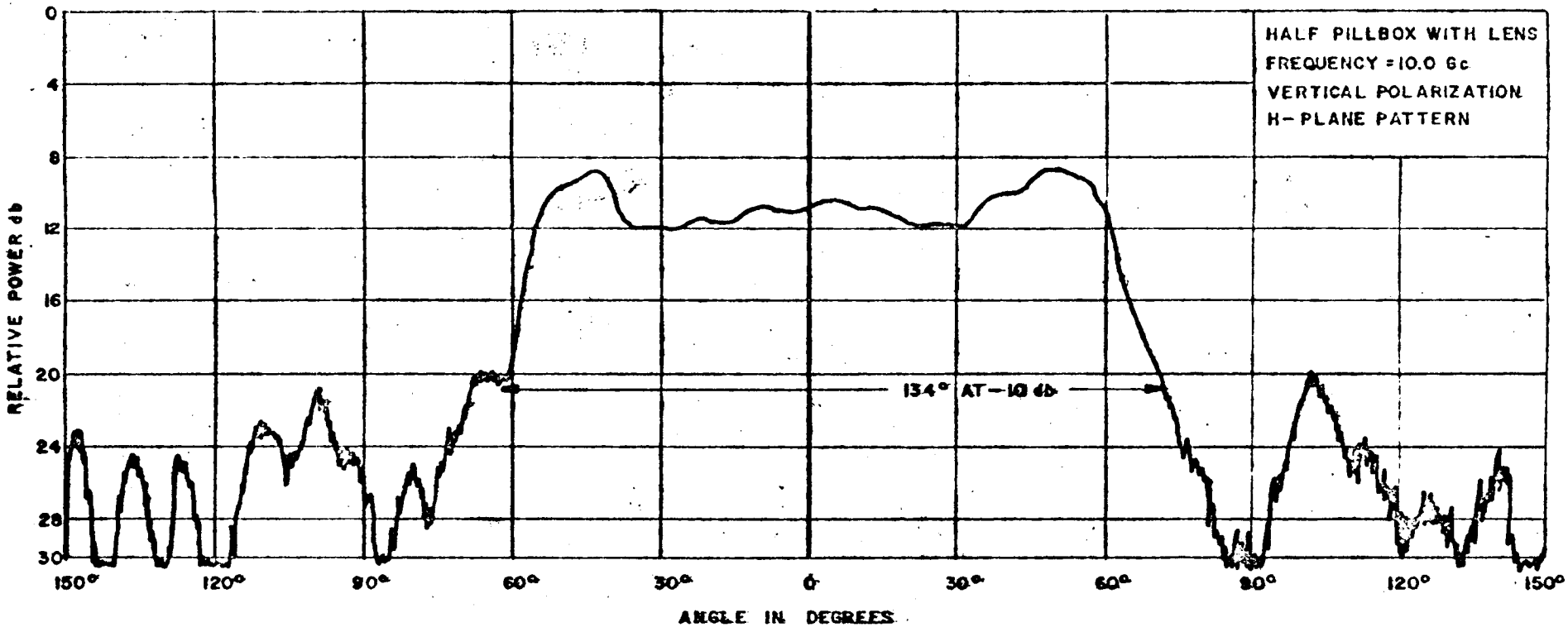

Figure 4-2. Sectoral Horn With Lens Primary Pattern.

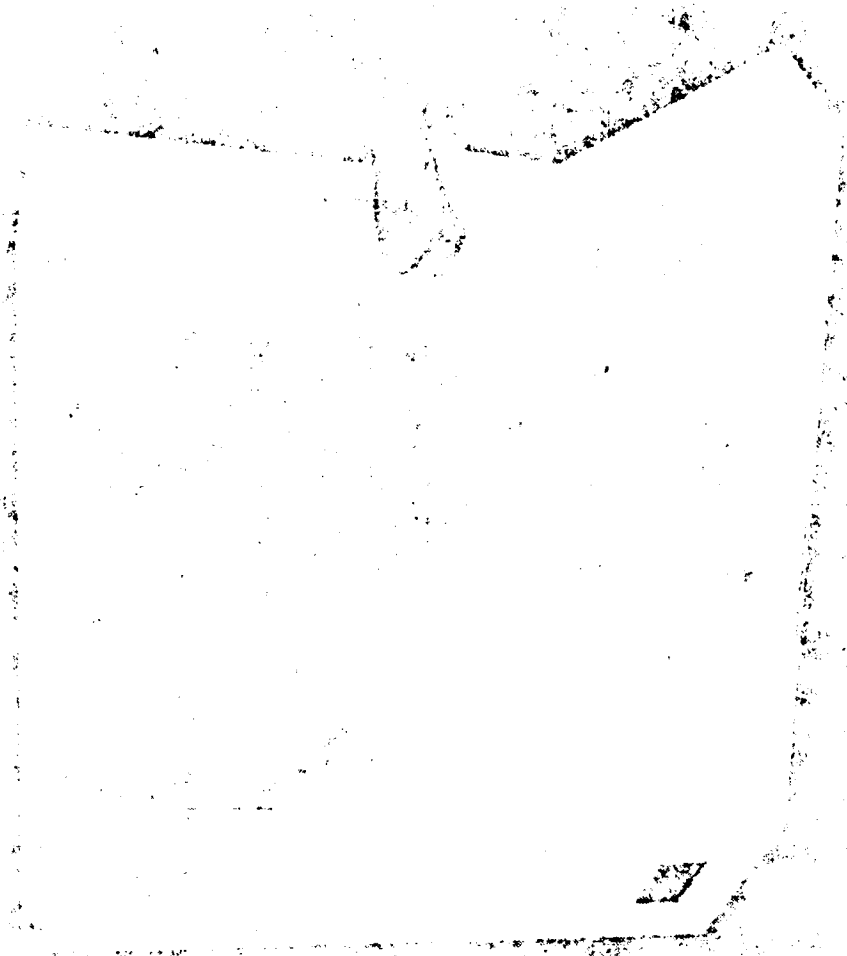

It should be mentioned that at all times during the program an attempt was made to develop feeds which would operate effectively in a circularly symmetric configuration. Evaluation of the various linear polarization feed system under experimentation was continually made in order to determine the operational characteristics of the feed as a function of polarization, loss characteristics, physical size, and other factors of importance. The early experimental effort utilized linear polarization feed structures due to the fabrication simplicity of these configurations coupled with the general validity of measurements made on these feeds at both polarizations in determining their circular polarization characteristics.

Various other dielectric lens feed systems were fabricated and experimental measurements taken. The principal horn lens structure employed in the program was a half-pillbox feed with a dielectric lens and a single waveguide input. This same configuration was modified for a dual waveguide input in order to simulate monopulse operation of this feed system. Figure 4-4 illustrates two of the waveguide primary feeds employed. One of these waveguides is simply an open guide; the other is tapered at the waveguide exit and contains a beam broadening post in its aperture. The latter feed system has a very broad beam energy distribution and effectively illuminates the entire extent of the dielectric lens surface. Figure 4-5 is a photograph showing the half-pillbox primary feed with dielectric lens. Figure 4-6 illustrates the same dielectric lens structure fed by means of a dual waveguide system simulating monopulse operation. The comparison horns to which the half-pillbox dielectric lens and paraboloidal cylinder reflector were compared are shown in Figure 4-7.. The primary pattern for the Sperry 56X1 standard gain horn is shown as Figure 4-8..

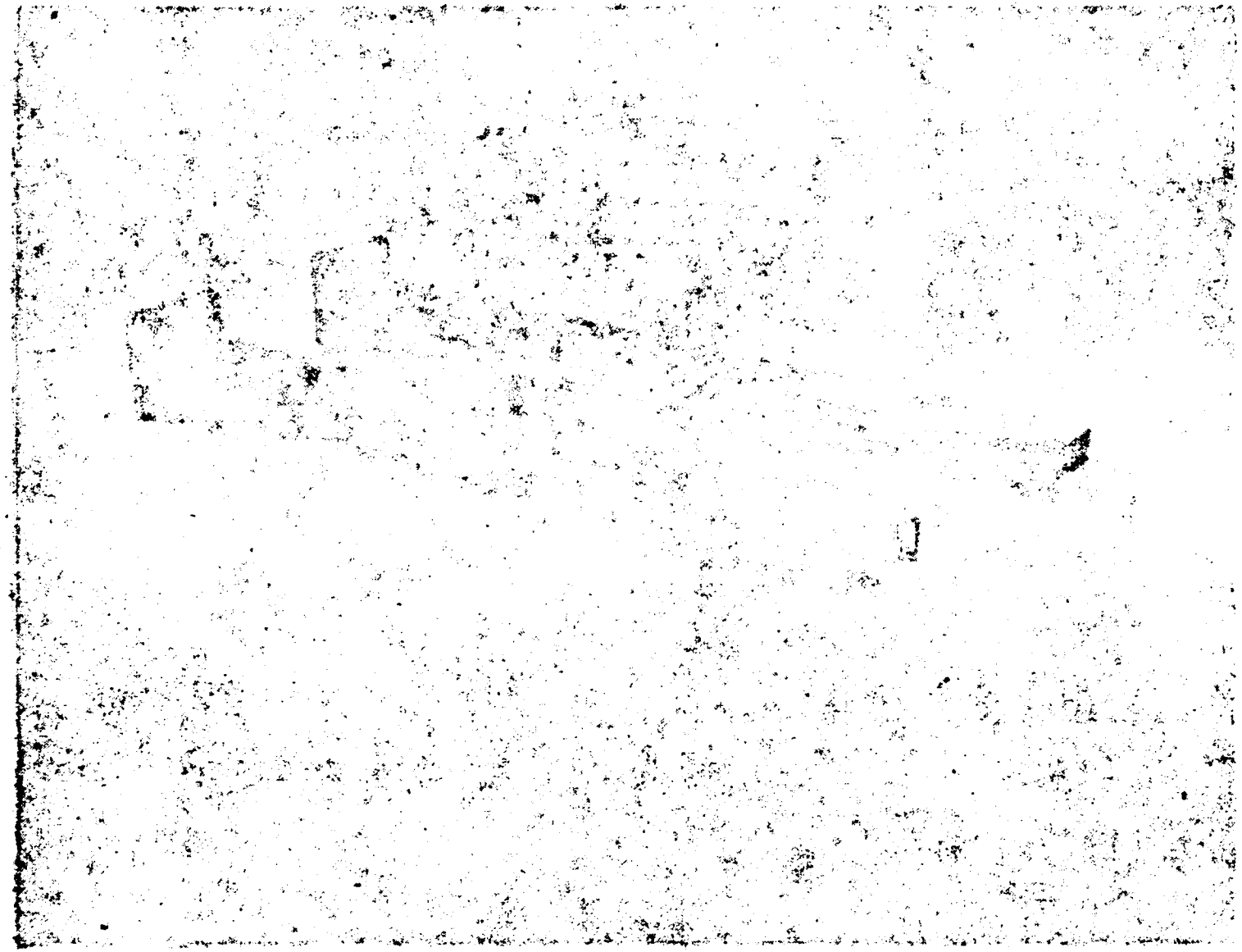

Figure 4-4. Open and Modified Open Waveguide Primary Feeds.

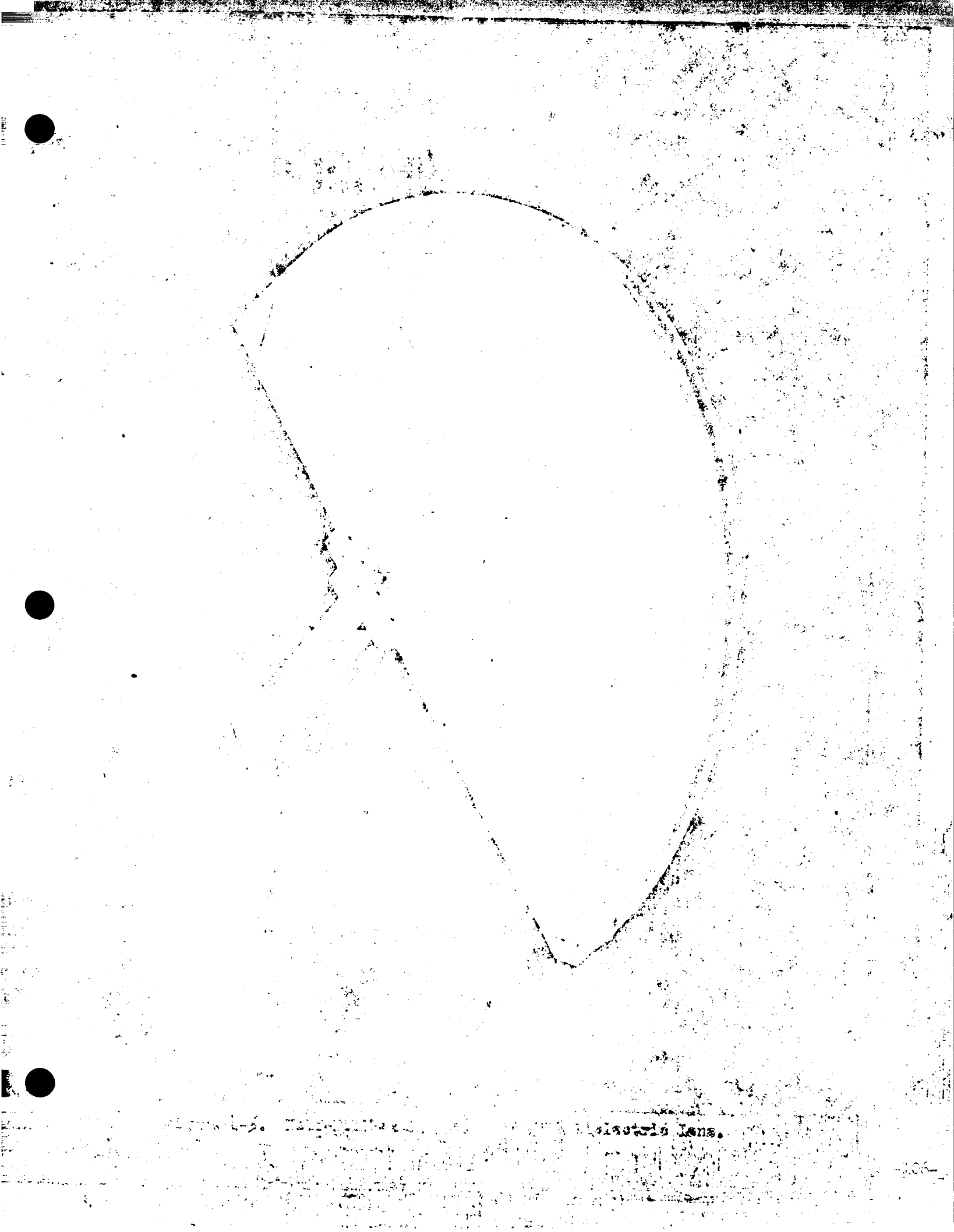

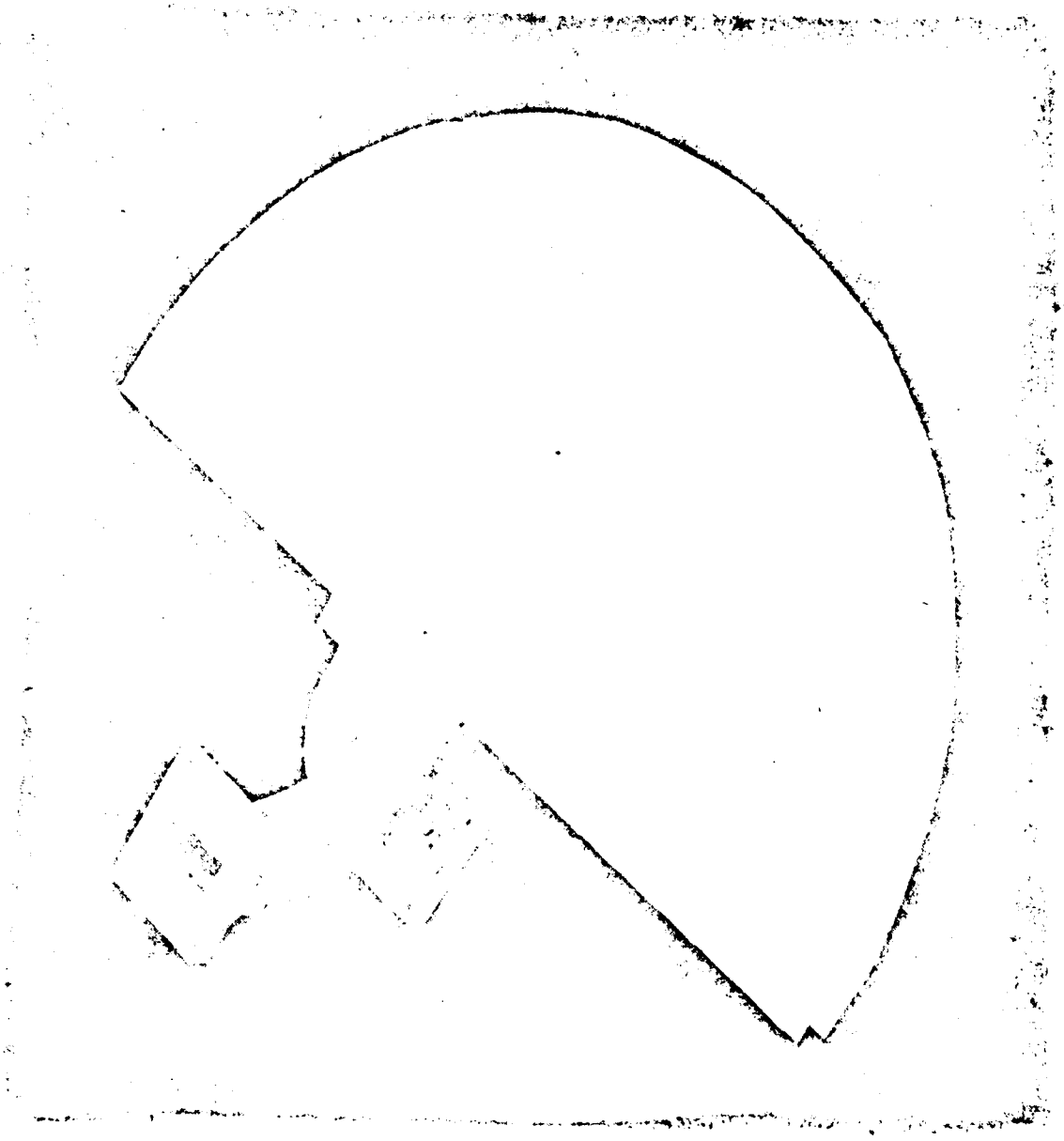

Figure 4-6. Half-Pillbox Primary Feed With Dielectric Lens In Monopulse Configuration.

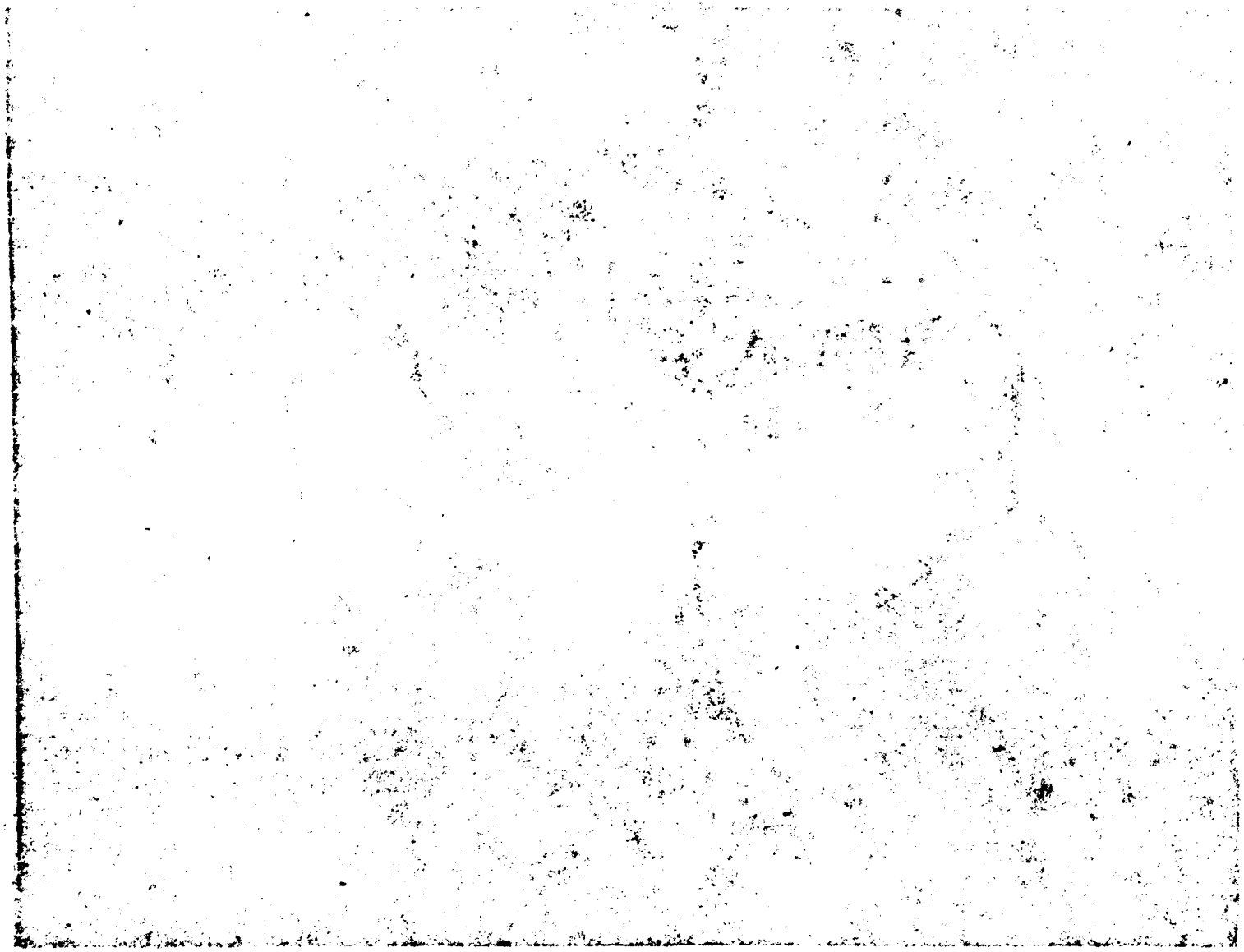

Figure 4-7. Flared Horn and Standard Gain Horn Primary Feeds.

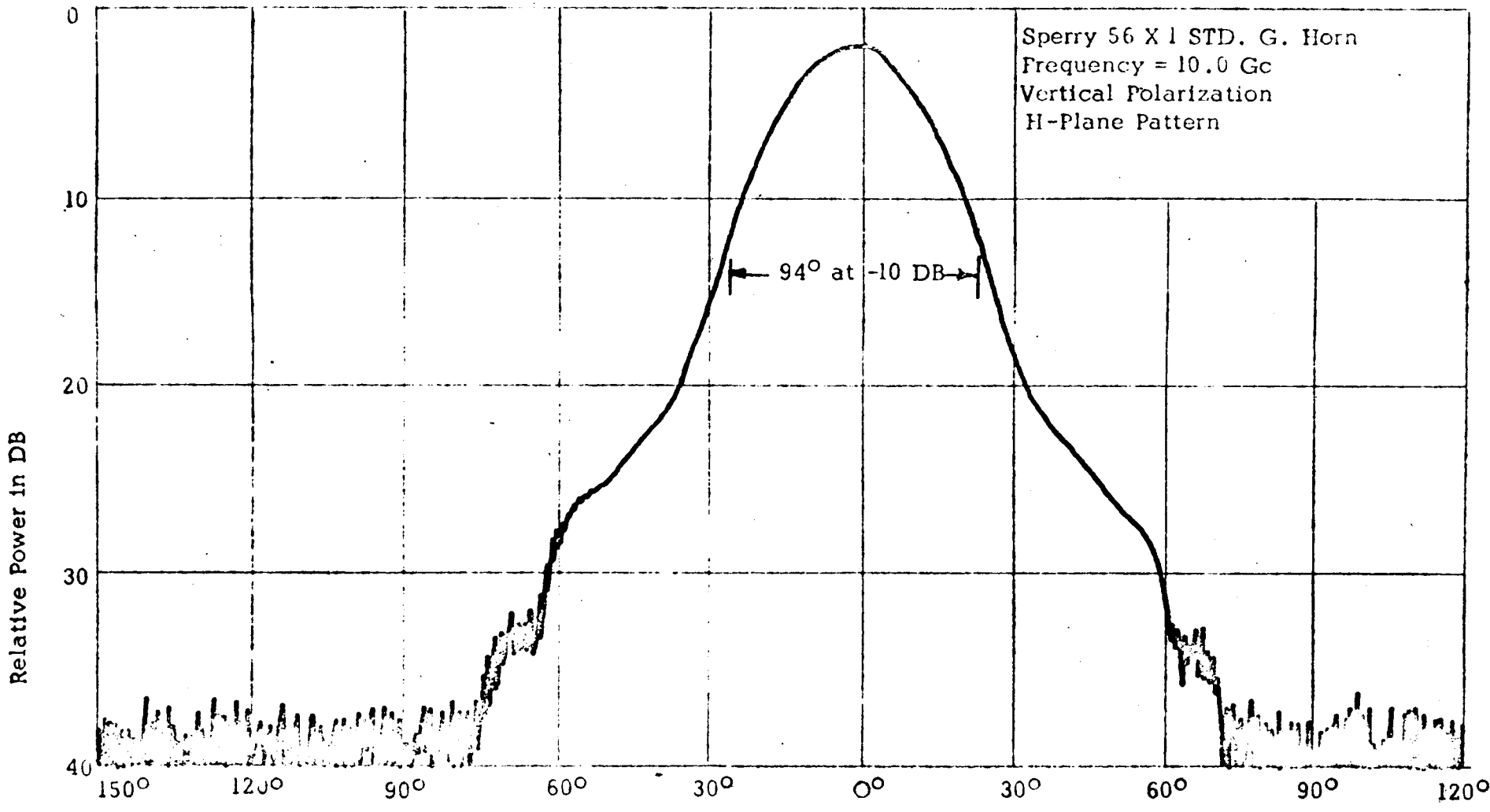

Figure 4-8. Standard Gain Horn (Sperry 56 X 1) Primary Pattern.

The coordinate geometry which has been employed in describing the primary pattern measurements and polarization orientations is given in Figure 4-9.. A similar pattern coordinate system geometry illustration but for secondary patterns is presented as Figure 4-10. In order to enable operation of the feed system with circular polarization, two open circular waveguide primary feeds were utilized; their measured primary patterns are presented as Figures 4-11 and 4-12. The primary pattern for the shorter of these two open circular waveguide feeds is shown in the latter figure.

Measurements taken for the half-pillbox feed system with the best obtainable illumination of the lens structure by the illuminating waveguide was found to offer promising results initially. These results are indicated by the primary pattern for the half-pillbox feed system using dielectric lens shown in Figure 4-13. Considerable difficulty was encountered in the experimental attempts to obtain desirable primary patterns from the same half-pillbox feed system operated in a monopulse configuration. Figure 4-14. illustrates a primary pattern for the half-pillbox feed system simulating a monopulse configuration and it is apparent that there is considerable assymetry in the response.

The primary pattern measurements of the various feed systems indicate several interesting features. The measurements were made initially as H-plane patterns for vertical polarization of the feed system using the feeds as receiving elements. The effect of the pin in the waveguide aperture for the illuminating waveguide employed with the dielectric lens structure was found to have a very marked influence. The open rectangular waveguide does not appear to be very desirable as a feed illumination method since the minor lobe energy level is quite high. The open waveguide illuminating feed containing a post in its aperture was found to provide

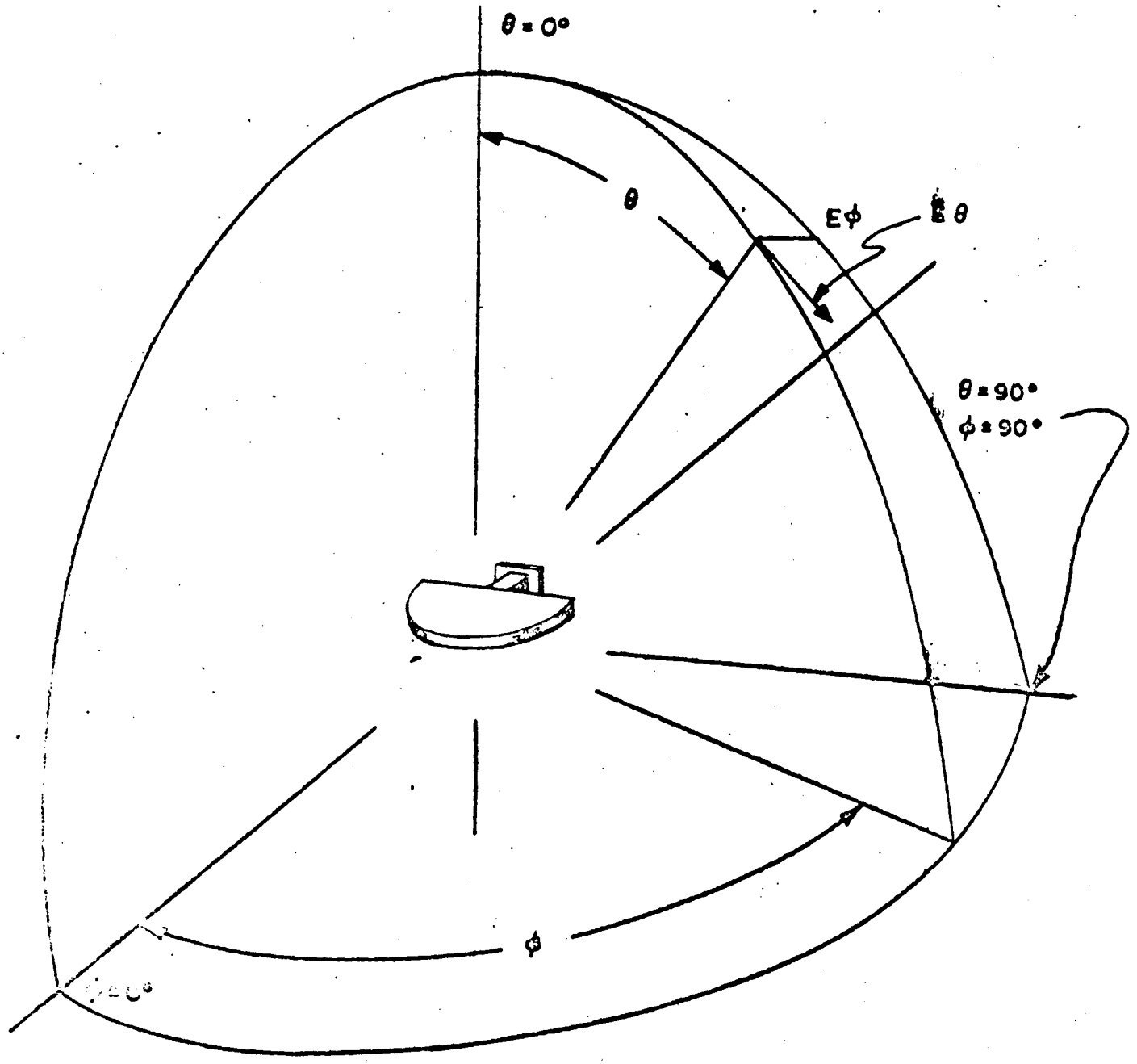

Figure 4-9. Coordinate Geometry For Primary Pattern Measurements.

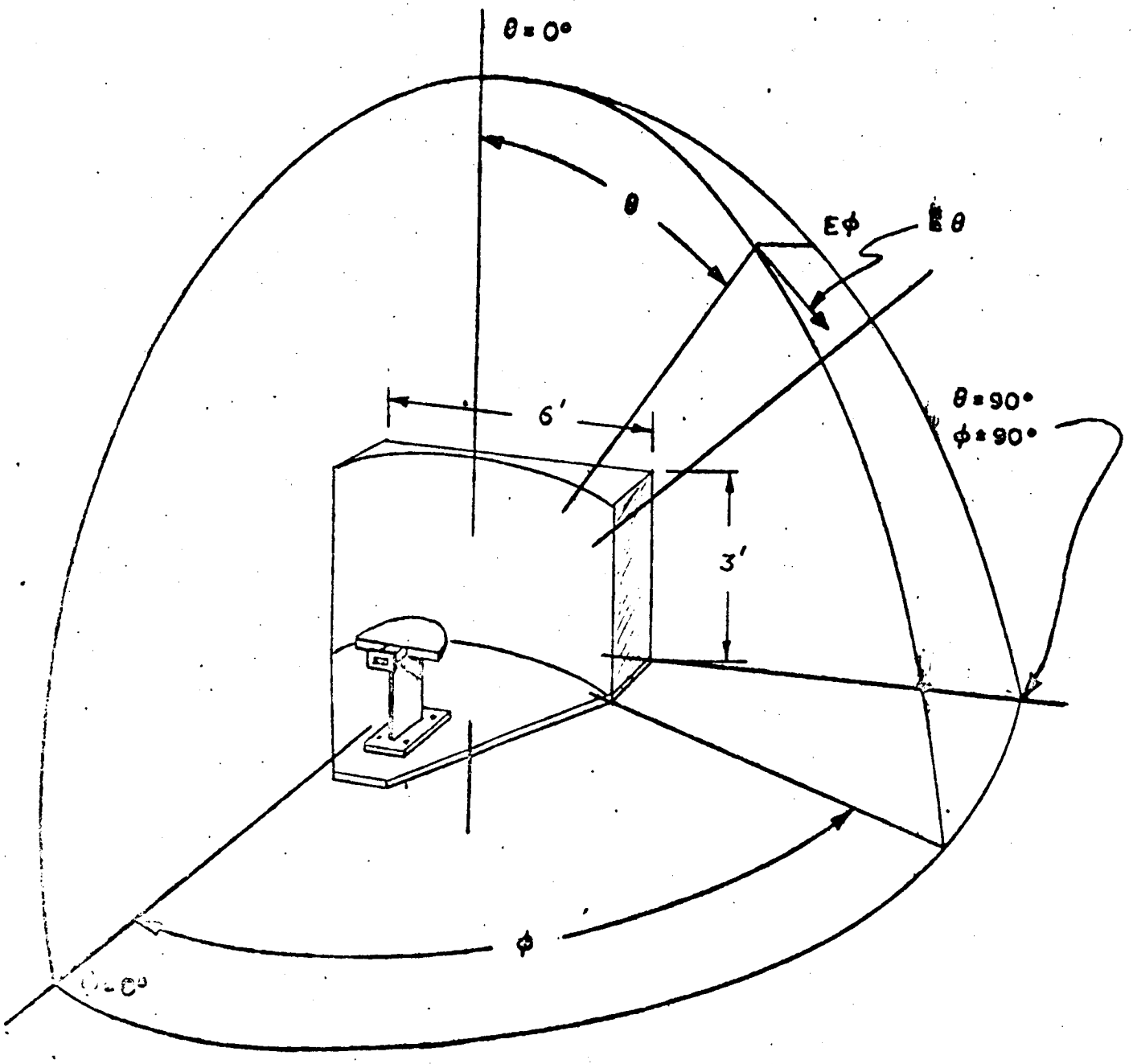

Figure 4-10. Coordinate Geometry For Secondary Pattern Measurements.

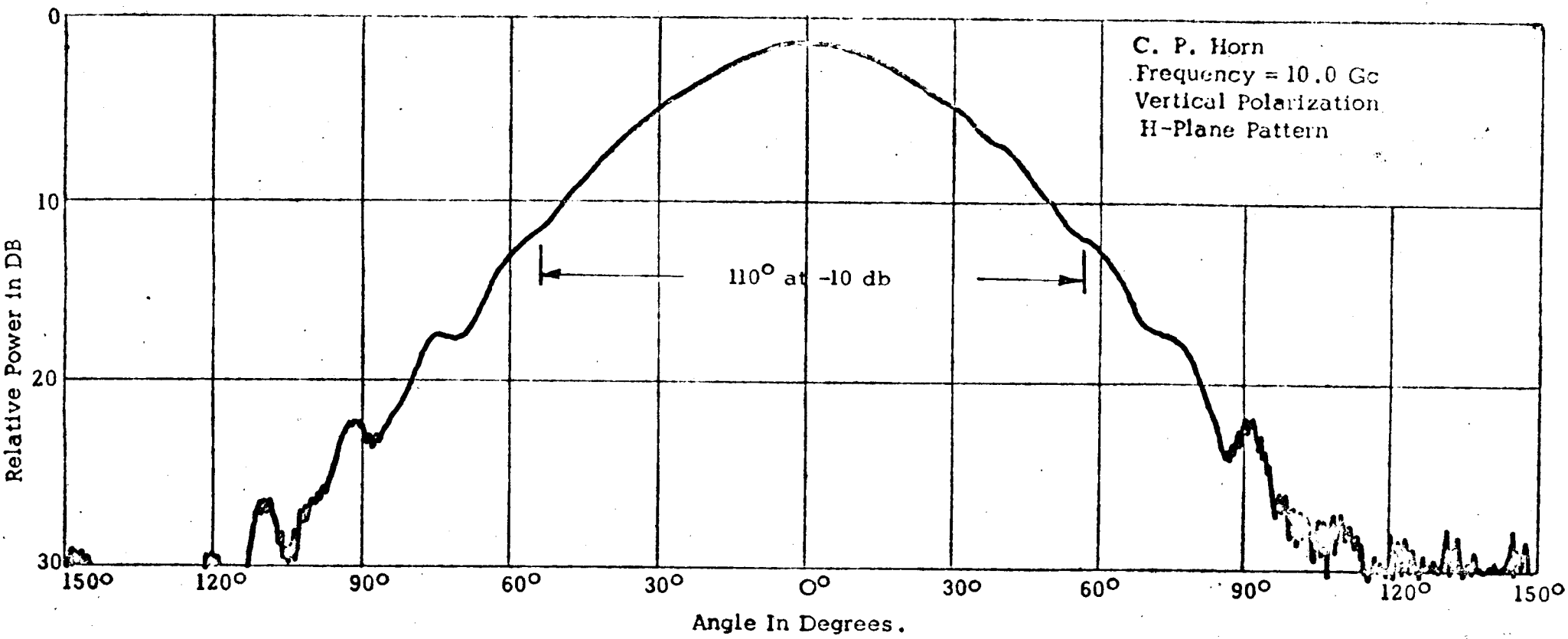

Figure 4-11. Open Circular Waveguide Feed Primary Pattern.

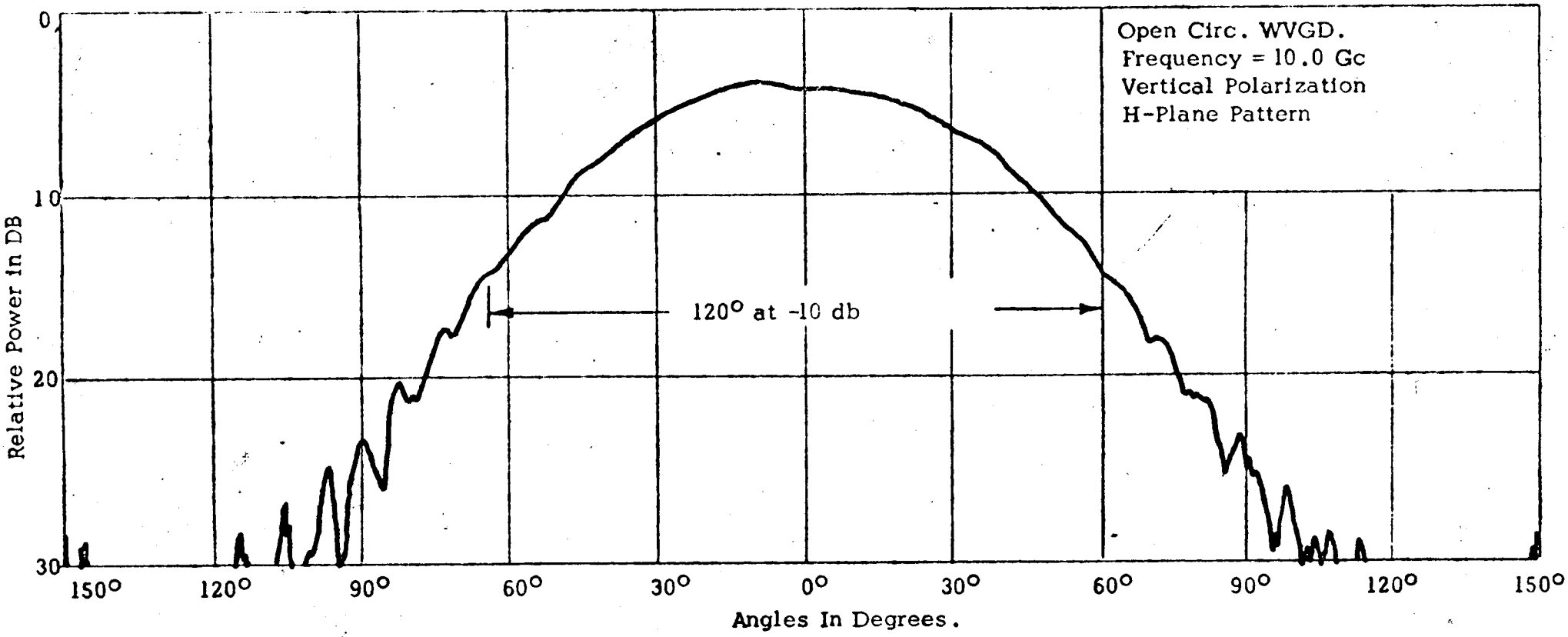

Figure 4-12. Open Circular Waveguide Feed Primary Pattern.

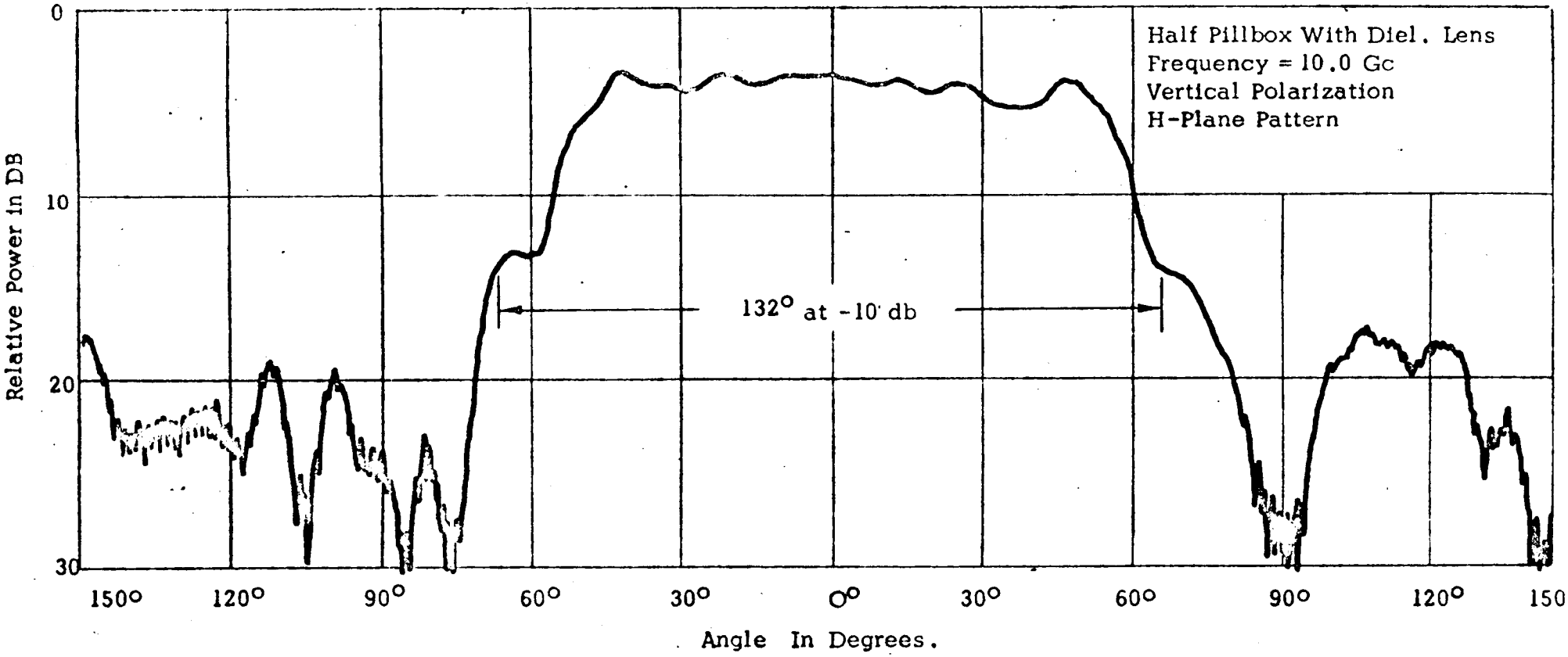

Figure 4-13. Half-Pillbox With Dielectric Lens Feed Primary Pattern.

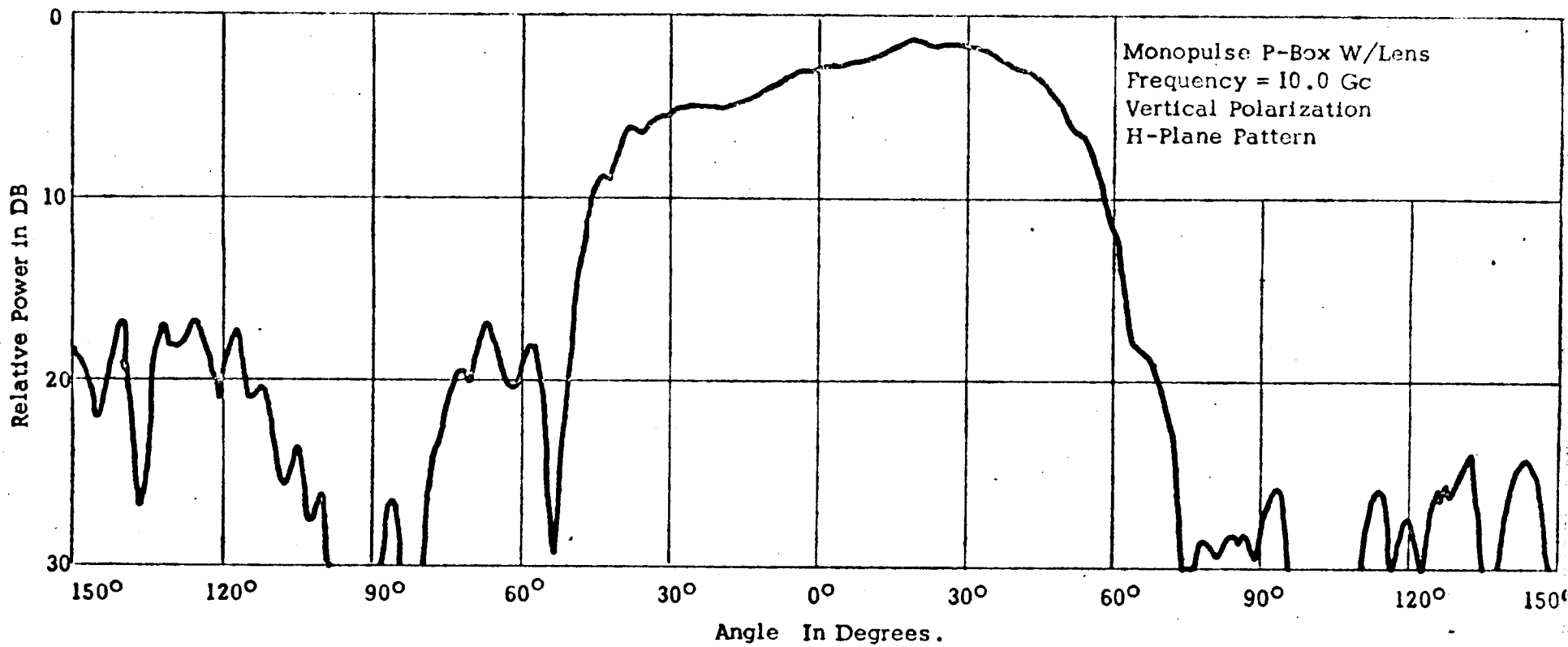

Figure 4-14. Half-Pillbox With Dielectric Lens Feed Primary Pattern For Monopulse Configuration.

good performance as a broad beam feed in illuminating the lens structure as well as in other primary feed applications. The primary pattern for sectoral horn flared in the H-plane, illustrated as Figure 4-15, , closely resembles a typical horn feed pattern with the exception that the side lobe energy is relatively high. The primary patterns obtained from open circular waveguide are very similar, as may be noted in Figures 4-11,12. The difference between the two feed structures appears principally as a beamwidth variation related to the internal dimensions of the waveguide employed which directly relates to the effective illuminating aperture. The side and back lobe energy from the circular polarization feeds is seen to be very low. For this reason some secondary patterns were taken using the circular polarization waveguide feed since it is believed that the low values of side and back-lobe energy levels would enable a good representation of the far-field patterns obtainable from a primary feed having approximately a 10 db beamwidth at the reflector aperture edge.

The primary patterns for the half-pillbox feed system with a dielectric lens was one of the first attempts at obtaining a reasonably constant illumination level over the physical aperture involved and of achieving a very rapid taper in the illumination pattern toward the edges of the reflector. The primary patterns for the half-pillbox feed systems illustrate that the energy distribution is indeed reasonably constant over the aperture; however, the illumination taper in the region of the aperture edge is not as sharply formed as desired. Also, it appears that the side and back-lobe energy is at a higher level than desired and some means appear necessary for reducing this level. The assymmetry shown in the monopulse configuration for the dielectric lens feed structure appears to be due primarily to the off-axis entrance into the feed structure of the waveguide

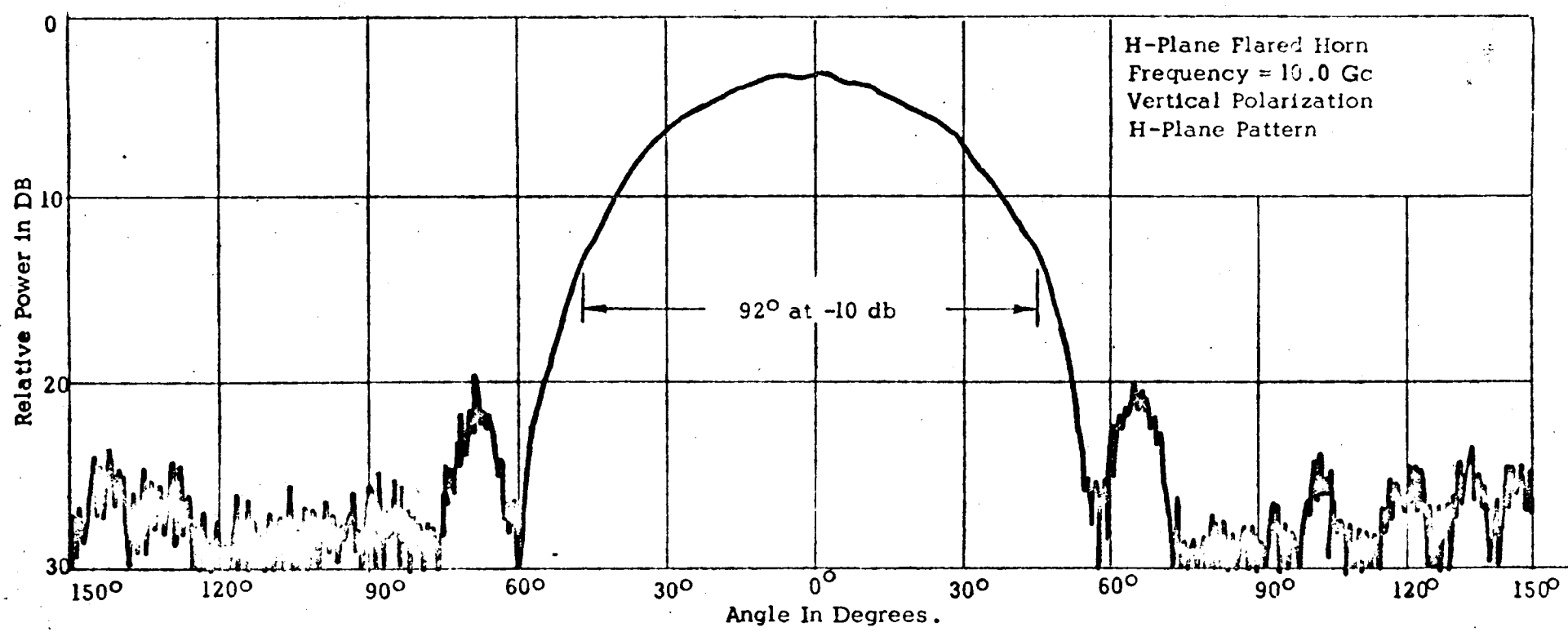

Figure 4-15. Sectoral Horn Flared In H-Plane Primary Pattern.

illuminating aperture.

4.2.3 Evaluation of Technique

The secondary patterns which were taken for both representative primary feed horn systems and the half-pillbox dielectric lens feed systems indicate significant improvements attainable by the use of dielectric lens configurations. The aperture angle required to be subtended by the primary feed for the f/D ratio of 0.42 established from the NASA 85 foot paraboloidal reflector geometry is approximately 124 degrees. This is quite a large beamwidth for reasonably uniform illumination to be required and it certainly appears that the dielectric lens technique offers some merit in meeting this requirement, especially for linear polarization. The principal objections which were found to this feed arrangement are in the primary pattern "ears" located approximately 8-10 db below the mid-beam average level at each extremity of the main beam. This effect was found to be difficult to correct and is possibly associated with the mode configuration and the scattering properties of the half-pillbox geometry and dielectric material. The additional disadvantage in the measured dielectric lens patterns of a reasonably high minor lobe energy distribution also caused some concern. For this reason the dielectric techniques employed within a pillbox were set aside in order to pursue possibly more advantageous means for obtaining the desired primary pattern illumination.

4.2.4 Dielectric Loss Noise Considerations

The use of dielectric materials as a surface wave mechanism to "trap" or redistribute part of the radiation field energy appears to be a worthwhile technique for certain primary feed applications. A significant improvement in the primary response pattern characteristics for a class of feed systems for use in low noise antenna applications has been experimentally noted. However, the use of dielectric materials in an antenna feed design for low noise application should be evaluated thoroughly to determine the extent of degradation in the effective antenna noise temperature due to the loss characteristics of the dielectric material. To this end, a determination follows of the ratio of the energy losses due to the properties of the dielectric employed to the total signal energy available at the antenna terminals. From this information a reasonably accurate indication may be obtained for the effective noise temperature degradation due to the dielectric loss properties.

Consider the amplitude of the received energy in the neighborhood of the antenna as having a simple periodic form represented by

$$E = E_o \cos \omega t,$$

where E_o is independent of time and $\omega/2\pi$ is the signal frequency. If a field of this nature has existed for a long duration compared to the polarization inertia time for the dielectric material, then the amplitude of the electric displacement, D, will be periodic in time. However, in general, D will not necessarily be in phase with E, but may show a phase shift, ϕ, expressed by

$$D = D_o \cos (\omega t - \phi)$$

$$D = D_o \cos \omega t \cos\phi + D_o \sin \omega t \sin \phi;$$

and setting

$$D_1 = D_o \cos \phi \text{ and } D_2 = D_o \sin \phi$$

we obtain,

$$D = D_1 \cos \omega t + D_2 \sin \omega t.$$

The ratio D_o/E_o usually depends upon frequency, hence for a given dielectric material it is necessary in general to use two differing dielectric constants to express its properties, i.e.,

$$D_1 = \varepsilon_1 E_o \quad \text{and} \quad D_2 = \varepsilon_2 E_o$$

Therefore we may write:

$$\frac{D_2}{D_1} = \frac{D_o \sin \phi}{D_o \cos \phi} = \tan \phi$$

hence,

$$\tan \phi = E_2/\varepsilon_1$$

The dielectric constant may be written in complex form as;

$$\varepsilon = \varepsilon_1 + j\varepsilon_2$$

Using exponential notation for the field, we have:

$$E = E_o e^{-j\omega t} = E_o(\cos \omega t - j \sin \omega t)$$

which may be used to write the conventional expression for the electric displacement as

$$D = \varepsilon E$$

considering the real part only.

Considering a linear isotropic dielectric in the presence of a periodic field, we may calculate, on an average over one period, the amount of electric energy which is transformed into heat. For isothermal conditions[1], we have

$$dU = dQ + \frac{E}{4\pi} dD = 0$$

and integrating over one period,

---

1. H. Frohlich, "Theory of Dielectrics", Oxford, Clarendon Press, 1958; p. 10.

$$Q = 1/4\ \pi \int_0^{2\pi/\omega} E \frac{dD}{dt}\ dt.$$

The heat produced per second per unit volume, or the rate of loss of energy from the field is therefore,

$$L = \frac{\omega}{8\pi^2} \int_0^{2\pi/\omega} E \frac{dD}{dt}\ dt.$$

Integrating and reducing, we obtain

$$L = \frac{\varepsilon_2 E_o^2 \omega}{8\pi}$$

which in terms of the phase angle becomes

$$L = \frac{\varepsilon_1 E_o^2 \omega}{8\pi} \tan \delta$$

Calculating the ratio of the electric losses to the total energy available we obtain:

$$K_o = \frac{k_1 L}{U} = \frac{k_1 (\varepsilon_1 E_o^2\ \omega/8\pi) \tan \phi}{E_o^2 / Z_o}$$

or

$$K_o = (k_1 \varepsilon_1 f\ Z_o/4) \tan \phi$$

$$K_o = (k_1 \varepsilon_o \varepsilon_m f\ Z_o/4) \tan \phi,$$

where k_1 represents the fraction of the total energy influenced by the dielectric material.

Choosing typical values for the parameters of this expression, we have

1. Surface wave plate or cone material - plexiglass of relative dielectric constant $\varepsilon_r = 2.6$ resulting in a dielectric constant $\varepsilon_1 = 2.6\ \varepsilon_o$ where $\varepsilon_o = 8.85 \times 10^{-12}$ farads/meter, and loss tangent, $\tan \phi = 5.7 \times 10^{-3}$

2. Frequency of operation, maximum f = 4.2 kMc,

or f = 4.2×10^9 cps.

3. Input impedance to antenna at antenna waveguide feed, $Z_o \approx 200\ \Omega$

4. Fraction of total energy influenced by dielectric material, k = 0.30

With these assumptions we obtain:

$$K_o = [0.3\ (2.6 \times 8.85 \times 10^{-12})\ (4.2 \times 10^9)\ (200)/4]\ (5.7 \times 10^{-3})$$

$$= 8.27 \times 10^{-4}$$

K_o = 0.083 percent

Converting this fraction of the total energy which appears as a loss in the dielectric to an effective noise temperature in terms of T_D, the dielectric loss noise equivalent temperature, we may write

$$T_D = T_o K_o \text{ deg. Kelvin}$$

$$= 290\ (8.27) \times 10^{-4}$$

$T_D = 0.24^\circ$ K

It therefore appears apparent from general consideration that the influence of the dielectric in the surface wave structure is quite small.

To verify the previous result by another technique we may consider the loss caused by an equivalent length of similar dielectric inserted in a waveguide. For a plane wave propagating through a lossy dielectric, we may write for the attenuation constant, α, in nepers per meter,

$$\alpha = \omega \left\{ \frac{\mu_o \varepsilon}{2} \left[1 + \frac{\sigma^2}{\omega^2 \varepsilon^2} \right]^{1/2} - 1 \right\}^{1/2}$$

where $\omega = 2\pi f$, μ_o = permeability of free space (or of dielectric in this case),

σ = conductivity of dielectric.

It may be shown that

$$\frac{\sigma}{\omega\varepsilon_1} = \tan\delta$$

which is the dielectric loss tangent.

Measured values[2] of loss for dielectric-filled waveguides operating in the TE_{10} mode including certain second order effects verify the basic form of the expression given. The expression in terms of the dielectric parameters, i.e., the loss tangent, tan δ, and the relative dielectric constant ε_1 may be written:

$$\alpha_D = 832 \frac{\tan\delta}{\lambda_o} \frac{\varepsilon_1}{\sqrt{\varepsilon_1 - \left(\frac{\lambda_o}{2a}\right)^2}}$$

where a is the H-plane waveguide dimension in centimeters.

Considering a one inch length of dielectric or relative dielectric constant $\varepsilon_1 = 2.6$ and loss tangent $\tan\delta = 5.7 \times 10^{-3}$, we obtain from plotted values a figure of 0.28 db/ft. For the one inch section this is equivalent to a loss of about 0.046 db, neglecting other factors such as standing wave effects, etc. The effective dielectric loss temperature for this length of dielectric may be written as

$$0.046 = 10 \log_{10} \left(1 - \frac{T_D'}{T_o}\right)$$

$$T_D' = 290\ (0.0106)$$

$$T_D' = 3.07^\circ K \text{ per inch}$$

This value is determined for a wavelength of 3 cm which is somewhat less than the minimum wavelength to be actually considered in the low noise antenna system.

---

2. G.D.M. Peeler, "Dielectric Losses", NRL Paper, April, 1953.

It also is practical and desirable to use dielectric materials of considerably lower loss characteristics than the material described. Polystyrene or teflon dielectrics are of essentially equivalent dielectric constant (2.5 and 2.1 respectively) but have loss tangents of 4×10^{-4} or better, a full order of magnitude better than plexiglass.

Considering, therefore, the lower frequency of operation and the use of lower loss dielectrics, the improvement in the calculated equivalent loss temperature per inch of dielectric may be obtained. The corrected value under these conditions is found to be

$$T_s' = 0.15^\circ K \text{ per inch.}$$

Assuming an extent of dielectric comparable to the length of the surface wave structures, we consider a length of approximately ten inches which appears realistic - or possibly somewhat pessimistic. The resulting value for the effective noise temperature degradation due to the dielectric properties of the feed calculated from the preceding approach appears to be

$$T_s' \text{ (total)} = 1.5^\circ K.$$

Both approaches therefore indicate that the extent of noise temperature degradation due to the use of dielectric material in the feed structure in the surface wave type of configuration is in the order of a degree Kelvin. The actual contribution under ideal conditions is probably considerably less than a degree Kelvin. However, it is felt that the surface contamination of the dielectric material including moisture absorption possibly degrade the dielectric characteristics to an extent. These influences indicate that an upper bound upon the dielectric degradation figure of about one degree Kelvin does not appear unreasonable. This magnitude of temperature is quite small and does not appear to be a serious problem. The use of dielectric

materials does appear feasible and practical from this aspect.

It might also be noted that there does not appear to be the need for dielectric structures at the higher microwave frequencies. And it is in this higher region in which the loss characteristics of the dielectric are least desirable. In the lower frequencies, the extent of dielectric necessary becomes large, but the loss is improved with lower frequency operation and in general the noise improvement possible in the lower regions is considerably restricted.

4.3 Surface Wave Structure Feeds

4.3.1 Electromagnetic Energy Trapping Mechanism

The re-distribution of the energy contained in an electromagnetic field existing in the vicinity of a reactive surface in such a manner that reinforcement occurs near the surface boundary is a well known and much employed physical phenomena. The actual mechanism at the basis of the surface wave "trapping" effect is in some contention[1], however, occurence of the physical phenomena may be easily verified.

It was desired to employ the surface wave "trapping" phenomena to the shaped beam feed design by extending energy trapping surfaces along each side of an illuminating feed aperture. For the proper set of conditions involving the orientation of the surface wave trapping surfaces, the beamwidth of the illuminating aperture and various other factors, it appeared that a three lobed pattern should be attainable by this technique. The first lobe, located at the center region of the primary beam would be the normal main load of the primary feed energy distribution; the other lobes would be those formed by the re-distribution of the feed energy in the vicinity of the energy trapping surfaces. It was also felt that this energy re-distribution should enable attainment of a reasonably good illumination taper for the entire structure at the limits of the secondary aperture edge. It also appeared that a technique of this type may be readily modified to a feed system of circular symmetry and that electrical characteristics independent of polarizations might be attainable.

---

1. S. A. Schelkunoff, "Anatomy of Surface Waves", IRE Transactions on Antennas and Propagation, Dec. 1959, pp. 133-139.

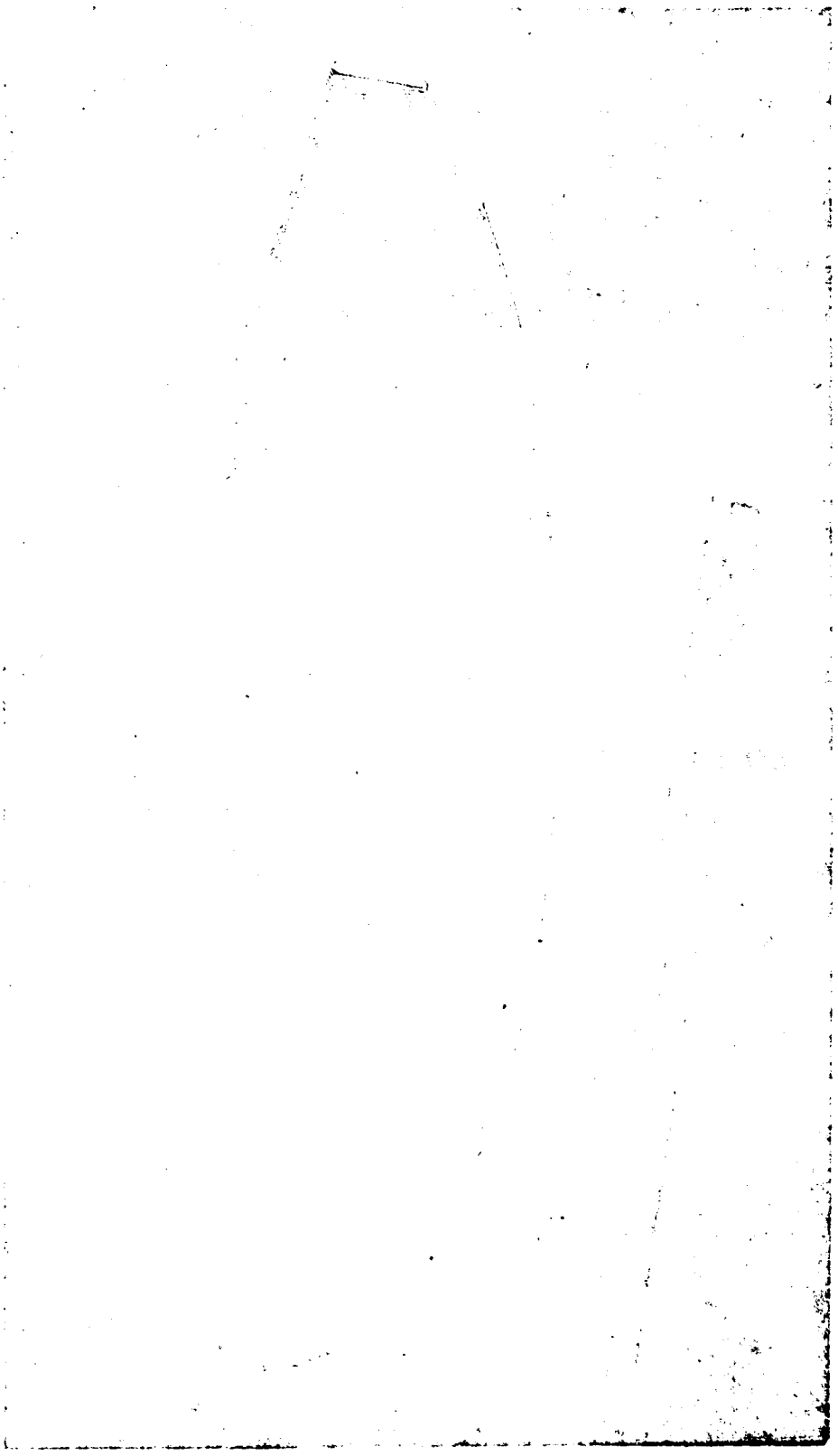

Figure 4-17. Corrugated Plate, Waveguide Fed Surface Wave Structure Primary Feed (Top Plate Removed).

Several surface wave feed designs were constructed and experimentally evaluated under a variety of conditions. Two classes of linear polarization structures were initially employed; a flat plate horn configuration using dielectric sheets and a quasi-horn configuration consisting of metallic corrugated surfaces enclosed top and bottom by metallic plates. Illumination of these primary feeds was provided by an open waveguide feed system employing a pattern broadening post in its aperture, and at lower frequencies by sleeve dipole radiators. Consistent with the effort discussed in the dielectric lens feed system section, a comprehensive study of single feed techniques employing linear feed polarization was the course taken initially. Investigations then progressed to both linear and circular polarizations and finally circular symmetry was established and the polarization and other feed problems associated with this mode of operation were investigated.

The dielectric plate surface wave structure was experimentally tested with solid metal plate backing, metallic tape backing, silver paint coating on the back surfaces and without metallic backing. The effects and results were then recorded for variations in the illuminating feed position, feed projection depth into the aperture, length of surface wave structure, polarization condition, included angle, and certain other factors.

4.3.2 Polarization Dependence

The principal feed structures which were tested and evaluated consisted of first, a waveguide fed dielectric sheet surface wave structure shown in Figure 4-16; second, a waveguide fed metallic corrugated surface structure consisting of milled aluminum blocks oriented between two metal plates as illustrated in Figure 4-17; and a third feed structure which was similar to the previous dielectric sheet

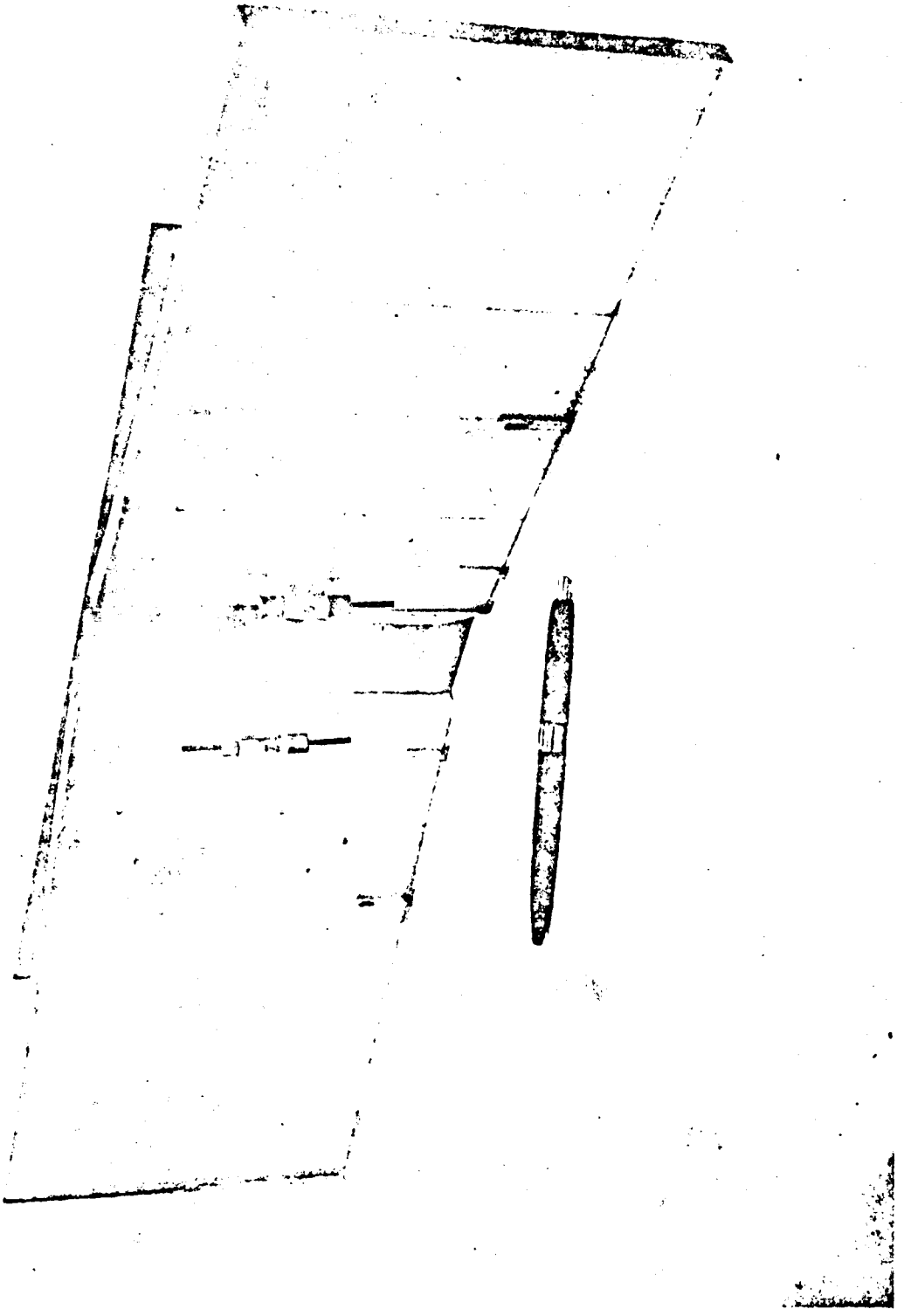

Figure 4-18. Dielectric Plate, Dipole Fed Primary Feed In Monopulse Configuration.

surface wave structure except that it was illuminated by a sleeve dipole. Evaluation of the dielectric plate surface wave feed structure arranged in a monopulse configuration was accomplished by menas of two sleeve dipoles. This configuration is illustrated in Figure 4-18.

Primary patterns for the various feed arrangements were taken with particular note made of the variation in pattern structure due to the various conditions of illumination, frequency of operation, feed projection distance, included angle, and polarization. Figure 4-19 illustrates some primary patterns taken for a dielectric plate surface wave feed showing the dependence upon polarization and included angle between the dielectric plates. Figure 4-20 shows some primary patterns for a surface wave feed structure showing the influence upon the pattern of the surface wave structure length. It is interesting to note that the rate of pattern taper in decibels per unit angle increases with the extent of the surface wave structure, as expected from aperture considerations. Figure 4-21 illustrates a primary pattern obtained for a sleeve dipole feed with a dielectric surface wave configuration. This surface wave feed pattern and the previous pattern for the feed structure illuminated with a waveguide horn indicate considerable potential for shaped beam feeds of this type. Excellent patterns were also obtained for the waveguide fed corrugated surface wave structure. A pattern for this feed system is presented in Figure 4-22.

The primary response patterns obtained for the dielectric plate surface wave feeds with aluminum tape backing utilizing a rectangular waveguide with a post in the aperture illumination were in general very satisfactory. Fairly constant illumination over the center portion of the primary beam was attained with a reasonably low value of minor lobe energy on either side. The 10 db beamwidth for one of these primary structures was found to be approximately 122 degrees which is quite

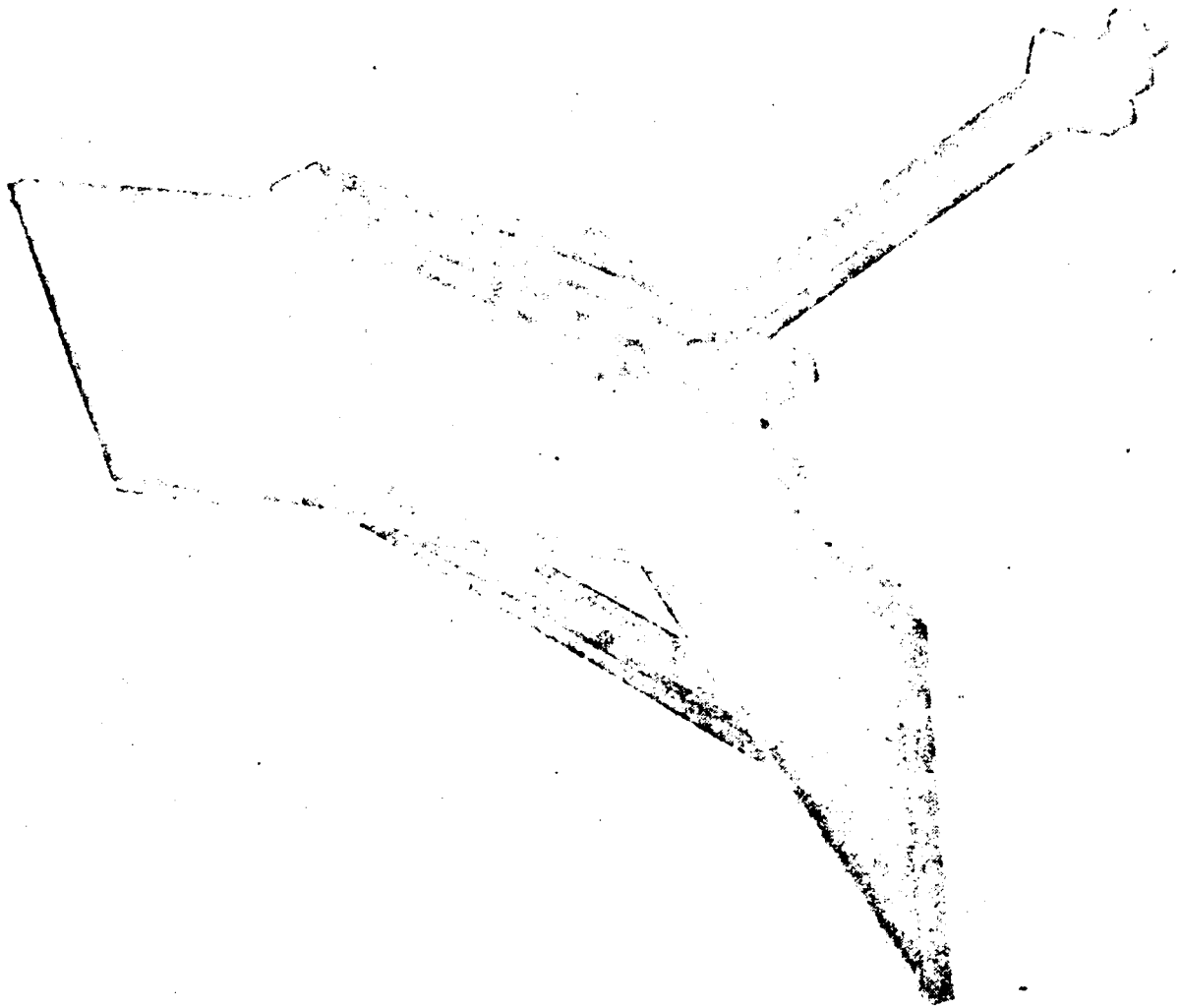

Figure 4-1[illegible]. Dielectric Plate, Waveguide Fed Surface Wave Structure Primary Feed.

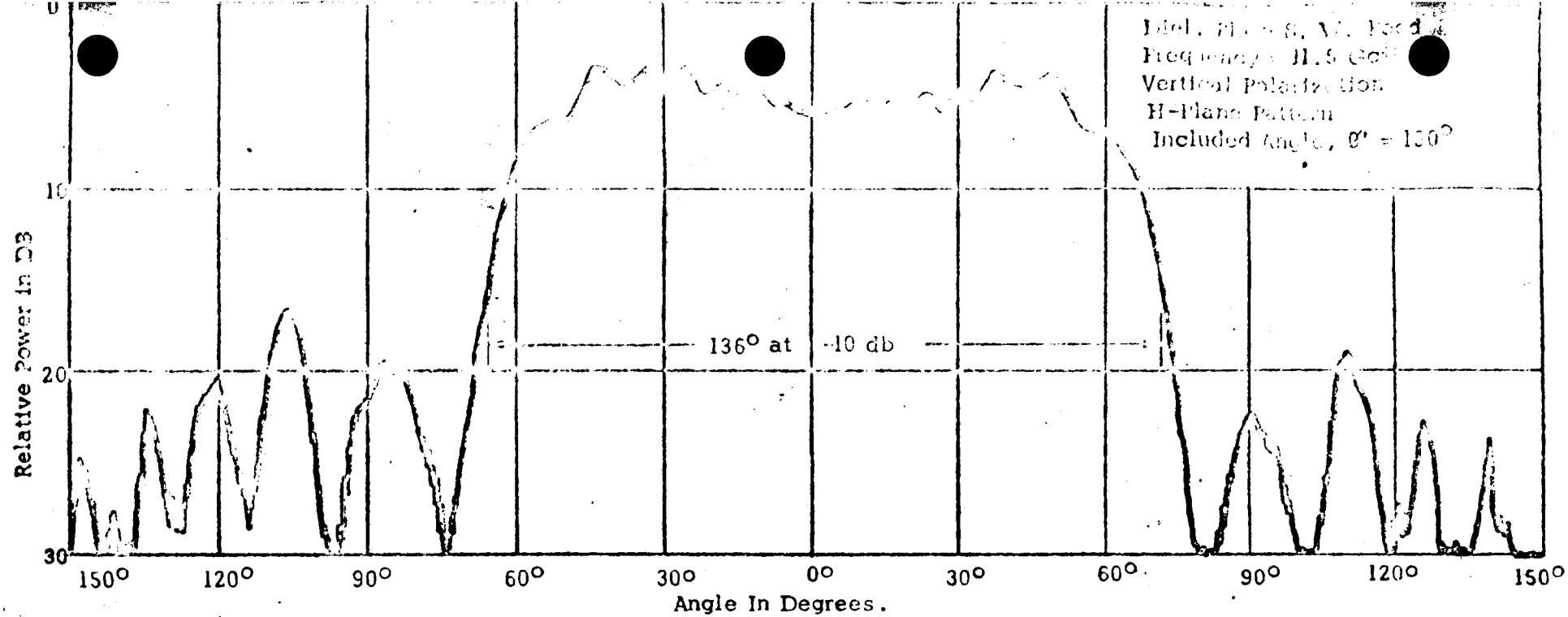

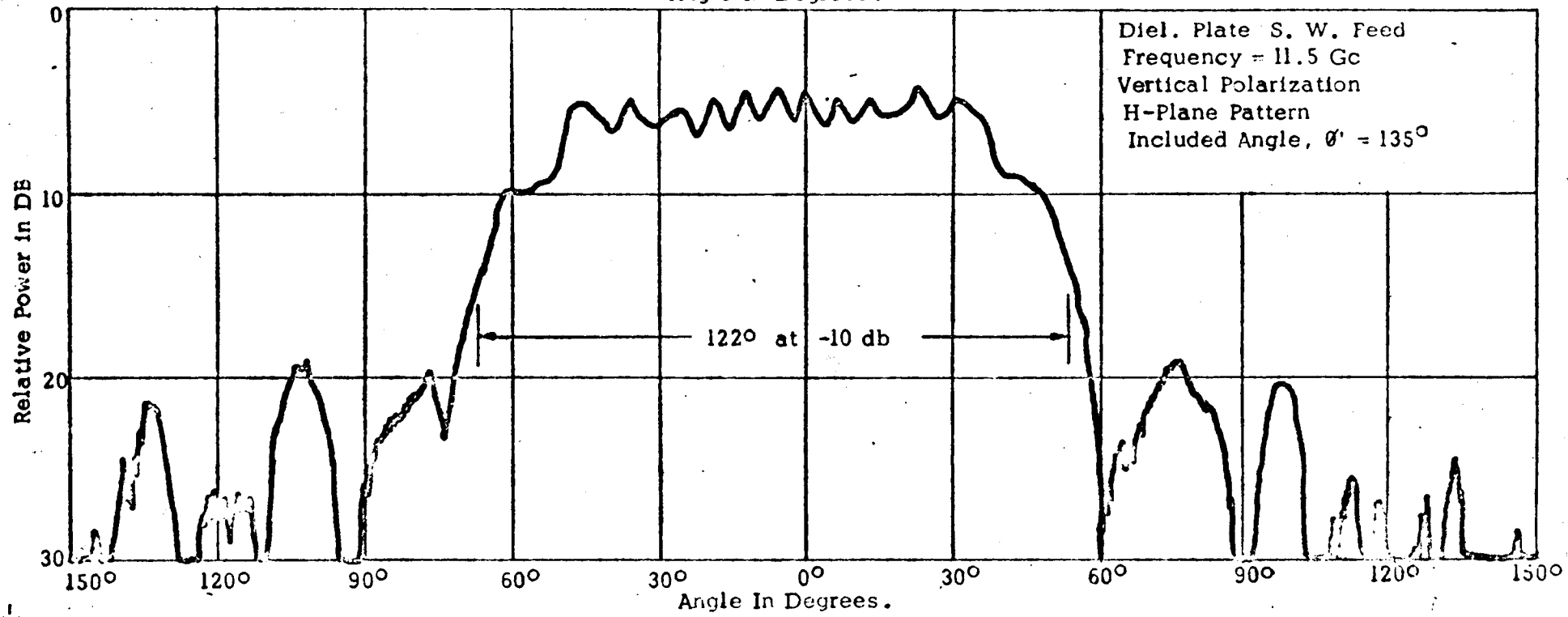

Figure 4-19. Dielectric Plate Surface Wave Feed Primary Patterns Showing Dependance Upon Included Angle.

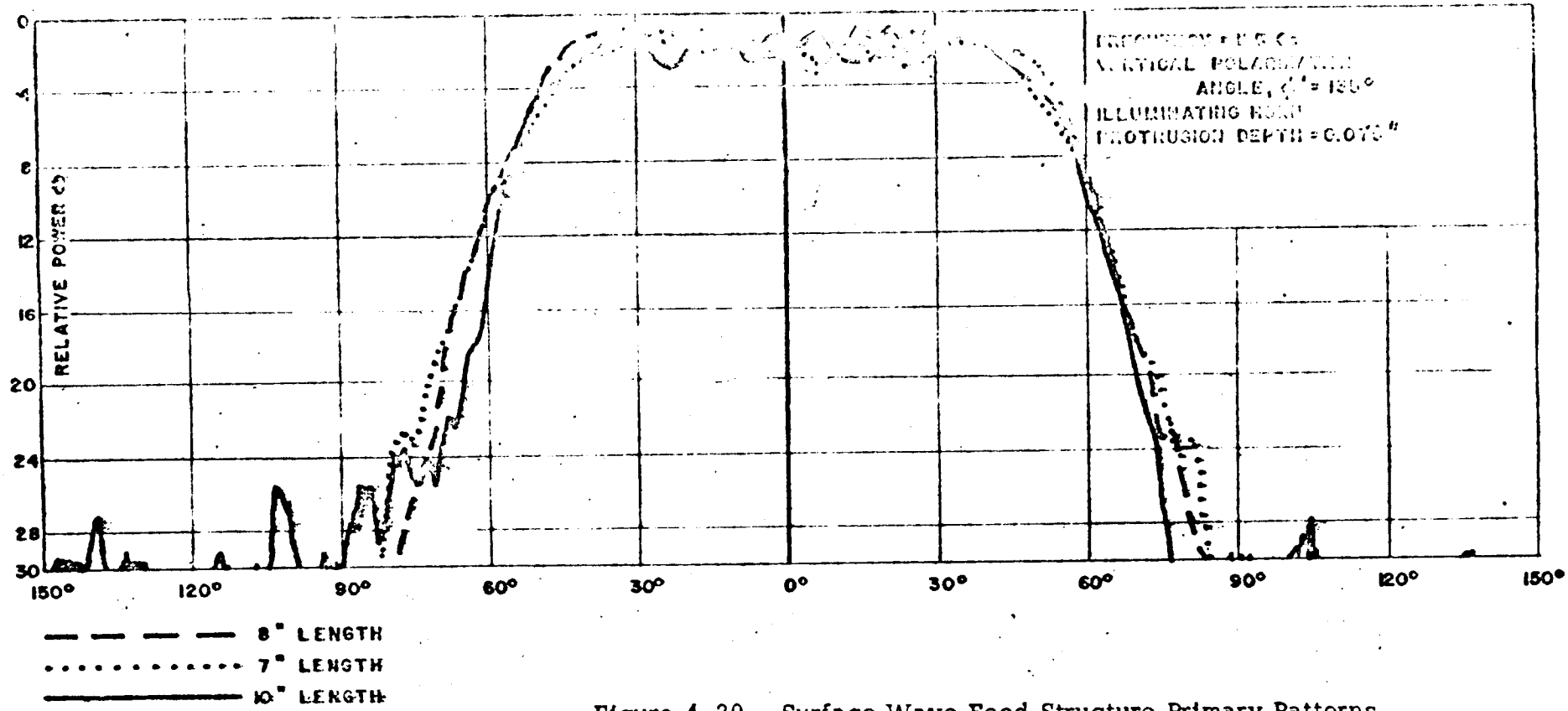

Figure 4-20. Surface Wave Feed Structure Primary Patterns Showing Dependance Upon Structure Length.

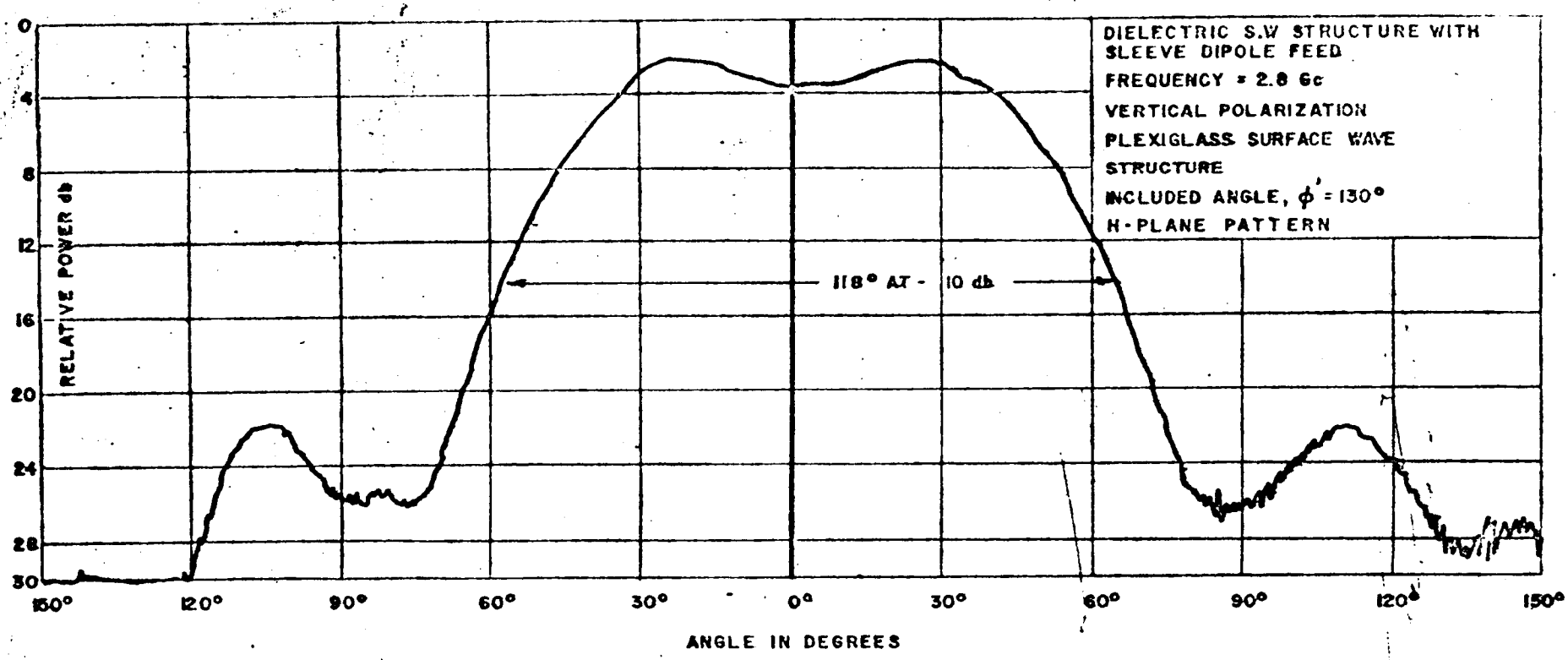

Figure 4-21. Sleeve Dipole Fed Dielectric Surface Wave Structure Primary Feed.

close to the desired 124 degree illumination. Metal plates were then added above and below the plexiglass sheets to enable the formation of a more conventional horn type arrangement. Again, a reasonably constant illumination over the center of the beam was realized with a 10 db beamwidth of about 119 degrees. The side lobe level for this primary feed was found to be of even lower value than the dielectric plate feed. The illumination horn protrusion depth was found to exhibit a marked influence upon the primary pattern shape and to a degree this was found beneficial but the pattern was found to be quite sensitive to minor illumination horn displacement. Protrusion of the waveguide feed into the surface wave structures generally resulted in a rise or depression in the center region of the response pattern which was formed. It appears that somewhat more effective trapping occurs along the surface regions of the structure for the condition of minimal protrusion depth.

Generally, it was found that minor influences in the region of the projection of the illumination horn into the surface wave structure caused appreciable variation in the form of the primary pattern obtained. The maximum values of side-lobe level occurred in the order of 20 db below the average center response of the surface wave feed.

A primary pattern obtained by the use of a metallic corrugated surface wave structure is illustrated in Figure 4-22. Two milled aluminum blocks were used placed at an included angle of about 130 degrees relative to each other and sandwiched between two metal plates as previously described. This surface wave feed achieved a 10 db beamwidth of approximately 121 degrees and maintained side lobes of approximately 18 db or less. For comparison purposes, a primary pattern for a smooth metal plate structure of the same general configuration as the corrugated surface wave feed is presented in Figure 4-23. These patterns have several significant differences which should be discussed. First, the decrease in the illumination toward the edges of the

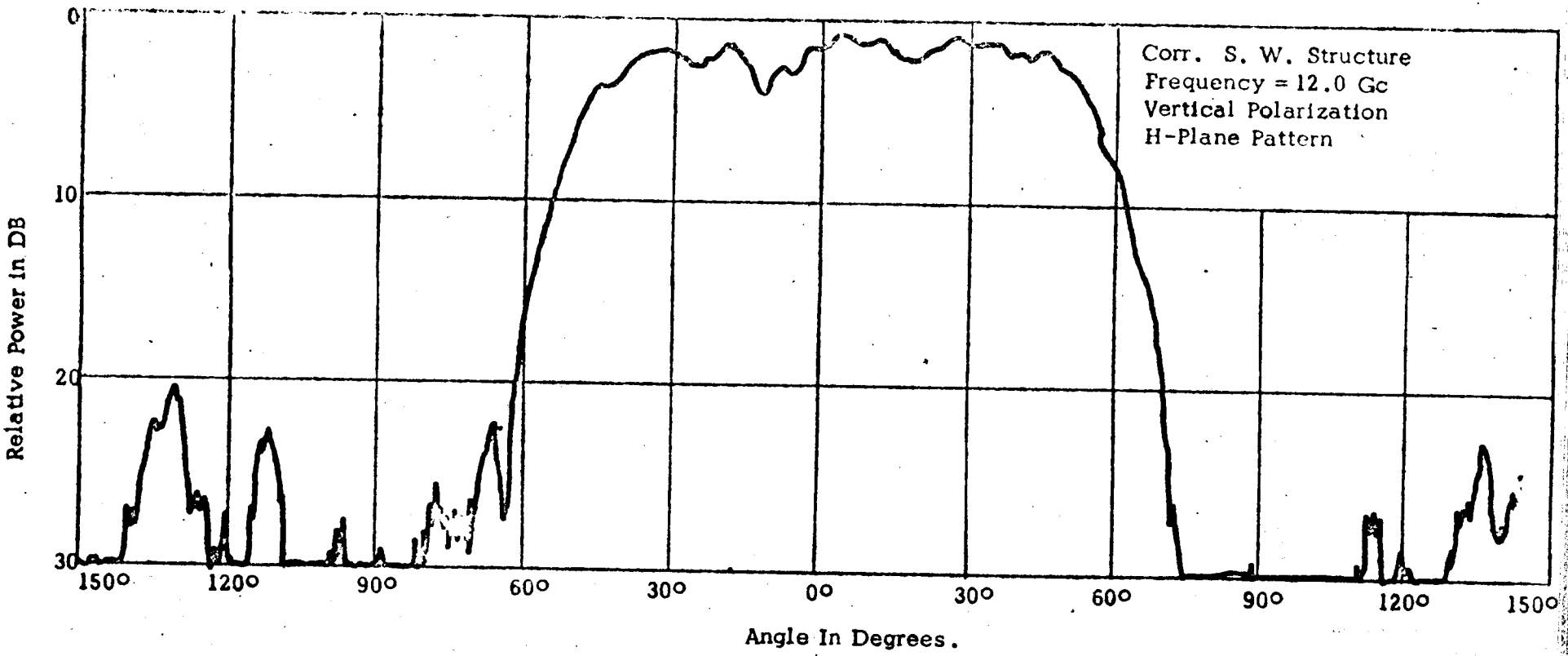

Figure 4-22. Waveguide Fed Corrugated Surface Wave Structure Primary Pattern.

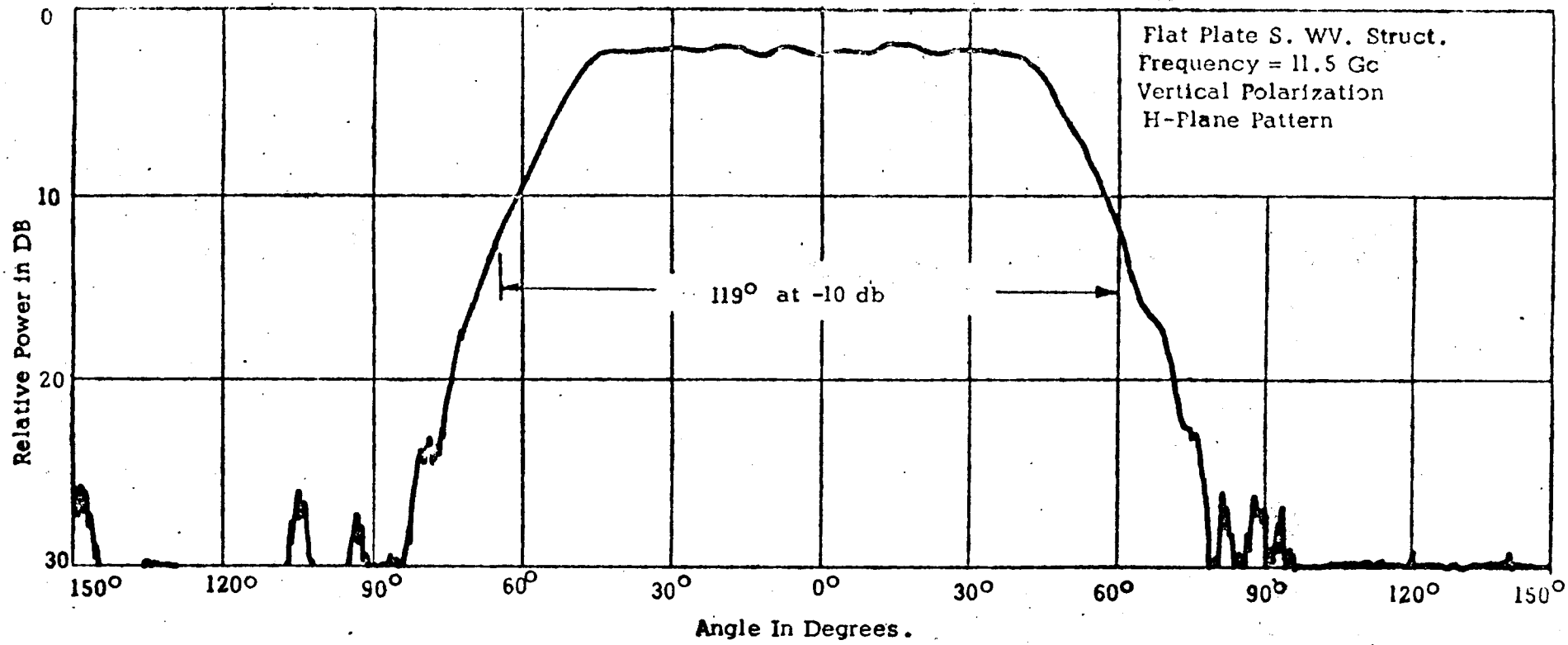

Figure 4-23. Waveguide Fed Metal Plate Surface Wave Structure Primary Pattern.

beam is much more gradual for the smooth plate structure than in the corrugated wave structure. Corrugated surfaces in general are considered to be more effective surface wave trapping mechanisms and hence the results obtained appear to verify previous information. The beamwidth at 10 db points is approximately 125 degrees for the smooth metallic plate surface wave structure which is quite close to the 121 degree beamwidth obtained for the corrugated surface. However, it is interesting to note that the slightly more narrow beam of the corrugated structure enabled a constant illumination beamwidth considering ± 2 db points of approximately 114 degrees while the smooth plates had a significantly smaller constant illumination region of about 96 degrees.

Figure 4-21 illustrates the primary pattern obtained for a dipole fed illumination of a surface wave feed structure consisting of a pair of dielectric plates oriented so as to form an included angle of 130 degrees. This primary feed system utilized a sleeve dipole arrangement operating at 2.8 Gc. The general pattern obtained appears quite acceptable and the side lobe levels in particular indicate promise for this mode of operation in that the side-lobe energy is 20 db or more below the main-lobe response for this feed system. It appears desirable to increase the taper rate in the illumination region towards the secondary aperture edge, however, accomplishment of this appears to be quite difficult unless sufficient primary aperture is available.

The aperture blocking effects of the lower frequency primary feeds may limit to a considerable extent the degree of primary pattern shaping desirable at the lower frequencies. Fortunately the spillover and minor lobe extent of the primary feed at the lower frequencies does not influence the overall antenna temperature to the extent prevalent in the higher frequency regions, i.e., those operating frequencies above about 1.Gc. However, the improvement in gain realized by the primary pattern shaping even at the low frequencies appears significant.

Beamwidths at the -10 db power level for the surface wave feeds were obtained for approximately 124 degrees without a great deal of effort. The various compromises, as design choices, available in a feed structure of this type include surface wave material, included angle, illumination feed type, horn protrusion depth and surface wave structure extent. This wide design latitude appears to place surface wave feeds in a generally desirable aspect. It is also interesting to note that the desired steep slope in the primary pattern at the outer extremity at the principal illuminating region was generally obtained. A subtended angle between the surface wave trapping regions, or simply the included angle between the plates surrounding the illuminating feed of 130-135 degrees appeared to enable the proper primary beamwidth of 124 degrees to be achieved. This condition, however, must be specified as the angle required for tangential polarization with reference to the trapping surface.

4.3.2 Polarization Dependence

Surface wave structures appear to be quite useful in realizing the desired feed properties since direct radiation from the launcher may be judiciously combined with the radiation from the surface wave structure in order to tailor the composite pattern. The characteristic which has been noted in the patterns presented previously concerning the beamwidth dependence upon polarization concerns the fact that radiation from a conducting surface occurs at a higher angle for tangential polarization than for polarization oriented normal or perpendicular to the surface. A simple surface wave structure exhibiting axial physical symmetry, for instance a wide angle cone, will produce unequal beamwidths in the E and H plane patterns. A symmetrical radiation pattern may be obtained in the linearly polarized case by flattening the cone i.e., separately adjusting the flare angles in the two planes, in order to

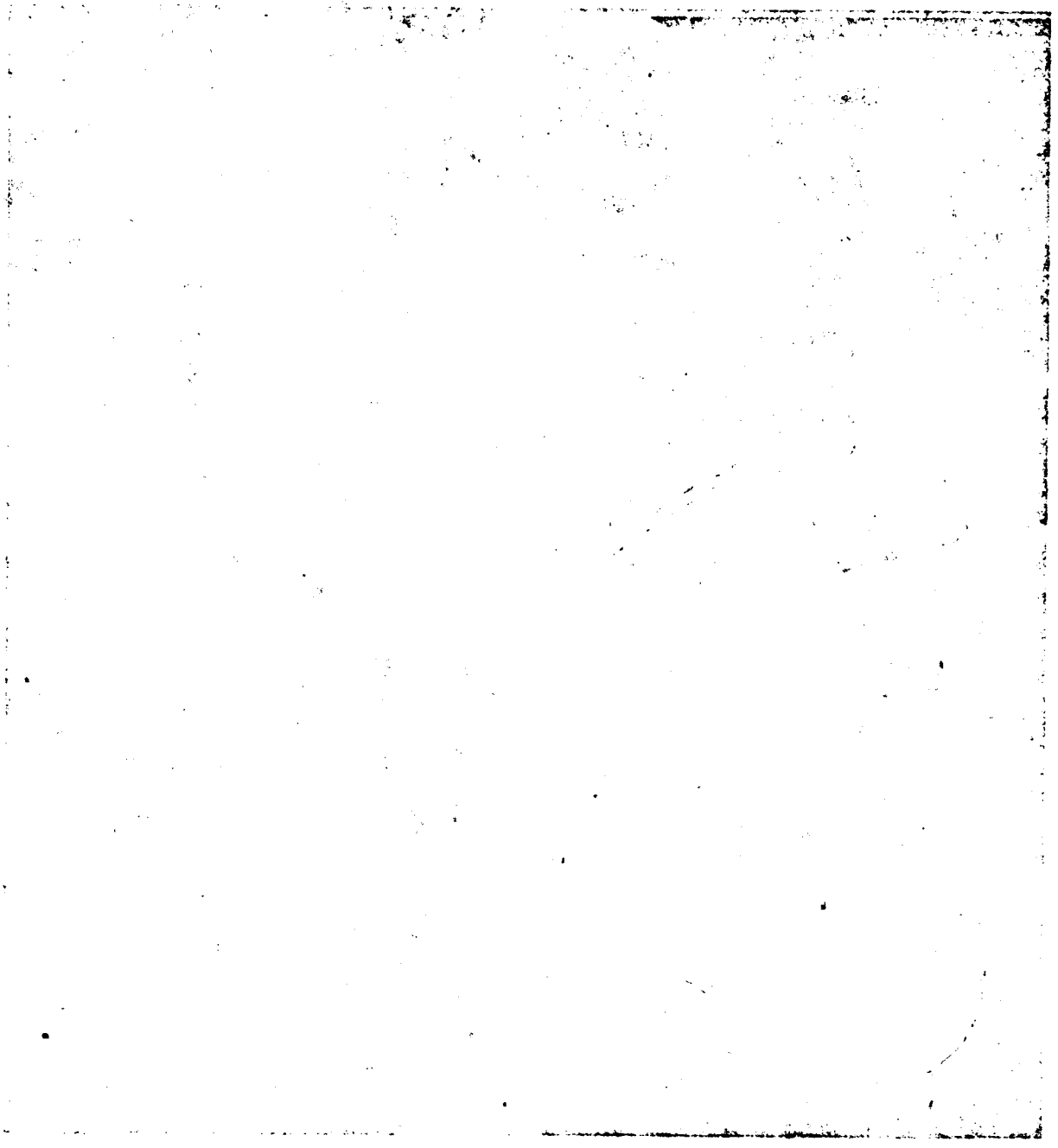

Figure 4-24. Surface Wave Cone Primary Feed

compensate for this difference in the surface polarization characteristics of the radiation energy. For the example mentioned, a cone elliptical in cross-section results. One important feed requirement in the circular polarization feed system involves the formation of equal and orthogonal field components in phase quadrature. For this reason, the elliptical cone arrangement mentioned is consequently restricted to linear polarization. A complex cone is required for circular polarization, one that has quite an unusual requirement attached to it. The circular polarization feed must have one flare angle or surface for tangential polarization and another surface of smaller flare angle for perpendicular polarization. It is also desirable that the energy for each polarization should not couple with the surface with the orthogonally polarized energy.

4.3.3 Linear Polarization Elliptical Cone

Several experimental cone surfaces were fabricated in order to determine the optimum feed placement and the feasibility of distorting the cone surface into the elliptical configuration. A photograph of a surface wave cone structure is shown as Figure 4-24. Primary patterns for the surface wave cone structure with a rectangular X-band illuminating feed operating into the 135 degree included angle cone are presented as Figures 4-25 and 4-26.. The former primary pattern is for a frequency of 12.5 Gc, vertical polarization and is an H-plane pattern. The beamwidth of the feed structure at -10 db power level is seen to be approximately 121 degrees. The primary pattern for the surface wave cone structure shown in the latter figure is for similar conditions of included angle and operating frequency, but is for horizontal polarization and is presented as an E-plane pattern. The feed system -10 db beamwidth in this case is approximately 140 degrees. The shape of the E-plane pattern appears to indicate that the trapped energy just

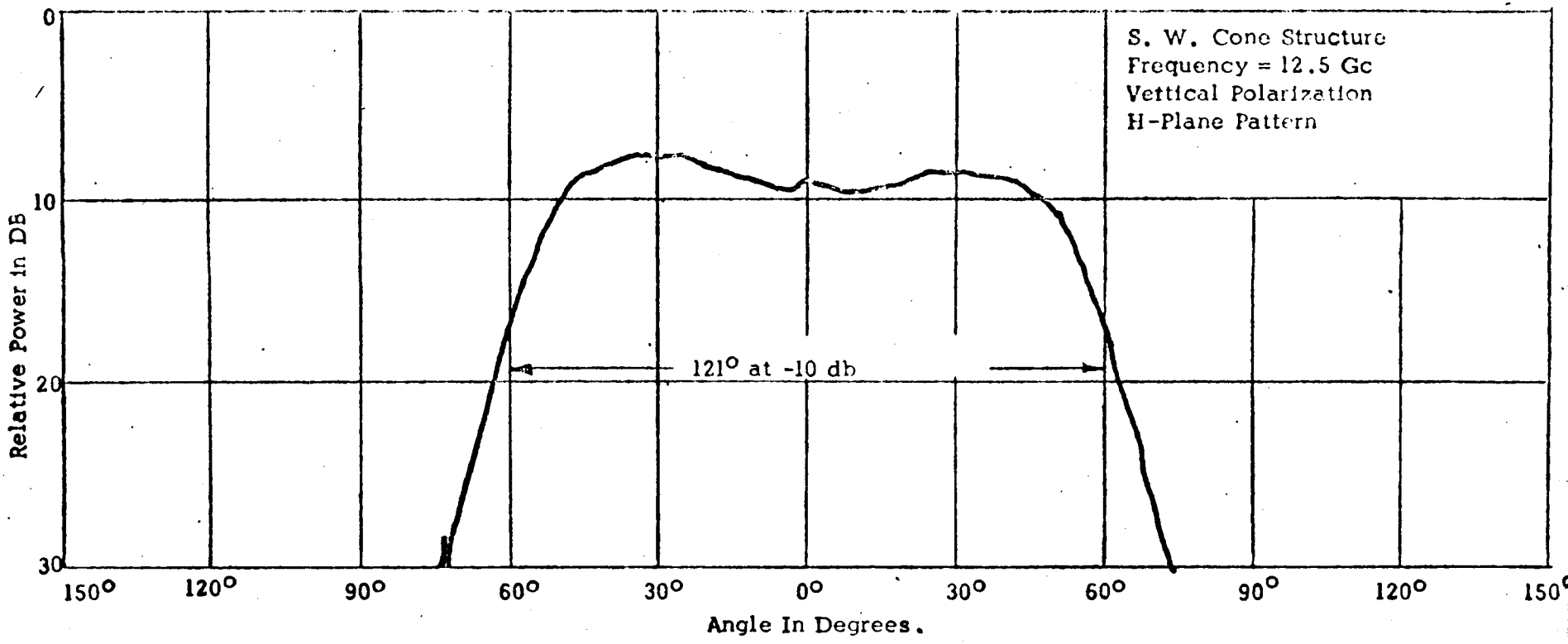

Figure 4-25. Waveguide Fed Surface Wave Cone Structure, Vertical Polarization.

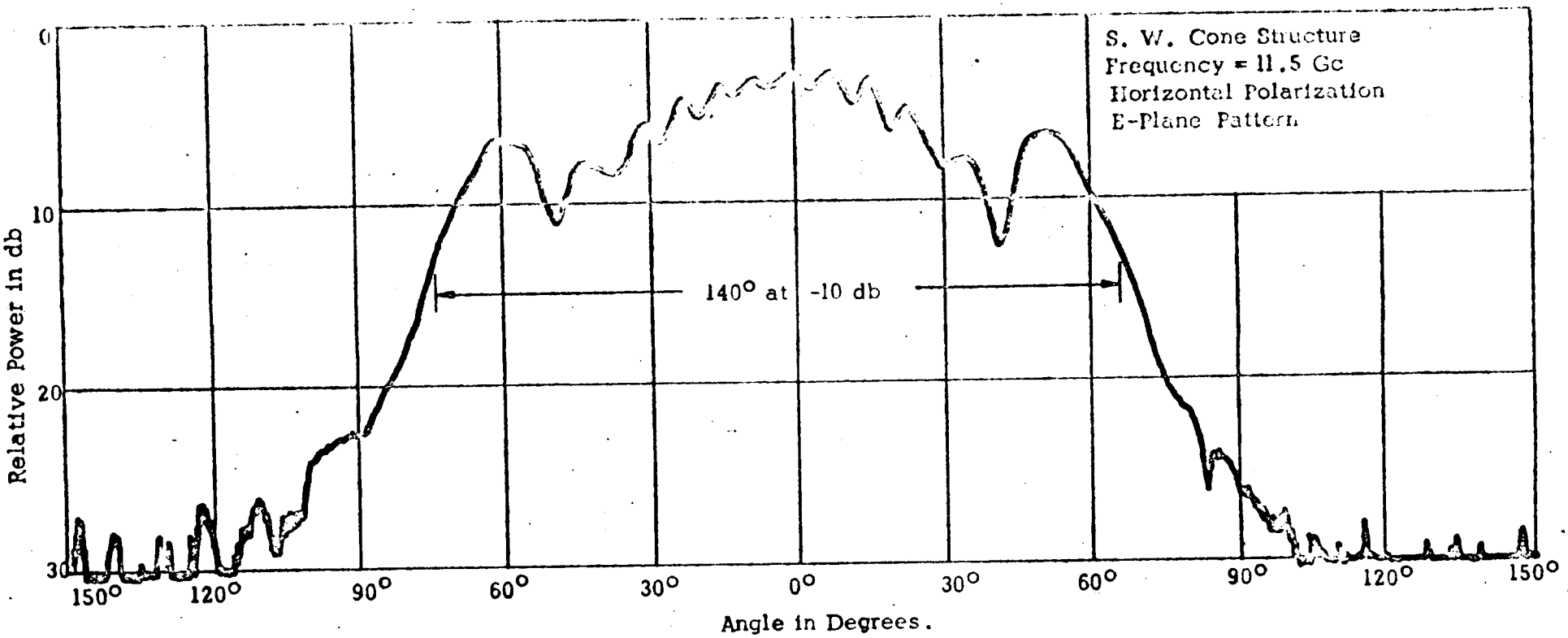

Figure 4-26. Waveguide Fed Surface Wave Cone Structure, Horizontal Polarization.

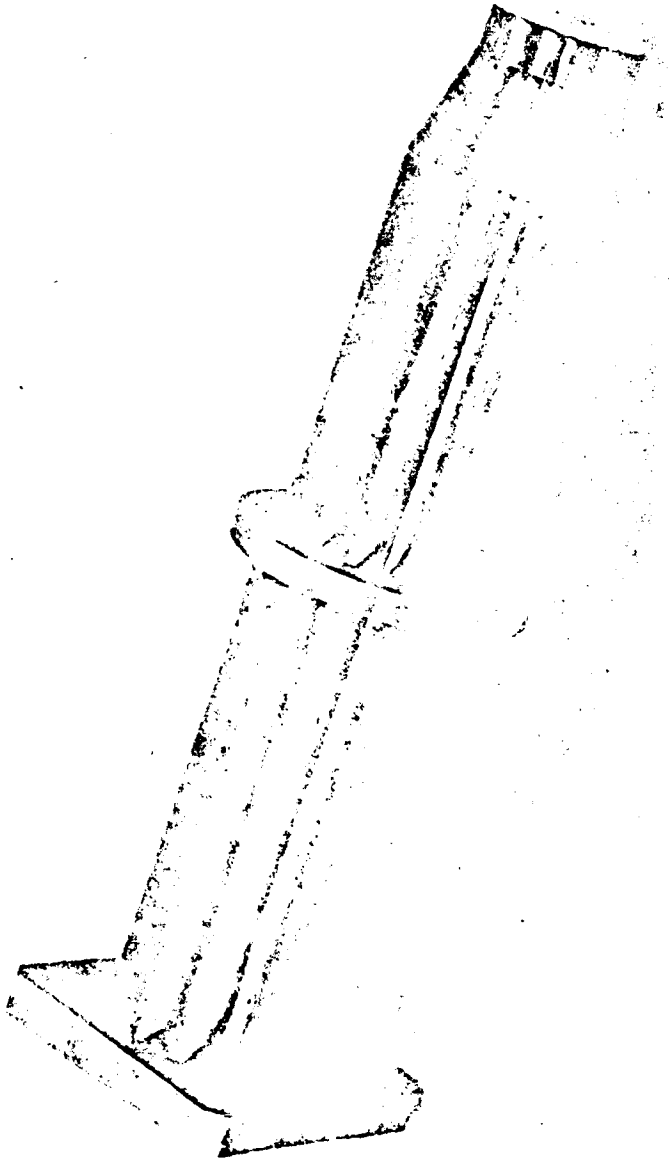

Figure 4-27 Circular Polarization Horn Used With Fluted Cone.

off the surface of the cone appears to be nearly separating from the direct energy received from the launching aperture. It is quite apparent that a more narrow cone surface is required in the E-plane.

The utility of a surfave wave feed structure designed for circular polarization may be somewhat limited if constrained to the use of rectangular waveguide illumination, a circular polarization horn illumination design was required. A waveguide horn was planned, however, the beamwidth of the circular polarization horn should be quite wide if it is to illuminate the conical surface wave structure properly. A conventional circular polarizatinn horn was employed, however, the aperture of the horn was tapered in order to broaden the beamwidth for the illumination. Figure 4-27 is a photograph of a circular polarization horn which was employed in these tests. Using this circular polarization horn with the cone surface wave structure reported upon previously an elliptical cone structure was made available with geometrical symmetry about the cone axis, allowing accurate evaluation of polarization influences in both planes.

The primary pattern shown in Figure 4-28 illustrates the primary response for the symmetrical surface wave cone structure illuminated by the circular polarization horn. The operating frequency is 11.5 Gc, the included angle for the cone is 135 degrees and the pattern is taken for an H-plane cut vertical polarization. The -10db power beamwidth is shown to be approximately 124 degrees. The E-plane pattern for a similar configuration is shown in Figure 4-29 and the perpendicular polarization influence has spread the beamwidth at -10 db power points to 147 degrees. This pattern markedly demonstrates the formation of three independent energy distributinns. The polarisation influences noted across the main beam of the pattern and the broadening effect of the entire beam appear to be in large measure independent of the illuminating feed.

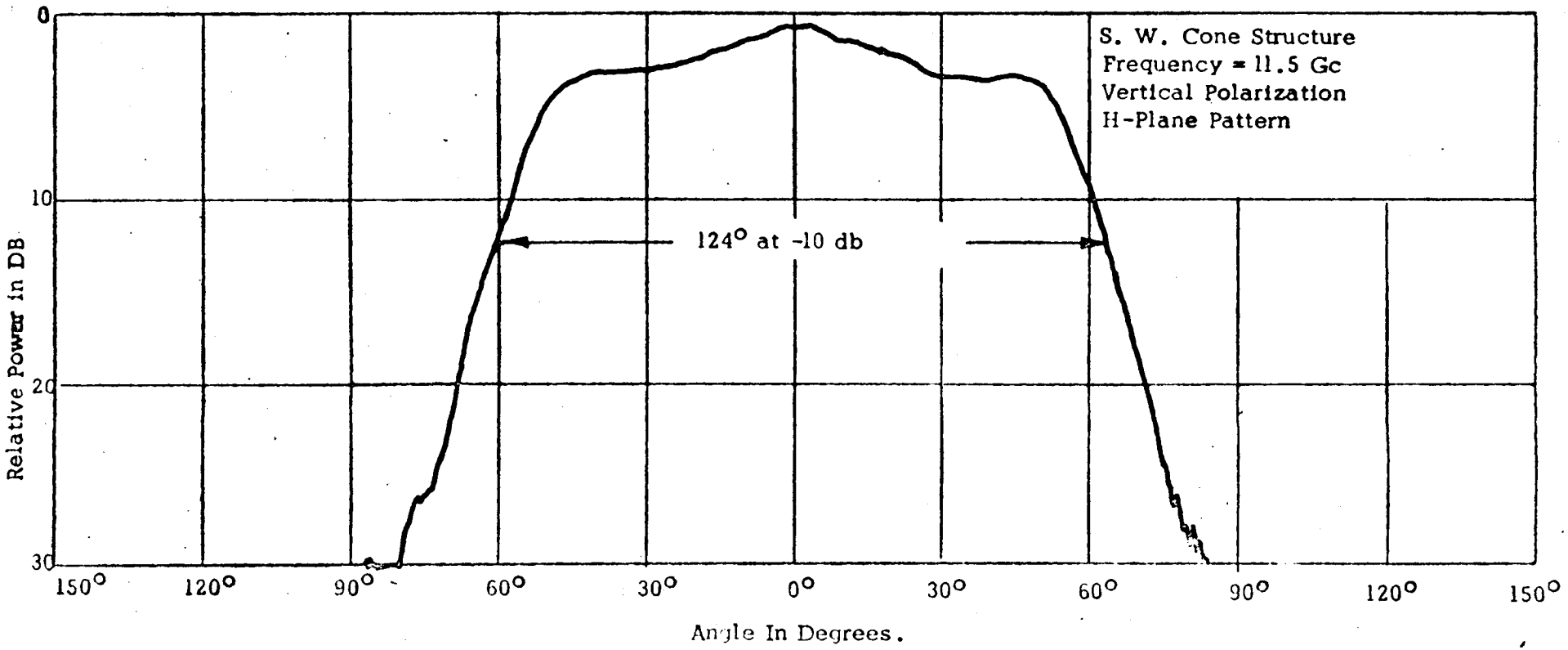

Figure 4-28. Surface Wave Cone Structure Primary Pattern, Vertical Polarization.

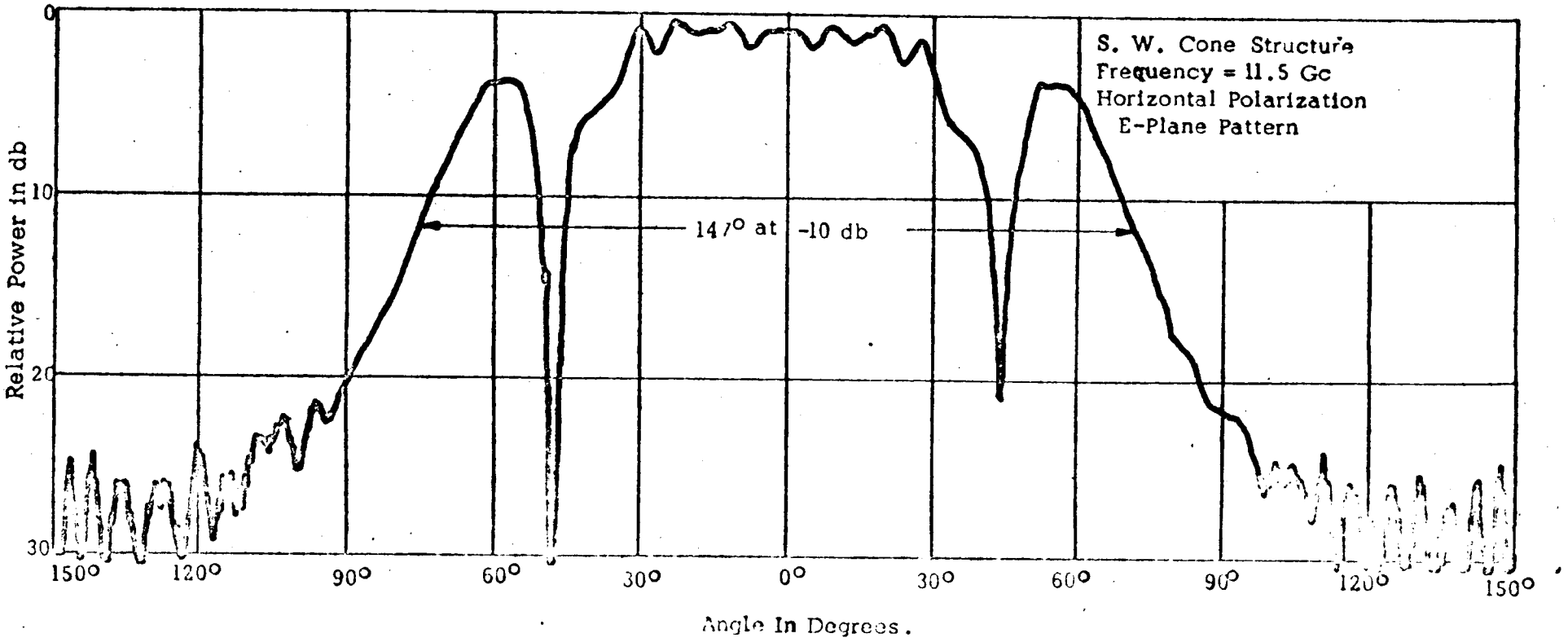

Figure 4-29. Surface Wave Cone Structure Primary Pattern, Horizontal Polarization.

Prior to altering the cone structure, it was desired to note the pattern variations due to several different values of illuminating feed protrusion depth for the 135 degree cone structure. The slant height for the cone during all of these measurements was constant at 8 inches. Figure 4-30 illustrates the variation in the H-plane patterns for vertical polarization as a function of the horn protrusion depth indicated on the plots. It might be noted that the principal influence is found to be in the region of the center of the feed pattern. Somewhat as expected, more energy may be placed in the pattern center by greater protrusion into the surface wave cone region. As the illuminating launch structure is moved back out of the surface wave region, a greater portion of the incident energy is trapped by the cone surface.

Surface wave cone structures were fabricated with included angles of 135 degrees and 110 degrees. These structures were illuminated with signals of both polarizations by broad-beam waveguide feeds and dipole feeds resulting in some interesting results. Figure 4-31 illustrates the primary patterns for both surface wave cone structures employing sleeve dipoles as the illuminating feeds. The H-plane primary pattern shown in the former figure employed the 135 degree included angle cone, and as may be seen in the pattern, attained a beamwidth at -10 db points of about 112 degrees. The E-plane pattern shown in the latter figure employed the 110 degree cone structure and attained a beamwidth at -10 db points of 126 degrees. These beamwidths are compatible with the 124 degree aperture beamwidth requirement for the primary feeds utilized with the large NASA dishes implying an f/D ratio of 0.42. The E-plane pattern particularly appears to be quite good and is certainly a vast improvement from the considerably spread three-lobed patterns obtained initially with the 135 degree cone. The H-plane pattern could be improved somewhat

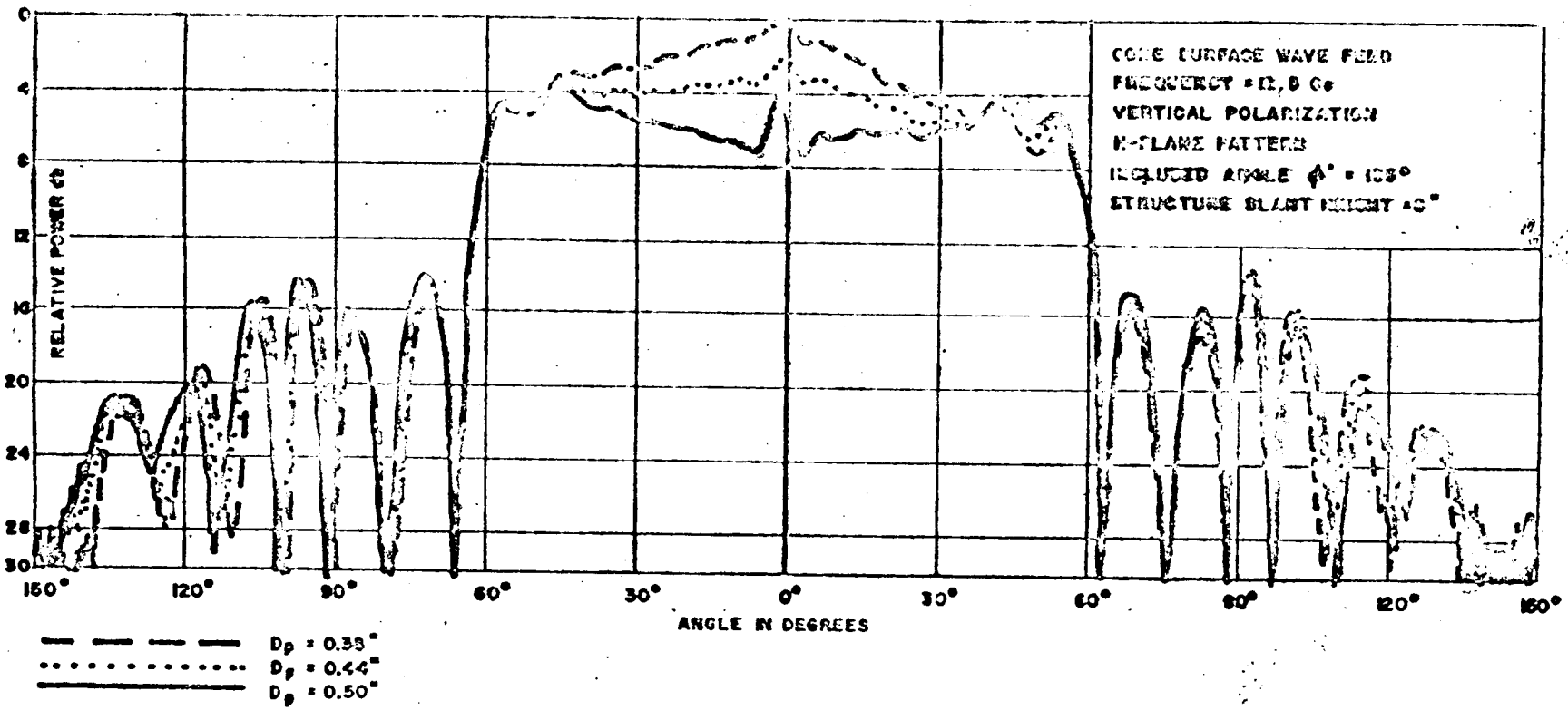

Primary Patterns for Cone Surface Wave Structure Showing Response Variation with Illuminating Horn Protrusion Depth

Figure 4-30.

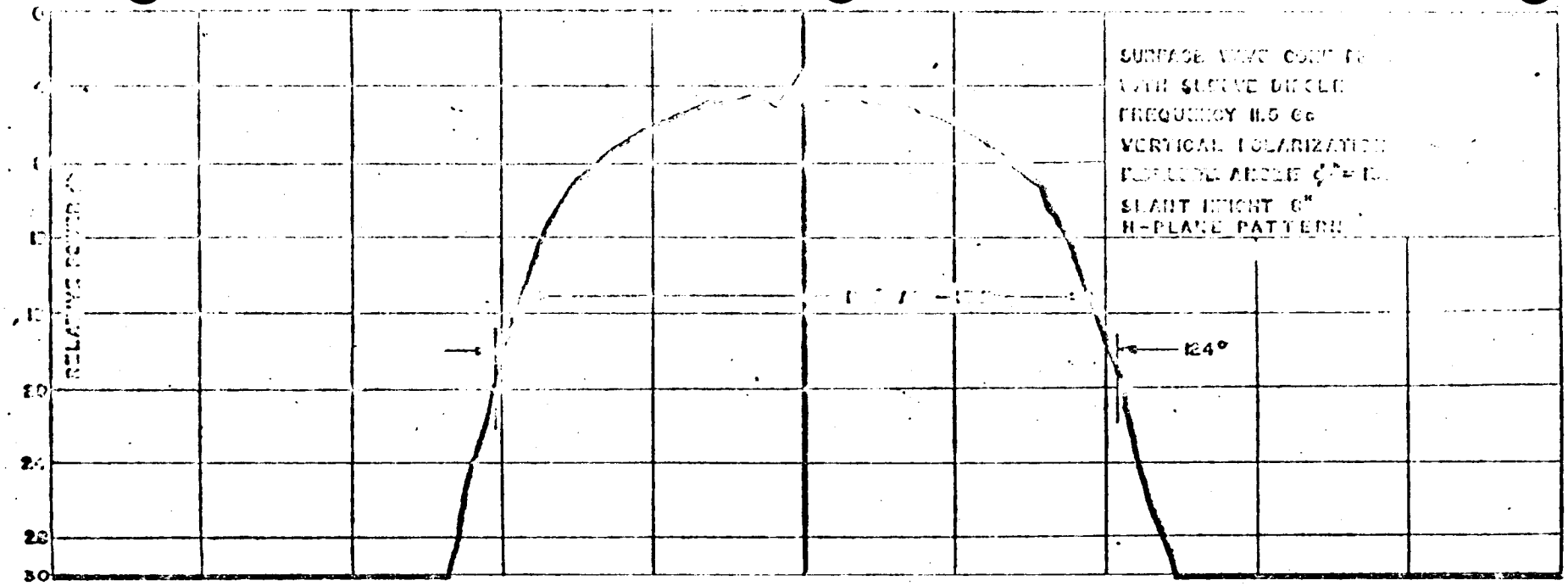

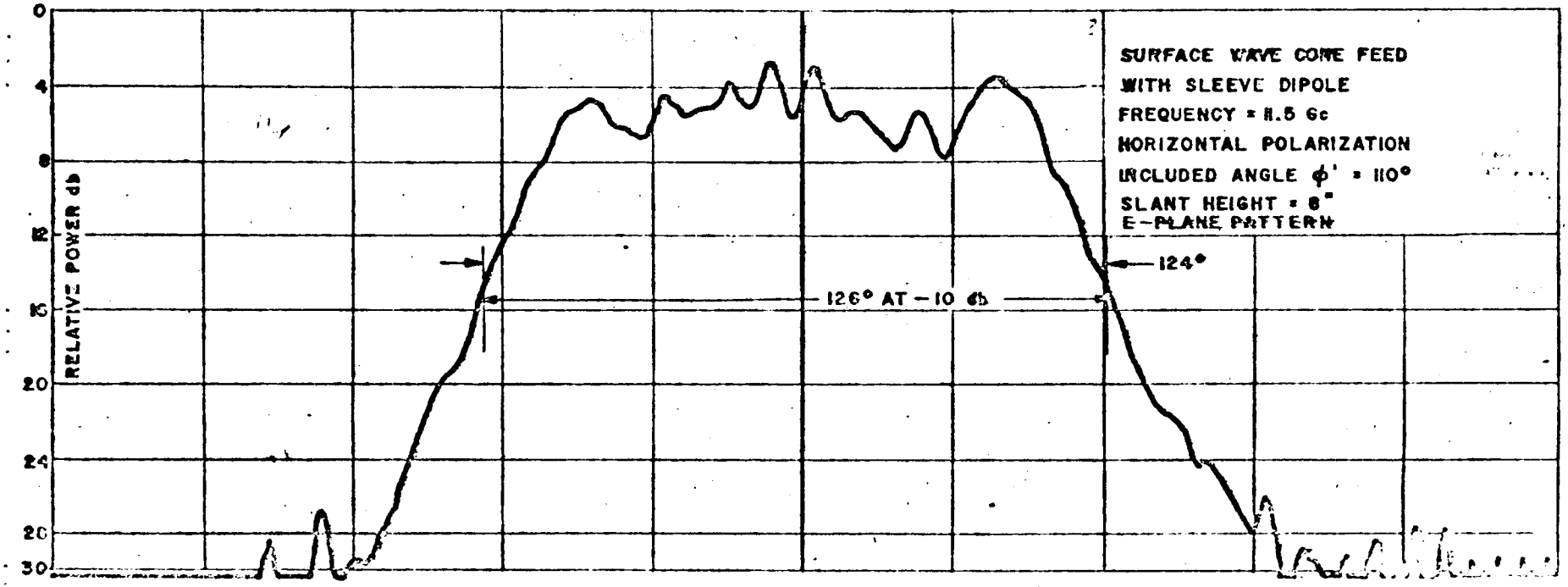

Figure 4-31. Sleeve Dipole Fed Surface Wave Cone Structure Primary Patterns.

by the use of possibly greater flare angle since the dipole radiation characteristic is not as broad in this plane as would be desired. The 110 degree and 135 degree cone flare angles were selected on the basis of test performed on plane surfaces utilizing principally waveguide feed structures and therefore deviation from these selected values for other feeds may be required.

Information was also obtained for the two surface wave cone structures utilizing a circularly polarized horn with a tapered apture. Figure 4-32 illustrates the E-plane and H-plane primary patterns for the surface wave cone structures fed by the circular polarization horn. The frequency of operation for these measurements was 11.5 Gc, the slant length of the cone structures in both cases was 8 inches, and included angles of 135 degrees for the H-plane pattern and 110 degrees for the E-plane pattern. The H-plane pattern shown in the figure is reasonably flat across the region of the secondary aperture and has reasonably rapid illumination taper towards the aperture edge. The -10 db beamwidth for this pattern is about 120 degrees comparing quite favorably with the desired 124 degree beam requirement. The E-plane pattern does not attain quite the illumination taper at the aperture edge of the H-plane plot but is quite uniform in response across the secondary aperture extent. The beamwidth obtained for this E-plane pattern measured at the -10 db points was found to be 127 degrees consistent with the measure H-plane beamwidth of 124 degrees. Both beamwidths compared quite favorably with the desired 124 degree secondary aperture included angle. These patterns appear quite satisfactory as primary feed patterns and indicate the feasibility of considerable improvement in both aperture efficiency and in minimizing the spill-over and minor lobe energy levels. The minor-lobe energy level for both

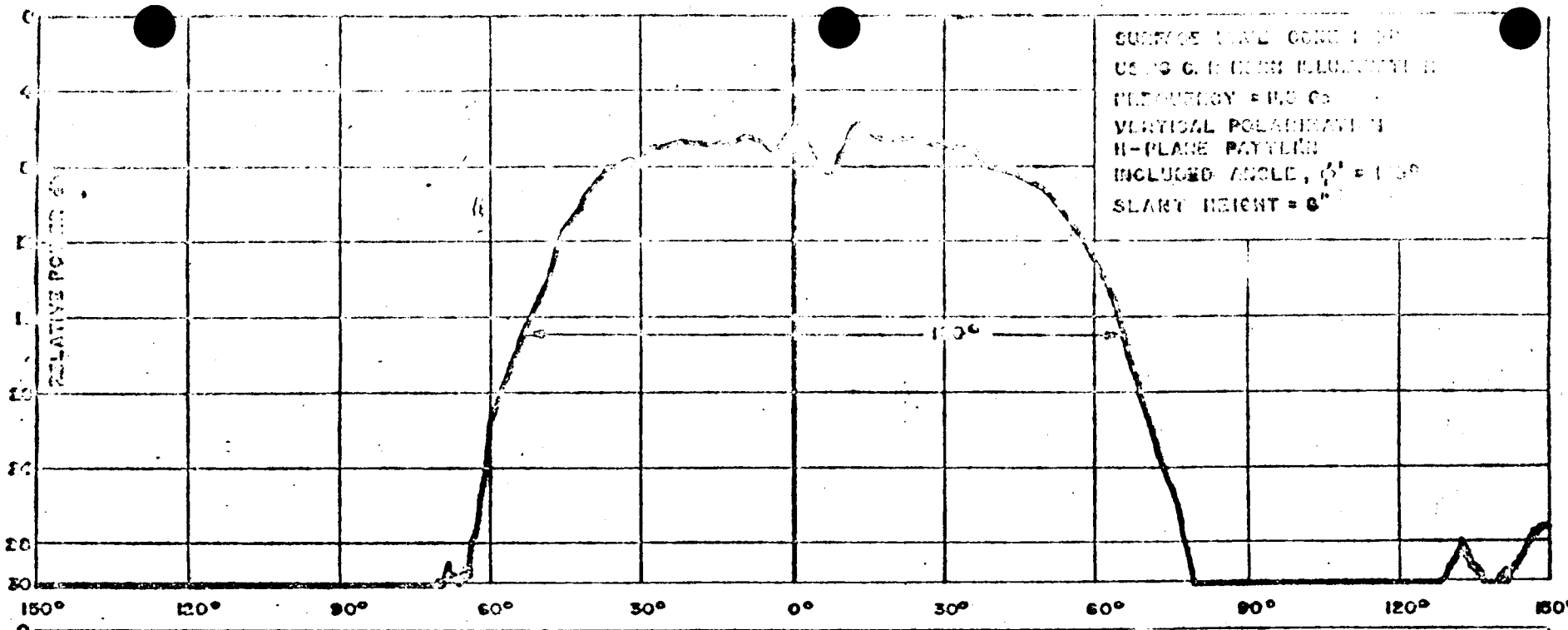

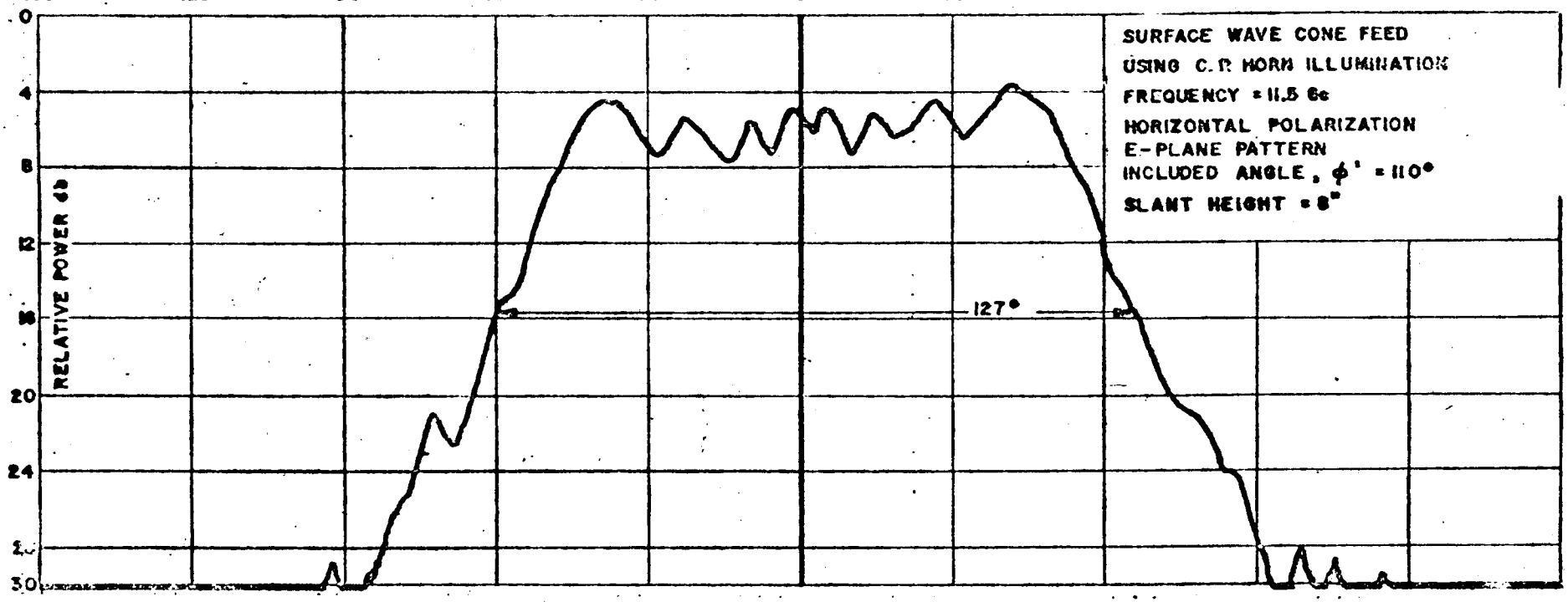

Figure 4-32. Circular Polarization Horn Fed Surface Wave Cone Structure Primary Patterns.

of these feed systems appears to be a reasonably small value. The reasonably rapid taper toward the aperture edge for both primary patterns i.e. in the region of + or - 62 degrees, should minimize the spillover energy which is one of the principal causes of the ground temperature degration of an antenna system.

It therefore appears that distortion of the cone surface into an electrical cone having a maximum flare of 135 degrees in one plane and a minimum flare of about 110 degrees in the perpendicular plane provides a simple, constant beamwidth surface wave feed for linear polarization that appears to be quite satisfactory for a large number of applications.

4.3.4 Circular Polarization Fluted Feed

The desirability of the surface wave cone feed structure has been demonstrated and has been shown to be a practical solution to the feed shaping requirement for linear polarization. A solution is required for the circular polarization case in which a cone of possibly complex configuration might be employed which has one flare angle or equivalent surface for tangential polarization and another equivalent surface of smaller flare angle for perpendicular polarization. It is also desired that the energy for each polarization condition should not couple with the surface for the orthogonal polarization. A novel approach has been devised to satisfy these requirements and consists of an arrangement of vertical conducting fins placed on the surface of the cone structure. The fins are placed in such a manner about the surface of the cone so that the interfin distances are less than half the wave length of the maximum frequency of feed operation. The fins are also tapered from the outer edge of the cone to the center illuminating feed system. The taper rate corresponds to an angle satisfying in the included angle requirement for the desired feed beamwidth in the perpendicular polarization case. The metallic plate

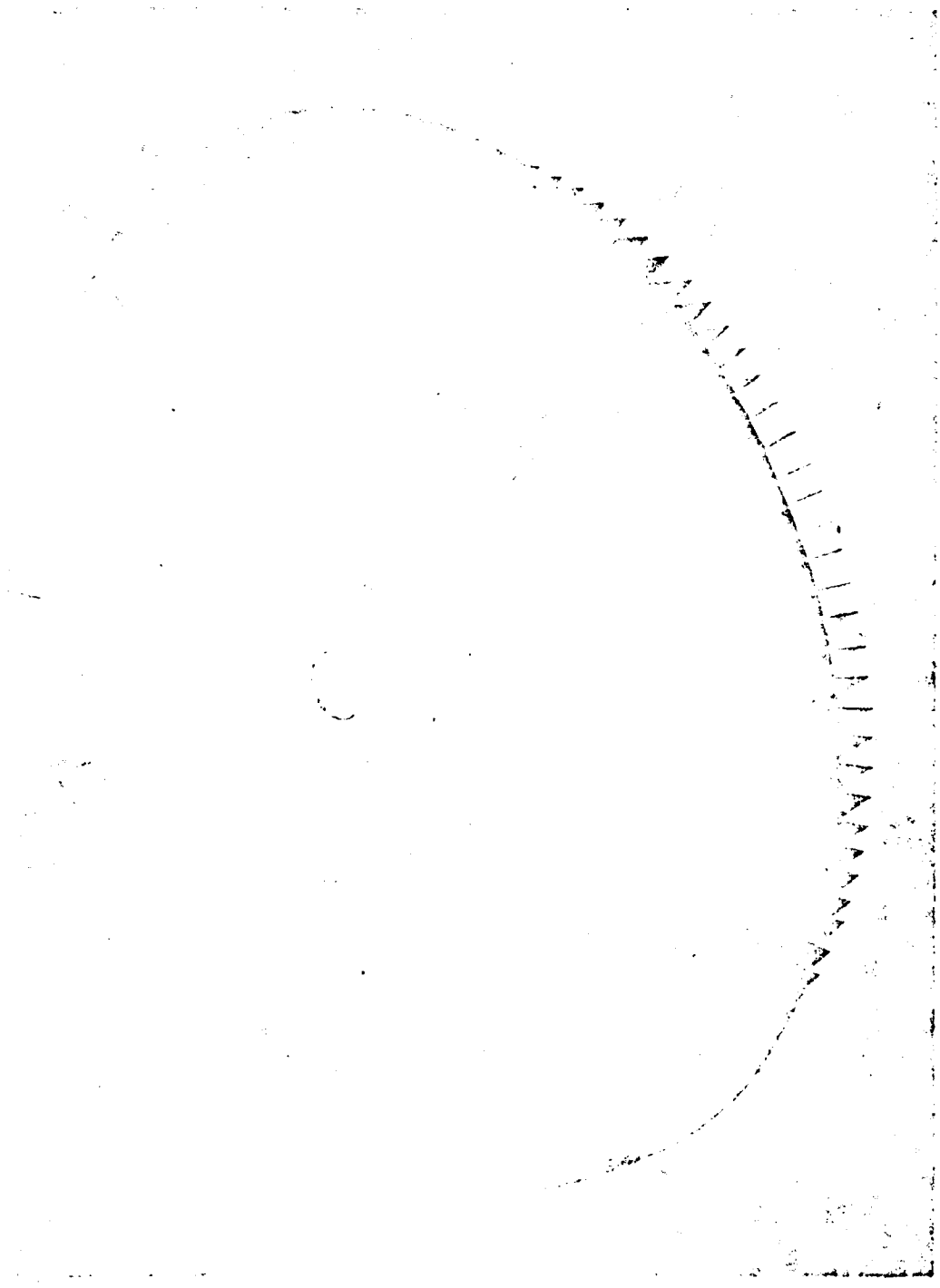

Figure 4-33. Fluted Feed Surface Wave Cone Structure

cone structure has an included angle corresponding to the required beamwidth surface wave cone for the tangential polarization condition. For this physical configuration the vertical fin system appears as a parallel plate multiple waveguide structure operating in the TE_{01} mode to an electric field normal to the surface of the wide angle cone. A condition exists in this region of a waveguide below cutoff in that the separation has been specified as less than half of a wavelength at the maximum frequency of operation. For this condition the perpendicular polarization energy will propagate along the reactive surface formed along the top edges of the tapered metallic fins. The metallic fins have an almost unnoticeable effect upon an electric field tangential to the wide angle cone surface. Therefore, tangentially polarized energy will propagate along the boundary determined by the wide angle cone surface. The fin configuration thus affords a technique for independently determining the energy trapping surface boundaries for parallel and perpendicular polarization components of the field energy.

Flat plate surface wave structures were then fabricated with tapered metallic fins in order to determine the desired fin taper and fin extent. These results were in surprisingly good agreement with theory indicating that the reactive surface formed by the tapered fin system behaved essentially as a solid metallic cone described by the top edges of the fin structure.

A surface wave cone structure employing the wedge shaped fin elements was designed and fabricated and is shown in Figure 4-33 . Due to the channelled appearance of the tapered vertical plates employed in the circular polarization surface wave cone structure, and to the length of any reasonably descriptive title for the feed, the device has been termed the fluted feed.

Primary patterns for the fluted feed are presented in Figure 4-34. It was necessary to compromise somewhat between the E and H-plane patterns in selecting an optimal protrusion depth for the circular polarization illuminating horn. Therefore, the optimal independent patterns were not attained in combination from the fluted feed. However, the form of the H-plane pattern shown in the figure indicates the response of the antenna to tangential polarization and the beamwidth obtained of 118° appeared satisfactory. The E-plane pattern shown in the figure corresponds to the perpendicular polarization condition and the beamwidth at -10 db points for this pattern is 122°. The general form of both of the primary patterns for this feed appear very good; the primary distribution of energy is reasonably flat, the pattern taper towards the aperture edge is reasonably high and the minor-lobe energy distribution is small, especially in the case for tangential polarization.

The measured performance characteristics of the fluted feed surface wave structure indicated that a considerable improvement in aperture efficiency antenna gain and minor-lobe energy level should be attainable by the fluted feed system over conventional feed systems. To investigate those advantages of the fluted feed, secondary patterns were taken for the fluted feed structure mounted in a paraboloidal reflector. The secondary aperture utilized was an 85 inch paraboloidal surface of revolution with an f/D ratio of 0.42 simulating the 85 foot paraboloidals in use by NASA at several locations. Figures 4-35 and 4-36 illustrate the E and H-plane patterns obtained with a conventional horn illumination in the paraboloidal reflector. It is interesting to note that the average back-lobe level in the region greater than 30° removed from the main beam is in the order of minus three decibels relative to the isotropic level for both of the patterns. This corresponds

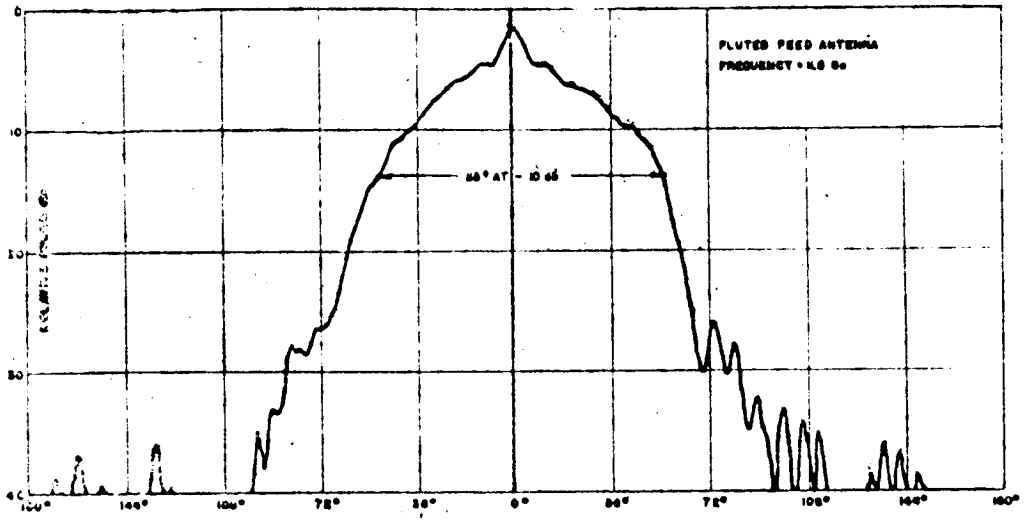

VERTICAL POLARIZATION, H-PLANE PATTERN

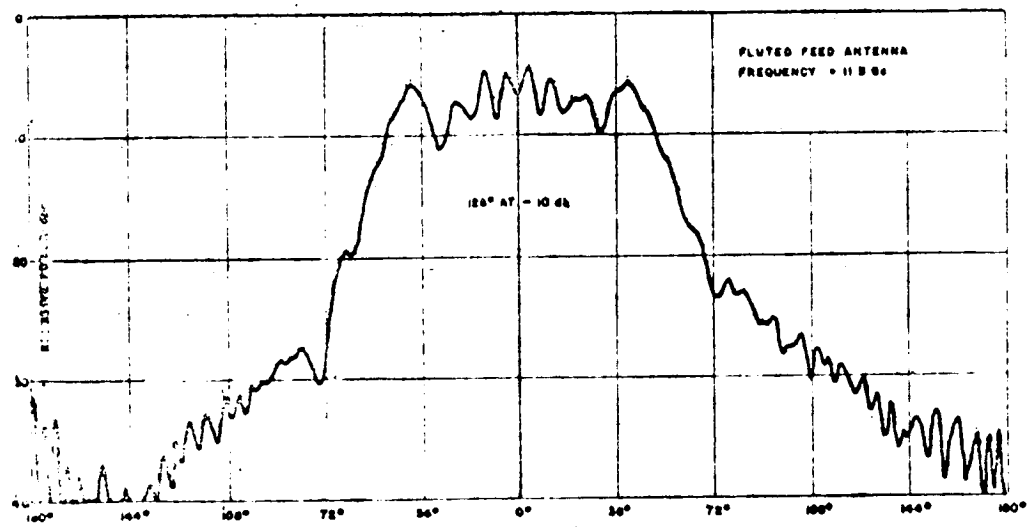

HORIZONTAL POLARIZATION, E-PLANE PATTERN

Figure 4-34. Fluted Feed Primary Patterns.

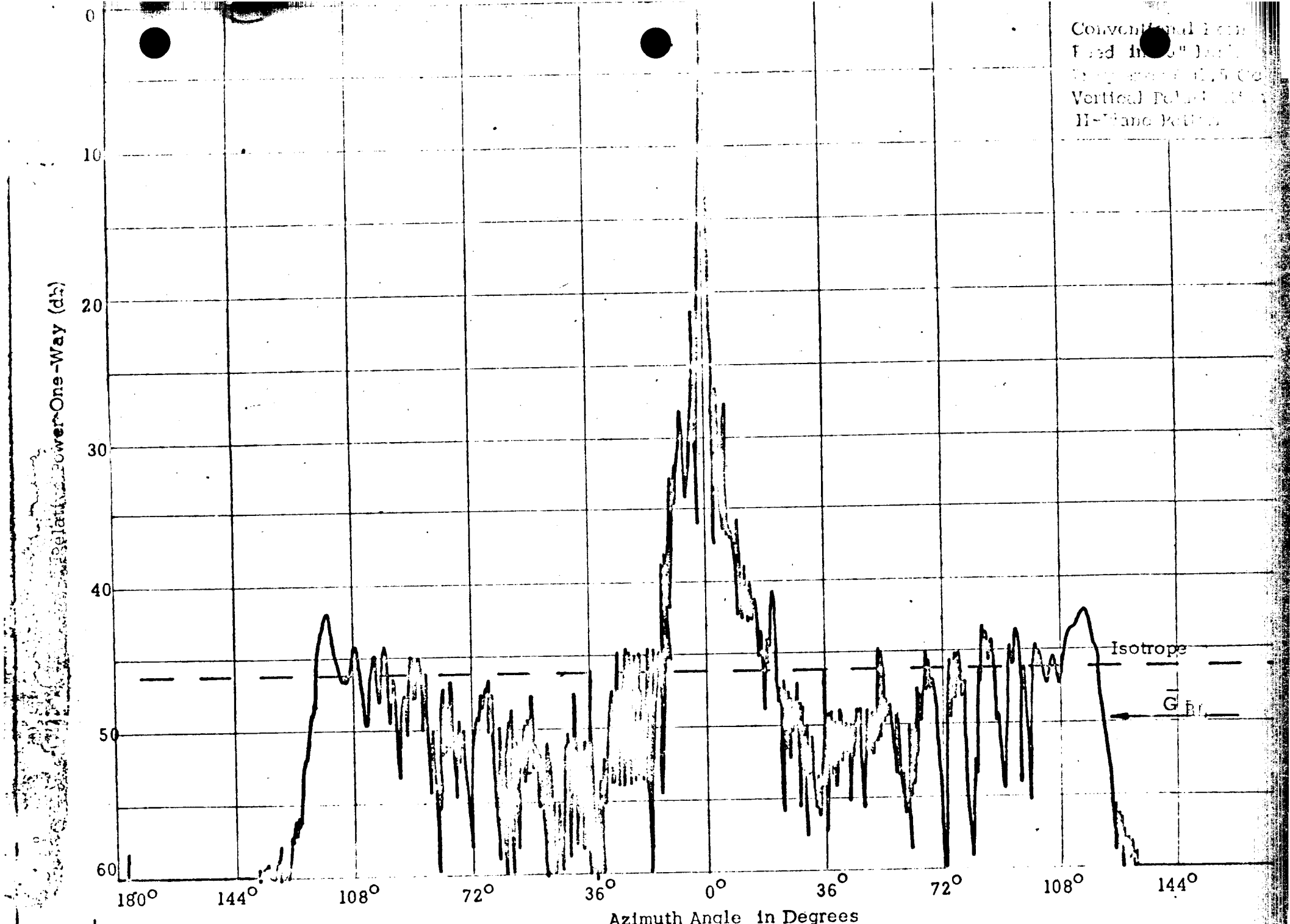

Figure 4-35. Secondary Pattern For Conventional Horn Illumination Of A Paraboloidal Reflector; H-Plane Pattern.

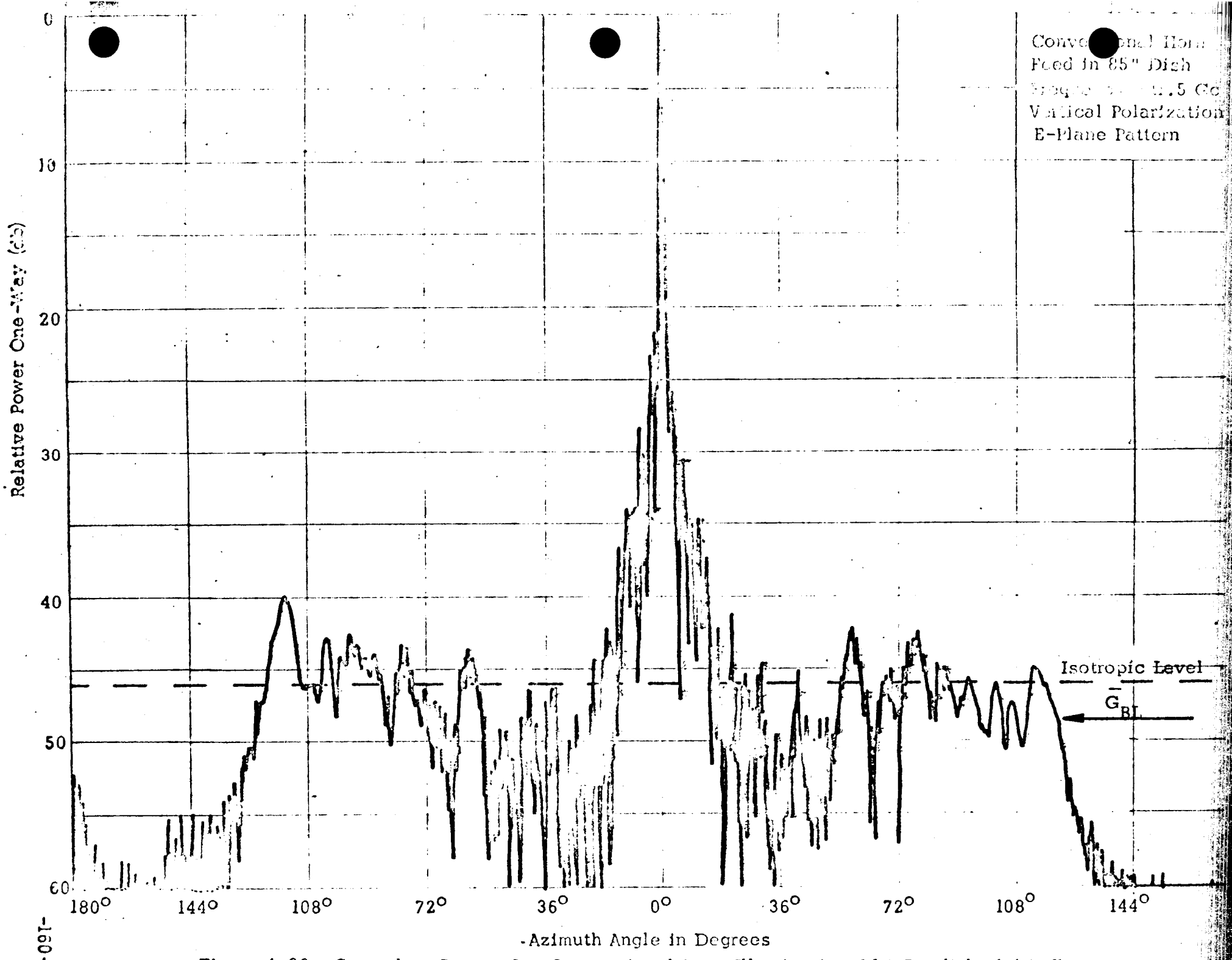

Figure 4-36. Secondary Pattern For Conventional Horn Illumination Of A Paraboloidal Reflector.

to a ground radiation contribution to the antenna effective noise temperature of approximately 60° Kelvin, which is a considerable degradation in antenna low noise performance due to this single factor. The secondary patterns taken for the 85 inch paraboloidal reflector were 60 db patterns in order to perform an adequate evaluation of the noise contributions due to the minor-lobe response. The E and H-plane secondary patterns for the fluted feed illuminating the paraboloidal reflector are presented in Figures 4-37 and 4-38 . An improvement in gain as anticipated, was measured for these patterns indicating a definite improvement in the aperture efficiency. As can be noted on the secondary patterns, the average backlobe level was found to be approximately 12 db below isotropic level, nearly an order of magnitude better than the performance obtained by the conventional horn illumination. The fluted feed system average minor lobe level corresponds to an effective antenna noise temperature contribution due to ground radiation of about 8° Kelvin. Figure 4-39 presents the E and H-plane primary patterns obtained for the conventional flared horn utilized with the 85 inch paraboloidal reflector for which the presented conventional horn illumination secondary patterns were obtained. Figure 4-34 shows the E and H-plane primary patterns obtained for the fluted feed system utilized with the 85" paraboloidal reflector. The fluted feed structure has obtained a rather startling performance advantage over a conventional horn feed in two important respects. First, the measured gain improvement for the fluted feed structure of about one db over a conventional circular polarization horn illumination indicates a significant increase in aperture efficiency for the fluted feed. The fluted feed aperture efficiency appears to be approximately 70 percent over the frequency of about 8.0 to 12.5 Gc which may be compared with a conventional horn efficiency of about 55 percent. Second, and

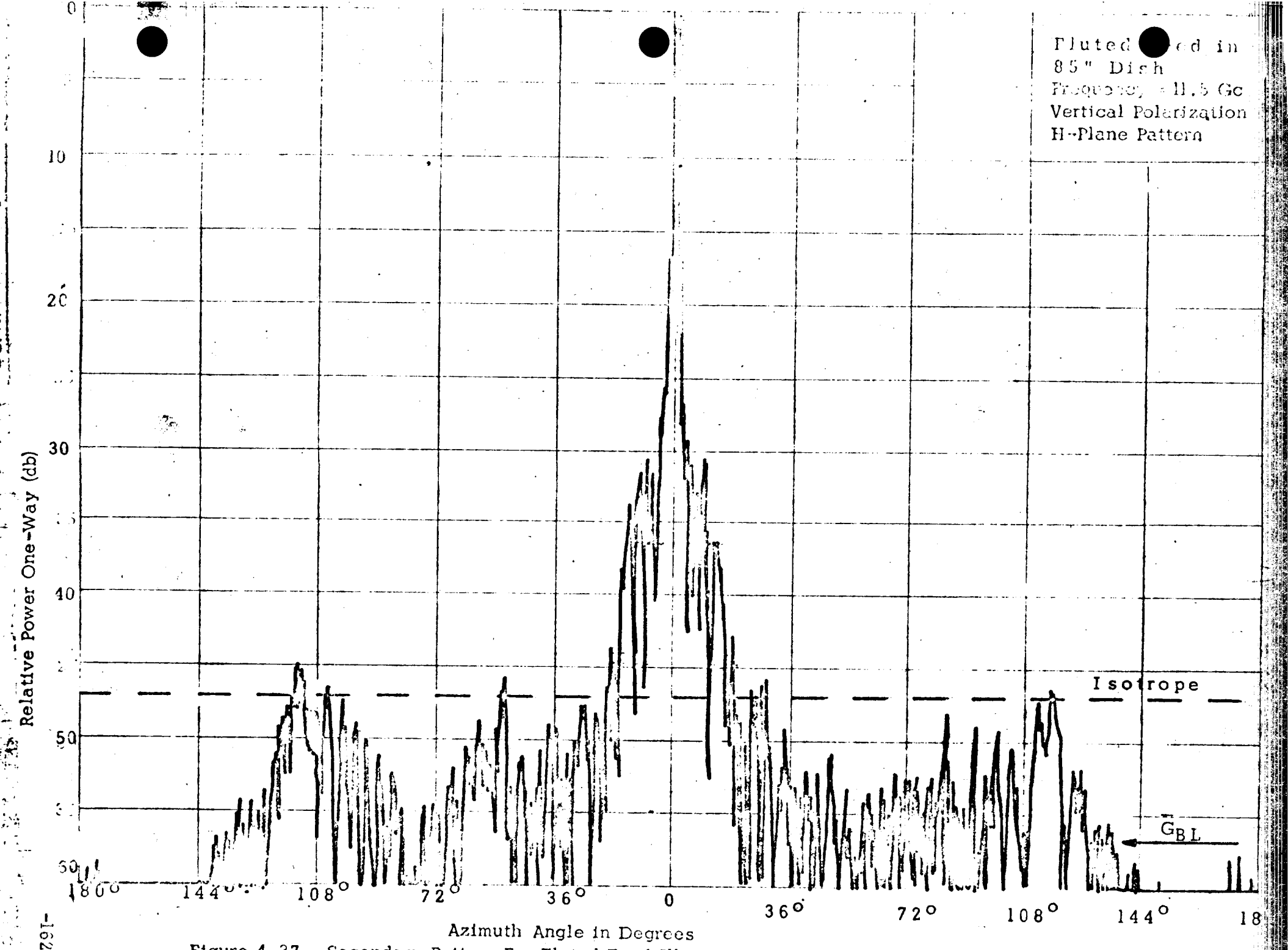

Figure 4-37. Secondary Pattern For Fluted Feed Illumination Of A Paraboloidal Reflector; E-Plane Pattern.

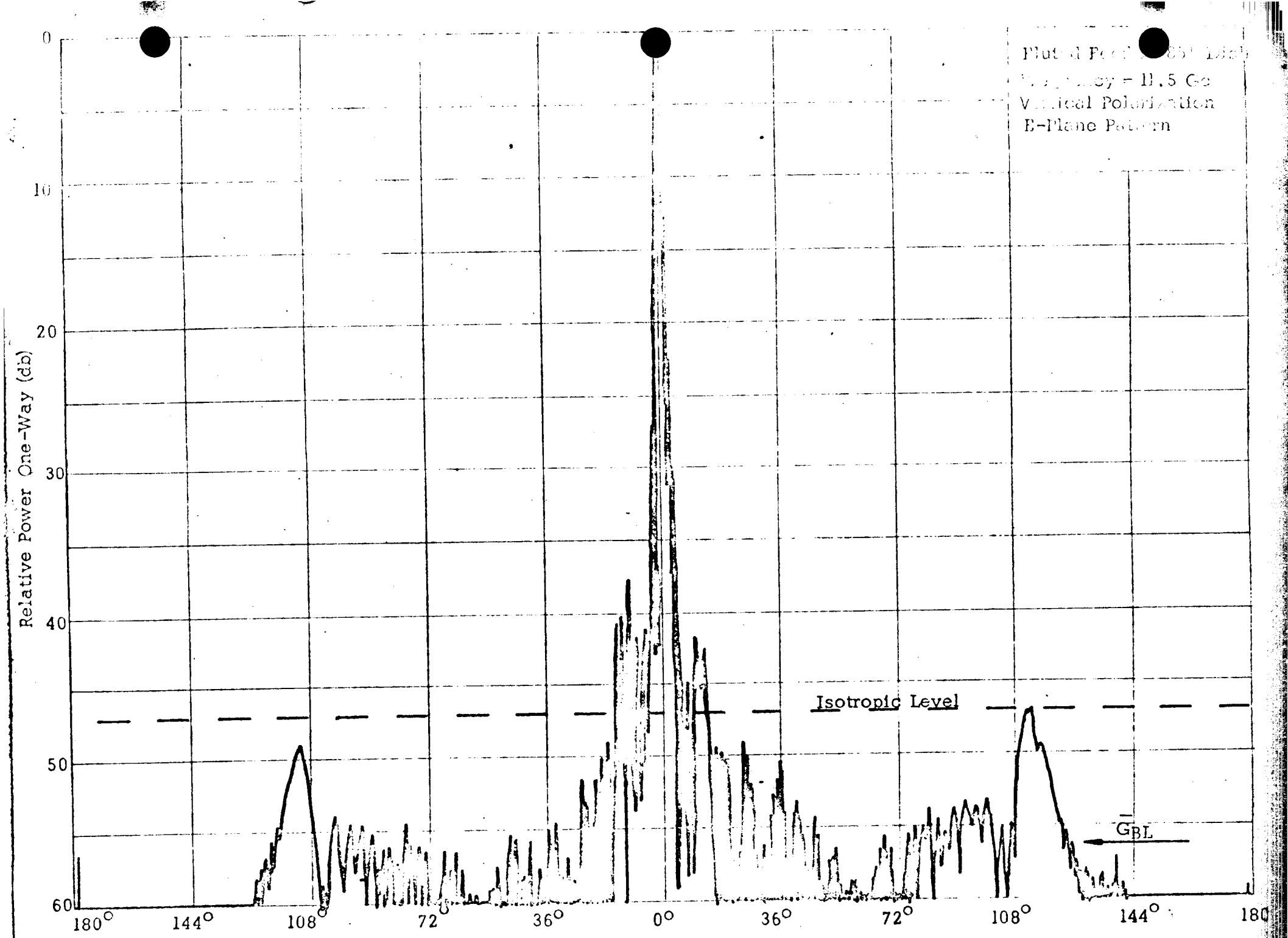

Figure 4-38. Secondary Patter · For Fluted Feed Illumination Of A Paraboloidal Reflector; E-Plane Pattern.

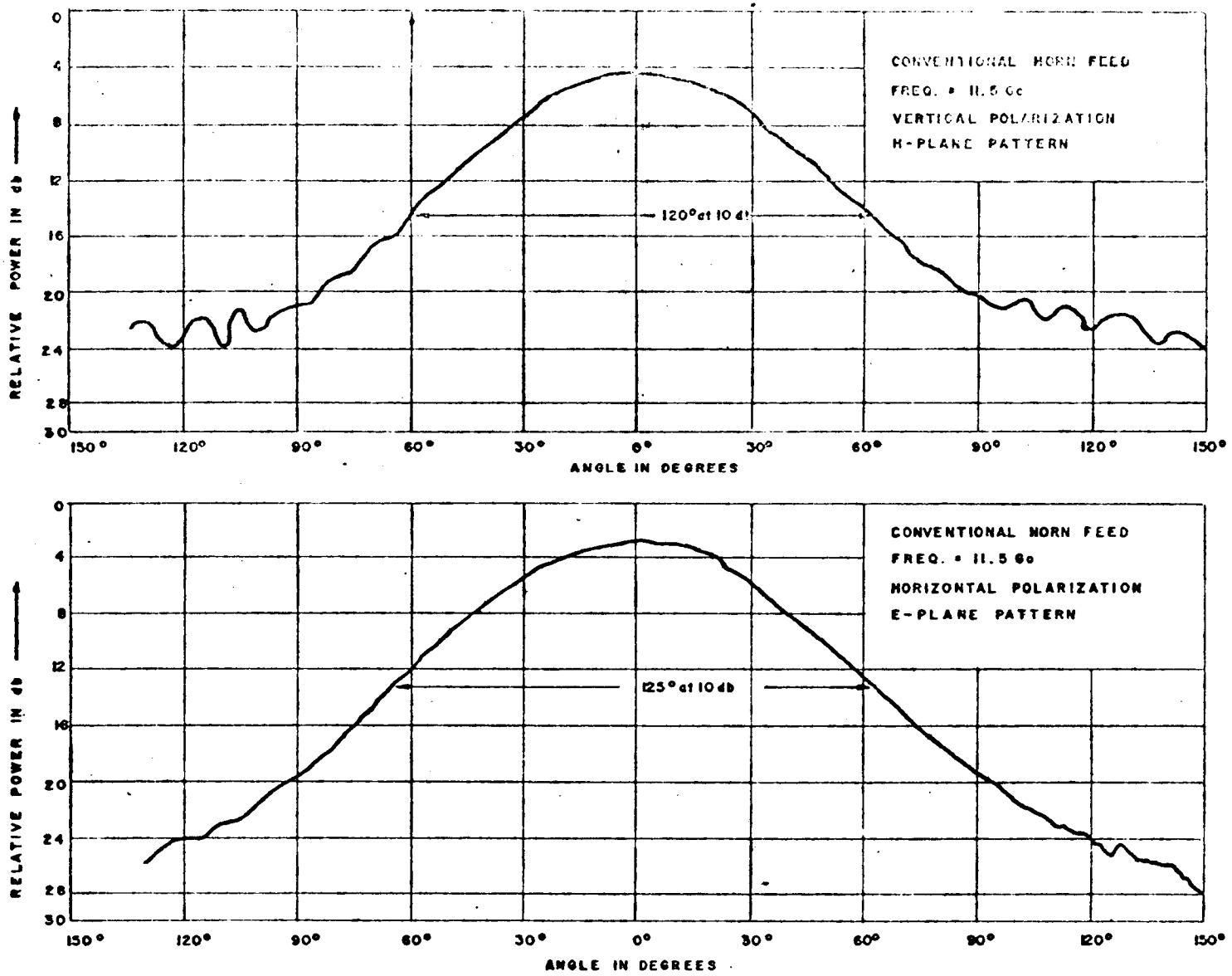

Figure 4-39. Primary Patterns For Conventional Flared Horn Feed Used With Paraboloidal Reflector.

related but undoubtedly more significant is the extreme improvement noted in the minor-lobe energy level attained by use of the fluted feed. The improvement in calculated antenna effective noise contribution from the ground region is based on the measured minor lobe levels in the region including the ground and assumes an equivalent black body radiation temperature for the ground of 240° Kelvin (including an emissivity correction equal to .83). For these reasonably valid, or nominal conditions, we realize an improvement in the antenna noise temperature contribution from ground radiation by use of the fluted feed of nine db, or nearly an order of magnitude over conventional horn illumination.

The fluted feed also appears amenable to monopulse operation. A typical way in which this may be implemented is illustrated in Figure 4-40. It was not possible to fabricate an additional fluted feed structure in order to investigate further the adaptability of the fluted feed structure to monopulse operation. However, with few reservations it does appear to offer a great deal of promise in providing an efficient low noise feed structure which may be utilized with existing large paraboloidal reflectors in improving to some extent the gain characteristics of the antennas and improving considerably the low noise characteristics of the system.

The advantages of the fluted feed surface wave antenna in low noise antenna systems might be reviewed. An antenna feed was desired with which nearly uniform illumination could be obtained across the secondary aperture with very little spillover and relatively low minor-lobe energy. Also, it was desired that the energy density at the secondary aperture edge be reasonably small which requires a rapid illumination taper of the primary illumination at the aperture edge. It was also desired to utilize this feed in circular polarization feed systems which required

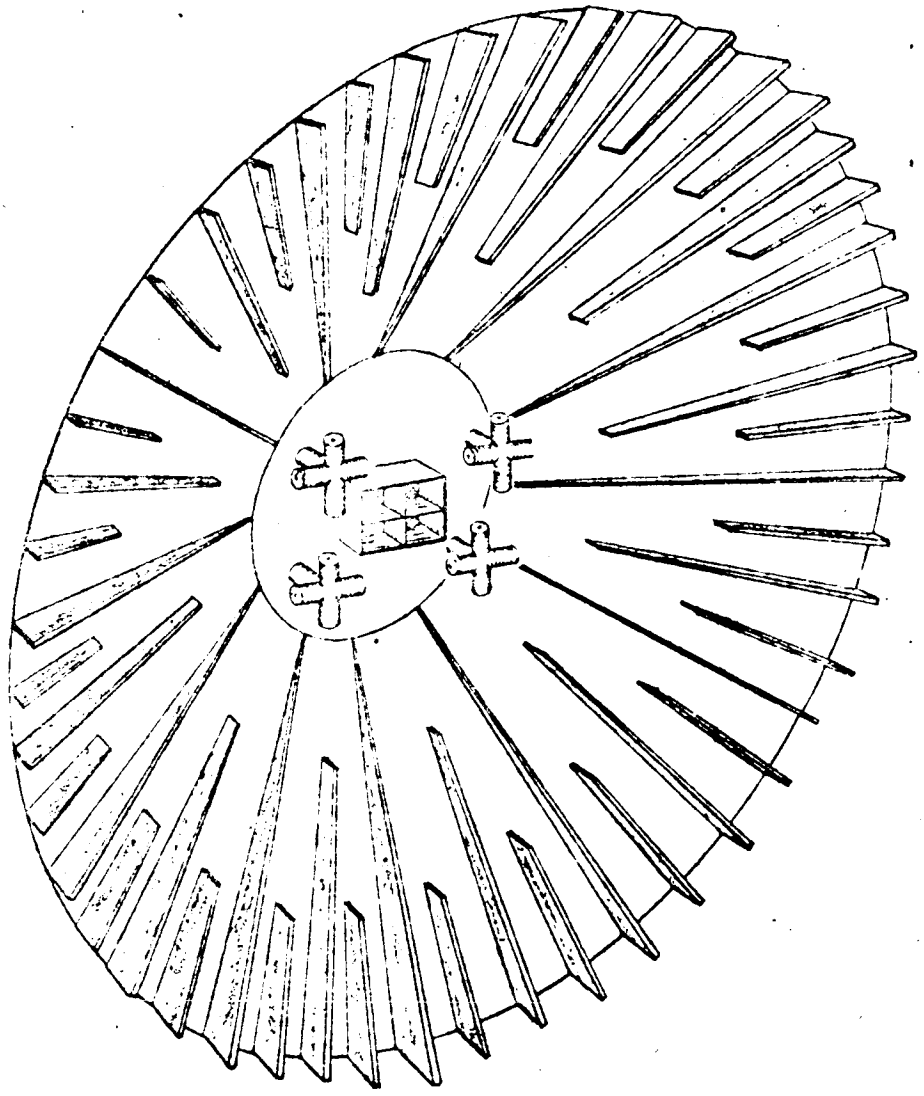

Figure 4-40. Monopulse Fluted Feed Configuration.

that the E and H-plane patterns be of equal beamwidth. It was also hoped that a design would be evolved which could be amenable to use with present paraboloidal antenna systems. The fluted feed accomplished all of these requirements. Indeed, the principal requirements placed upon the desired feed structure are found to be its main advantages. These advantages may be listed as follows.

(1) Nearly uniform reflector illumination.

(2) No spillover at reflector edges.

(3) E and H-plane patterns with equal beamwidths.

(4) Complete polarization flexibility.

(5) Negligible aperture blocking in high gain applications.

(6) Improved performance by retrofit of existing paraboloids.

In summary, a comparative performance evaluation of the fluted feed structure with a conventional horn feed indicates an appreciable improvement in the aperture efficiency of the antenna system with a resulting gain increase and an order of magnitude improvement in the antenna noise temperature performance characteristics of the antenna system.

4.3.5 Aperture Blocking Efforts

Due to the physical size of the surface wave structures used as pattern shaping elements with the primary feeds, it appears desirable to determine the magnitude of the influences on the far field pattern caused by the physical extent of the primary feed structure. The aperture blocking effect is the principal cause investigated. This effect generally results in a degradation of the side lobe levels present in the secondary response of the antenna.

In order to determine rigorously the perturbation in the secondary field due to aperture blocking it is necessary to evaluate the far field response resulting

from a modified field configuration near the secondary surface. The modified field configuration is caused by the combined scattering, absorbtion, re-radiation and reflection of the primary structure. This influence may be approximated for analysis as an additional source of field energy which replaces the primary feed structure appearing in this region as a cancellation field; i.e., a field described in the region of influence by field components of the same amplitude but of opposite phase relation to the original field existing in the region.

Fortunately, it is not necessary to set up or solve the boundary value problem involved since a reasonably accurate approximation procedure exists[1]. Silver[2] and others have also investigated the problem from the fundamental considerations and may be referred to for a justification of the cited approximation procedure. Feed blocking in general increases the minor-lobe level, decreases the gain and sharpens somewhat the main beam. The latter two effects are negligible for most practical cases, but the increase in minor-lobe level is significant. A close approximation to the lobe level obtained with feed horn blocking may be obtained by first calculating the far field pattern from a knowledge of the primary feed characteristics and the resulting aperture illumination, neglecting the feed blocking effects. This establishes the normalized minor-lobe level without feed horn blocking. The normalized value for the minor-lobes including the effects of feed horn blocking may be obtained by adding to the minor-lobe level previously obtained a term equal to twice the ratio of the feed horn area to the total aperture

---

1. R. L. Mattingly, "Radar Antennas", Chapter 25 in "Antenna Engineering Handbook" edited by H. Jasik, McGraw-Hill Book Co., N. Y., 1961, p. 25-3.

2. S. Silver, "Microwave Antenna Theory and Design," McGraw-Hill Book Co., N. Y., pp. 190-192.

effect of feed may be expressed as

$$P_b \approx P_o + 2A_b/A_o$$

or

$$P_b \text{ (db)} \approx 10 \log (P_o + 2A_b/A_o)$$

where P_o is the minor-lobe power level neglecting feed blocking, A_b is the effective area of the feed blocking, A_o is the effective area of the total secondary aperture, and P_b, is the resulting minor-lobe power level including the effects of feed blocking. P_b (db) is the same as P_b but is expressed in decibels. This may also be written in terms of the diameters involved in the case of circular symmetry for both feed and aperture as:

$$P_b \text{ (db)} \approx 10 \log_{10} \left[P_o + 2(D_f/D_a)^2 \right]$$

where D_f is the feed diameter and D_a is the aperture diameter.

Figure 4-41 is a plot of the degradation of the principal minor-lobe level as a function of primary feed extent normalized in terms of feed and aperture diameters expressed in terms of wavelength. The plot assumes a uniformly illuminated aperture. The examples given are for an 85 foot reflector operating at 4 Gc and 2 Gc and indicate degradation levels of approximately 0.1 db and 0.5 db for an effective primary feed diameter of about 10 wavelengths. This degradation does not appear to be a particularly restricting factor on the use of reasonably large surface wave structures as primary feed elements.

Figure 4-42 is a plot of a family of curves relating the ratio of feed to aperture diameters to the aperture diameter in feet for selected frequencies between one and ten Gc. The plots assume a primary feed extent of ten wavelengths. This figure may be used to determine the D_f/D_D ratio for use with the previous figure from the antenna aperture size and frequency of operation.

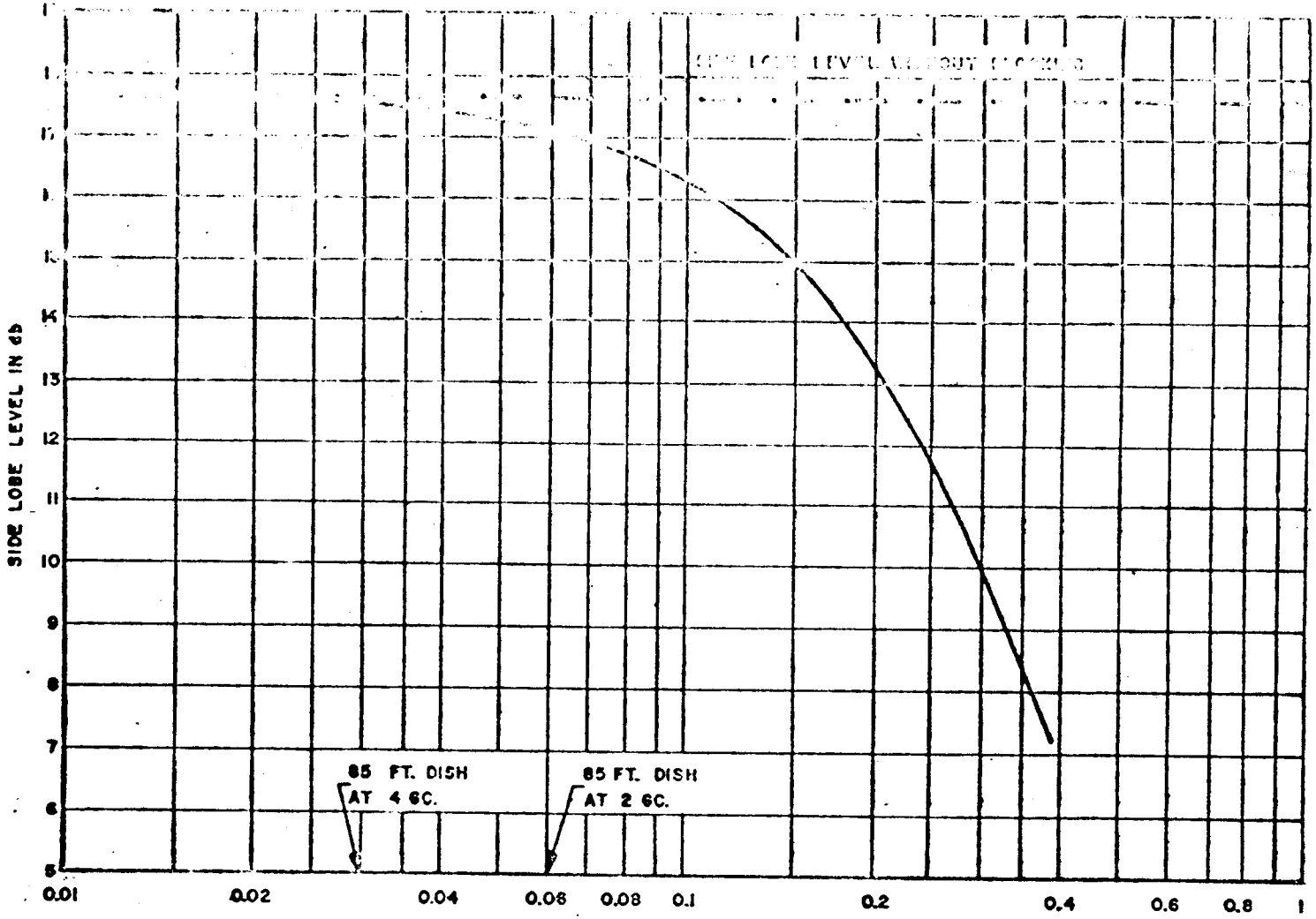

Figure 4-41. Minor-Lobe Level Degradation As A Function Of Feed Extent.

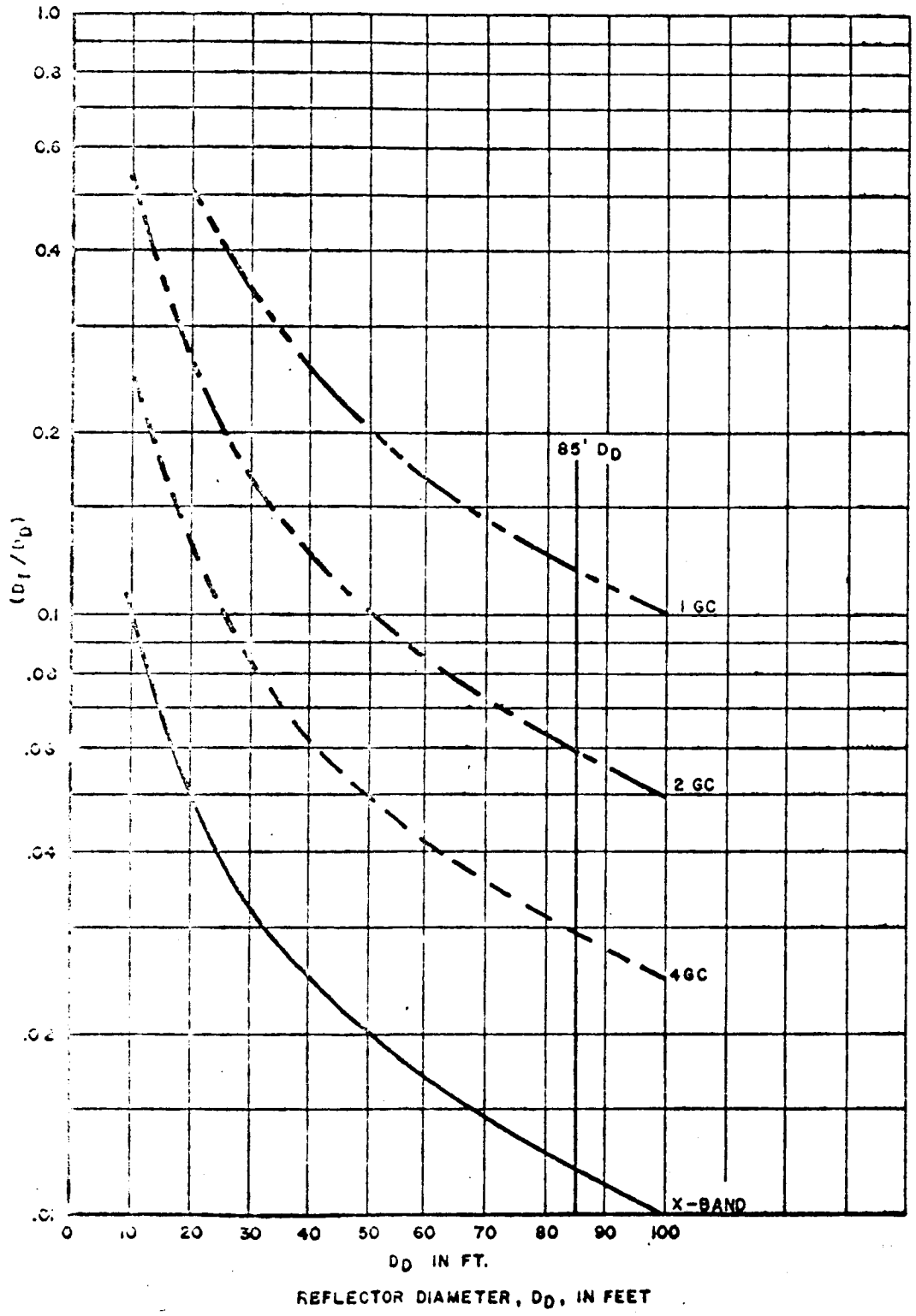

Figure 4-42. Feed To Aperture Diameter Ratio As A Function Of Total Aperture Diameter For A Given Feed Extent.

4.3.6 Evaluation of Technique

Employment of surface wave structures to obtain a composite polarization insensitive primary feed system or as single surface elements arranged in an elliptical fashion for linear polarization illumination, provides a very powerful technique for feed shaping of the primary energy distribution. The evolution of the fluted feed structure for use in circular polarization feed systems from the linear polarization surface wave criteria is felt to be a significant contribution to low noise feed systems. The device generally meets all of the requirements for feed shaping placed upon it initially and appears to have additional potential limited only by the feed aperture considerations.

It is believed that one of the most significant achievements during the Low Noise Study program has been the development of the low noise high efficiency fluted feed structure. Techniques which have been used in the fluted feed design and in the other material presented in this report are certainly amenable to use with other feed configurations. Application of certain of these principles should enable low noise modifications to be performed on many existing antenna systems and should influence the design and system operating capabilities of future paraboloidal reflector antenna systems.

V CASSEGRAINIAN SYSTEMS

5.1 Cassegrainian System Approaches

The Cassegrainian approach to the low noise antenna problem has certain inherent advantages and has gained considerable acceptance for use in low noise receiving systems. The conventional Cassegrainian configuration utilizing a hyperboloidal sub-reflector and a paraboloidal reflector has been treated extensively in the literature, and it is not the intent of the study to re-evaluate the conventional Cassegrainian systems which are presently in use. However, it was considered desirable to obtain a reasonable estimate of the principal advantages and disadvantages of Cassegrainian systems, the limitations of the technique, and to investigate any particular feature which appeared to offer promise for the improvement of Cassegrainian antenna performance. It was also desired to evaluate a Cassegrainian sectoral horn-reflector system which had been discussed in the early part of the program.

The significant advantage of the Cassegrainian configuration is the relocation of the spillover energy associated with the primary feed illumination from the relatively high effective noise temperature ground region into the relatively low noise sky region. The principal disadvantages of the Cassegrainian antenna appear to be the degradation in aperture efficiency due to the difficulty in providing proper illumination to the hyperboloidal sub-reflector, the increased phase error losses associated with a dual reflector configuration, and aperture blocking by the sub-reflector. The convex configuration of the hyperboloidal sub-reflector used with conventional Cassegrainian antennas, results in a divergence of the primary energy over the secondary aperture. It is therefore necessary to illuminate the relatively small sub-reflector with an energy distribution similar to that desired at the secondary surface but of usually smaller angular extent. These considerations usually dictate a larger primary feed aperture resulting in general in a more complex feed requirement

than necessary for the same illumination of a conventional horn-reflector system. A large primary feed aperture is often not readily obtainable and primary feeds are employed which generally result in high levels of forward spill-over energy past the hyperboloidal sub-reflector and high values of current density at the edges of the secondary reflector. An unusual geometry for the Cassegrainian system which appears to overcome certain of the disadvantages inherent in the conventional Cassegrainian configuration is the use of an ellipsoidal sub-reflector as the feed focusing element for the secondary dish. This technique is discussed, and primary patterns for the ellipsoidal sub-reflector configuration are presented.

Some quite surprising and very encouraging results were obtained in the investigation of the Cassegrainian sectoral horn - reflector system designated the KSK antenna. This antenna utilizes many of the desirable features of the sectoral horn-reflector system as employed recently by BTL in their Telstar communications satellite program and commonly referred to as the "sugar scoop" antenna. The KSK antenna utilizes a Cassegrainian approach to avoid most of the inherent mechanical disadvantages of the "sugar scoop" antenna and appears possibly to have developed into an antenna configuration which operationally may be considered at present the state-of-the-art in low noise antenna designs.

5.2 Ellipsoidal Sub-Reflector Configuration

5.2.1 Ray Tracing Feed Shape Determination.

The principle of operation of the Cassegrainian antenna as conventionally employed is to image the focus of the paraboloidal secondary surface to a point near the center of the secondary surface by means of a sub-reflector providing the appropriate reflecting surface for the incident energy. Hyperboloidal reflectors are conventionally used, however, an ellipsoidal reflector is equally satisfactory.

Hyperboloidal sub-reflectors are necessary if the sub-reflector is to be located between the focus of the paraboloidal surface and the surface itself; ellipsoidal sub-reflectors are necessary if the sub-reflector is to be located at a distance from the center of the surface greater than the focal length of the surface.

The focii of the ellipsoid are then arranged such that the far focus for the ellipsoid corresponds to the phase center of the primary feed and the near focus of the ellipsoid is set as the common focus of the paraboloidal surface and the ellipsoid, as illustrated in figure 5-1 . It should be noted in the figure that as in the case of a hyperboloidal sub-reflector there is a diverging effect caused by the ellipsoidal sub-reflector of the energy from the primary feed after reflection. This is to say that the angle θ in the figure relating the ray path leading from sub-reflector surface to the paraboloidal surface is greater than the angle of incidence of the same energy measured as angle α , indicating the ray path from the phase center of the primary feed to the sub-reflector surface. The desired configuration for an ellipsoidal Cassegrainian system may be easily determined to a first order approximation by utilizing simple ray tracing techniques. In this manner the physical extent of the sub-reflector and the location of the focii for the selected ellipsoidal surface may be determined in conjunction with the paraboloidal surface characteristics. As shown in the figure, it appears desirable to use a waveguide feed protruding through the secondary surface and well into the region of the ellipsoidal sub-reflector. This arrangement minimizes the required primary aperture desired for conventional horn illumination and allows some flexibility in primary beam shaping techniques for illuminating the sub-reflector.

5.2.2 General Illumination Characteristics

The Cassegrainian system has found considerable use in the recent years

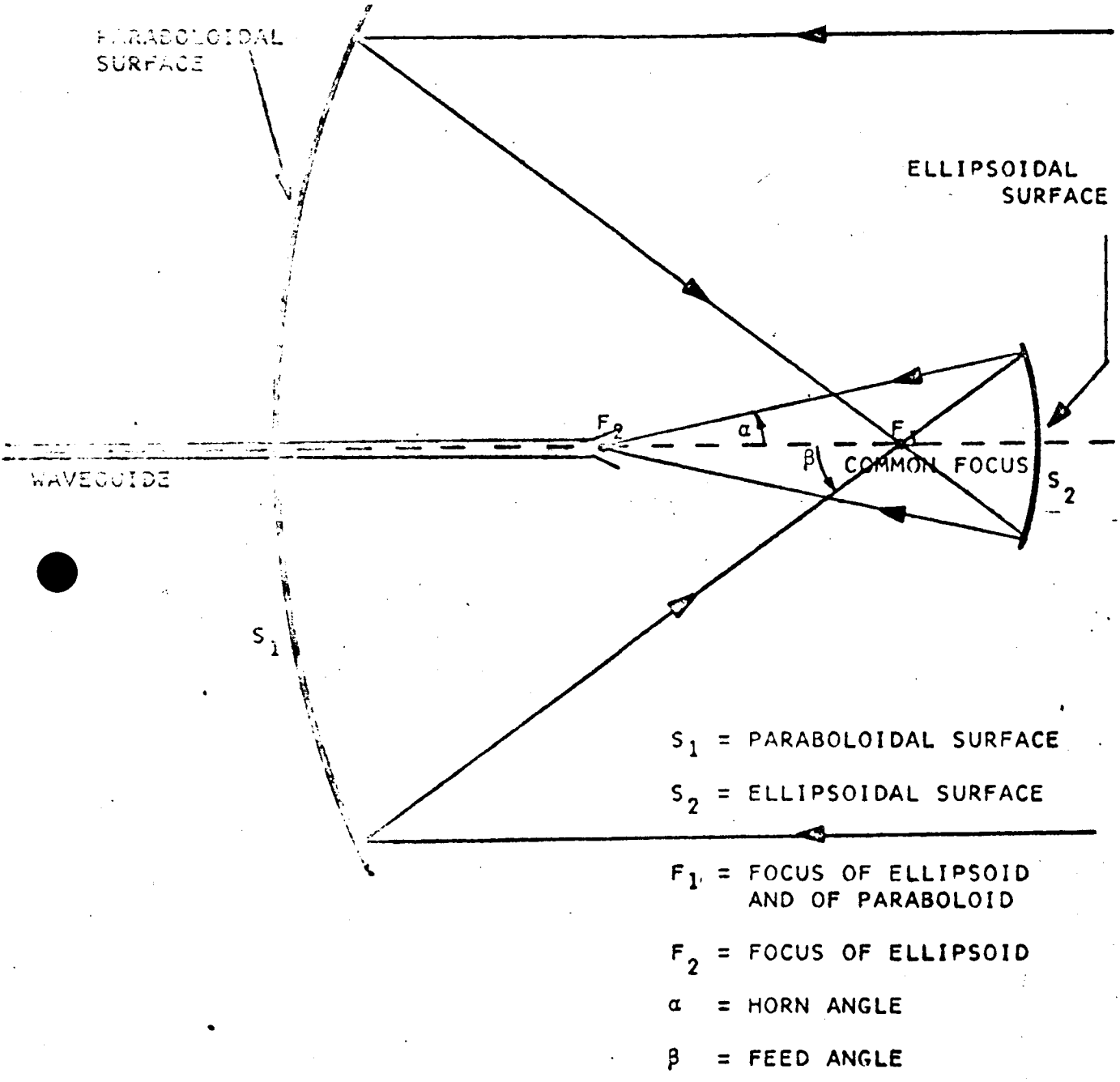

Figure 5-1. A Low Noise Cassegrain Antenna Utilizing An Ellipsoidal Sub-Reflector.

in a wide variety of radar and microwave antennas. Conventional Cassegrainian antennas are in use which have beamwidths ranging from about 2^{o} down to small fractions of a degree. The Cassegrain principal utilizing double reflector illumination certainly assists in removal of the spill-over energy from the region behind the reflector and places the spill-over which does occur in the vicinity of the pointing direction. This is advantageous at high frequencies in optimizing low noise performance, since the sky noise temperature is considerably less than the ground noise temperature. A Cassegrainian arrangement also appears to be generally compatible with the conventional paraboloidal reflectors such as the many NASA facilities of this type in present use.

In order to evaluate the ellipsoidal sub-reflector, characteristics in a typical Cassegrainian antenna system, a metallic plate ellipsoidal cylinder sub-reflector was fabricated for use with a line source feed. A slotted waveguide line source feed was also fabricated and placed at the focus of the ellipsoidal sub-reflector. The sub-reflector and line source feed are shown in Figures 5-2 and 5-3 . This system was fabricated to evaluate primary patterns for the ellipsoidal sub-reflector and to possibly evaluate far field patterns in utilizing this system with the paraboloidal cylinder fabricated earlier in the program. An ellipsoid of revolution fabricated of plaster with a surface of conducting silver paint was completed and planned for use with the 85 inch paraboloidal reflector utilized with other feed system far field pattern measurements. Primary patterns were also obtained for the ellipsoidal cylinder sub-reflector utilizing a circular polarization horn similar to that described previously. Figure 5-4 is a typical pattern for the general illumination characteristics obtained for the ellipsoidal cylinder sub-reflector employing a circular polarization feed. The conditions for this particular primary pattern are

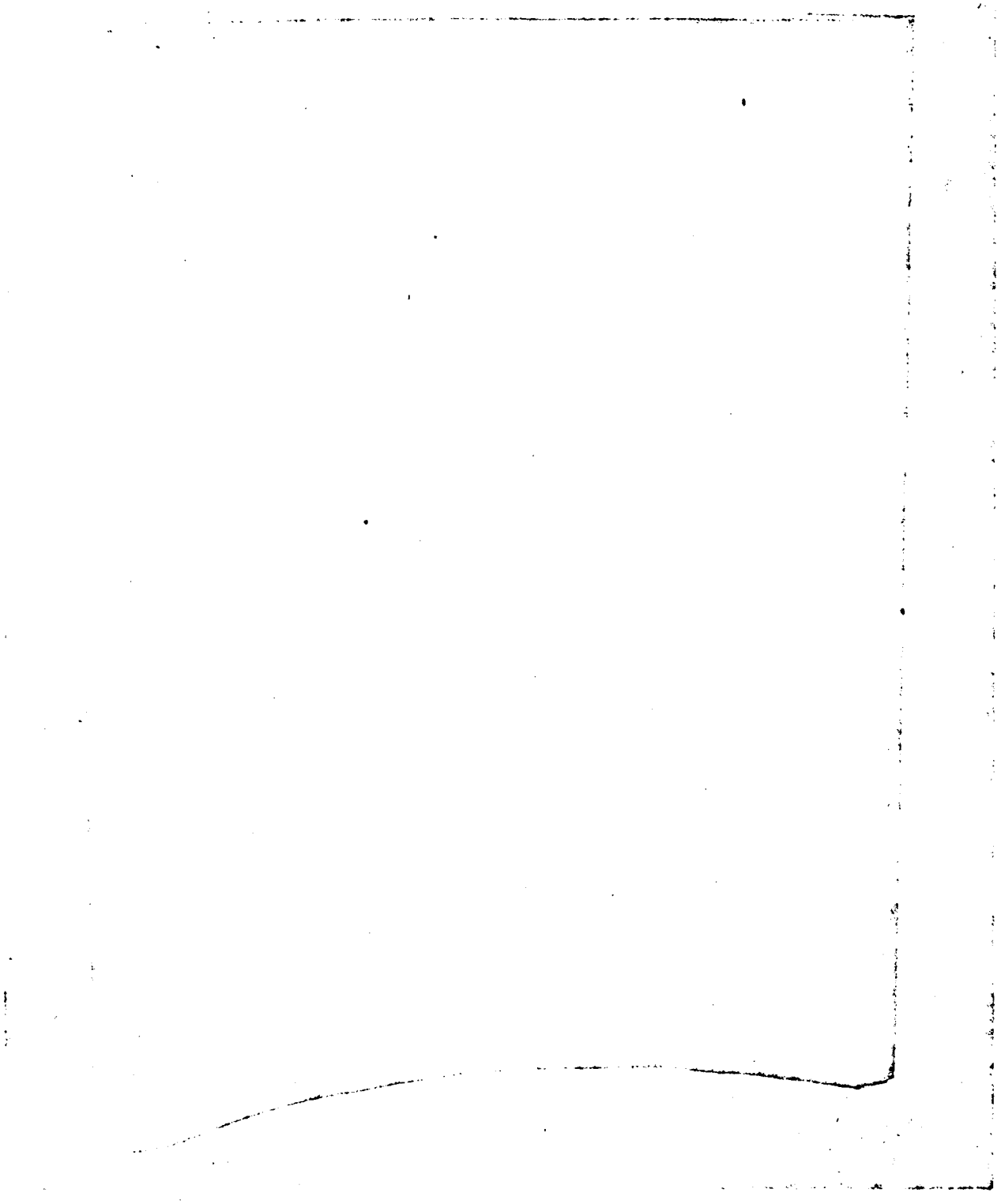

Figure 5-2. Ellipsoidal Sub-Reflector For Use With Cassegrain Antenna

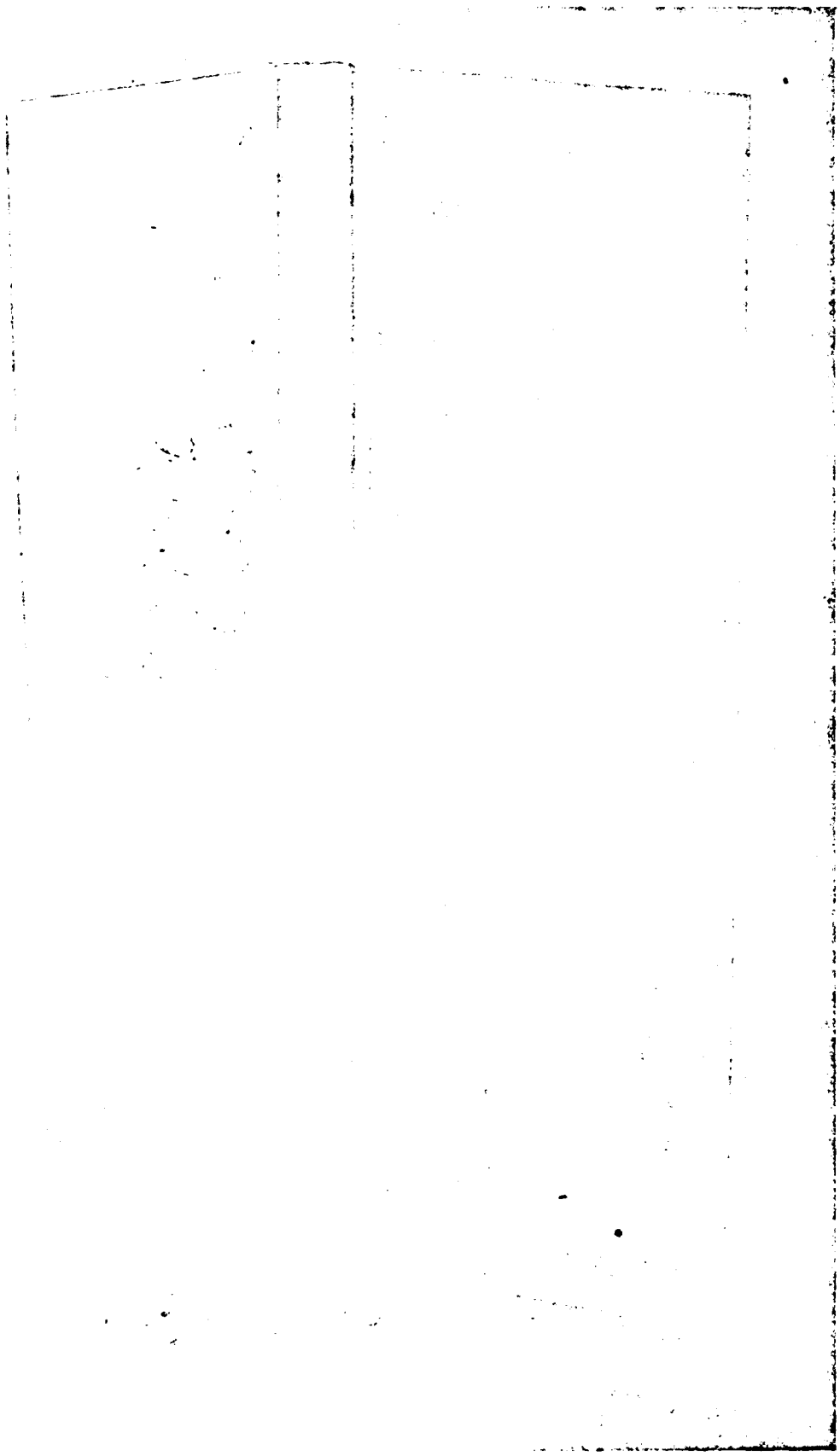

Figure 5-3. Slotted Waveguide Line-Source Feed For Use With Cassegrain Antenna.

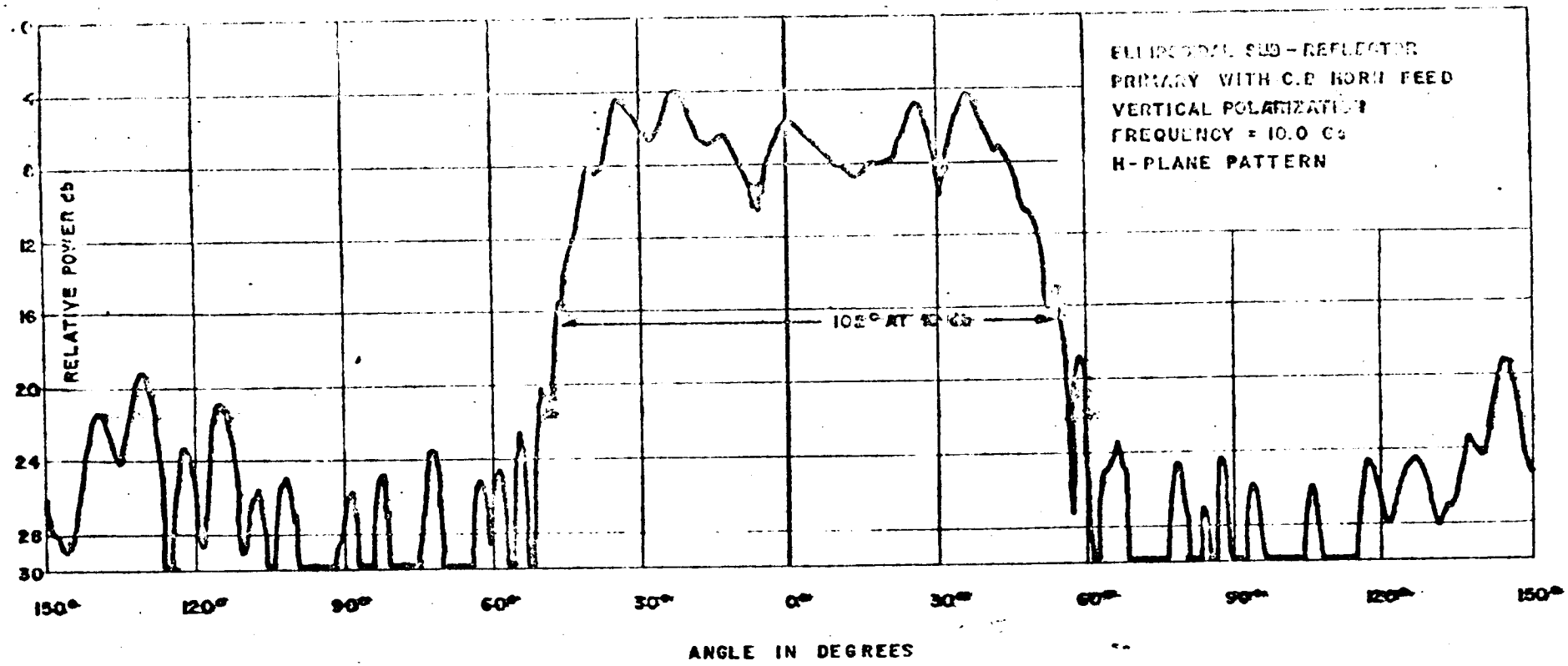

Figure 5-4. Primary Pattern For Ellipsoidal Cylinder Sub-Reflector.

that the frequency of operation was 10.0 Gc, vertical polarization was used, and the pattern is for an H-plane measurement. This technique appears to have merit in that the primary illumination is reasonably uniform over its extent and decreases to a fairly low spill-over level in the region extending from its beamwidth edge at approximately -10 db points to well beyond 90°. The average sidelobe energy due to the primary pattern in this region is seen to be greater than 20 db below the average level of the main portion of the primary illumination. The measured beamwidth of the primary illumination is 101° at the -10 db response points, but this is considered satisfactory since the illuminating circular polarization horn had a reasonably narrow beam pattern in itself.

5.2.3 Discussion of Technique

There is believed to be considerable merit in the use of an ellipsoidal sub-reflector as the primary pattern forming focusing surface in Cassegrainian configurations. Primary patterns taken for a typical ellipsoidal sub-reflector illuminated with a circular polarization horn indicate reasonably constant primary illumination patterns over the surface of the secondary aperture, and in general indicate a quite promising feed technique. It might be noted that modification of existing large antennas by means of an optimal Cassegrainian sub-reflector appears to a feasible approach to minimizing the effect of ground radiation contributions to the antenna noise temperature and thereby improving the sensitivity of many present antenna installations.

5.3 MSI Antenna

The MSI antenna is basically a Cassegrainian sectoral horn type of reflector system which is an adaptation of the sectoral horn-reflector antenna which has achieved general recognition as one of the leading low noise antenna systems available. A sectoral horn antenna, commonly referred to as a "sugar scoop" antenna, of reasonably

large aperture size (about 1600 square feet) was recently employed operationally by the Bell Telephone Laboratories in their Telstar communication satellite program.

The sectoral horn antenna presently being used in the Telstar system suffers from three basic problems. First, a relatively high diffraction lobe of approximately 30 db associated with energy from the reflector aperture exists, which appears to be disturbed by the presence of the large ring gear near the aperture. The exact cause of this lobe is difficult to predict. It is quite possible that some type of mode configuration within the horn is responsible. Previous experience has indicated that many obstacles can be placed in the vicinity of a collimating beam without drastically effecting the beam. However, the accepted explanation is that of diffraction past the ring gear. Another problem associated with the existing antenna is that of assymetrical amplitude distribution across the aperture in the plane containing the apex of the sectoral horn. This is a basic problem since it arises out of the geometry of the horn itself. This assymetrical distribution results in relatively high side-lobes close in to the main beam. Values of the order of 15 db are common. It is difficult to imagine any design techniques capable of eliminating this problem. If one considers that this particular antenna has been studied at the Bell Telephone Laboratories since 1948, and if one realizes the capability existing at that Institution, it is doubtful that any solution exists.

Another problem associated with the sectoral horn-reflector antenna is that of excessive size compared to its effective aperture. The shielded aperture offers great advantage for reducing back-lobe radiation but in this instance it is achieved only by using a configuration with maximum dimensions greater than twice the aperture dimension. Such a structure presents structural problems and windloading problems. As a result, it must be housed in a radome and the radome itself must be relatively

large compared to the available effective aperture. The existence of the radome introduces noise into the communication system so that a very excellent antenna design is degraded.

Figure 5-5 illustrates the principle of operation of the Cassegrainian sectoral horn-reflector often referred to as the KSK antenna after the innovator of the technique. The use of surface S2 as the hyperboloidal sub-reflector imaging the paraboloidal surface focal point back to the feed point along the surface S1 is the basic innovation which converts the sectoral horn-reflector horn system to the Cassegrainian mode of operation. A front three-quarter view of this system is shown in Figure 5-6 . Figure 5-7 illustrates both the KSK antenna and the BTL sectoral horn antenna to an equivalent aperture scale.

The Cassegrainian adaptation of the sectoral horn-reflector system which has been investigated during the program represents a significant improvement in many respects over the BTL sectoral horn. A simple analysis shows the areas of improvement. First, the configuration itself as illustrated permits a more conventional antenna support structure allowing removal of the ring gear presently used in the sectoral horn, hence no obstacle exists near the aperture. The KSK horn utilizes two reflecting surfaces so that an infinite selection of surface pairs are available which may be employed to achieve the collimated beam. One is therefore not necessarily restricted to the paraboloidal geometry but is free to choose from any number of surface pairs. The optimum pair would be that which provides symmetrical illumination in the plane where the sectoral horn is plagued with assymmetry. The development of such an optimum pair of surfaces requires a great deal of effort. However, a quite valid comparison of this technique with the sectoral horn-reflector configuration may be made by utilizing the conventional paraboloidal and hyperboloidal surfaces in a

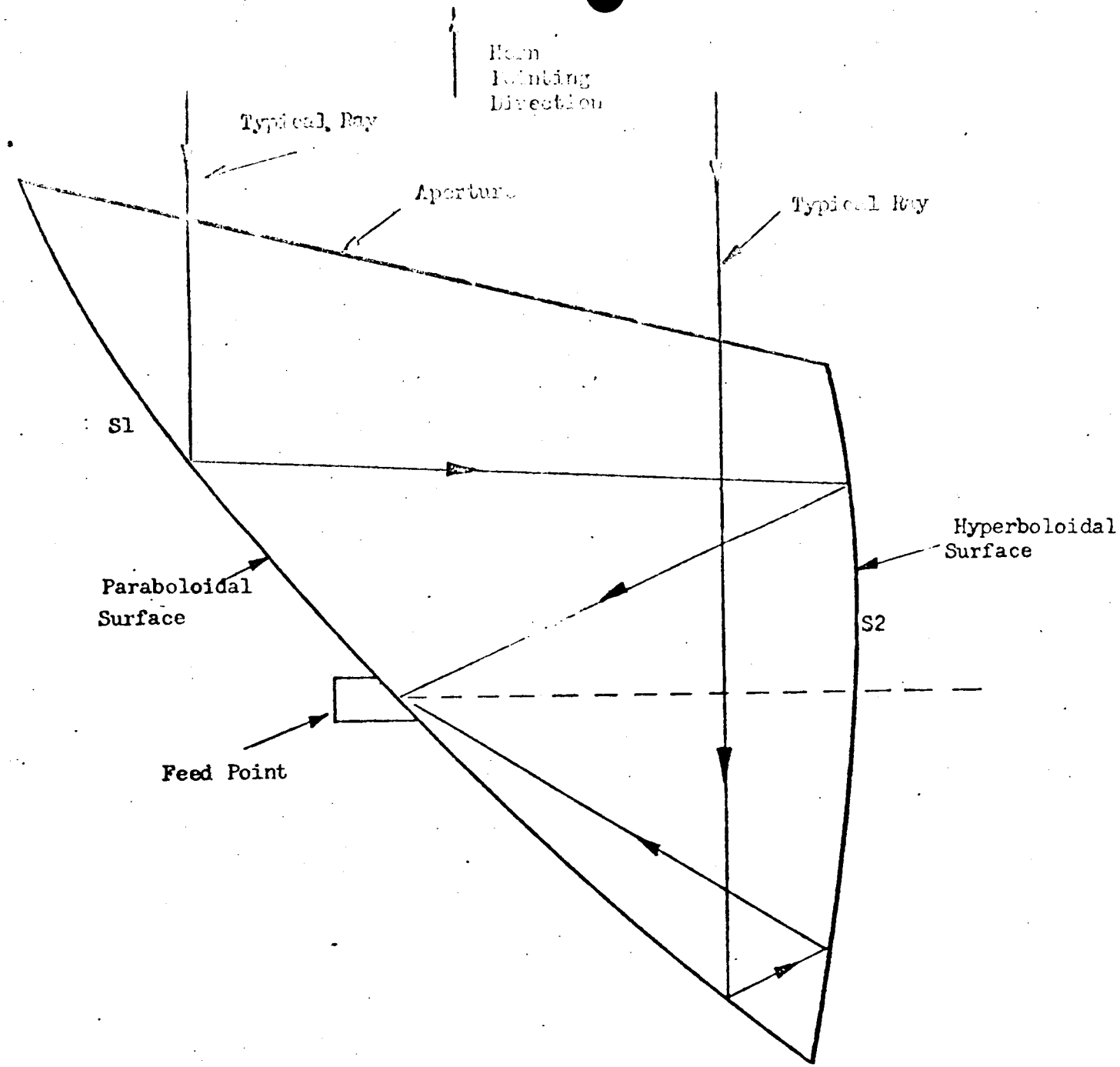

Figure 5-5. Cassegrainian Sectoral Horn-Reflector Antenna (KSK Antenna); Section Detail.

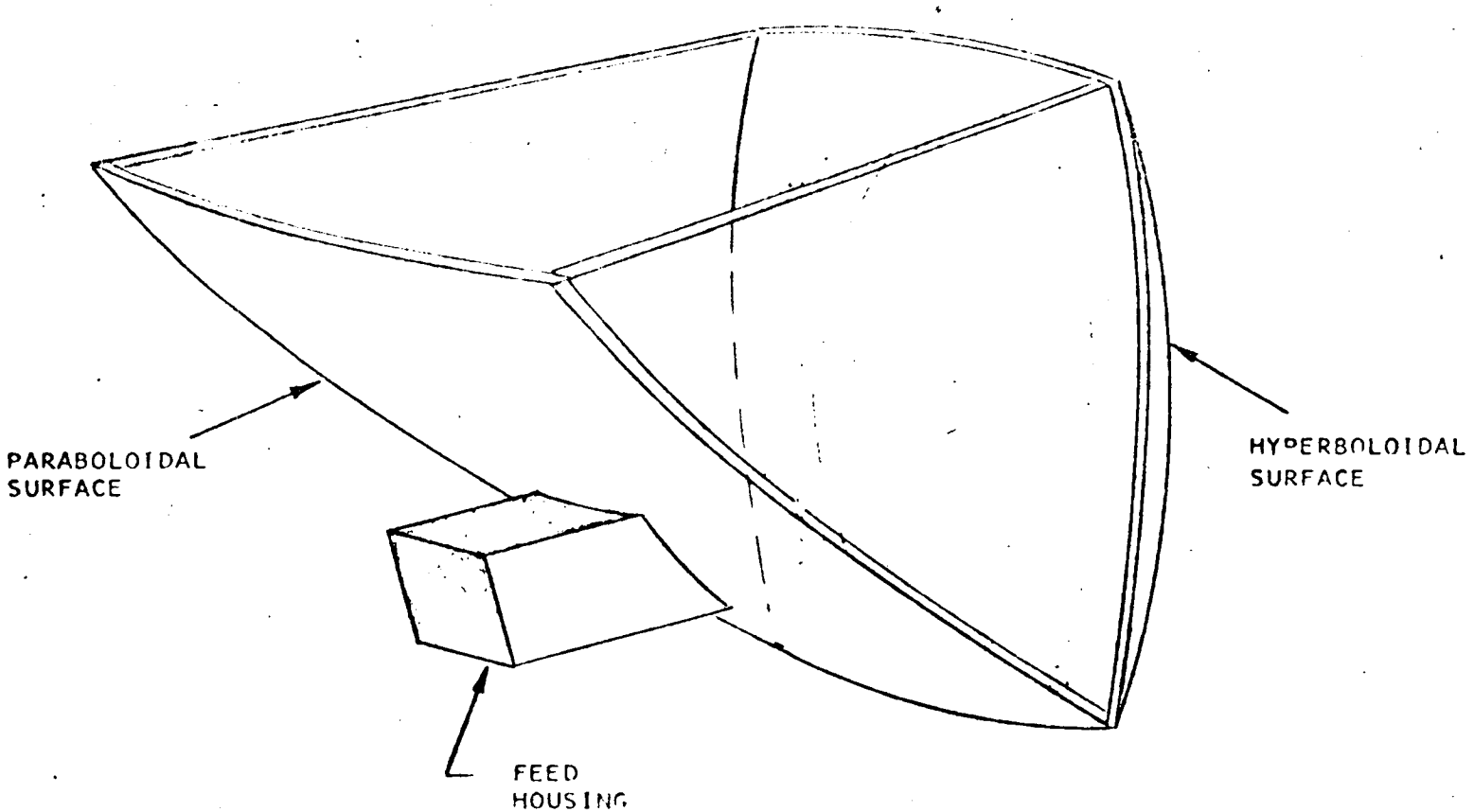

Figure 5-6. Cassegrainian Sectoral Horn-Reflector Antenna (KSK Antenna); Three Quarter View.

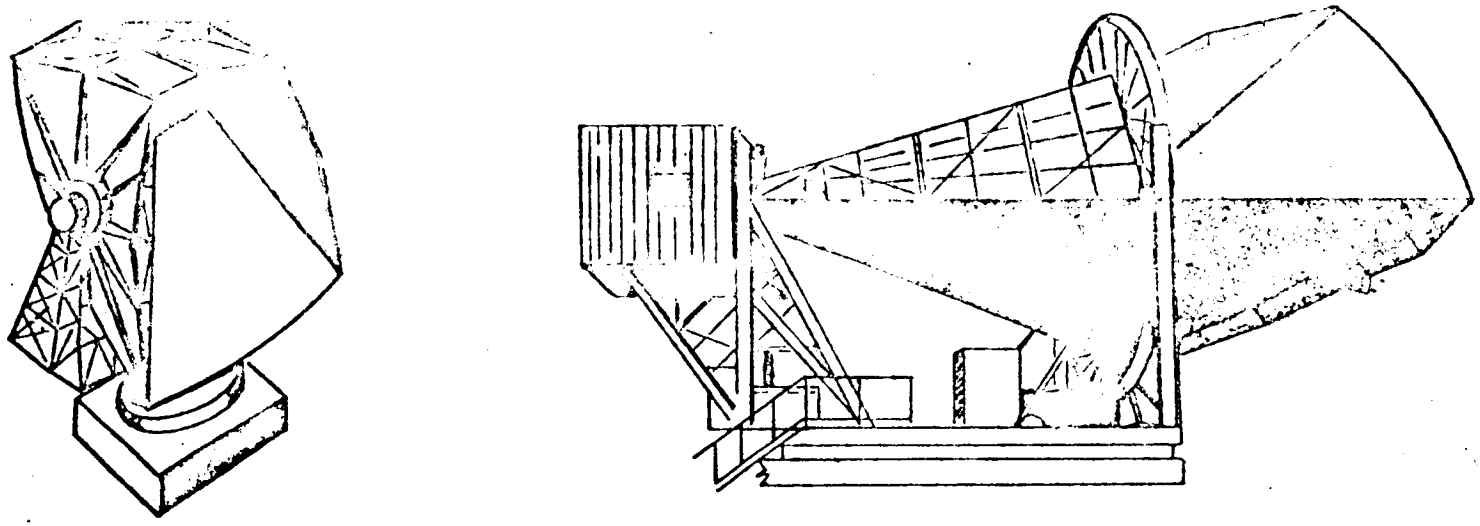

A.G.A. TYPE

B.T.L. TYPE

Figure 5-7. Equivalent Aperture Comparison Of KSK Antenna With BTL Horn-Reflector Antenna.

configuration such as that illustrated as the KSK antenna.

The use of the Cassegrainian approach in modifying the sectoral horn drastically reduces the horn size. It is possible to achieve configurations in which the maximum dimension of this antenna closely approximates the radiating aperture dimensions. This single factor provides an impetus for detailed investigations of this new low noise antenna. If it were possible to obtain a more compact structure, one might readily eliminate the radome with its increased noise and could conceivably obtain an antenna system where cost closely approximates that of the conventional 85 foot reflector antennas.

5.3.1 Geometrical Optics Design

Figure 5-8 illustrates the general principle involved in the KSK antenna. Surface S1 is a parabolic paraboloidal surface, surface S2 is a hyperboloidal surface, and the sides of the structure are flat plates forming a sectoral horn. Approaching the KSK antenna from the standpoint of geometrical optics, it may be seen that typical collimated rays entering the aperture from above are reflected by the paraboloidal surface towards its focal point. Prior to reaching the focal point for the paraboloidal surface, the rays are reflected from a hyperboloidal surface and focused at point P1. Surface S2 provides the transforming surface necessary to image the paraboloidal focus at the desired feed point, point P1. The primary feed is then placed with its phase center at point P1 and with an illumination function for the hyperboloidal surface as desired.

5.3.2 Model Fabrication

Fabrication of a model of the Cassegrainian sectoral horn reflector, the KSK antenna, utilizing a hyperboloid of revolution as a sub-reflector and an inclined paraboloidal surface as a secondary surface was completed during the program. Figures 5-8 and 5-9 illustrate the design geometry for this model.

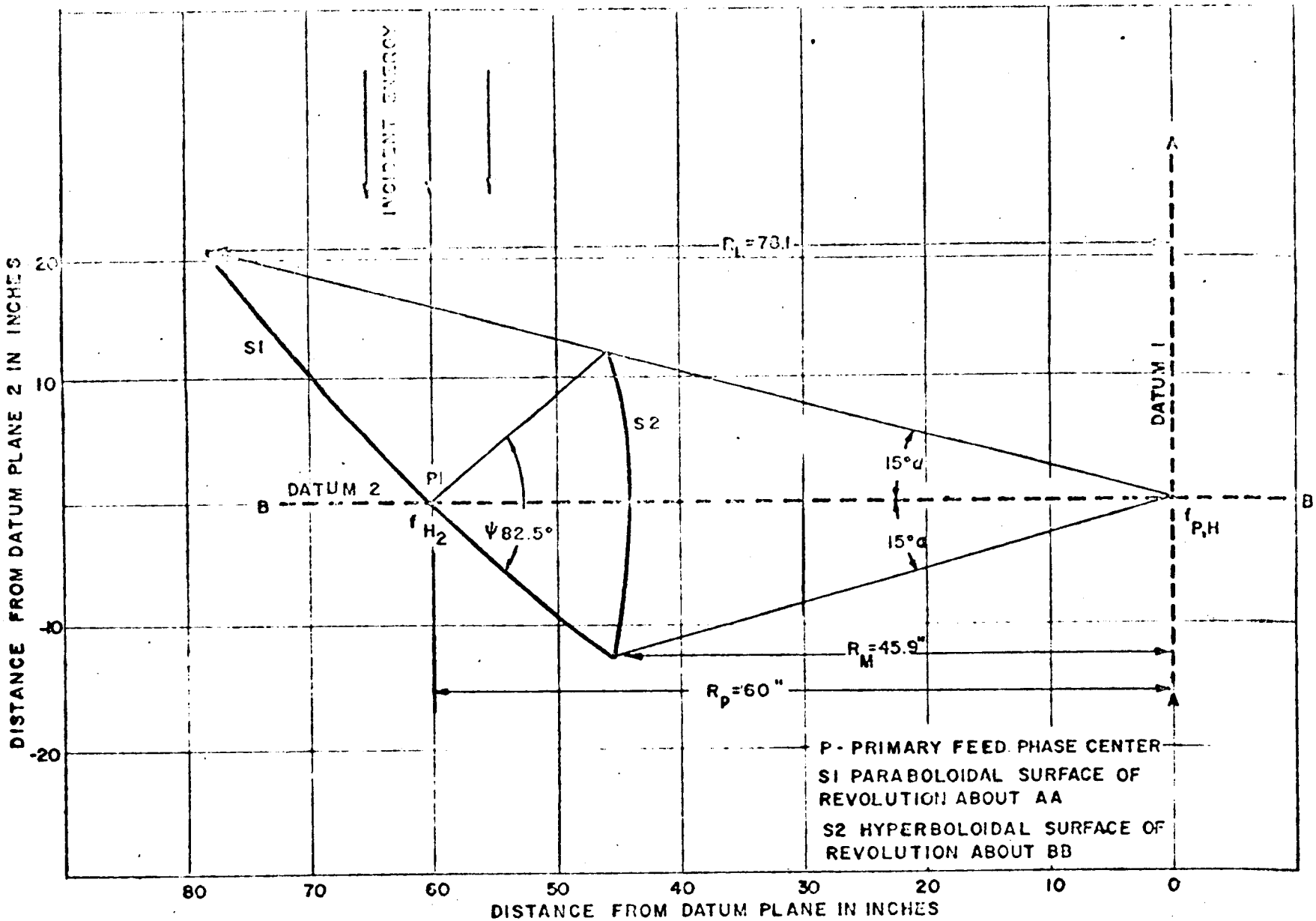

CASSEGRAINIAN SECTORAL HORN-REFLECTOR ANTENNA MODEL GEOMETRY, VERTICAL SECTION VIEW

Figure 5-8.

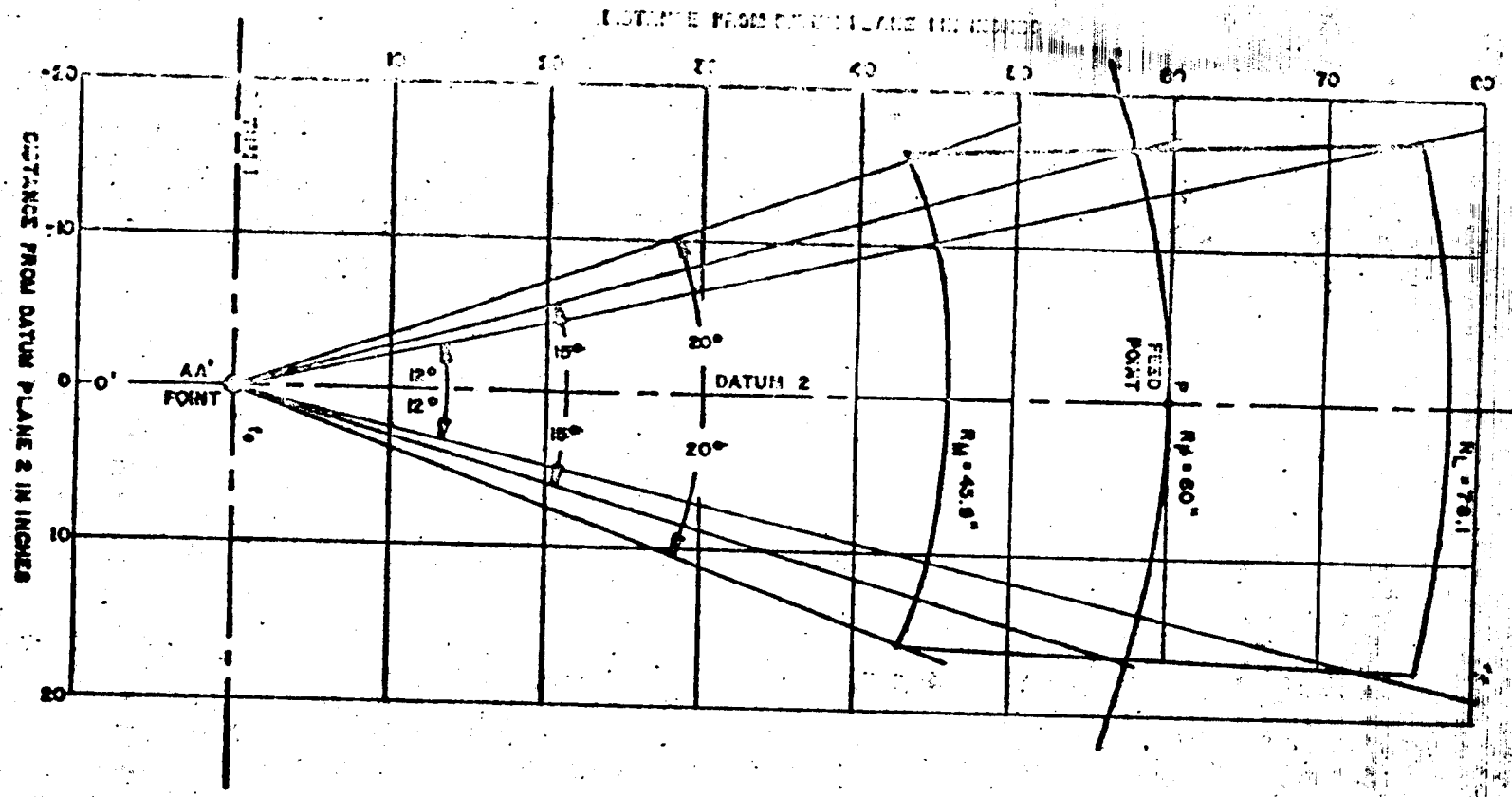

CASSEGRAINIAN SECTORAL HORN-REFLECTOR ANTENNA MODEL GEOMETRY, HORIZONTAL SECTION VIEW

Figure 5-9.

Figure 5-10 illustrates the completed operating test model of the KSK antenna. The hyperboloid of revolution was formed as a swept surface in a plaster mold. The paraboloidal section was initially formed as a swept surface in a plaster mold, and later transferred to a fiberglass selectron impregnated matte which was attached firmly to rib sections to insure structural rigidity of this surface. Final corrections were made on both the hyperboloidal and paraboloidal surfaces by means of reasonably accurate guided templates forming finished plaster surfaces. The surface was further smoothed by means of sanding and application of soft finishing plastic putty which enabled reasonable surface tolerances to be maintained. The exposed faces of both surfaces were then given several coats of conductive silver paint. A plywood housing was constructed for the surfaces as shown in the figure which incorporated means for adjusting both surfaces to the required orientation. Metallic side plates were not incorporated into the model structure, hence the azimuth plane patterns were expected to be possibly degraded somewhat. The estimated surface tolerance to which the model surfaces were held is approximately plus or minus one eighth of an inch. This value corresponds to about an eighth of a wavelength error at the maximum test frequency.

Initial alignment of the KSK antenna was reasonably straight forward. The surfaces were generally adjusted for maximum received signal level from a medium power transmitting source located some distance away. Alignment of the original surfaces was accomplished by minor corrections applied to the measured geometric design configuration. Final focusing was accomplished by feed horn placement in the aperture. This operation was simplified by the fact that the feed was oriented along the hyperboloidal axis and it was possible to adjust the placement of the feed along this axis to a reasonable extent. The designed beamwidth for the primary illumination required by a circular polarization horn at the feed point was set as approximately 80 degrees.

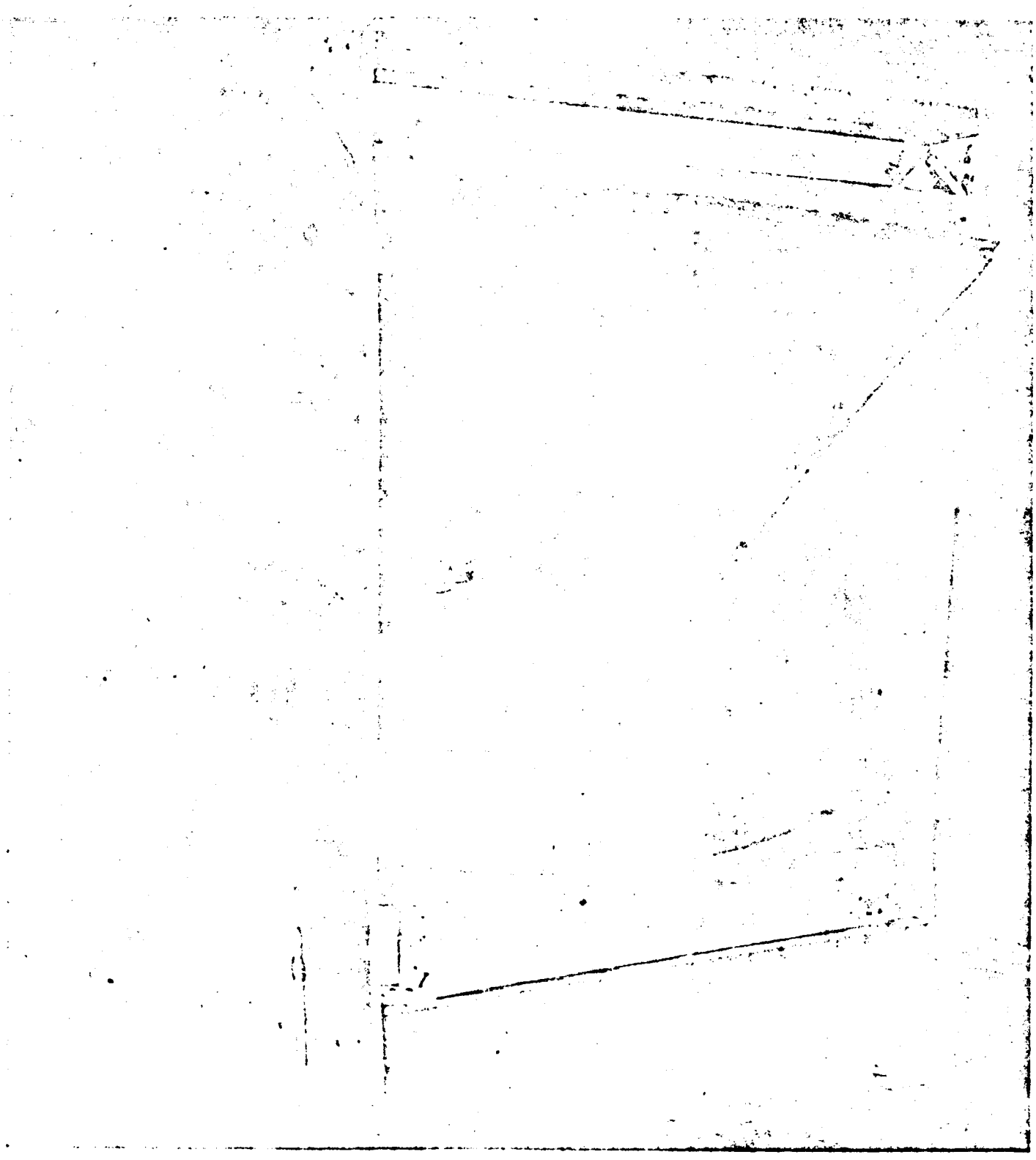

Figure 5-10 Cassegrainian Sectoral Horn-Reflector (KSK) Antenna Operating Model.

Figure 5-11 illustrates both E and H-plane patterns for the circular polarization horn utilized with the antenna. The aperture dimensions of the KSK antenna model are approximately 26 inches square. However, due to the surface of revolution construction of the hyperboloidal structure, certain portions of the paraboloid were not utilized decreasing the usable aperture by about 10 percent to a value of approximately 600 square inches.

5.3.3 Experimental Measurements

The secondary patterns taken for the KSK antenna were measured at X-band and recorded for a 60 db range of response. The patterns were taken by means of the use of high power signal source located about 650 feet from the antenna under measurement. The source signal was generated by a 10 watt traveling wave tube amplifier fed by a conventional low power stable signal generator. A four foot paraboloidal reflector antenna was employed at the source in order to provide a relatively high energy density available at the antenna measurement site. Power levels of this intensity were required in order to evaluate the important minor-lobe behavior of the antenna response. An evaluation of the minimum distance at which the antenna may be considered as in its far field, or Fraunhofer region, may be calculated from the familiar $L = 2D^2/h$ criteria. The effective aperture dimension for the KSK antenna may be taken as approximately 26 inches and for the X-band frequency range, and may be assumed to be roughly one inch. For these conditions, the expression may be evaluated as a distance of approximately 112 feet for a phase variation over the aperture surface of approximately 1/20th of a wavelength. The distance employed of 650 feet is well in the Fraunhofer region for the KSK antenna and hence the far field results presented in the secondary patterns appear to be quite acceptable.

The pattern measurements were made by means of a conventional bolometer detector

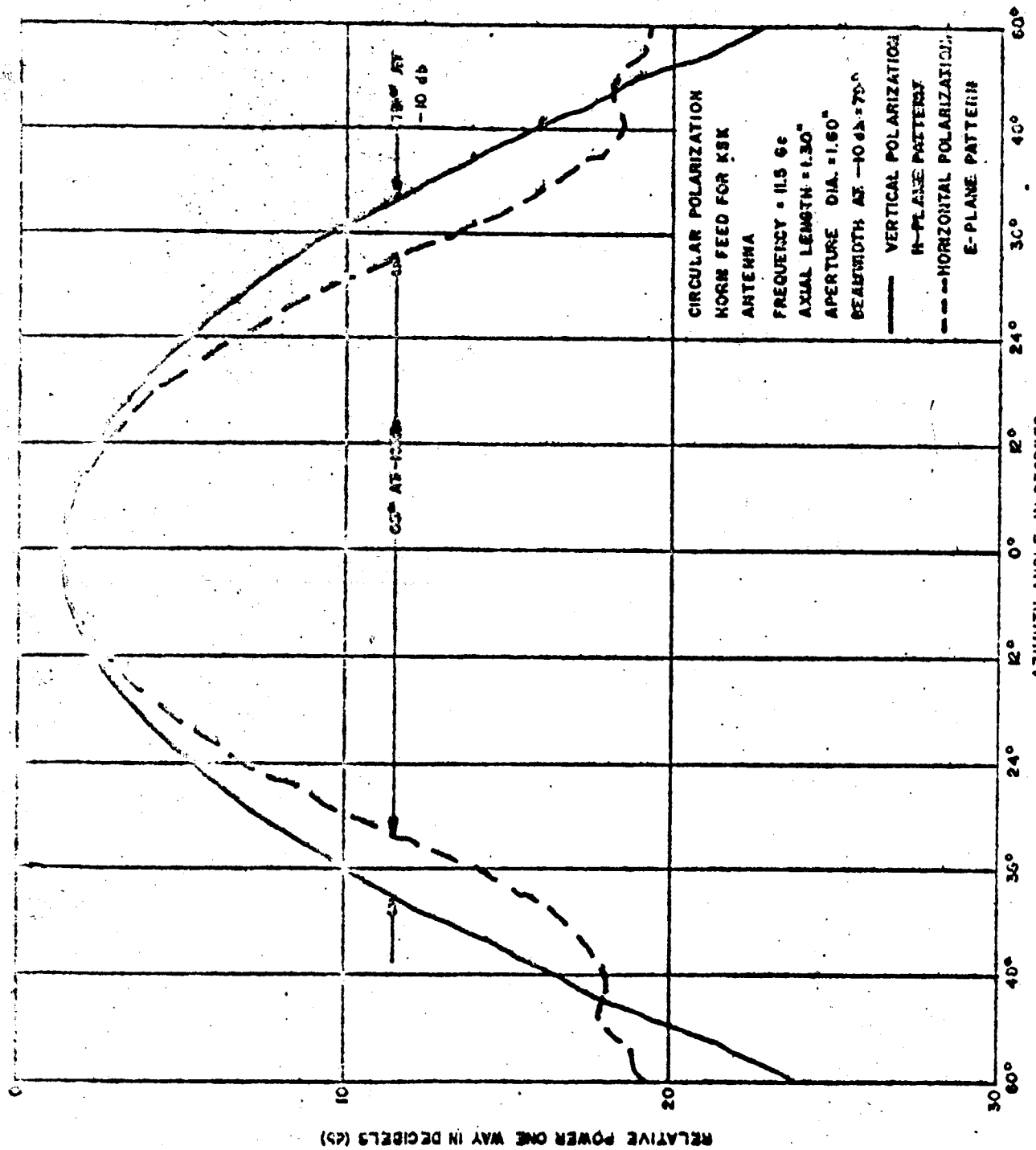

Figure 5-11. Primary Patterns For Circular Polarization Horn Feed Used With The KSK Antenna.

and a 40 db pattern recorder. The 60 db patterns were obtained as composite patterns for the same measurement performed at sensitivity scales altered by 20 db. The full sensitivity of the recorder amplifier was utilized to obtain the 40 db patterns containing the minor-lobe information. Employment of an accurate 20 db attenuator in the line allowed measurements to be performed for the top 20 db of pattern information containing the main lobe and at times the first minor-lobes for the antenna system. An X-band standard gain horn calibrated in the range of frequencies in which measurements were obtained was utilized in determining the measured isotropic level values for the antenna measurements.

Measurements were initially taken for the KSK antenna for the frequency range from 8.0 to 12.5 Gc. A final set of secondary pattern measurements were made for the KSK antenna in all four pattern aspects for the frequency range from 10.0 gc to 12.5 gc. For the KSK operating model antenna test configuration illustrated previously, patterns were taken at every 0.5 Gc for both E and H-plane polarization conditions and for both azimuth and elevation plane antenna operation. A typical set of these results is included as Figures 5-12 through 5-15. This set is for a frequency of 11.0 gc and presents rather complete information on the performance behavior of the KSK antenna.

Figure 5-12 illustrates the secondary response of the KSK antenna at a frequency of 11.0 Gc for vertical polarization and is shown as an H-plane pattern. The measured isotropic level was found to be 36.3 db below the maximum level of the main beam and is indicated on the pattern. The minor-lobe energy is seen to taper off sharply in the region of the main beam and to reach a value approximating 25 db below isotropic in a region greater than 90 degrees separated from the center of the main beam. The average back-lobe level was calculated for this response pattern

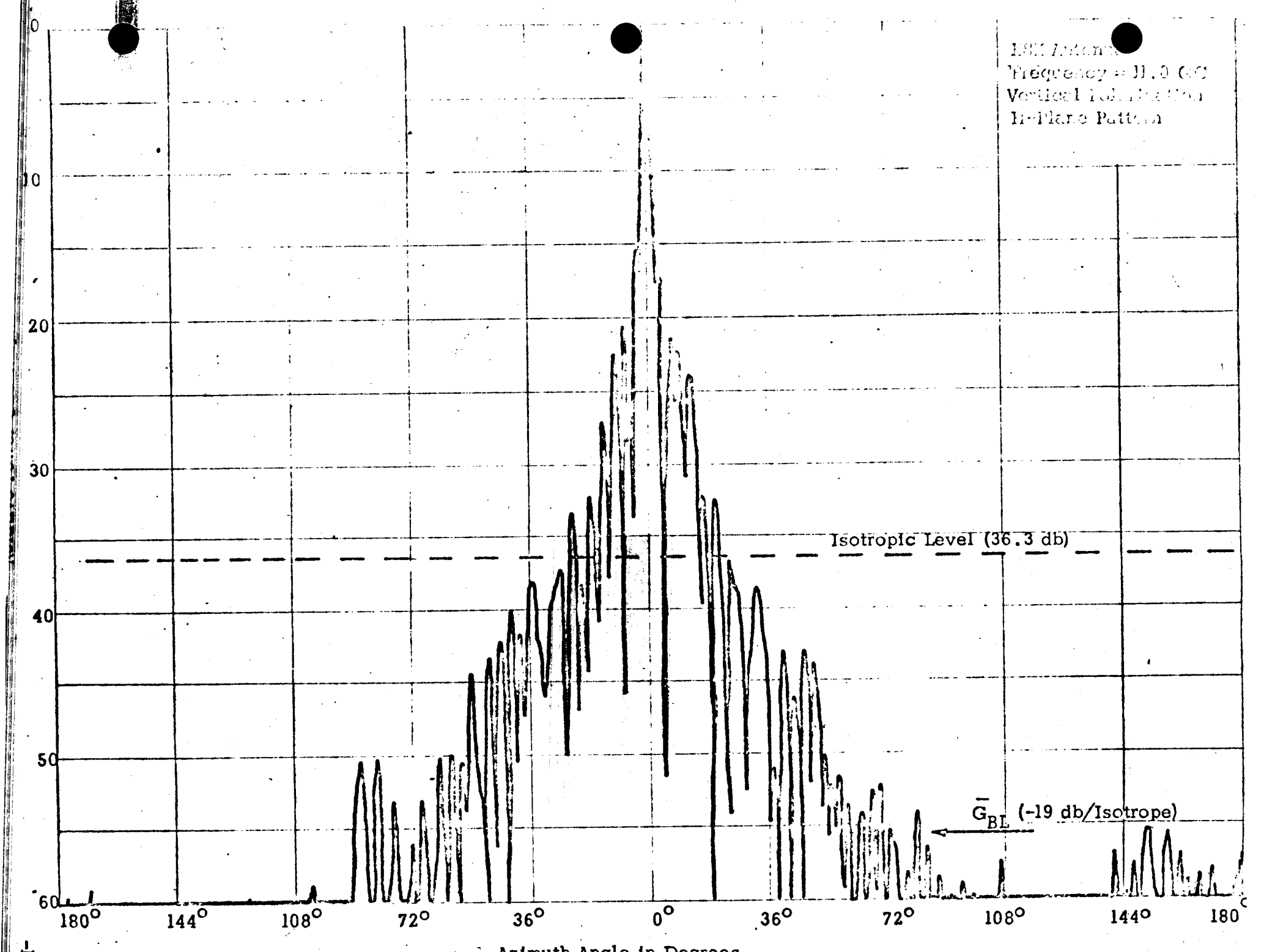

Figure 5-12. KSK Antenna Far Field Response, 11.0 Gc, Vertical Polarization, H-Plane Pattern.

considering the region exceeding 30° separation from the main beam and was found in this case to have an average value of 19 db below the isotropic level.

The average minor-lobe level is important since the noise temperature contribution from the ground radiation may be easily calculated to a first order approximation from this average level. An average level of 20 db below isotropic corresponds to a noise temperature contribution from the ground of 1.5 degrees Kelvin. The effective ground radiation noise temperature contribution for these various values of average minor-lobe level may be quite simply computed by referring to Figure 3-10 which illustrates the relation between the average back-lobe energy level in the half space containing the ground and the equivalent temperature. In most operating positions of the antenna the average minor-lobe level due to the lobes intercepting the ground half-space will be considerably less than the average minor-lobe level for the entire pattern as calculated from the pattern response excluding only the solid angle containing the main beam and all side-lobes within 30° of the main beam. However, to be as conservative as possible in rating the antenna performance from the experimental results, the worst case values are taken assuming that all of the minor-lobe energy in the region greater than 30° from the main beam is considered as the energy being averaged over the ground half-space. The actual improvement in the performance due to this approximation which may be realistically assumed from the geometry of the antenna configuration and the normal operating mode of the antenna indicates an improvement of about four to ten db, and possibly more.

Figure 5-13 is a secondary response plot for the KSK antenna at the same operating frequency of 11.0 Gc, but is an E-Plane pattern taken for horizontal polarization. This azimuth plane plot also demonstrates an extremely low minor-lobe level especially at orientations greater than 30 degrees removed from the main beam. The

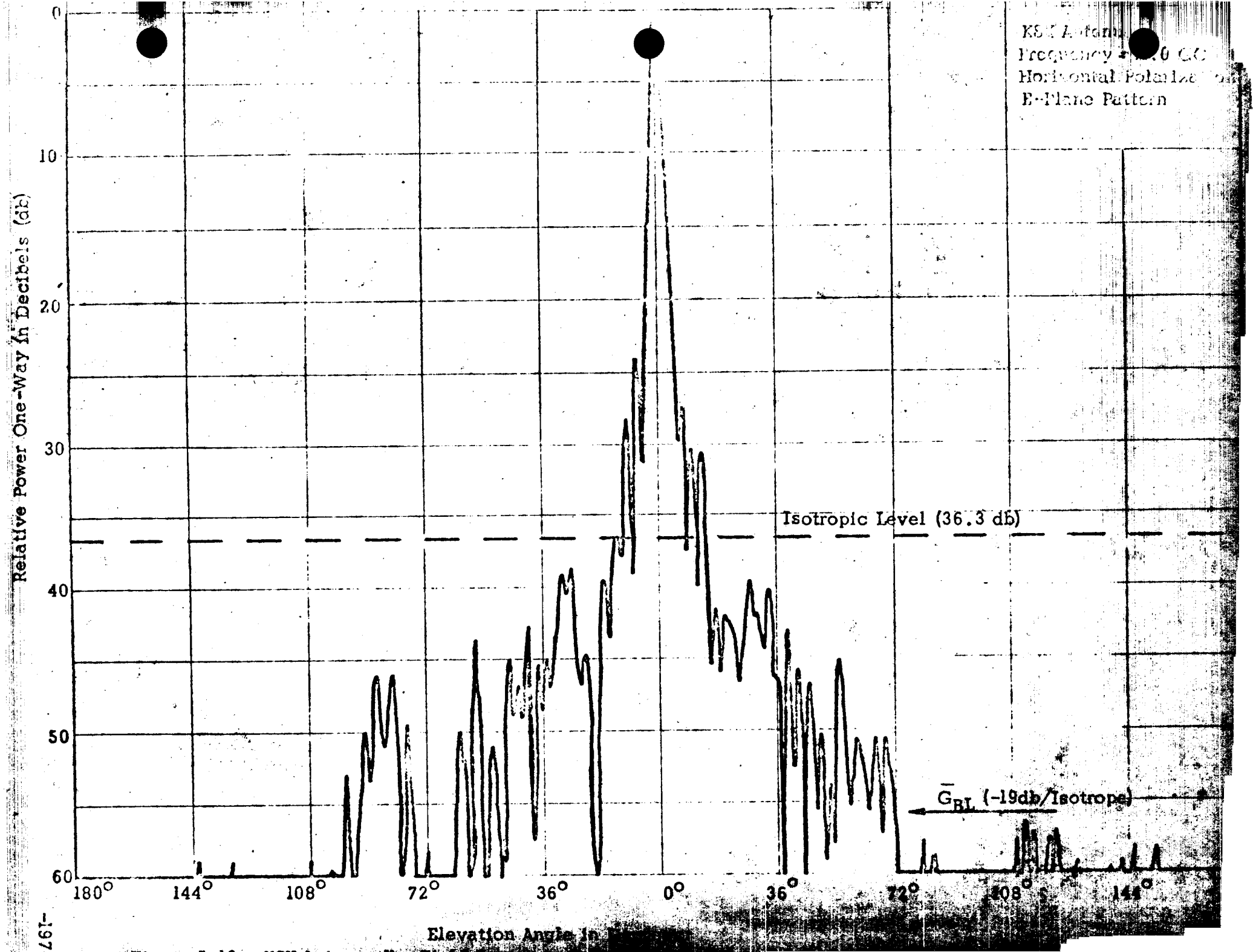

Figure 5-13. KSK Antenna Far Field

calculated average minor-lobe level which is determined by measurements made from the response pattern, appears to be about 19 db below the isotropic level.

Elevation plane patterns for the KSK antenna are shown in Figure 5-14 and 5-15, for a frequency of 11.0 Gc. The former is an E-plane pattern for vertical polarization and the latter is an H-plane pattern for horizontal polarization. These patterns in general have characteristics similar to the azimuth plane patterns of rapidly decreasing minor-lobe energy, however, a spill-over lobe may be noted in both patterns at about $+66^{\circ}$. This spill-over energy is apparently due to the paraboloidal surface being a few inches too short. It was found that this spill-over lobe could be improved by 6 to 10 db by covering the forward part of the hyperboloidal surface. This indicates that a ray path from the feed phase center incident on the forward surface of the hyperboloid would not be intercepted or reflected by the paraboloidal surface. Conversely it appears that the hyperboloidal surface provides an effective reflecting region for an orientation somewhat removed from the main beam. This deficiency should be easily corrected by extending the length of the paraboloidal surface. The average minor-lobe level for the E-plane pattern was found to be approximately 15 db below isotropic level. The spill-over lobe in the H-plane pattern is more pronounced and is believed to be caused by the wider H-plane beamwidth of the primary feed employed. Again it was noted that absorber material placed in the forward area of the hyperboloidal surface decreased the spill-over energy considerably without greatly effecting the performance of the antenna in the other regions. For these reasons it is believed that a minor design modification extending the paraboloidal leading surface would overcome most of the elevation plane spill-over effects.

Figures 5-16 and 5-17 illustrates the operation of the KSK antenna at frequencies of 10.0 gc and 12.0 gc. These response patterns are shown for frequencies

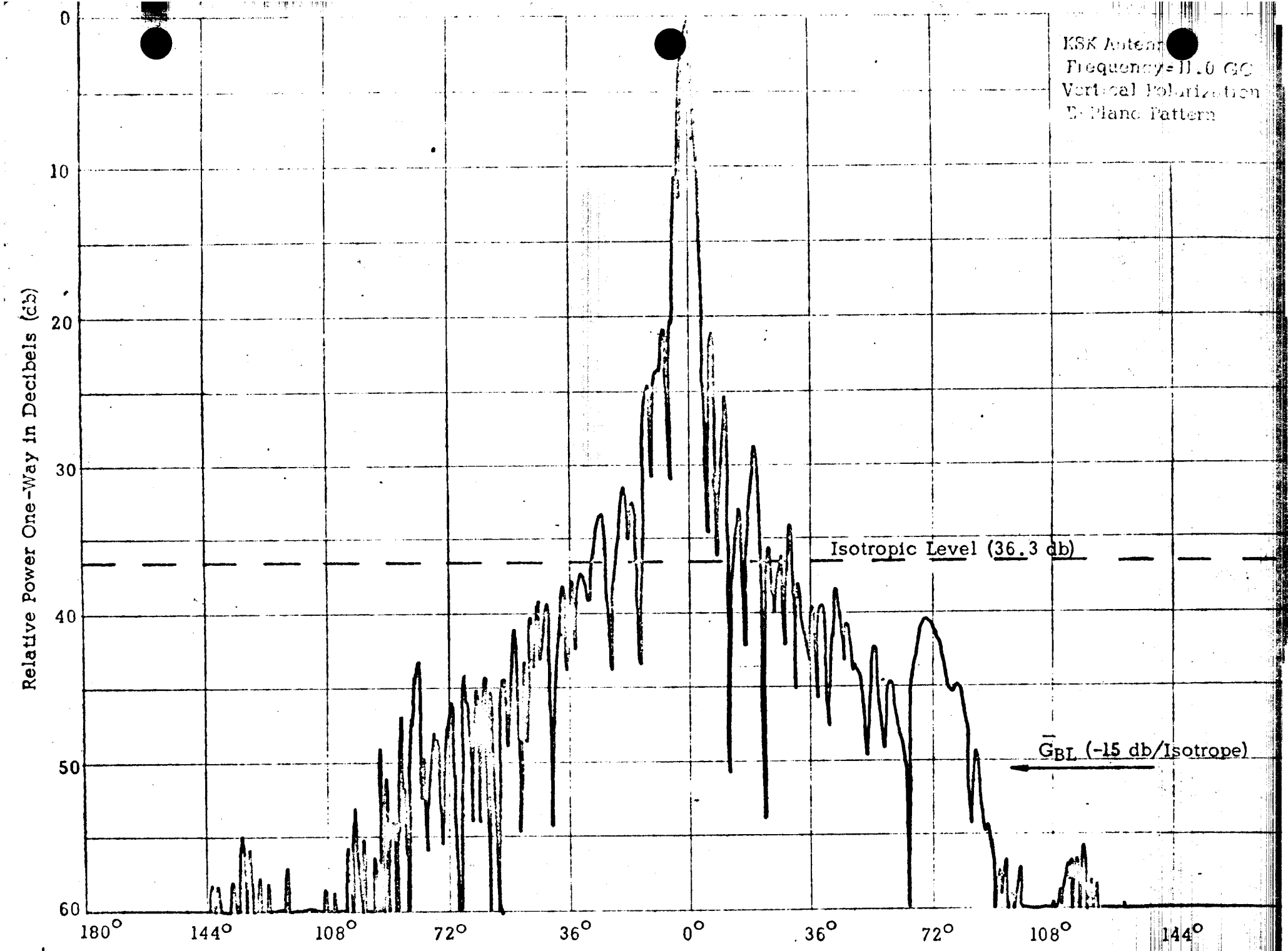

Figure 5-14. KSK Antenna Far Field Response, 11.0 Gc, Vertical Polarization, E-Plane Pattern.

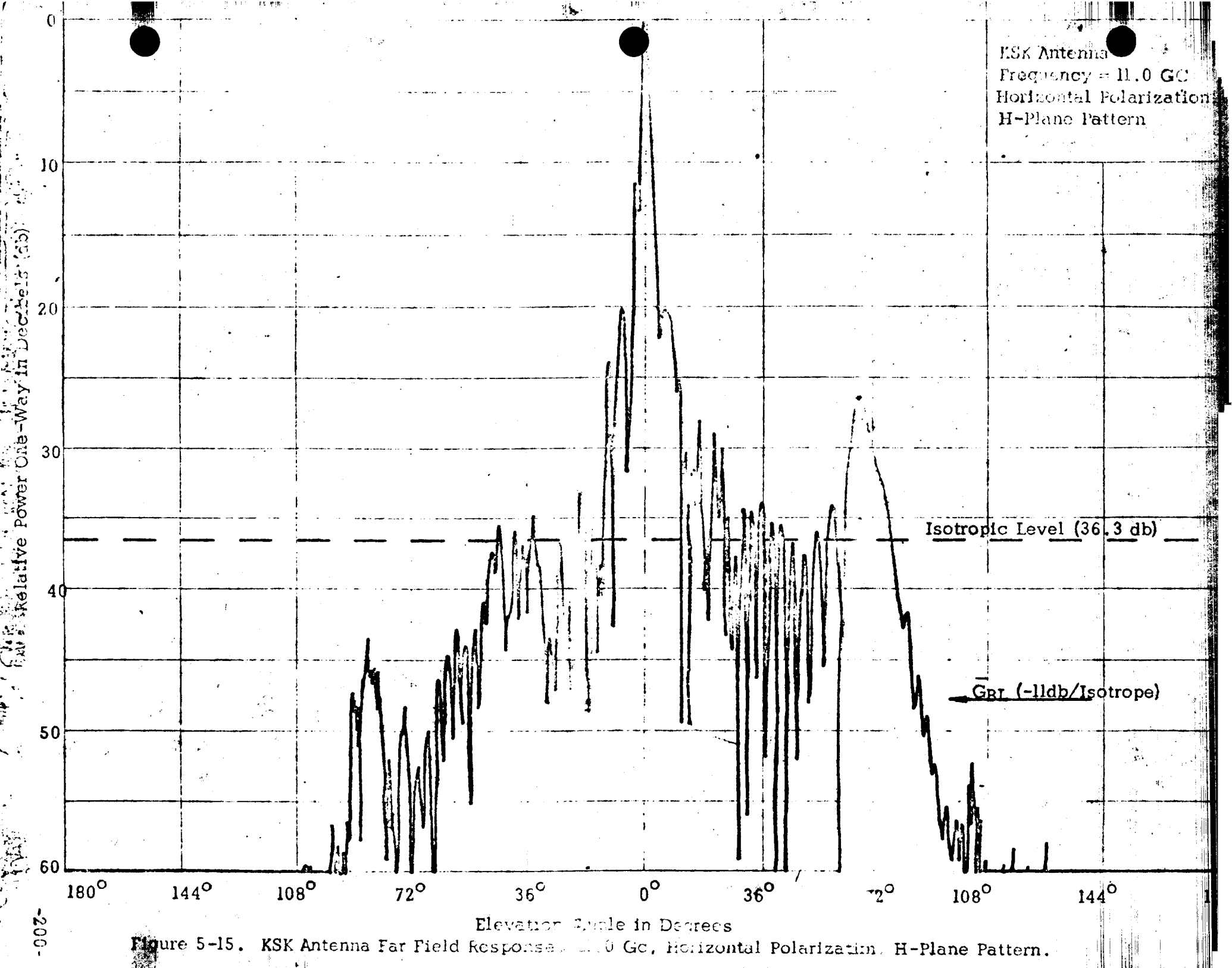

Figure 5-15. KSK Antenna Far Field Response ... 0 Gc, Horizontal Polarization, H-Plane Pattern.

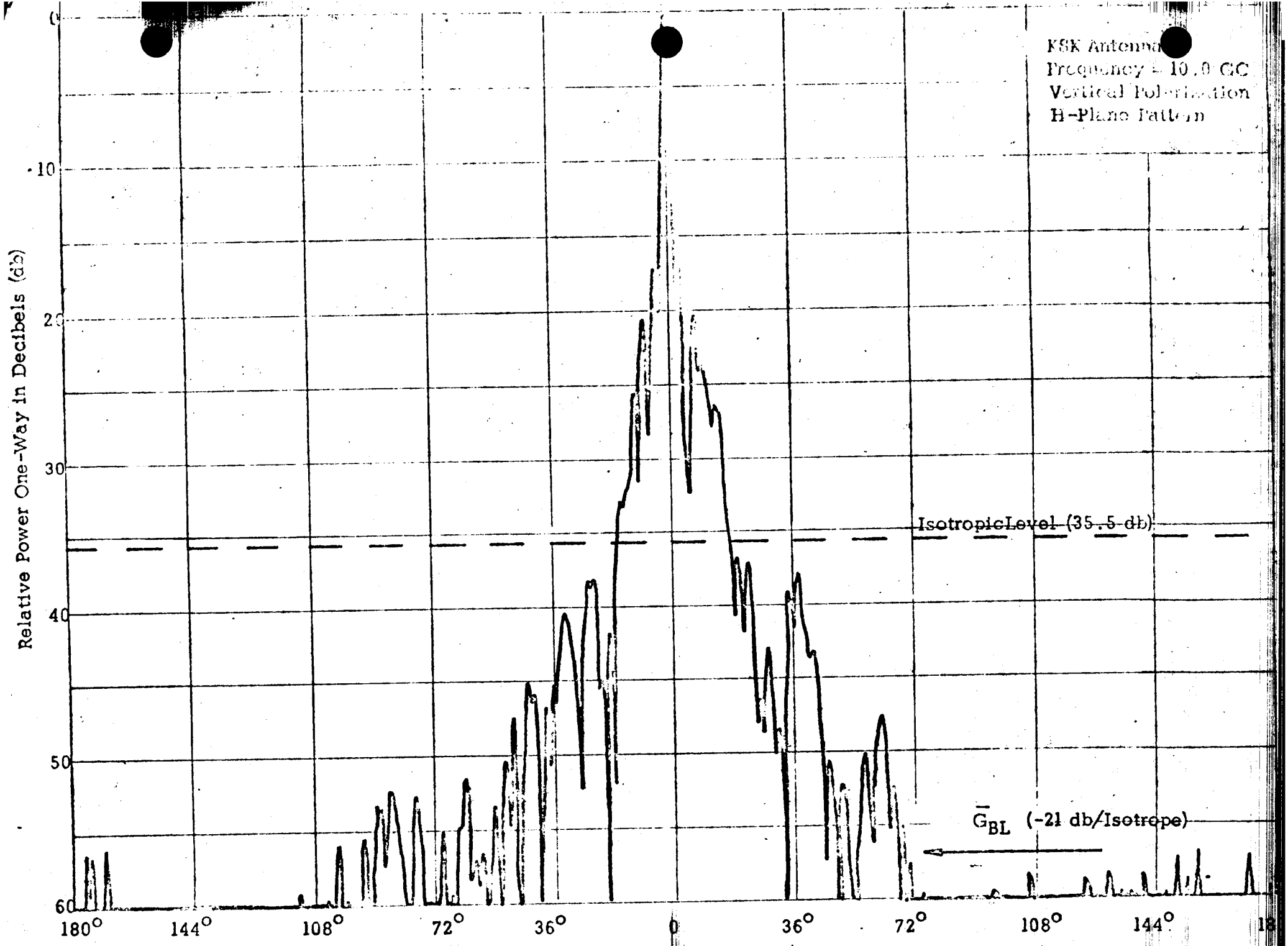

Figure 5-16. KSK Antenna Far Field Response, 10.0 Gc, Vertical Polarization, H-Plane Pattern.

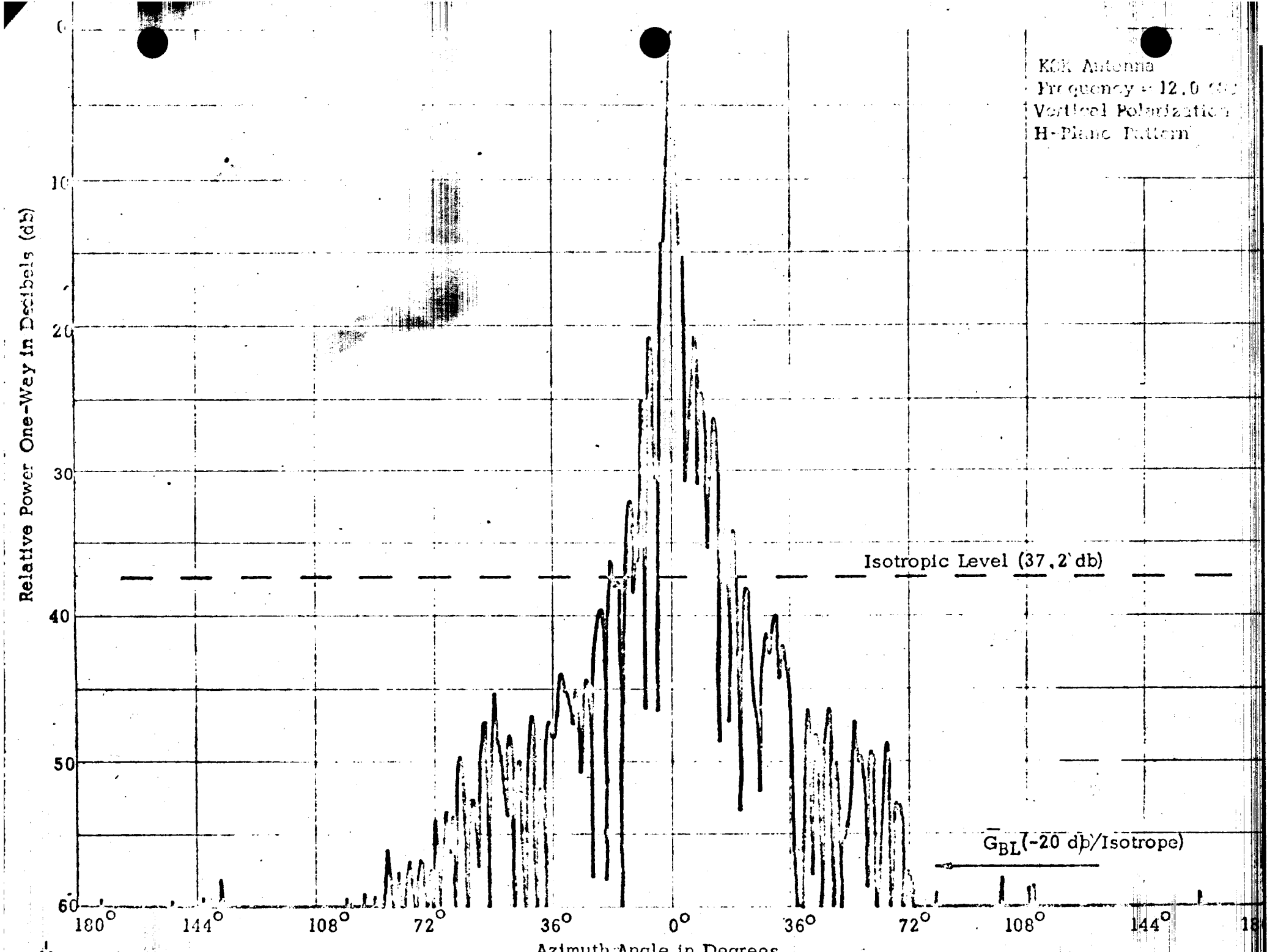

Figure 5-17. KSK Antenna Far Field Response, 12.0 Gc, Vertical Polarization, H-Plane Pattern.

approximately 1 Gc above and below the previous patterns and are presented in both cases as H-plane patterns for vertical polarization. It might be noted in these patterns that the average minor-lobe level was found to be 20 db or more below isotropic level corresponding to a ground radiation noise temperature of approximately one degree Kelvin or less.

5.3.4 Performance Comparisons

The performance characteristics for the Cassegrainian adaptation of the sectoral horn-reflector system, the KSK antenna, appeared to be outstanding. Using the performance criteria originally discussed of maintaining minor-lobe energy over the spacial extent of the antenna response which intercepted the ground energy of better than 10 db below the isotropic level, the KSK antenna is found to present a considerable improvement over other antenna systems.

For an average ground radiation temperature of approximately 300°K the total effective antenna noise temperature due to the ground radiation contribution for the antenna response at isotropic level would be approximately 150°K. Taking into account the ground emissivity which may reduce the equivalent black body radiating temperature for the ground region to a figure possibly as low as 120°K. It is apparent that a truly low noise antenna system should maintain side-lobe energy of better than 10 db below the isotropic level which would correspond to a ground radiation antenna equivalent noise temperature contribution of approximately 12°K. It might be mentioned that few antennas are capable of maintaining this average minor-lobe level and hence have considerably higher noise temperature contributions from the ground radiation. In general, only Cassegrainian systems are competitive in this respect and for conventional Cassegrainian configurations the ground spill-over lobes are suppressed at the expense of poor aperture efficiency, with consequent reduction

in gain. However, the KSK antenna should provide good aperture efficiency, a corresponding relatively high gain, and average minor-lobe levels of approximately 15 to 20 db below isotropic level.

The minor-lobe structure characteristics of all of the presented KSK antenna secondary patterns should move in somewhat closer to the main beam for an operational antenna. The average aperture dimension in terms of wavelength for the model KSK antenna at the frequency range of interest is only approximately 25. However, for aperture dimensions comparable to the aperture area of the present NASA 85 foot paraboloidal antennas, i. e., for a KSK antenna of roughly 75 feet square aperture, the number of wavelengths contained in the nominal aperture dimension would be in the order of 33 to 330, for the operating frequencies between 400 mcs and 4.1 Gc. For a typical operating frequency, for example 1.7 Gc, a large KSK antenna might contain 130 wavelengths across the aperture. This indicates that the lobe structure, which may be seen on the six presented KSK antenna patterns, which now decrease from the main beam to about -20 db below isotropic at 60 to 70 degrees away from the main beam should now decrease to about 20 db below isotropic within 12° of the main beam. In any case, the degradation is reasonably fast for normal operating frequencies and even for the 400 mc operation it appears that most of the minor lobe energy will be rearing 15 to 20 db below the isotropic level at approximately 30 to 40 degrees away from the main beam. For a KSK antenna of somewhat smaller size which may be more practical due to the improved aperture efficiency, resulting gain improvement, and improved low noise performance, we might assume an antenna size of approximately that utilized in the present BTL Telstar communication satellite tracking antenna. This would indicate an aperture dimension of approximately 40 feet square. For the two higher ranges of NASA frequencies, at about 1.7 Gc and 4.1 Gc,

the antenna would maintain essentially all of its minor-lobe energy associated with the main beam to within an angular extent of approximately 20° from the main beam or less. Operation at 400 mcs would have minor-lobe energy associated with the main beam spread out essentially throughout the region within 90° of the main beam. The antenna therefore, would optimally perform at zenith and be degraded slightly for elevation angles departing slightly from the zenith, with increased ground radiation noise temperature degradation occurring as the antenna is oriented closer and closer to the horizon, in which case the higher level minor-lobe components would intersect the ground. However, it is felt that the KSK antenna even for a considerably more limited aperture dimension, and operating at about the lowest range in which it appears feasible to operate from noise consideration, the KSK antenna should improve the performance characteristics considerably over any known antenna of comparable aperture dimensions.

The gain characteristics for the KSK antenna were calculated from the aperture considerations and also measured by means of a standard gain horn. A check on these methods was also performed by measuring the antenna pattern beamwidths and calculating the equivalent gain for the antenna from the familiar expression relating the E and H-plane beamwidths to the gain. The results of these measurements and calculations are shown in Figure 5-18, for the range of frequencies from 10 to 12.5 Gc. The three methods agreed quite closely indicating both reasonably good measurements and fairly valid approximations for the antenna aperture area and the primary feed system illumination characteristics, which determine the aperture efficiency. An aperture efficiency of 55 percent was taken, since no special beam shaping provisions were included in the primary feed. It is felt that the aperture efficiency can be improved above this level, probably to the 70 - 80 percent region by the use

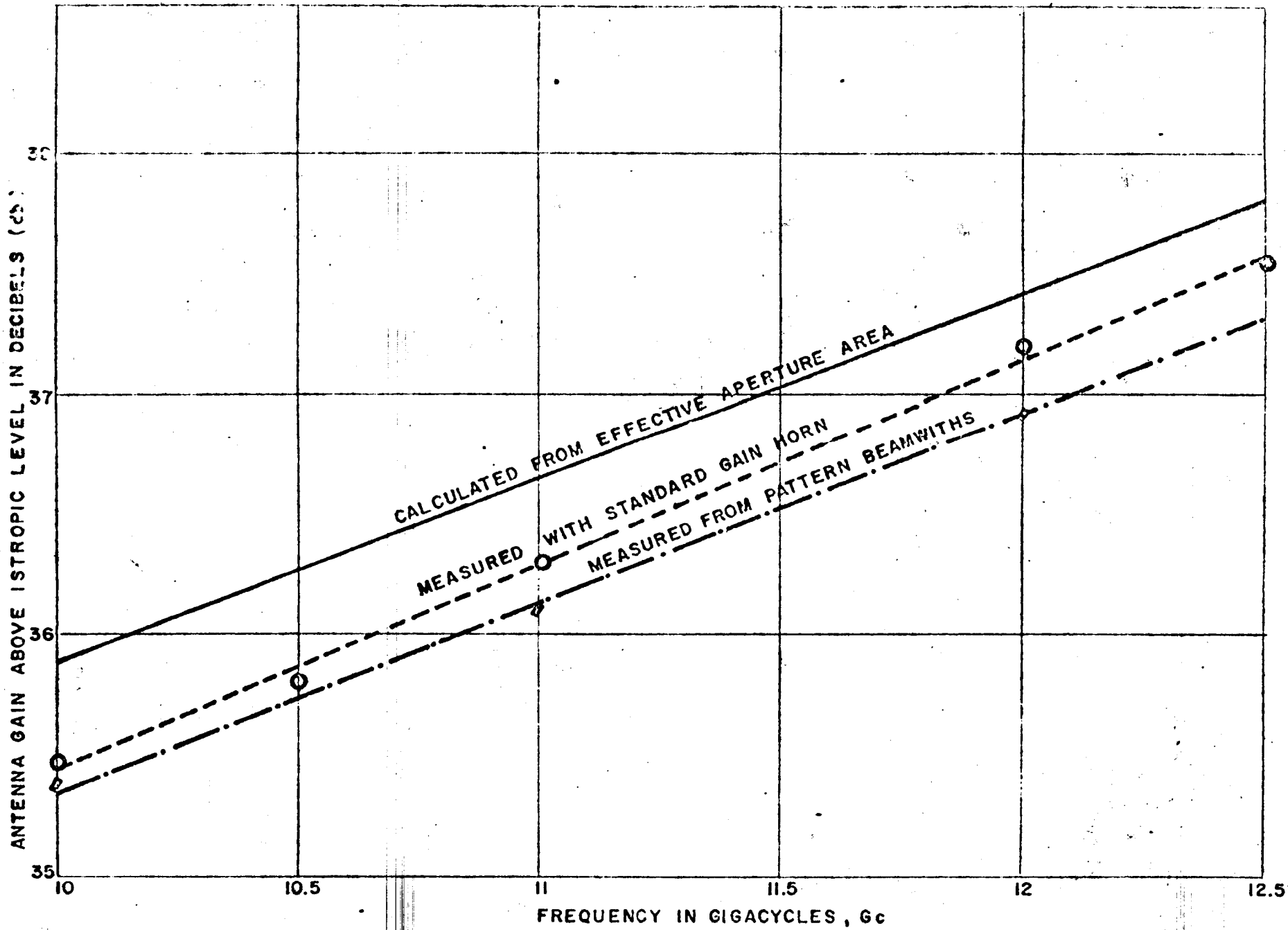

Figure 5-18. K.SK HORN GAIN vs FREQUENCY CHARACTERISTICS

of beam shaping techniques.

A performance comparison was made of the KSK antenna with the best information available for the BTL sectoral horn-reflector system, or "sugar scoop" antenna, as it is popularly know. Most of the information available concerning the sectoral horn-reflector system radiation pattern in the longitudinal plane and for longitudinal polarization described was obtained from a report by Crawford, Hogg and Hunt of the Bell Telephone Laboratories in their NASA Technical Note (D-1131) for the project ECHO HORN-REFLECTOR antenna for space communication. The extended radiation pattern in the longitudinal plane for longitudinal polarization indicates two spill-over lobes, both of which are approximately 6 to 13 db above the isotropic level. The BTL system described in this report has a spill-over lobe at approximately 70° of about 6 db above the isotropic level and a spill-over lobe at 342° i. e., about 18° from the main beam, of about 13 db above isotropic. It is also quite surprising to note that the average minor-lobe level in the region for which the antenna response pattern is available does not appear at any point to be greater than six or eight db below isotropic. The average level calculated by the same technique in which the KSK antenna minor-lobe levels were calculated appears to be only 3 to 5 db below isotropic. However, it should be mentioned that the pattern information is somewhat limited in that only the one polarization condition is included and patterns are available in this polarization for only approximately 40° in one direction and 110° in the other, relative to the main beam. The BTL aperture size for this antenna system was approximately 20 by 20 feet, the structure was about 50 feet in length and the weight was about 18 tons. The frequency of operation for this particular system was at 2.39 Gc. The aperture efficiency for the antenna was quite good, reaching a measured value of 76 percent. The KSK antenna from all performance evaluation, appears to maintain considerably lower minor-lobe levels than

the horn-reflector antennas for which published data is available. This however, is not considered an inherent advantage of the KSK antenna; the conventional horn-reflector antenna should perform in this respect equally as well. However, the mechanical considerations usually involved in the fabrication and implementation of the horn-reflector system appears to degrade the electrical performance to an extent. The mentioned difficulty concerning diffraction around the large ring gear in the BTL Telstar system is an example.

The requirement for operation of the BTL sectoral horn-reflector antenna with a radome in order to avoid wind loading is another serious problem. The most recent information concerning the radome indicates that radome noise temperature degradation is approximately 19°K. This certainly presents a drastic limitation upon the noise performance of the antenna system and appears to make the massive size and expense of the "sugar scoop" type of horn-reflector configuration questionable. The much improved likelihood and distinct possibility of operating the KSK antenna without a radome by means of designing the much smaller structure to meet the necessary wind loading is one of the principal factors in favor of the Cassegrainian adaptation of the sectoral horn-reflector.

5.3.5 Evaluation of Technique

Table V-1 lists the estimated total antenna noise temperatures for various low noise antenna systems. This information has been compiled from the best source material available in the form of either measured data, performance results interpreted from limited measured data, or verified values contained in the literature. The systems which have been considered are the conventional paraboloidal reflector with a focal point feed, a Cassegrainian system employing a hyperboloidal sub-reflector, a sectoral horn-reflector system, or "sugar scoop" antenna, and the

	SKY NOISE IN MAIN BEAM	GROUND NOISE FROM MINOR LOBES	SCATTERING-ABSORBTION BY FEED SUPPORTS	TOTAL
PARABOLOIDAL REFLECTOR WITH FOCAL POINT FEED	3.0 °K	29 °K	8.0 °K	≥ 40 °K
CASSEGRAIN HYPERBOLOIDAL SUB-REFLECTOR	3.5 °K	3.0 °K	3.0 °K	≥ 9.5 °K
HORN-REFLECTOR "SUGAR SCOOP" ANTENNA	3.5 °K	2.5 °K	- - -	~ 6 °K
BSK HORN CASSEGRAINIAN HORN-REFLECTOR	3.5 °K	1.5 °K	- - -	~ 5 °K

Table V-1.

Estimated Antenna Noise Temperatures
For Various Low Noise Antenna Systems.

Cassegrainian sectoral horn-reflector, the KSK antenna.

The principal degrading influence of paraboloidal reflectors with focal point feeds is the spill-over energy which intercepts relatively high temperature ground radiation. Table V-1 shows a breakdown of the noise temperature contributions from the various regions, and it can be noticed that the most significant contributions are from the ground thermal radiation noise entering the antennas through the minor lobes. A frequency of approximately 1,000 mcs was assumed for this table in order to place the antennas on a similar basis.

The sky noise contribution at this frequency is a combination of galactic noise and atmospheric absorption losses and is taken as approximately 3.5°K for the pointing direction of the antennas, which in all cases was assumed to be at the Zenith. The scattering and absorption losses due to the feed supports are an additional important contributing factor to the paraboloidal reflector system effective noise temperature and may be considerably higher than the value which is presented. As stated earlier, these values include the best results obtainable, but it appears that certain techniques are available for reducing the scattering and absorption noise due to feed supports to the range which is shown. *1

The typical total equivalent antenna noise temperature for the paraboloidal reflector employing the focal point feed is seen to be approximately 35° Kelvin. The best Cassegrainian systems available utilizing a paraboloidal surface of revolution with a hyperboloidal sub-reflector offer a considerable improvement in the low noise performance for an equivalent aperture. The principal reason for this improvement

---

*1. D. C. Hogg and R. A. Semplak, "Characteristics of a Prototype Near-Field Cassegrainian Antenna", Memo for Record, Bell Telephone Labs., INC., 17 January, 1962.

is the transfer of the main spill-over energy from the ground region into the relatively quiet sky region.

Figure 5-19 illustrates the quite interesting fact that feed spill-over considerations may often govern the choice of antenna for operation at a particular frequency range of interest. The principal design criteria is the achievement of a maximal antenna gain to noise temperature ratio. This infers that for similar antennas, optimal performance may be achieved if the spill-over energy is directed to the minimal noise distribution, whether this is toward the region of the ground or the sky. Referring to the figure it is apparent that the region of Cassegrainian advantage appears to have an upper level bound due to atmospheric absorption effects and definitely has a lower bound at about 150 Mc, which may vary from approximately 100 Mc to 500 Mc. Conversely, the regions defined by those bounds as the lower and upper bounds respectively are the regions in which conventional feed-reflector antennas have the operating advantage. This is simply stating that in the frequency ranges above about 30 Gc and below 150 Mc the ground temperature is less than the sky temperature; hence, the conventional feed-reflector system advantage, and that from about 150 Mc to 35 Gc the sky temperature is less than the ground temperature, hence the Cassegrainian system advantage. For the frequencies of principal current operational interest to NASA of 136 Mc to 4.1 Gc, it is significant to note that from spill-over considerations and neglecting the increased probability of solar degradation through the minor lobes, the Cassegrainian antenna system has a rather clear operating advantage at all bands of operation except the lowest.

The Cassegrainian system discussed is one of an advanced type developed by Potter and Rusch of JPL [*1], and has a total equivalent antenna noise temperature

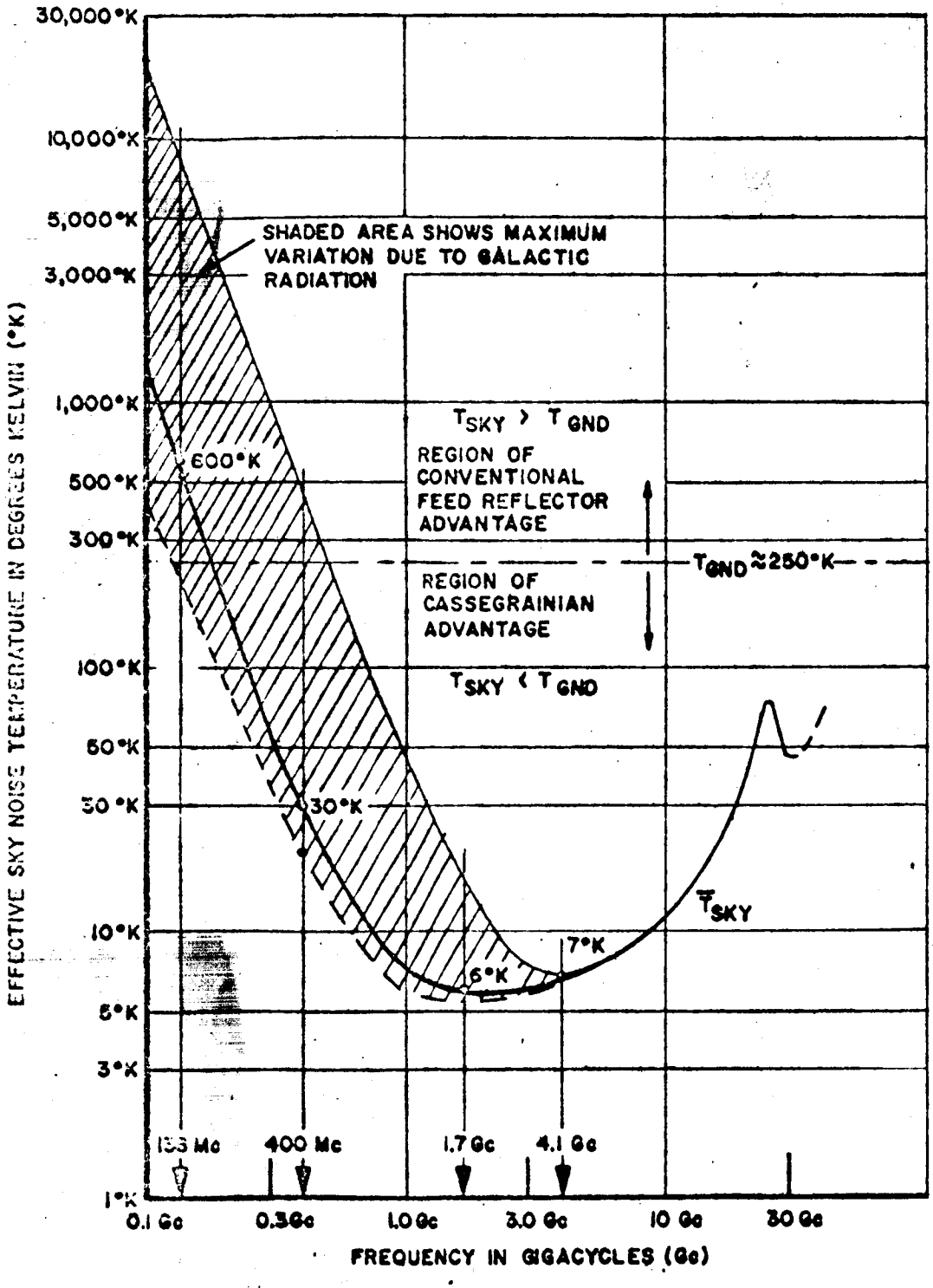

Figure 5-19. Environmental Noise Temperature Influence.

of approximately 9.5°K, the components being broken down as shown in the table. This Cassegrainian system is quite good and should be considered somewhat superior to other Cassegrainian systems operationally available at this time.

The sectoral horn-reflector system or "sugar scoop" antenna has no feed supports and therefore holds this loss to zero. The minor-lobe noise due to contributions from the ground radiation are taken from the best information quoted by BTL and is not for the measured sectoral horn-reflector patterns, which appear generally somewhat worse than the corresponding operational values. It appears that an effective antenna noise temperature of about 6° Kelvin is attainable by the sectoral horn-reflector system. If it is realized that the limiting value beyond which no further improvement is possible corresponds to the noise power density contained in the main beam of about 3.5° Kelvin, it is apparent that the "sugar scoop" horn-reflector system is an exceedingly low noise antenna.

The KSK antenna, however, appears in certain respects to out perform the sectoral horn-reflector system. Measured values indicate that minor-lobe levels for the KSK antenna are significantly below those of the sectoral horn-reflector system enabling an improvement in the contribution to the antenna noise temperature from the ground radiation. In all other favorable respects, the KSK antenna performance matches the sectoral horn-reflector. But this factor allows an improved equivalent antenna noise temperature by about a degree Kelvin. The KSK antenna, rated at about 5° Kelvin, attains a low noise performance equivalent to less than 2° Kelvin from the theoretical minimum.

Not included in the low noise antenna evaluation table, but a very significant contributing factor, is the equivalent antenna noise contribution due to the radome

structure which has been previously estimated at approximately 19° Kelvin. However, assuming operation without the radome, the most optimistic equivalent antenna noise temperature performance figures for the sectoral horn-reflector system are as shown in the table.

The Cassegrainian sectoral horn-reflector system, the KSK antenna, from all indications appears somewhat better in minor-lobe content and is indicated as such in the table. It is therefore apparent that effective antenna noise temperatures exclusive of additional transmission line losses, receiver system noise, and certain other factors not associated directly with antenna performance, of approximately 5° are obtainable by means of either the Cassegrainian sectoral horn configuration, designated the KSK antenna, or the sectoral horn-reflector "sugar scoop" antenna as employed by BTL.

It is believed that the significant operational advantage gained by the KSK antenna design is in the simplification of the antenna structure eliminating certain diffraction and wind loading problems present in the considerably more massive sectoral horn-reflector design. It is also important to recognize the feasibility of the KSK design in possibly enabling operation of the antenna without a radome.

It appears that conventional Cassegrainian systems may attain a noise temperature of approximately 10°K with a sacrifice in aperture efficiency and resulting gain loss. Conventional paraboloidal feed-reflector systems appear to be capable of attaining operation in the range of noise temperatures of 30 to 50° Kelvin utilizing conventional feed systems. It should be pointed out that utilizing appropriate feed shaping techniques such as those investigated during this program, the effective antenna noise temperature of paraboloidal reflector systems may be improved considerably with an attendant increased aperture efficiency and gain improvement.

The Cassegrainian principal appears to offer considerable merit in low noise systems, and application of this principle to the conventional sectoral horn-reflector antenna appears to provide a compact, mechanically simple antenna configuration of outstanding electrical characteristics and minimal effective antenna noise temperature. The principal advantages of the KSK antenna are presented in Table V-2 in summary form.

TABLE V-2

ADVANTAGES OF THE KSK ANTENNA.

1. Exceptionally low noise with high effeciency.
2. Physically compact.
3. Mechanically simple.
4. Negligible aperture blocking.
5. May operate without radome.
6. Easily adaptable to monopulse operation.
7. Economically practical.

VI SUMMARY AND CONCLUSIONS

6.1 Design Guides

The general background information presented in this report provides both considerable data and a comprehensive discussion concerning the principal factors influencing the performance characteristics of low noise antenna systems. Information has been presented relating the galactic and atmospheric noise contributions as a function of frequency, antenna pointing direction, and certain other factors. The influence of aperture efficiency, aperture energy distribution and minor-lobe levels have been discussed and quantitatively evaluated. A straightforward technique has been derived and presented for the evaluation of antenna primary feed systems by a pattern integration method which should prove a valuable tool in the design, development, and selection of low noise antenna feeds. A method for evaluating the performance of low noise antenna systems from considerations concerning their feed properties or from certain characteristics of their measured secondary patterns has also been presented. The influence upon the total effective antenna noise temperature of the average minor-lobe levels has been derived, discussed, and plotted.

The evolution of practicable feed shaping techniques by several approaches has been presented. One very desirable surface wave beam shaping technique was developed which offers many advantages and enables a considerable performance improvement over conventional horn feeds. This feed system appears to provide a feasible means for improving significantly the antenna noise temperature characteristics of passive paraboloidal reflectors. The fluted feed surface wave structure was fabricated and tested during the program and the experimental information, as well as other design guides utilized, have been included to allow

the design of similar feed structures to particular NASA requirements. The design approaches utilized in the development of the Cassegrainian adaptation of the sectoral horn-reflector system have also been included with measured pattern data and other information concerning a particular design of this type which has been evaluated.

6.2 Major Accomplishments

A summary of the major accomplishments during the study program is presented as Table VI-1.

The two most important areas in which worthwhile contributions were made are believed to be in the development of the high efficiency low noise fluted feed surface wave structure and in the development of the Cassegrainian sectoral horn-reflector configuration, the KSK antenna.

The development of the fluted feed is significant in that it may be adapted for use with existing paraboloidal reflectors, thereby improving their gain characteristics and decreasing considerably the antenna noise temperature. Adaptations of the fluted feed for multi-band use appear practical, in that the fluted feed is inherently a wide band device. Monopulse configurations utilizing the fluted feed geometry also appear practical and certain suggested configurations for operation in this manner have been suggested.

The KSK antenna is a practical Cassegrainian adaptation of the sectoral horn-reflector configuration and it has been experimentally verified to have outstanding electrical characteristics. The KSK antenna appears in nearly all respects to out-perform in low noise and other characteristics all known antennas of comparable aperture.

TABLE VI-1

SUMMARY OF MAJOR ACCOMPLISHMENTS DURING PROGRAM

1. DEVELOPMENT OF THE KSK ANTENNA

   - an entirely new, exceptionally low noise antenna system.

2. DEVELOPMENT OF THE FLUTED FEED

   - a broad beamwidth, uniform illumination, all-polarization primary feed system which greatly improves the efficiency and low noise performance of conventional paraboloidal reflector antennas.

3. DERIVATION AND EXPERIMENTAL VERIFICATION OF DESIGN CRITERIA

   - for several classes of low noise primary feed systems, including dielectric lens and surface wave feed configurations.

4. DEVELOPMENT OF LOW NOISE ANTENNA EVALUATION TECHNIQUES

   - for determining the low noise characteristics and relative merit of a feed design, reflector configuration, or antenna system from the measured or estimated pattern characteristics.

5. INVESTIGATION OF THE ELLIPSOIDAL SUB-REFLECTOR CASSEGRAIN

   - a novel low noise antenna configuration.

6. CONSOLIDATION AND ORGANIZATION OF FUNDAMENTAL INFORMATION

   - concerning the origin, distribution and analysis of noise sources influencing low noise antenna performance.

The development of primary and secondary pattern evaluation techniques was accomplished during the program. The primary pattern integration technique provides a powerful tool for determining the merit of a particular feed system or a feed system combination of feed and sub-reflector. The simplification of this technique for the evaluation of secondary patterns by the use of the average minor-lobe level provides a direct, reasonably accurate method for secondary pattern evaluation.

An investigation of the ellipsoidal sub-reflector for use with Cassegrainian antenna systems was performed during the program. The ellipsoid-paraboloid configuration was presented as an example of a class of typical Cassegrainian configurations which may have considerable merit. Since there are a large number of surface combinations which may be utilized in the design of a Cassegrainian antenna, the ellipsoidal sub-reflector was utilized as a familiar surface which appears to have certain advantages when used in a rather unorthodox Cassegrainian configuration.

Possibly one of the most important functions of the program was the consolidation, organization, and evaluation of a considerable amount of fundamental information relating to the low noise antenna field. A large number of plotted data, figures, tables, and antenna patterns have been presented in order to place in convenient and readily interpretable form the fundamental information necessary to an intelligent analysis of low noise antenna systems.

6.3 Promising Developments

During the course of the study a number of promising areas in which further developmental work appears worthwhile were encountered. However, two developments in particular appeared to be especially promising, the fluted feed surface structure

and the KSK antenna. A brief discussion of these areas follows.

6.3.1 Fluted Feed for Existing Antennas

The fluted feed surface wave structure was the culmination of a considerable effort in the development of shaped beam primary feed techniques and is believed to provide an optimal illumination by means for many antenna systems, and in particular the paraboloidal reflector. The circular symmetry of the polarization characteristics of the feed system coupled with its combined nearly uniform illumination over a large beamwidth and reasonably rapid taper towards the outer region of its beamwidth affords a feed structure presenting many excellent characteristics. The high aperture efficiency attainable with this feed indicates that improvements of approximately one db may be expected in the gain characteristics of antennas utilizing the fluted feed system over that possible by conventional horn feed illuminations. Suppression of minor-lobe energy due to the rapid taper of the primary beam in the region of the secondary aperture edge and the resulting low spill-over and small values of diffraction lobes appears to be another significant feature of the feed system. For a conventional paraboloidal reflector antenna system it is significant to note that the fluted feed advantages of combined higher gain, decreased spillover and reduced minor-lobe levels affords an improvement of about six to ten db in the gain to antenna equivalent noise temperature ratio. The corresponding improvement in the communication system sensitivity for a given signal-to-noise ratio will be determined by the noise temperature characteristics of the receiving system and will always be less but generally comparable to the gain to antenna noise temperature improvement. This improvement is based upon operating conditions for which the antenna noise and the receiver noise are the principal system limitations. The stated results appear reasonable and valid for system

employing modern low noise receiver techniques. For operational advantages of this improvement are plainly significant in that the low noise feed shaping techniques applied to existing antenna systems may improve their range tracking capabilities by a factor of two or more; or put in another way, the transmitter power required from a satellite or space probe may be decreased by a factor of four to eight while maintaining the same information transfer rate and signal-to-noise ratio.

6.3.2 KSK Antennas as a New Technique

The Cassegrainian adaptation of the sectoral horn-reflector system appears to offer a new antenna technique of significant electrical and mechanical advantages. The KSK antenna design provides a compact structure, an extremely low antenna noise temperature, feasibility of operating without a radome, and high aperture efficiency, coupled with broadband capability. Experimental measurements obtained for this antenna and comparable information evaluated from other sources indicate that the KSK antenna establishes a practical operational antenna system which if implemented appears reasonably certain of becoming the low noise antenna state-of-the-art. Evaluation of the operating features and limiting factors indicate performance superiority for the KSK antenna to all other antennas of comparable aperture in nearly all low noise respects.

6.4 Recommended Areas for Future Effort

The principal areas which are recommended for future effort may be summarized as follows:

(1) The KSK Antenna

(2) The Fluted Feed.

(3) Development of a Cassegrainian modification for existing paraboloids.

(4) A further study of advanced low noise

6.4.1 The KSK Antenna

The model test experimental results on the KSK antenna indicate the feasibility of the Cassegrainian adaptation of the sectoral horn-reflector system as an antenna design of extreme low noise characteristics and a mechanically high gain configuration. It appears advantageous to proceed further with this novel, compact low noise antenna system by possibly optimizing the design somewhat further and by fabrication of a larger model or an operational full scale antenna system of moderate size. The antenna system certainly has a great deal of merit and possibly could provide an optimum antenna system of compact configuration for future utilization in the space tracking and communication fields.

6.4.2 The Fluted Feed

The optimization of the noise characteristics of an arbitrary secondary reflecting surface by means of beam shaping of the illumination energy incident to the surface is an essential for combined antenna low noise performance and optimal gain performance. The fluted feed structure is a means by which these requirements have been successfully met.

The novel manner in which the fluted feed surface wave structure obtains a constant beamwidth independent of the applied polarization appears to be of definite benefit in many applications. The immediate application of the fluted feed appears to be in the retrofit of existing paraboloidal reflector antenna feed systems with fluted feeds in order to improve their aperture efficiency and reduce their effective antenna noise temperatures.

The fluted feed structure may also be used in any application requiring effective illumination of an aperture in a uniform manner and requiring minimization of the energy contained in the region not subtended by the secondary surface. The

fluted feed principle could very well be utilized as an effective primary feed for Cassegrainian systems, especially since Cassegrainian systems often suffer from poor aperture efficiency. Use of the fluted feed as a primary element with the MSK antenna may prove to advantage. It is felt that further investigation of the fluted feed principle in the development of wide band and monopulse high efficiency uniform illumination feed systems would be of considerable benefit to NASA's effort in providing excellent low noise antenna systems with but a moderate effort in system re-design.

6.4.3 Cassegrainian Modification of Existing Paraboloids

The Cassegrainian method of operation has certain inherent advantages over feed-reflector systems which are often quite important in achieving low noise system performance. A distinct advantage of the Cassegrainian system is its ability to place the spillover energy from the primary feed in the relatively low noise temperature sky region instead of in the relatively high noise temperature ground region. There are also many operational advantages to be found in locating the receiving equipment, such as maser, parametric, and other low noise amplifiers and similar equipment behind the secondary surface, instead of at the focal point of the paraboloidal surface.

Many difficulties arise from the location of maser and other low-noise receivers at the feed point. Included among these is the necessity for using more sturdy feed supports to hold the equipment stable with attendant noise degradation due to absorption or reflection from these supports; the cooling difficulties encountered in operating the maser amplifier at some distance from a source of cooling media; the remote adjustment, alignment and optimizing problems associated with the amplifiers and feed system; and various other factors associated with

furnishing power or other services to the sensitive receiver equipment at the feed point. Since many of the existing NASA large paraboloidal reflector tracking stations are planned for conversion to maser and other low noise receiving systems, it appears desirable to optimize the antenna configuration so that maximum performance compatability with the planned receiver system may be achieved. For these reasons it is believed that a worthwhile area for rather immediate future effort is in the Cassegrainian modification of existing paraboloidal reflectors for use with low noise receiver systems. An investigation of the optimum technique by which this may be accomplished should possibly consider sub-reflectors other than the conventional hyperboloid. The choice of a satisfactory sub-reflector and a desirable high efficiency illuminating feed containing the desired multi-band monopulse feed elements presents a reasonably complex problem but one which is believed amenable to solution by techniques similar to those developed during this program.

6.4.4 Study of Advanced Low Noise Techniques

Further study into the basic optimization criteria involved in the development of advanced low noise antenna system appears to be of considerable value.

A STUDY OF TECHNIQUES FOR REDUCING THE NOISE

TEMPERATURE OF PASSIVE PARABALOIDAL REFLECTORS

Bibliography of Works Conducted

1. S. V. C. Aiya, "Atmospheric Noise Interference to Short Wave Broadcasting", Proc. IRE, Vol. 45, No. 3, pp. 580-588; March, 1958

2. S. V. C. Aiya, "Atmospheric Noise Interference to Medium Wave Broadcasting", Proc. IRE, Vol. 46, No. 8, pp. 1502-1509; August, 1958.

3. ----- "Antenna Noise Temperature Study", Final Report 3304-11on Contract DA-49-170-sc-1547, Airborne Instruments Lab., Nov. 1957.

4. C. M. Angulo and J. P. Rhina, "Antenna Resolution as Limited by Atmospheric Turbulence", Report R-96, Control Sys. Lab., Univ. of Ill.; July, 1957.

5. L. V. Blake, "Antenna and Receiving System Noise-Temperature Calculation, " NRL Report 5668, September 19, 1961.

6. R. H. Brown and C. Hazard, "A Model of the Radio-Frequency Radiation from the Galaxy", Phil Mag., Vol. 44, p. 939; September, 1953.

7. R. H. Brown and C. Hazard, "A Model of the Radio-Frequency Radiation from the Galaxy" Phil. Mag., Ser. 7, Vol. 44, pp. 939-963; September, 1953.

8. R. J. Coates, "Measurements of Solar Radiation and Atmospheric Attenuation at 4.3-Millimeters Wavelength", Proc. IRE, Vol. 46, No. 1, pp. 122-126, January, 1958.

9. H. V. Cottony and J. R. Johler, "Cosmic Radio Noise Intensities in the VHF Band", Proc. IRE, Vol. 40, pp. 1053-1060; September, 1952.

10. A. B. Crawford, D. C. Hogg, and L. E. Hunt, "Project Echo - Horn-Reflector Antenna for Space Communication", NASA Technical Note D-1131(TN D-1131), NASA, Washington, D. C.; December, 1961.

11. R. H. Dicke, et. at., "Atmospheric Absorption Measurements with a Microwave Radiometer", Phys. Rev., Vol. 70, p. 340; 1946.

12. F. D. Drake, "Radio Resolution of the Galactic Nucleus", Sky and Telescope, Vol. 18, No. 8, pp. 428-429; June 1959.

13. A. Feiner and D. Savage, "The Effects of Low Noise Techniques on Tropospheric Scatter", presented at National Symposium on Global Communications, St. Petersburg, Fla; December, 1958.

14. H. T. Friis and W. D. Lewis, "Radar Antennas", Bell System Technical Journal, Vol. 26, pp. 219-317; April, 1947.

15. R. C. Hansen and R. G. Stephenson, "Communications at Megamile Ranges", J. Brit, IRE, Vol. 22, pp. 329-345; October, 1961.

16. R. C. Hansen, "Low Noise Antennas", The Microwave Journal, Vol. 3, p. 19; June, 1959.

17. H. A. Haus and R. B. Adler, "Circuit Theory of Linear Noisy Networks," The Technology Press, 1959.

18. H. A. Haus and R. B. Adler, "An Extension of the Noise Figure Definition", Proc. IRE, Vol. 45, p. 690; 1957.

19. A. H. Hausman, "Dependence of the Maximum Range of Tropospheric Scatter Communications on Antenna and Receiver Noise Temperatures", Trans. IRE, Vol. CS-6, pp. 35-38; December, 1958.

20. D. C. Hogg and W. W. Mumford, "The Effective Noise Temperature of the Sky", Microwave Journal, Vol. 3, pp. 80-84; March, 1960.

21. D. C. Hogg, "Effective Antenna Temperatures due to Oxygen and Water Vapor in the Atmosphere", J. Appl. Phys, Vol. 30, pp. 1417-1419; September, 1959.

22. D. C. Hogg and R. A. Semplak, "Characteristics of a Prototype Near-Field Cassegrainian Antenna", BTL Memorandum for Record, Jan. 17, 1961.

23. F. Horner, "Extra-Terrestrial Radio Noise as a Source of Interference in the Frequency Range 30-1000 Mc/s", Proc. IRE, Vol. 107, Pt. B, pp. 373-376; July, 1960.

24. E. Jahnke and F. Emde, "Tables of Functions," 4th Edition, Dover Publications, N. Y., 1945.

25. K. G. Jansky, "Electrical Disturbances Apparently of Extraterrestrial Origin", Proc. IRE, Vol. 21, No. 10, p. 1387; October, 1933.

26. G. Joos "Theoretical Physics," Third Edition, Hofner Publ. Co., N. Y. 1950.

27. H. C. Ko, "The Distribution of Cosmic Radio Background Radiation", Proc. IRE, Vol. 46, pp. 208-215; January, 1958.

28. J. D. Kraus and H. C. Ko, "Celestial Radio Radiations", Technical Note TN-57-537, AFCRC Contract No. AF19(604)-1591, AD-117273; Ohio State University Research Foundation, Columbus, Ohio; May, 1957.

29. J. D. Kraus "Solar System Radio Radiation", Technical Note TN-59-148, AFCRC Contract No. AF19(604)-1591, AD211944; Ohio State University Research Foundation, Columbus, Onio; December, 1958.

30. J. L. Lawson and G. E. Unlenback, "Threshold Signals", Vol. 24 of MIT Radiation Laboratory Series, McGraw-Hill Book Co., New York, N. Y., pp. 103-108; 1950.

31. M. L. Livingston, "The Effect of Antenna Characteristics on Antenna Noise Temperature and System SNR", Trans. IRE, PGSET, pp. 71-79; September, 1961.

32. B. Lovell and T. A. Clegg, "Radio Astronomy", John Wiley and Sons, Inc., New York; 1952.

33. -------- "Low Noise Vital to Ground Stations," Electronic Design, Jan. 18, 1962.

34. D. F. Martin, "Temperature Radiation from the Quiet Sun in the Radio Spectrum", Nature, Vol. 158, pp. 632-633; November 2, 1956.

35. C. H. Mayer, et. al. "Measurement of Planetary Radiation at Centimeter Wavelengths, "Proc. IRE, Vol. 46, pp. 260-266; January, 1958.

36. A. Maxwell, G. Swarup, and A. R. Thompson, "The Radio Spectrum of Solar Activity", Proc. IRE, Vol. 46, No. 1, pp. 142-148; January, 1958.

37. D. H. Menzel, "Cosmic Noise Survey", Dept. of Defense Contract DA-49-170-SC-2386, Harvard Observatory, Cambridge, Mass.

38. D. H. Menzel, "The Radio Noise Spectrum", Harvard Univ. Press, pp. 151-176; 1960.

39. B. Y. Mills, A. G. Little and K. V. Sheridan, "Emission Nebulas as Radio Sources", Australian Journal of Physics, pp. 218-227; 1956.

40. G. H. Millman, "Atmospheric Effects on VHF and UHF Propagation", Proc. IRE, Vol. 46, pp. 1492-1501; August, 1958.

41. H. Nyquist, "Thermal Agitation of Electric Charge in Conductors", Phys, Rev., Vol. 32, p. 110; July, 1928.

42. J. L. Pawsey and R. N. Bracewell, "Radio Astronomy", Oxford University Press, London, England, pp. 189-190, 343-347; 1955.

43. S. Perlman, et. al. "Concerning Optimum Frequencies for Space Vehicular Communications", IRE Record of National Symposium on Extended Range and Space Communications, Geo. Wash. Univ., pp. 24-31; 1958. (IRE-PGCS, Oct. 1958, pp. 24-31).

44. J. H. Piddington and G. H. Trent, "A Survey of Cosmic Radio Emission at 600 Mc/s", Australian Journal of Physics, Vol. 9, pp. 481-493; 1956.

45. J. R. Pierce and R. Kompfner, "Transoceanic Communication by Means of Satellites", Record of National Symposium on Extended Range and Space Communications, IRE-PGCS, Oct. 1958, pp. 55-64; October, 1958.

46. P. D. Potter, "The Application of the Cassegrainian Principle to Ground Antennas for Space Communication," IRE Transactions on Space Electronics and Telemetry, Vol. SET-8, June 1962, pp. 154-158.

47. P. D. Potter, "A Simple Beamshaping Device for Cassegrainian Antennas," JPL Technical Report No. 32-214, January 31, 1962.

48. P. D. Potter and W. ViTiRusch, "A Cassegrainian Type Low-Noise Antenna Feed For Radio and Radar Astronomy," JPL Report, April, 1962

49. H. J. Pratt, "Propagation, Noise and General Systems Considerations in Earth-Space Communications", Trans. IRE, (Communication Systems), Vol. CS-8, pp. 214-221; December, 1960.

50. R. P. Rafuse, "Characterization of Noise in Receiving Systems", in E. J. Baghdady's "Lectures on Communication System Theory", McGraw-Hill Book Co., New York, N. Y., pp. 369-399; 1961.

51. J. F. Ramsay, "Fourier Transforms in Antenna Theory", Marconi Rev., Vol. 9, p. 139; October-December, 1946.

52. ----- "Reference Data for Radio Engineers" 4th ed. International Telephone and Telegraph Corp., New York; 1956.

53. S. A. Schelkunoff and H. T. Friis, "Antennas: Theory and Practice", John Wiley and Sons, Inc., New York, 1952.

54. D. Schuster, C. T. Stelzried and G. S. Levy, "The Determination of Noise Temperatures of Large Antennas", JPL Technical Report, pp. 32-97; May 1, 1961.

55. C. L. Seeger, G. Westerhout and H. C. Van De Hulst, "The Flux Densities of Some Radio Sources at 400 Mc/s", Bulletin of the Astronomical Institute of the Netherlands, Vol. 13, No. 472, pp. 89-99, 1956.

56. I. S. Shklovsky, "Cosmic Radio Waves," Harvard University Press, Cambridge, Mass., 1960.

57. S. Silver, "Microwave Antenna Theory and Design", McGraw-Hill Book Co., Inc., New York; 1949.

58. A. G. Smith; "Extraterrestrial Noise as a Factor in Space Communications", Proc. IRE, Vol. 48, pp. 593-599; April, 1960.

59. R. C. Spencer, "Fourier Integral Methods of Pattern Analysis", M.I.T. Radiation Lab. Report 762-1; Jan. 21, 1946.

60. P. D. Strum; "Considerations in High-Sensitivity Microwave Radiometry", Proc. IRE, Vol. 46, p. 43; January, 1948.

61. ------- "Standards on Electron Devices: Methods of Measurements of Noise", Proc. IRE, Vol. 41, pp. 890-896; July, 1953.

62. -------- "IRE Standards on Receivers: Definition of Terms"; Proc. IRE, Vol. 40, pp. 1681-1685; December, 1952.

63. -------- IRE Standards on Receivers, 52 IRE 17.81 (Definition of Terms), Proc. IRE, Vol. 40, p. 168; December, 1952; also, IRE Standards on Electron Devices, 53 IRE 7.S1 (Methods of Measuring Noise), Proc. IRE, Vol. 41, pp. 890-896; July, 1953. IRE Standards on Electron Tubes: Definition of Terms; 1957, 57 IRE 7.S2, Proc. IRE, Vol. 45, p. 983; July 1957. IRE Standards on Methods of Measuring Noise in Linear Two Ports, 1959, 59 IRE 20.S1, Proc. IRE, Vol. 48, p. 60; January, 1960.

64. T. T. Taylor, "Proc. IRE", Vol. 36, p. 1135; September, 1948.

65. L. C. Van Atta and T. J. Keary, "Microwave Antenna Theory and Design", McGraw-Hill Book Co. Inc., New York, p. 465; 1949.

66. J. H. Van Vleck, Physics Rev., Vol. 71, p. 413, 427; 1947.

67. J. H. Vogelman, "Propagation and Communications Problems in Space", Proc, IRE, Vol. 48, pp. 567-469; April, 1960.